Finite Element Analysis of Interlocking Timber Connections in Plywood Diaphragm Floors Optimizing Form for Strength

Wielinga, Elise

Award date:
2023

EINDHOVEN UNIVERSITY OF TECHNOLOGY

Department of the Built Environment
Architecture, Building and Planning
Structural Engineering and Design

Finite Element Analysis of Interlocking Timber Connections in Plywood Diaphragm Floors: Optimizing Form for Strength

Master Thesis

E. Wielinga
1017980

Supervisors:

prof.dr.ir. A.S.J. Suiker
Chair of Applied Mechanics

ir. A.P.H.W. Habraken
Chair of Innovative Structural Design

ir. G.J. Rozemeijer
Director at Adviesbureau Lüning

Final version

Eindhoven, June 2023

Abstract

In this thesis, Linear Elastic Finite Element Analyses are performed to analyse the influence of the shape of interlocking timber connections on their strength capacity. Dovetail, arrow and yin yang shaped connections with varying geometric parameters are investigated. Their height, width, radii and fillet radii are varied. Parametric scripts are created for automated creation of the Finite Element Models and for post-processing the results. The strength optimization study was performed using two failure criteria, where the peak or average stresses are compared to the design strength of the 18 mm thick spruce plywood. The connections will be applied in plywood diaphragm floor seams, therefore two critical load conditions are determined including tension and shear. The interlocking timber connection with the largest tension strength capacity made from 18 mm thick spruce plywood is a dovetail with h_1 of 180 mm, w_1 of 80 mm, w_2 of 20 mm and fr_1 of 15 mm. The interlocking timber connection with the largest shear strength capacity is a dovetail with h_1 of 190 mm, w_1 80 of mm, w_2 of 20 mm and fr_1 of 15 mm. The most important factor was the area for contact pressure. The dovetail was able to accommodate the largest space to transfer the stresses from one component to the other. Tension stress parallel was critical for most tension load case designs whereas tension stress perpendicular was critical for all shear load case designs. An example of application of interlocking timber connections in conventional structures is given on the first floor of the WikiHouse.

Preface

While coming across some research and projects on interlocking timber joinery I was immediately inspired. Creativity, robotic fabrication, structural innovation and the use of natural materials have always fascinated me. Interlocking timber connections gives ancient craftmanship a new guise while making its aesthetics very appealing.

I want to thank my supervisors for their guidance throughout my graduation project. In specific, prof.dr.ir. A.S.J. (Akke) Suiker for his knowledge on Finite Element Analysis, ir. A.P.H.W. (Arjan) Habraken for his advise on optimized structures and ir. G.J. (Gert-Jan) Rozemeijer for his experience with timber structures and its practical application. Moreover, I want to thank my colleagues at *Adviesbureau Lüning – Ingenieurs in houtconstructies* for their encouragement and enthusiasm on timber structures. And last but not least, my family and friends who have always supported me.

Elise Wielinga

Eindhoven, June 2023

Contents

Nomenclature

Abbreviations

CLT	Cross Laminated Timber
CNC	Computer Numerical Control
FEA	Finite Element Analysis
FEM	Finite Element Method
Glulam	Glued Laminated Timber
L	Longitudinal direction
LEFEA	Linear Elastic Finite Element Analysis
LVL	Laminated Veneer Lumber
OOP	Object Oriented Programming
OSB	Orientated Strand Board
R	Radial direction
S11	Axial stress parallel to the grain
S12	Shear stress (panel shear)
S22	Axial stress perpendicular to the grain
S33	Axial stress normal to the grain
SLS	Serviceability Limit State
T	Transverse direction
ULS	Ultimate Limit State

Symbols

E	Young's Modulus
$\boldsymbol{\varepsilon}$	Normal strain
$\boldsymbol{f_{c,0,d}}$	Design compression strength parallel to the grain
$\boldsymbol{f_{c,90,d}}$	Design compression strength perpendicular to the grain
$\boldsymbol{f_{t,0,d}}$	Design tension strength parallel to the grain
$\boldsymbol{f_{t,90,d}}$	Design tension strength perpendicular to the grain
$\boldsymbol{f_{v,d}}$	Design shear strength (panel)
$\boldsymbol{f_{c,0,k}}$	Characteristic compression strength parallel to the grain
$\boldsymbol{f_{c,90,k}}$	Characteristic compression strength perpendicular to the grain
$\boldsymbol{f_{t,0,k}}$	Characteristic tension strength parallel to the grain
$\boldsymbol{f_{t,90,k}}$	Characteristic tension strength perpendicular to the grain
$\boldsymbol{f_{v,k}}$	Characteristic shear strength (panel)
G	Shear Modulus
$\boldsymbol{\gamma}$	Shear strain
$\boldsymbol{\gamma_M}$	Material factor timber
$\boldsymbol{k_{mod}}$	Duration factor timber
$\boldsymbol{\upsilon}$	Poisson's ratio
$\boldsymbol{\sigma_{c,0,d}}$	Design compression stress parallel to the grain
$\boldsymbol{\sigma_{c,90,d}}$	Design compression stress perpendicular to the grain
$\boldsymbol{\sigma_{t,0,d}}$	Design tension stress parallel to the grain
$\boldsymbol{\sigma_{t,90,d}}$	Design tension stress perpendicular to the grain
$\boldsymbol{\sigma_{v,d}}$	Design shear stress (panel)
$\boldsymbol{\sigma_{c,0,k}}$	Characteristic compression stress parallel to the grain
$\boldsymbol{\sigma_{c,90,k}}$	Characteristic compression stress perpendicular to the grain
$\boldsymbol{\sigma_{t,0,k}}$	Characteristic tension stress parallel to the grain
$\boldsymbol{\sigma_{t,90,k}}$	Characteristic tension stress perpendicular to the grain
$\boldsymbol{\sigma_{v,k}}$	Characteristic shear stress (panel)
$\boldsymbol{\rho}$	Density

1 Introduction

1.1 Problem definition

The popularity of timber as building material has intensified over the past decades due to growing awareness for sustainability of building constructions and demand for prefabricated solutions. Timber has a favourable weight-to-strength ratio, stores carbon-dioxide and is a low-energy production material. These characteristics contribute to the negative carbon footprint of timber [1], [2]. The United Nations target to transform construction and development to net zero emissions by 2050 [3], which affects the building industry of The Netherlands among others as well [4]. Next to that, many cities worldwide are facing housing shortage [5]–[7]. In The Netherlands, there is a growing shortage of almost 400.000 houses in 2022 [6]. Building new residential houses mostly takes years, inducing a demand for quicker construction [7], [8].

Timber connections are essential to the structural behaviour of timber constructions since they affect the internal force distribution in the entire structure [9]. In the past, traditional timber connections such as mortise-tenon and scarf joints were used worldwide. The interlocking nature of traditional joinery can allow for more sustainable, non-destructive disassembly of timber structures, as demonstrated by historic shrines in Japan [10]. However nowadays traditional joinery techniques have been substituted by mechanical fasteners for quicker, more efficient and more economic designs. Metallic dowel-type connectors are commonly used in timber structures due to their higher load-carrying capacity and ductile behaviour. Nonetheless, the use of metallic fasteners in timber connections often leads to stress concentrations in the connection members due to the large difference of stiffness between the connectors and timber. Another common method involves the use of synthetic adhesives with or without mechanical connectors. A high connection efficiency can be achieved but they deficit on the sustainability aspect of using timber [11]. Moreover, the use of certain types of mechanical fasteners (e.g. nail plates) and adhesives often result in a one-life span design [2]. Due to innovations in the digital production industry, interlocking timber joinery might offer a revival in the building industry [2], [10]. Computer Numerical Control (CNC) can manufacture timber elements with high accuracy [12]. Recent examples of combining traditional joinery techniques with CNC manufacturing include the Hexbox Canopy (Australia, 2019) and the Vidy-Lausanne Theatre (Switzerland, 2017) [13], [14].

Applying interlocking timber joinery to conventional buildings, such as residential houses and offices, could offer a solution to quicker, more sustainable and demountable construction on a large scale. While numerical analyses of interlocking timber connections are not widely available in literature at the moment and structural validation is needed for large scale application [15], this study will investigate and optimize the strength of interlocking timber joinery using Finite Element Analysis (FEA). To address the applicability to conventional buildings, WikiHouse is adopted as case study. Further explanation is given in chapters ‘2. Preliminary study’ and ‘3. Structural analysis Wikihouse’.

1.2 Research objective

The goal of this study is to optimize the design shape and dimensions of the interlocking timber connection to maximize its tension and shear strength by means of a FEA based variation study. Interlocking timber connections might offer a rebirth in conventional timber structures if they have enough strength capacity to transfer the loads and compete with mechanical fasteners. Moreover, FEA of interlocking timber connections could reveal weak spots in the design which can then be improved. This study focusses on applying interlocking timber connections in plywood diaphragm floor seams. Therefore, the main research question is as follows:

What are the optimal design parameters to maximize the tension and shear strength of interlocking timber joinery in plywood diaphragm floor seams?

Several sub questions will be addressed in order to answer the main question:

- What geometric parameters influence the force transmission in the connection?
- What are the optimization criteria?
- What is the tension and shear strength of the interlocking timber connection and what design performs best under which load type?
- What are the corresponding deformations?
- Do the optimized interlocking timber joints have enough strength to be applied in the first floor of the WikiHouse?
- How to locate these connections in the WikiHouse floor seam?

When the tension and shear strength of certain connection geometries vary under different load applications, not only optimization of the geometry is possible but optimization on the placement of the connection can also be achieved. Tension-optimized connections can be placed in tension dominated zones in the diaphragm floor while shear-optimized connections can be placed in shear dominated zones.

1.3 Scope

Not much research is available on digitally manufactured interlocking timber joinery. Therefore, this study focusses on strength optimization of the connection which is analysed numerically. Many more aspects are important to address before structural validation can be achieved, such as experimental research and joint stiffness. Whereas the joint stiffness is highly dependent on the tightness of the joint, shrinkage and swelling of the timber, manufacturing tolerances and friction coefficient.

1.4 Thesis outline

The structure of this thesis comprises roughly three parts: preparatory investigation, variation study and application of research. The first part consists of chapters ‘2. Preliminary study’ and ‘3. Structural analysis WikiHouse’. Here, timber products, existing interlocking timber connections, CNC production and failure criteria are explored. The case study WikiHouse is analysed to acquire a realistic reference for the application of interlocking timber connections to conventional buildings.

The second part consist of the variation study for which a numerical model is made by utilizing parametric scripts. The numerical model is defined in chapter ‘4. Numerical model’ and the parametric scripts are explained in chapter ‘5. Parametric scripts’. Hereafter, the results are analysed in chapter ‘6. Variation study’.

In the last part, the research is applied to the case study WikiHouse in chapter ‘7. Example: Application to WikiHouse. The thesis finalizes with a conclusion and recommendation.

References and additional information are presented in chapters ‘Bibliography’ and ‘Appendix’ respectively.

2 Preliminary study

This chapter studies different types of timber, existing interlocking timber connections, CNC production techniques and failure criteria to determine beneficial design strategies.

2.1 Timber products

Timber is a natural material with anisotropic properties. This means that the mechanical and physical properties of the timber vary depending on the direction of the grain and the direction of the applied load. Timber has significantly higher strength and stiffness properties parallel to the grain than perpendicular and normal to the grain [16]. Furthermore, moisture and temperature fluctuations cause the timber to shrink and swell. The largest deformations resulting from this can be found in the tangential and radial direction whereas the deformation in longitudinal direction is much smaller [16]. The longitudinal (L), transverse (T) and radial (R) direction in relation to the grain of the timber are illustrated in Figure 1.

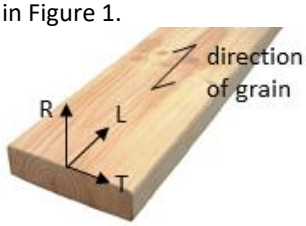

Figure 1: Sawn timber with anisotropic directions [17]

Several types of timber products are commonly available including sawn timber and various engineered timber products such as Glued Laminated Timber (Glulam), Cross Laminated Timber (CLT), plywood, Laminated Veneer Lumber (LVL) and Orientated Strand Board (OSB).

Sawn timber is a cut from logs and thus has its main strengths and stiffness in the longitudinal direction. On top of that, knots and other defects are commonly present in the timber due to branching of the trees which has a negative impact on the mechanical properties.

Glulam consists of multiple layers of lumber that are glued together of which the direction of the grain of all layers are parallel to the length of the structural element [18]. Whereas CLT is made by gluing together layers of sawn timber at right angles to each other. While the top and bottom faces of CLT are glued, the side faces are generally not glued. Additionally, some CLT panels feature additional stress-cuts between the side faces. [1]. Both Glulam and CLT commonly contain knots, holes and other defects [1].

Plywood and LVL are both produced by rotary peeling wood logs. Adhesives are applied on the veneers which are pressed together to create a strong and stable structural member. The veneers of plywood are mainly stacked orthogonally to each other whereas the veneers of LVL are predominantly or exclusively stacked in the longitudinal direction [18]. During the manufacturing process, defects such as knots are removed from the veneers. Besides, the probability that defects in the veneers are stacked in the same region is very low if they are still present.

OSB is manufactured from thin wood strands which are bonded together with adhesives under heat and pressure [18]. Strand orientation plays a major factor on the mechanical properties. Several types of boards exist such as unidirectionally oriented homogeneous boards, cross-oriented three-layer board, oriented three-layer board with random core layer and randomly oriented homogeneous board [19], [20].

Plywood and LVL seem to be the most suitable timber products for the application of interlocking timber joinery. They have excellent homogeneity throughout the material and advanced engineered strength in longitudinal and transverse direction. Contrarily, sawn timber, Glulam and CLT generally contain defects which should not collide with interlocking joint geometries. Despite the homogeneity of OSB, it is uncertain is local failure of strands might occur when using interlocking geometries. Additionally, plywood and LVL can be used as plate material. Then, the loads on the interlocking timber joints can be spread over a larger distance compared to timber frame structures and thus result in smaller loads per connection. WikiHouse, which is adopted as case study and elaborated in the next chapter, is made from plywood and therefore this study will implement plywood as material for the interlocking timber joints.

2.2 Interlocking timber joinery

Interlocking timber joinery has been used widely in the past. Additionally, recent studies and projects attempted to create new designs for interlocking timber connections while utilizing digital fabrication. Both old and new forms are briefed below.

Traditional joinery

Some well-known examples of traditional joinery are the mortise-tenon, scarf and dovetail joint (Figure 2). The mortise-tenon joint can be fastened by applying timber dowels or pegs. The scarf joint is illustrated in its simplest form in Figure 2, however numerous variations exist to improve interlocking abilities as demonstrated in Figure 4. The dovetail knows more complex design variations as well as illustrated in Figure 3. Where the mortise-tenon and scarf joints are more suitable for connecting columns and beams, the dovetail joint can be used to connect plates as well.

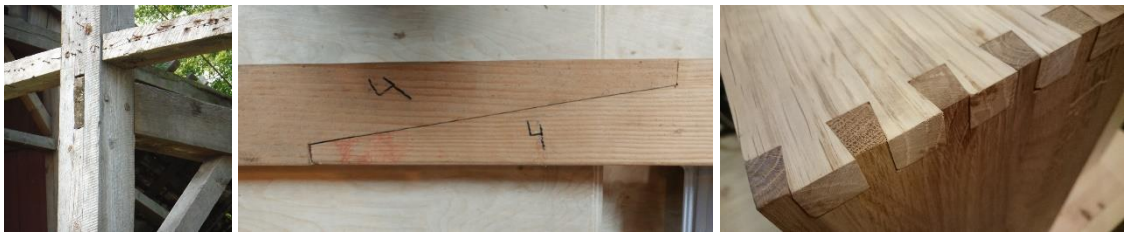

Figure 2: Traditional joinery: (a) mortise-tenon joint, (b) scarf joint, (c) dovetail joint [21]–[23]

Japanese joinery

Japanese wood craftmanship includes complex interlocking geometries which are crafted for structures and furniture. Extreme handcraft precision is needed to fit the joints. Some joints require rotation or movement of multiple components to fasten the joint. As they might be able to provide good interlocking properties and aesthetics, it could be difficult to implement 'rotating' joints in the building industry when a certain order of construction is needed. Other construction elements like beams or walls might be obstructing the joint component that needs to be rotated into the other joint component. Moreover, when the size of the joint elements increases (e.g. a 5 m long beam) it will be more difficult to precisely assemble the joint. There are numerous types and variations of joints where some are best applied to columns or beams and others to plates. A selection of Japanese joinery is illustrated in Figure 3.

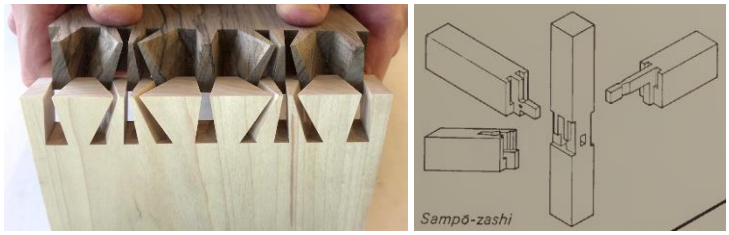

Figure 3: Japanese joinery: (a) sunrise dovetail joint, (b) Sampo-zashi joint [24], [25]

Joinery fastened with wedges

Another variation on joinery is to tighten the timber joints by hammering pegs or wedges in the joint as illustrated in Figure 4. The interlocking properties can be improved extensively compared to the basic mortise-tenon and scarf joint presented in Figure 2. Additionally, the stiffness of the joint is improved by ensuring the tightness of the joint. Joinery fastened with wedges is particularly suitable for joining beams and columns.

Figure 4: Joints fastened with pegs: (a) tusk-tenon joint and (b) mortised rabbeted oblique scarf joint ('Kanawa Tsugi') [26], [27]

Joint inlays

A different approach is to use loose insertion parts, commonly called keys or inlays, to join timber elements. A broad variety of shapes is possible like the butterfly, dog bone and jigsaw key joints in Figure 5. Possible advantages include that the keys can be assembled one by one when applied in a floor or wall element and that the key could be made from a stronger timber species which might increase the overall strength of the joint.

Figure 5: Joint inlays: (a) butterfly key joint, (b) dog bone key joint and (c) jigsaw key joint [28]–[30]

Snap-fit joints

Recent studies [1], [31] investigate the potential of applying snap-fit joints in the timber building industry as they are commonly used in the automotive and consumer electronics industry. Snap-fit joints consist of a protruding component, such as a hook, stud or bead, which is briefly deflected during the joining process. After insertion, the protruding component will be stuck in an undercut of the mating component and the snap-fit features should return to a stress-free condition, see Figure 6. A snap-fit joint might be separable or inseparable after construction, depending on the design. [32]

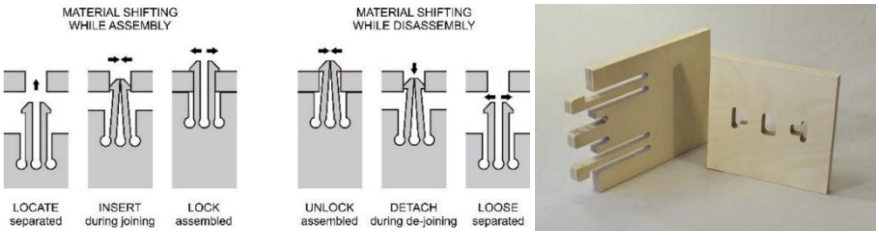

Figure 6: Snap-fit joint (a) assembly and (b) disassembly [28], [31]

The decision has been made to analyse traditional and Japanese inspired joint types because they can be implemented along the length of a plate. The loads on the interlocking timber joinery in the plywood diaphragm floor seams will thus be smaller per connection. Joint inlays might also offer great applicability with the possibility to use stronger timber species for the inlays themselves. However, joint inlays will not be covered in this thesis. Snap-fit joints are deemed less suitable due to the more complicated construction process and limited disassembly potential. Wedges could offer additional joint stiffness and could be considered in a future study as well.

2.3 Computer Numerical Control (CNC) production

Several topics need attention when creating interlocking timber connections with CNC machines. CNC machines use a miller with a certain radius that follows a toolpath to create the design. Therefore, sharp corners like the corners of a traditional dovetail joint cannot be created. Rounded corners or cutting notches will be created at these sharp corners instead, see Figure 7. The cutting notches might be in favour of the interlocking joint's strength by reducing peak stresses at the corners. However, it is also possible that the cutting notches reduce the joint stiffness and thus have a negative impact.

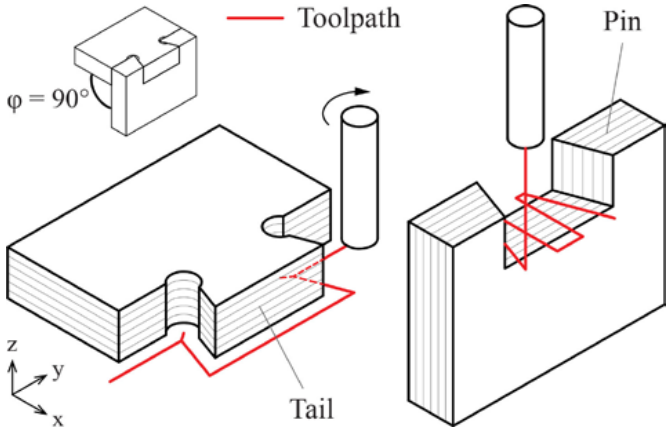

Figure 7: Cutting notches due to CNC toolpath (3-axis) [33]

Furthermore, CNC manufacturing is a very precise production technique where 0.01 mm precision is possible for milling the WikiHouseUK [34]. However, timber shrinks and swells which could cause the interlocking timber connections to not fit anymore. Therefore, it is extremely important to store the timber elements in a climate-controlled environment prior to construction.

Lastly, several degrees of motion are available for CNC machines, namely 3-axis, 4-axis and 5-axis milling. For 3-axis milling, the spindle can move in the x, y and z direction while the specimen is fixed. For 4-axis and 5-axis milling the spindle can move in the x, y and z direction and the specimen or spindle can rotate around one or two axes respectively. An example of what can be achieved by a 5-axis CNC machine is illustrated in Figure 8.

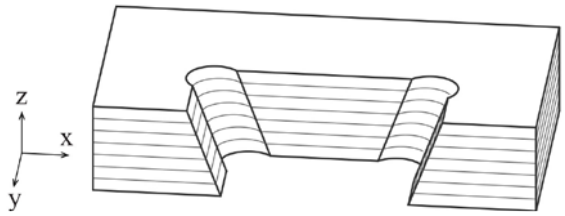

Figure 8: 5-axis CNC milled dovetail [33]

2.4 Failure criteria

Failure criteria will be used to assess the strength capacity of the interlocking timber joint designs. The failure mechanisms of plywood play an important role in the formulation of these criteria. Wang et al. studied the in-plane mechanical properties of birch plywood through experimental research [35]. It is expected that the interlocking timber connections will have similar failure mechanisms. The stress-strain relationships of the specimen loaded in tension, compression and shear are presented in Figure 9.

Application of the interlocking timber connections will be aligned to the direction of the grain (0°). These stress-strain relationships are illustrated by the black continuous curves in Figure 9. The failure mechanism of plywood loaded in tension is brittle. The stress-strain curve is mainly linear and failure happens without warning. The failure mechanisms of plywood loaded in compression and in shear show some plastic behaviour before failure. This means that the peak stresses, average stresses and difference between these stresses need to be investigated in the numerical analyses.

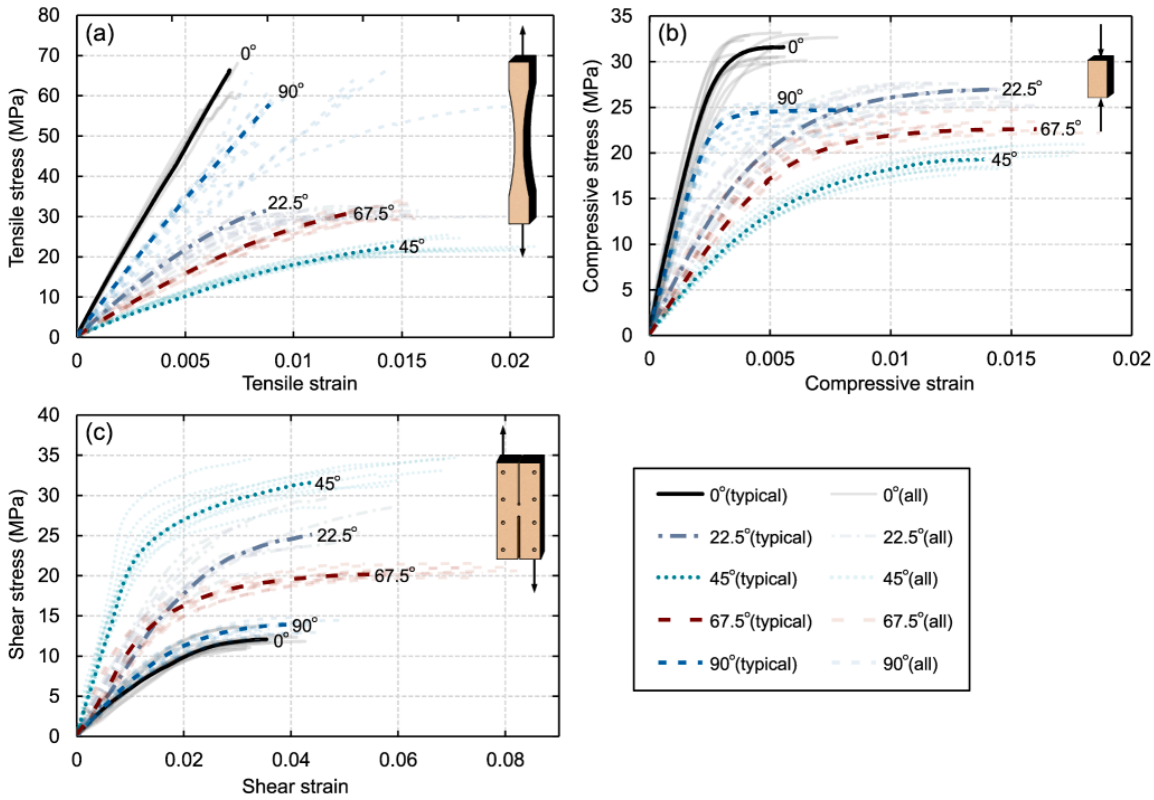

Figure 9: Stress-strain relationships of birch plywood specimens in (a) tension, (b) compression and (c) shear [35]

Furthermore, the intention is to apply the interlocking timber joints to conventional buildings to accommodate large scale application. The joints need to suffice the Dutch norm when applied on structures in the Netherlands. Therefore, the resulting stresses from the numerical analysis need to be evaluated to the design strength of the plywood. The design strengths are determined according to the Dutch norm (Eq. 1-5) [36].

$$f_{t,0,d} = \frac{f_{t,0,k}}{\gamma_M} \cdot k_{mod} \quad (1)$$

$$f_{t,90,d} = \frac{f_{t,90,k}}{\gamma_M} \cdot k_{mod} \quad (2)$$

$$f_{c,0,d} = \frac{f_{c,0,k}}{\gamma_M} \cdot k_{mod} \quad (3)$$

$$f_{c,90,d} = \frac{f_{c,90,k}}{\gamma_M} \cdot k_{mod} \quad (4)$$

$$f_{v,d} = \frac{f_{v,k}}{\gamma_M} \cdot k_{mod} \quad (5)$$

Where γ_M is the material factor, k_{mod} is the duration factor and subscripts *d* and *k* relate to the design and characteristic strength respectively.

The peak stresses in the numerical model do not necessarily mean failure of the complete connection. The relation between the design, characteristic and ultimate strengths from the study by Wang et al. is analysed in Table 1. Except for compression perpendicular to the grain, the ultimate strengths are higher than the characteristic and design strength. Since the degree of redistribution of stresses in the interlocking timber joints is unknown. Two failure criteria will be adopted for the variation study.

Table 1: Relation between plywood design, characteristic and ultimate strength

	Tension		Compression		Shear	
	0°	90°	0°	90°	0°	90°
Strength [MPa]						
Design strength	29.25*	27*	20.25*	18.75*	7.13*	7.13*
Characteristic strength	39**	36**	27**	25**	9.5**	9.5**
Ultimate strength	62.5***	56.7***	31.3***	23.9***	11.9***	13.2***
Strength percentage compared to the design strength [%]						
Design strength	100	100	100	100	100	100
Characteristic strength	133	133	133	133	133	133
Ultimate strength	213	210	154	127	167	185

* Determined according to Dutch norm [36]
** Handbook of Finnish Plywood [37]
*** Experimental data from study by Wang et al. [35]

Failure criterium 1

The first failure criterium exclusively assumes elastic behaviour, i.e. the linear part of the stress-strain curves. Each design will be assessed by this criterium. The maximum occurring stress in the interlocking timber connection may not exceed the design strength of the material (Eq. 6-8). The lower the score, the higher the strength of the connection. Brittle failure is assumed for failure due to tension stresses, therefore failure criterium 1 should be able to accurately predict the tension strength. Failure due to compression and shear loads will have some plastic behaviour, however the degree of redistribution is unknown. Therefore, this failure criteria will be on the safe side for these failure modes.

$$\frac{\sigma_{11,max}}{f_{t,0,d}} \leq 1.0 \quad and \quad \frac{\sigma_{11,min}}{f_{c,0,d}} \leq 1.0 \tag{6}$$

$$\frac{\sigma_{22,max}}{f_{t,90,d}} \leq 1.0 \quad and \quad \frac{\sigma_{22,min}}{f_{c,90,d}} \leq 1.0 \tag{7}$$

$$\frac{\sigma_{12,max}}{f_{v,d}} \leq 1.0 \quad and \quad \frac{\sigma_{12,min}}{f_{v,d}} \leq 1.0 \tag{8}$$

Where subscript *t* is tension, *c* is compression and *v* is shear. Subscripts *0* and *90* correlate to the longitudinal (0°) and transverse direction (90°) of the timber.

Failure criterium 2

The second failure criterium assumes plastic behaviour for the compression and shear load cases. After the optimization procedure by failure criterium 1, a selection of designs will be assessed by failure criterium 2. The average stresses along a section should not exceed the design strength of the material (Eq. 9-11). Again, a lower score means that the connection is stronger.

$$\frac{\sigma_{11,c,mean}}{f_{c,0,d}} \leq 1.0 \tag{9}$$

$$\frac{\sigma_{22,c,mean}}{f_{c,90,d}} \leq 1.0 \tag{10}$$

$$\frac{\sigma_{12,mean}}{f_{v,d}} \leq 1.0 \tag{11}$$

In addition, it is important to look at the difference between the peak stress and average stress. This stress distribution check is not only important for compression and shear stresses but also for tension stresses. By analysing the stress distribution, a speculation can be made if the connection will be able to redistribute the peak stresses. What is the difference between peak and average stresses and along what distance does the peak occur?

Lastly, if different designs perform equally well but have a different governing stress, the design with governing compression or shear stress is favoured above the design with governing tension stresses. The reason for this is because ductile behaviour is preferred over brittle behaviour due to warning aspect before failure.

3 Structural analysis WikiHouse

WikiHouse is adopted as case study to obtain a realistic reference for the application of interlocking timber joints in conventional buildings. In specific, a WikiHouse from phase 2 at The Stripmaker in Almere which consists of 2 storeys, 9 modules and a 45° pitched roof is considered. In this chapter, the general concept of the WikiHouse is explained after which an elaborated structural analysis is performed. First, the structure is analysed on a global level after which the scale is decreased to connection level. Figure 10 illustrates some of the WikiHouses from phase 2 that are built at The Stripmaker in Almere, The Netherlands.

Figure 10: Wikihouse phase 2 at The Stripmaker in Almere, The Netherlands [38], [39]

3.1 General concept WikiHouse

WikiHouse is an open-source modular timber building concept that enables users to select or create digital designs. The design is CNC manufactured locally after structural verification. The DIY package is delivered on site, making it possible to build it yourself or hire a contractor. The WikiHouse can be used for several functions, including but not limited to residential homes and offices. Currently, multiple WikiHouses have been built in The Netherlands, United Kingdom, Austria, China and New Zealand. The material choice, self-building aspect and relatively short construction time make it affordable homes [34], [40].

The lightweight structure of the WikiHouse consists of a plywood box-like construction that facilitates efficient material placement resulting in minimal material use (Figure 11). Moreover, the precise, digital and dry production process results in less waste and a circular demountable design. The timber elements fit like puzzle pieces and are fastened by screws, with insulation placed inside the box-like construction. The structural systems of WikiHouse differ over the years and per country (e.g. Wren, Blackbird, Swift and Skylark), but in all cases the structure can be built quickly. The Dutch WikiHouse construction can be completed in a few months. Whereas the chassis of the UK WikiHouse can be built in 2 to 4 days, and its construction can be completed in 4 to 12 weeks [34], [40].

Figure 11: Plywood box-like structure [41], [42]

3.2 Global structural analysis

A WikiHouse of 2 storeys, 9 modules and a 45° pitched roof is assumed. Each module is 1.2 m long, resulting in a total length of 10.8 m. The ridge height is 8.2 m. Structural drawings are added in Appendix A. The spruce plywood box-like structure acts as main load bearing structure (Figure 11). The seams between these boxes are fixed with screws: an additional plate of plywood is placed on the flanges of the boxes which together are fixated with screws, see Figure 12. Four screws were applied at these seams every 50 to 200 mm, resulting in about 7000 screws per building. The highest concentration of screws is found in the first-floor seams. A screw plan is added in Appendix A: Figure A-III.

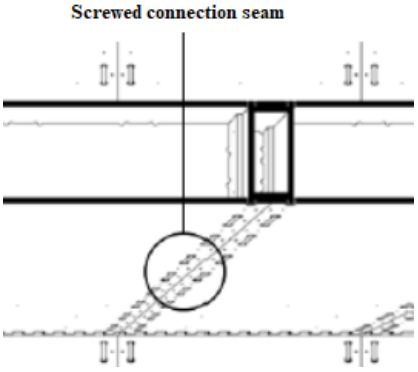

Figure 12: Connection seam [42]

Stability principles are illustrated in Figure 13. The stability in longitudinal direction is assured by the two adjacent façade walls, which act as a diaphragm. By increasing the stiffness of corner profiles, which are made from single-piece birch plywood, the stability of the frame is enhanced. To provide stability in the transverse direction, the first floor works as a diaphragm floor and an additional CLT stability wall with a length of 2.65 m is placed on the ground floor between modules 4 and 6.

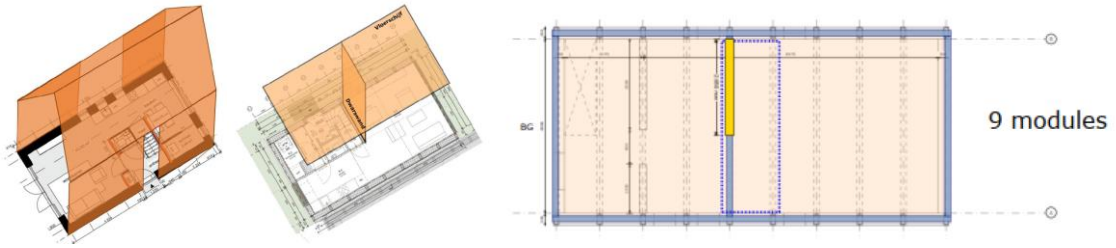

Figure 13: Stability principles: (a) walls and roof as diaphragm, (b) first floor as diaphragm with stability wall and (c) placement of stability wall [41]

The structure is calculated by a 2D frame study according to Dutch norms [36], [43], an elaborated structural report is added in Appendix B. The highest forces occur in the first floor at the location of the stability wall. The critical load combination is an Ultimate Limit State (ULS) load combination which includes wind left (i.e. wind load on the longest façade) and wind overpressure. The maximum normal force is 19.21 kN, the maximum shear force is 43.90 kN and the maximum bending moment is 131.71 kNm. Force diagrams for the critical load combination are presented in Figure 14.

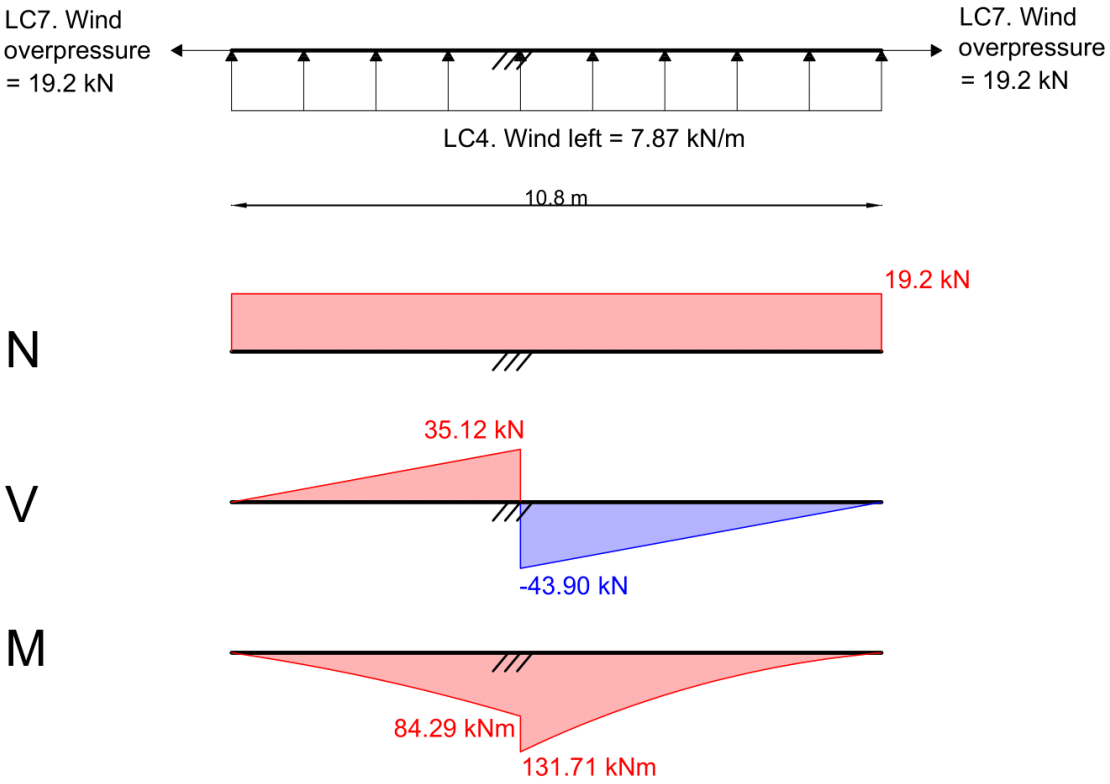

Figure 14: Critical load combination: Normal force diagram (N), Shear force diagram (V) and Moment diagram (M)

3.3 Local structural analysis

The first floor is analysed in more detail since this location was critical in the global analysis. A 2D Linear Elastic Finite Element Analysis (LEFEA) of the floor is conducted in Abaqus to determine the stresses at the floor seams. These results will be compared to analytically obtained stress results for validation. It is assumed that the interlocking connections will be applied only in the top flanges of the plywood box-structure. Therefore, only the top plate of 18 mm thick plywood is modelled and considered as a single stiff plate instead of 9 separate modules. The critical load combination consists of wind left and wind overpressure, see Figure 15. Vertical loading (normal to the floor plane), such as dead load and live load, is not considered.

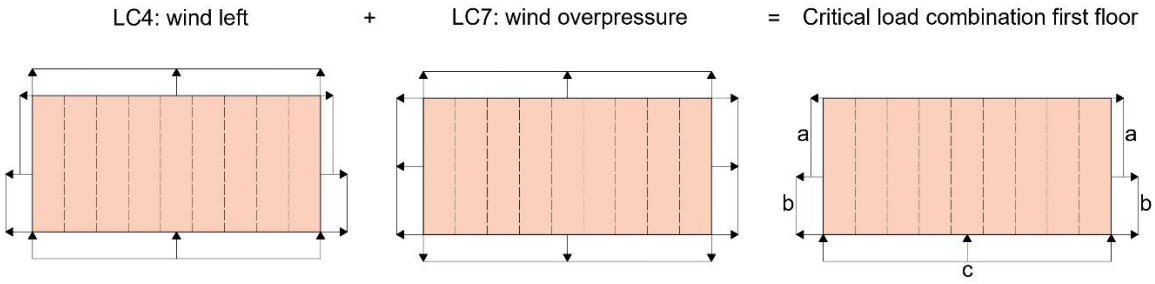

Figure 15: Load combination 2D analysis WikiHouse first floor with resultant forces of (a) $q_{x,1,res} = 3.20\ kN/m$, (b) $q_{x,2,res} = 4.54\ kN/m$ and (c) $q_{y,res} = 7.87\ kN/m$

The geometry and boundary conditions are illustrated in Figure 16. The translational displacement in U3 direction is restrained at the top and bottom edges. At the location where the first floor is supported by the stability wall (marked red), translational displacement in both U2 and U3 direction is constrained. Finally, the translational displacement in U1 direction is constrained along the whole width of the floor module at the same location as the stability wall (black centre line). This constraint was added to prevent large rotations around the stability wall corners since these rotations led to unrealistic stress patterns.

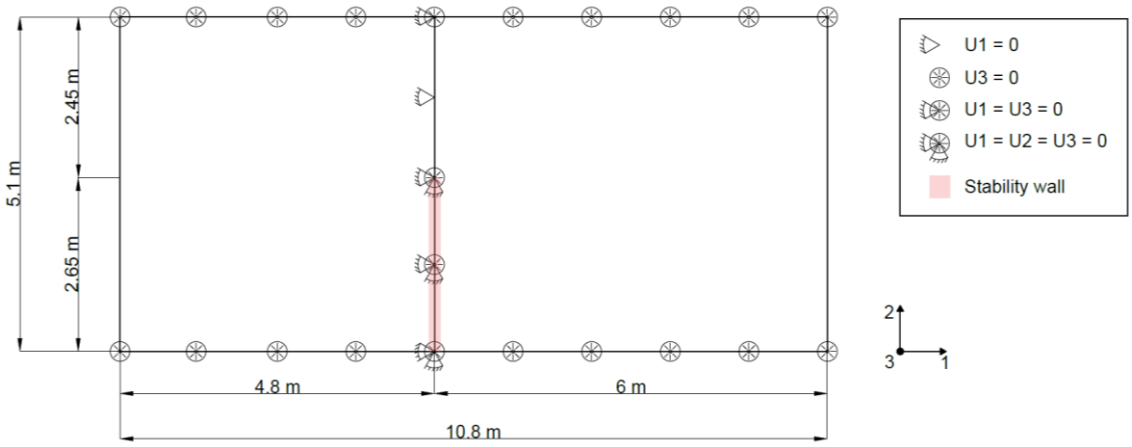

Figure 16: Boundary conditions 2D analysis WikiHouse first floor

The floor is modelled as a 2D planar deformable shell with a shell thickness of 18 mm. A Simpson integration rule with 5 integration points throughout the thickness is used. First-order quadrilateral elements are applied with a size of 0.1 m. The material is assumed to be solid homogeneous isotropic with density ρ of $4.60 \cdot 10^2\ kg/m^3$, Young's modulus E of $6.68 \cdot 10^6\ kN/m^2$ and Poisson's ratio υ of 0.3.

The results from the numerical study are presented in Figures 17-19. The maximum stresses were found at the stability wall (floor seam between modules 4 and 5). To avoid peak stresses due to boundary conditions, the location of maximum stresses is assumed at 0.5 m right from the stability wall. Here, a maximum tension stress of 2.51 MPa, a maximum compression stress of -1.86 MPa and a maximum shear stress of 0.83 MPa was found. The maximum stresses from the analytical calculation include a tension stress of 2.07 MPa, a maximum compression stress of -1.64 MPa and a maximum shear stress of 0.77 MPa. The analytical calculation can be found in Appendix B. The maximum results of both calculation methods are in the same range. The maximum tension, compression and shear stresses from the numerical study are 21%, 13% and 8% higher than the stresses from the analytical calculation. The analytical calculation is based on the Euler-Bernoulli beam theory whereas the numerical study is based on plate theory. Therefore, it makes sense that the maximum stresses determined by the plate theory somewhat differ from the maximum stresses determined by the Euler-Bernoulli beam theory. It can be assumed that the results from the numerical analysis are sufficiently accurate. Therefore, the maximum stresses from the numerical analysis will be used to determine the loads on the interlocking timber connections.

It is noticed that the shear stress curve along the floor seam tends to have a more parabolic shape when further away from the stability wall. The stresses in the floor seam between modules 5 and 6 are illustrated in Figure 19, this is the first seam 1.2 m right from the stability wall. Here, a maximum tension stress of 1.37 MPa, a maximum compression stress of -1.25 MPa and a maximum shear stress of 0.59 MPa was found. These values are 55%, 67% and 71% of the maximum tension, compression and shear stresses found at 0.5 m right from the stability wall respectively. In other words, a substantial decrease of stresses is noticed when moving away from the stability wall.

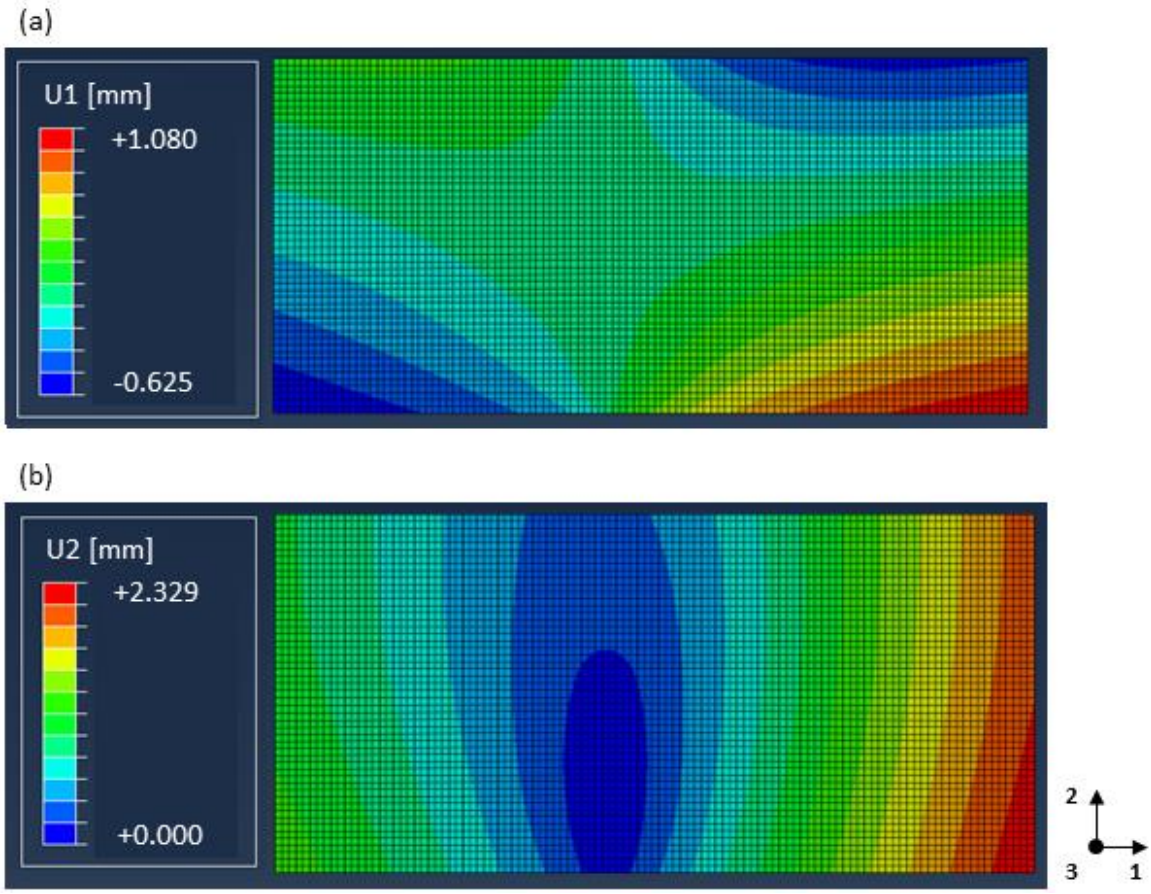

Figure 17: Displacements (a) U1 and (b) U2

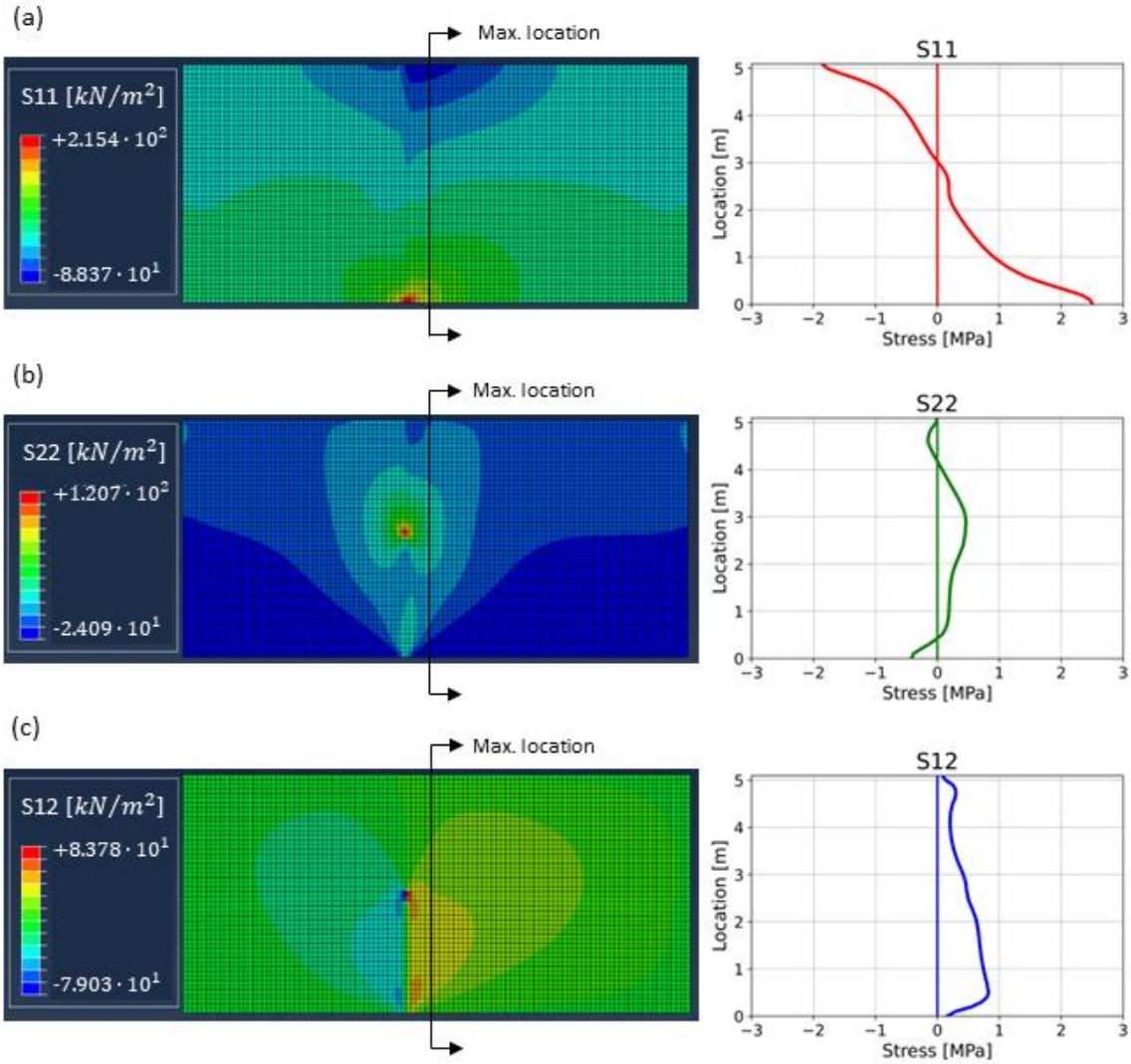

Figure 18: Stresses at max. location in floor: (a) axial stress S11, (b) axial stress S22 and (c) shear stress S12

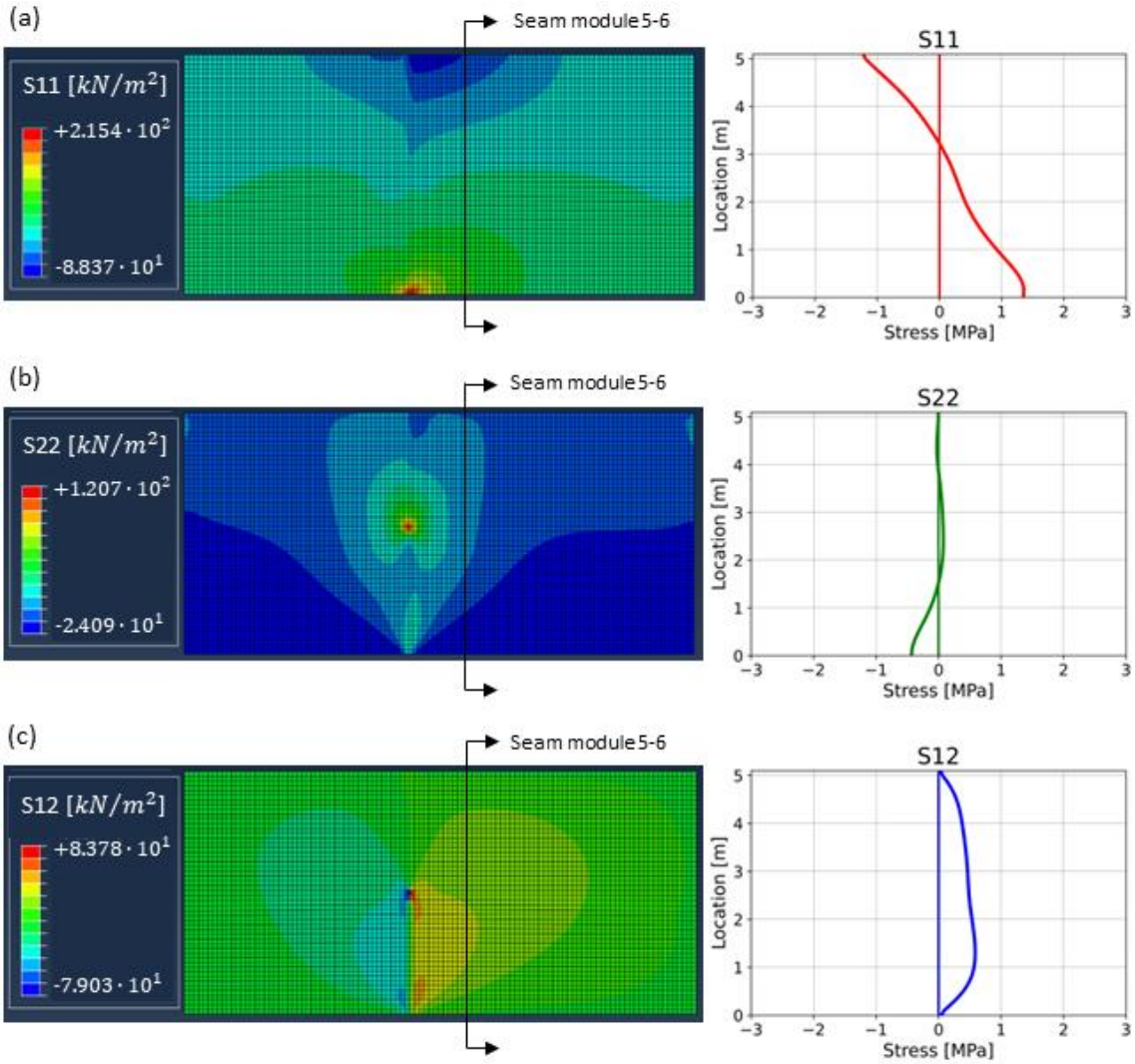

Figure 19: Stresses at seam between module 5 and 6: (a) axial stress S11, (b) axial stress S22 and (c) shear stress S12

3.4 Conclusion

The critical load combination consisting of wind left and wind overpressure at the first floor was used to determine the loads which will be applied on the interlocking timber connections. This load is assumed to be either the maximum tension, compression or shear stress which were found in the numerical analysis of the first floor. Even though multiple stresses are present at the same time at the same location in the floor seam, there will be no analysis on combined loading conditions. Optimization of the connection shape and dimensions will be done on single loading conditions, i.e. optimizing for tension or shear strength. When assuming that there will be 10 interlocking timber connection per meter floor seam length. The maximum forces on a connection will be a tension force of 4518 N, a compression force of -3348 N or a shear force of 1494 N. These loads will be applied in the variation study.

The tension, compression and shear stress vary over the length of the floor seams. Therefore, optimisation of the placement of connections can also be applied. Tension optimized connections can be applied in the tension-dominated zones and compression-dominated zones. The reason for this is because the wind load can be applied either on the left or on the right, thus the tension and compression patterns switch. Shear optimized connections can be applied in shear-dominated zones. Additionally, it is possible to create a transition zone between the tension-dominated zone and the shear-dominated zone.

Some first design ideas are created for application in a plywood diaphragm floor, see Figure 20. Different shapes or scales of interlocking timber joint designs could be applied at different locations in the floor seam. The connection that has the best tension strength properties can be applied in a tension-dominated zone whereas a connection that has the best shear strength properties can be applied in a shear-dominated zone.

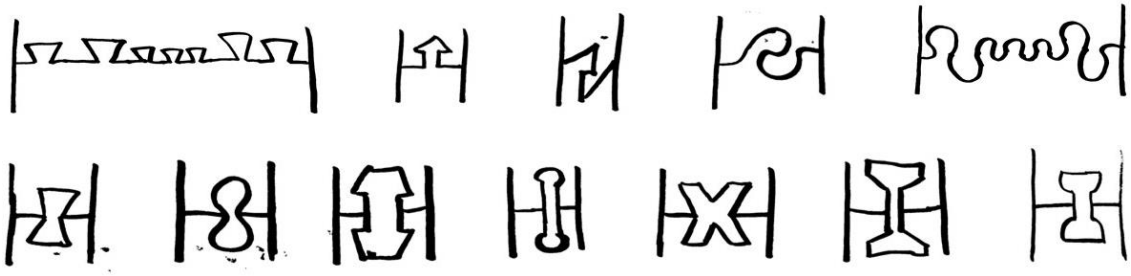

Figure 20: Design ideas sketches

4 Numerical model

The optimal form of the connection is investigated by a numerical study. Linear Elastic Finite Element Analyses (LEFEA) are performed in Abaqus. The goal is to investigate which connection performs best strength-wise. The exact loads at which the connections fail are not obtained from the LEFEA, more advanced numerical analysis or experimental research would be necessary for that purpose. This chapter explains the principles of the numerical analysis, the results are presented in chapter '6. Variation study'.

4.1 Geometries

Three main connection shapes are picked for the variation study in this thesis which are the dovetail, arrow and yin yang. The reason that these shapes are picked for the analysis is because they differ quite a lot from each other. For example, a jigsaw joint is very similar to a dovetail joint with large fillet radii. The dovetail is widely used in traditional joinery, the reason could be that it is relatively simple to make or that it is an efficient shape for connections. The yin yang has very round shapes and is not traditionally used as this would be very complex to make. However, CNC machines do not stumble on this problem which means new round shapes might offer good strength-capacity.

Figures 21-23 illustrate the geometric parameters per connection shape. In all studies, it is assumed that there are 10 connections per meter floor length, which means that the total width of the connection w_t is 100 mm. The total height of the connection h_t is assumed to be 100 mm as well. For each variation study, one parameter is varied while all other parameters remain constant to determine the influence of each parameter. The yin yang joints are modelled as two mirrored joints due to their asymmetric shape, they represent two adjacent joins in the floor seam.

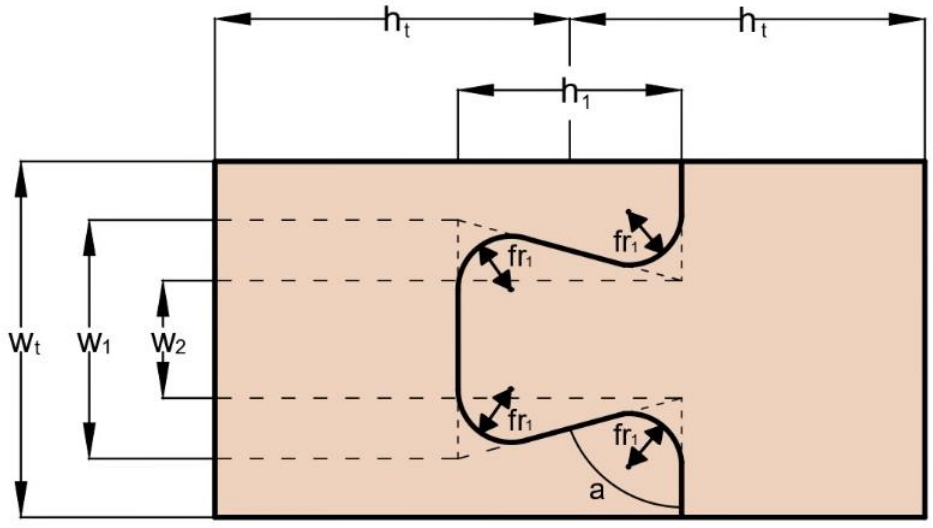

Dovetail parameters
Total width w_t [mm]
Width dovetail head w_1 [mm]
Width dovetail neck w_2 [mm]
Total height h_t [mm]
Height dovetail h_1 [mm]
Fillet radius f_{r1} [mm]
Dovetail angle a [°]

Figure 21: Dovetail geometric parameters

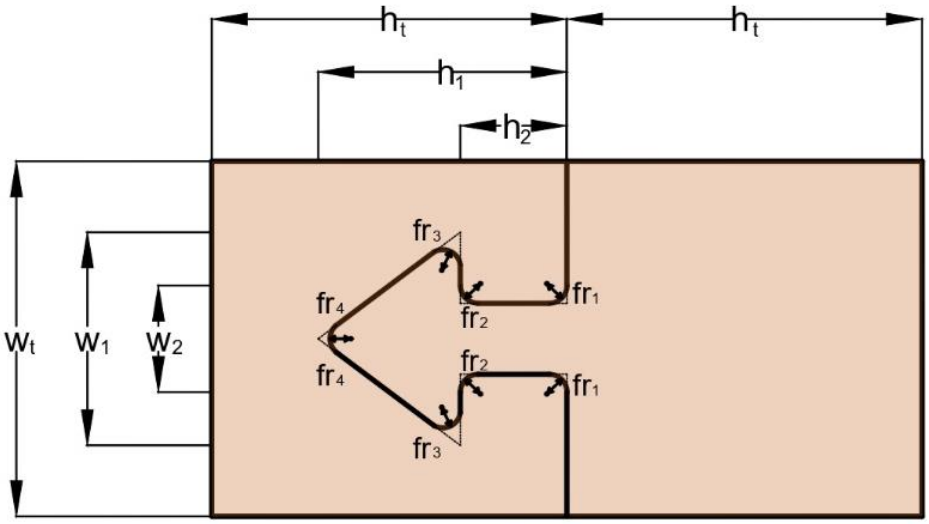

Arrow parameters
Total width w_t [mm]
Width arrow head w_1 [mm]
Width arrow neck w_2 [mm]
Total height h_t [mm]
Height arrow h_1 [mm]
Height arrow neck h_2 [mm]
Fillet radii $f_{r1,2,3,4}$ [mm]

Figure 22: Arrow geometric parameters

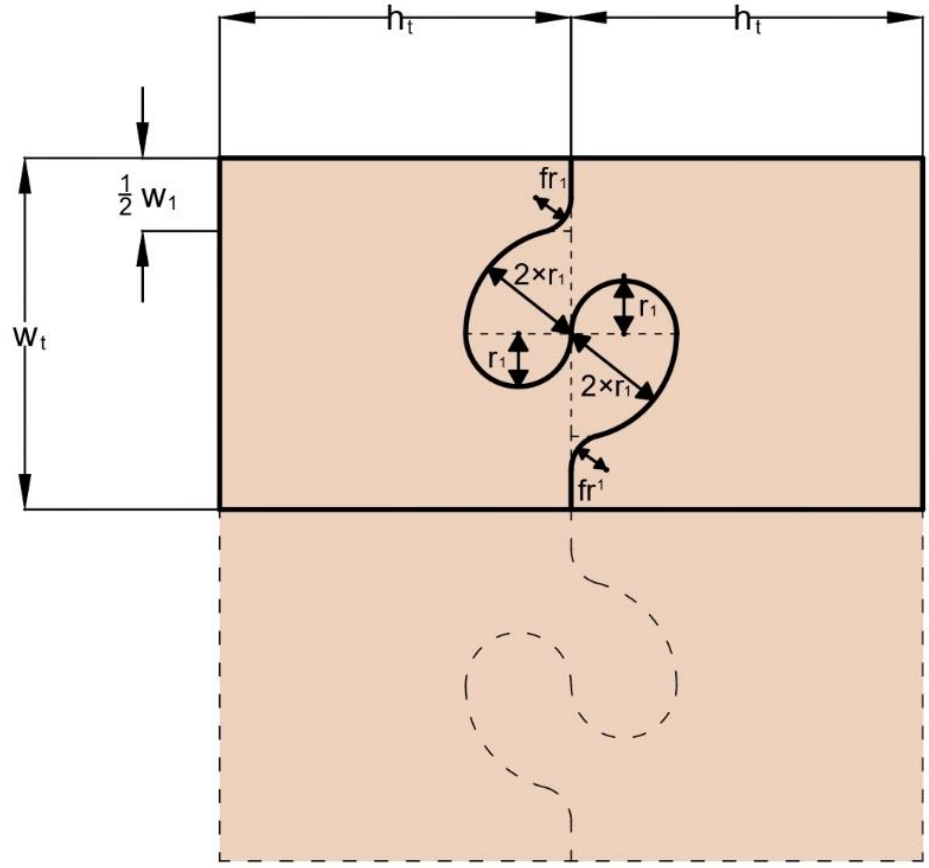

Yin Yang parameters
Total width w_t [mm]
Width between YY w_1 [mm]
Total height h_t [mm]
Radius r_1 [mm]
Fillet radius f_{r1} [mm]

Figure 23: Yin Yang geometric parameters

The thickness of the floor plate (18 mm) is significantly smaller than its length (5100 mm) and width (1200 mm). Moreover, the stresses in the thickness direction (S33) are negligible which is proven by comparing the axial stresses from a 3D solid homogeneous dovetail model of which the results are presented in Figure 24. Stress S33 is about 100 times smaller than S22. Therefore, the variation study can be performed by modelling 2D planar shell elements [44] which leads to a reduction in computation time.

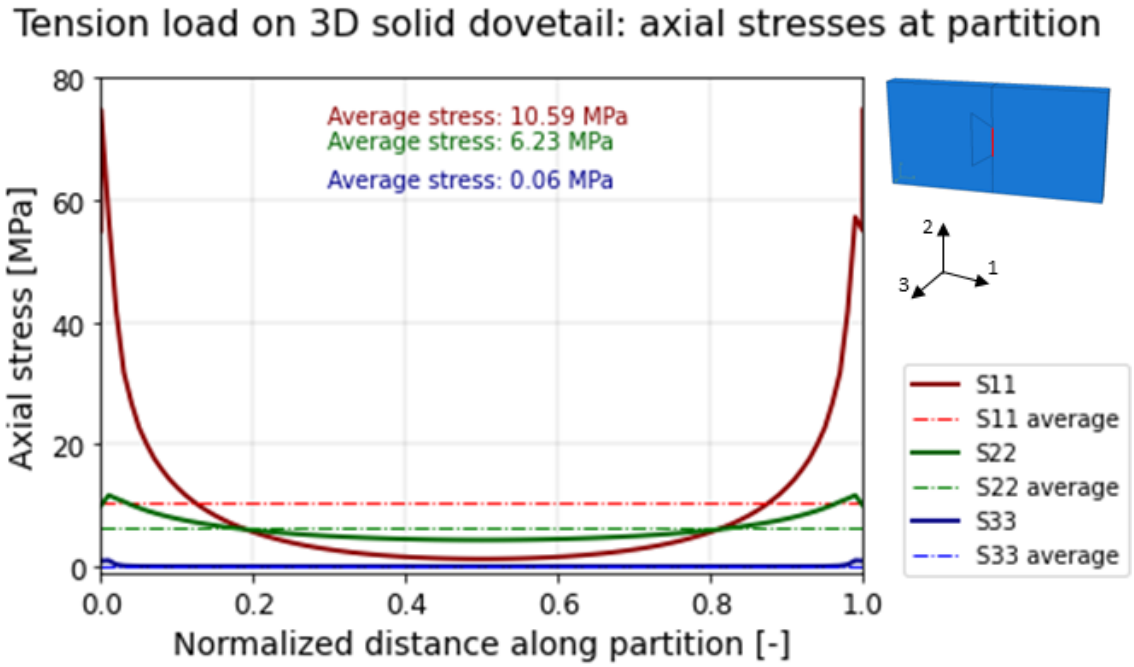

Figure 24: Comparison of axial stresses at red-marked partition of 3D solid dovetail model loaded in tension parallel to the grain

4.2 Boundary conditions

Single connections are modelled to simulate the loading transferred by a whole floor element. The variation study focuses on a tension load case and a shear load case. The compression load case is not included in the variation study because the whole contact area can be used to transfer the compression forces. Therefore, compression loads are not critical for the interlocking timber connections. Stresses due to compression loads were tremendously smaller then stresses due to tension or shear loads. This could be concluded from a preliminary study where some first designs were analysed. The loading conditions are illustrated in Figure 25, where the tension load case is presented on the left and the shear load case on the right. The main direction of the grain is aligned with axis 1. The dovetail is used as an example geometry, but the loading conditions remain the same for all different shapes.

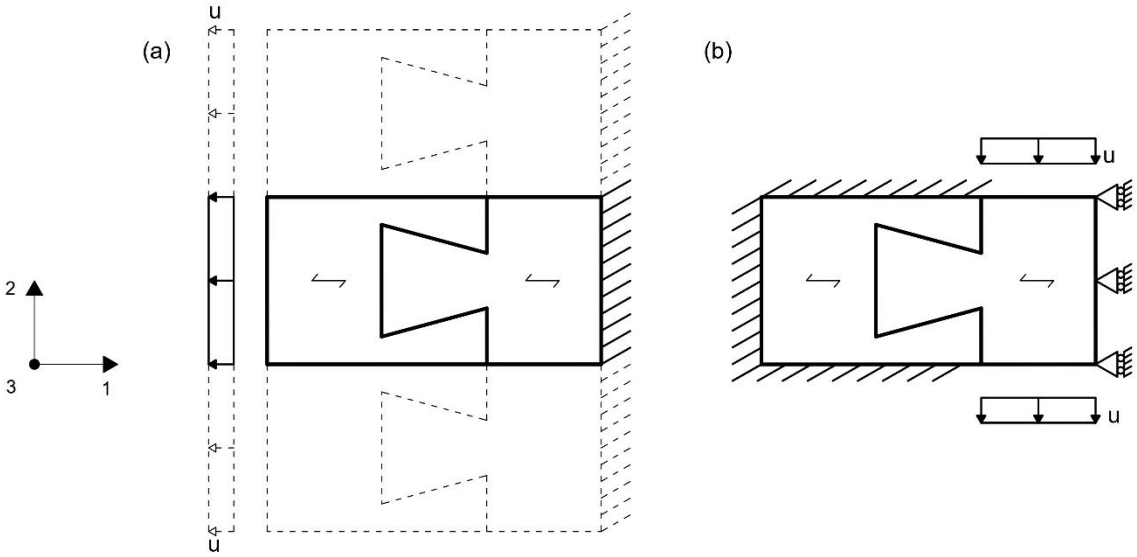

Figure 25: Boundary conditions of the (a) tension load case and (b) shear load case on a dovetail joint

Pure tension

The connection loaded in tension parallel to the grain is fixed (U1 = U2 = UR3 = 0) at the right edge. The tension load is applied at the left edge. Displacement-controlled loading conditions are used to prevent bending at the load application. Both the translational and rotational degrees of freedom of the nodes are associated to each other and therefore the constituent elements do not deform [44]. Y-symmetry axes (U2 = UR1 = UR3 = 0) are applied at the top and bottom edges (dashed illustration). By applying these constraints, the stiffness of the much larger floor plate is mimicked when simulating a single connection. Additionally, the loading pattern is comparable to when surrounded by other connections in the floor.

A compression load case can be easily created by using the same boundary conditions but reversing the direction of the load.

Pure shear

The connection loaded in shear is fixed (U1 = U2 = UR3 = 0) at all outer edges of the left component. The displacement-controlled shear load is applied at the top and bottom edge of the right component. An additional roller (U1 = 0) is applied at the right edge of the right component to prevent rotation of the right component.

4.3 Material properties

The material of the interlocking timber connections is spruce plywood with a total thickness of 18 mm which consists of 7 equally thick laminations stacked in a 0°-90°-0°-90°-0°-90°-0° sequence. Because of this ply lay-up the material can be assumed to be quite homogeneous. Therefore, the plywood is modelled as a solid homogeneous orthotropic material using equivalent material properties (Eq. 12).

$$\begin{Bmatrix} \varepsilon_{11} \\ \varepsilon_{22} \\ \varepsilon_{33} \\ \gamma_{12} \\ \gamma_{13} \\ \gamma_{23} \end{Bmatrix} = \begin{bmatrix} 1/E_1 & -\nu_{21}/E_2 & -\nu_{31}/E_3 & 0 & 0 & 0 \\ -\nu_{12}/E_1 & 1/E_2 & -\nu_{32}/E_3 & 0 & 0 & 0 \\ -\nu_{13}/E_1 & -\nu_{23}/E_2 & 1/E_3 & 0 & 0 & 0 \\ 0 & 0 & 0 & 1/G_{12} & 0 & 0 \\ 0 & 0 & 0 & 0 & 1/G_{13} & 0 \\ 0 & 0 & 0 & 0 & 0 & 1/G_{23} \end{bmatrix} \begin{Bmatrix} \sigma_{11} \\ \sigma_{22} \\ \sigma_{33} \\ \sigma_{12} \\ \sigma_{13} \\ \sigma_{23} \end{Bmatrix} \tag{12}$$

The density, Young's modulus and shear modulus of the equivalent plate material were retrieved from the Handbook of Finnish Plywood [37]. Since the equivalent Poisson's ratios were unknown they were determined according to the classical lamination theory [45]. The Poisson's ratios of spruce timber in the three planes were used to calculate the equivalent Poisson's ratios (Eq. 13-15).

$$\nu_{12} = \frac{\nu_{LT} E_T T}{E_T T_a + E_L T_b} \tag{13}$$

$$\nu_{23} = \nu_{TR} \frac{T_a}{T} + \nu_{LR} \frac{T_b}{T} \tag{14}$$

$$\nu_{13} = \nu_{LR} \frac{T_a}{T} + \nu_{TR} \frac{T_b}{T} \tag{15}$$

Both the material properties of spruce timber used for the classical lamination theory calculation and the equivalent material properties of the plywood are presented in Table 2.

Table 2: Material properties

Material properties of spruce			
Young's modulus	E_L	11000*	N/mm^2
	E_T	370*	N/mm^2
	E_R	370*	N/mm^2
Poisson's ratio	ν_{LT}	0.530*	-
	ν_{TR}	0.019*	-
	ν_{LR}	0.420*	-
Equivalent material properties of spruce plywood			
Density	ρ	460**	kg/m^3
Young's modulus	E_1	6682**	N/mm^2
	E_2	5318**	N/mm^2
	E_3	5318**	N/mm^2
Shear modulus	G_{12}	350**	N/mm^2
	G_{13}	52**	N/mm^2
	G_{23}	38**	N/mm^2
Poisson's ratio	ν_{12}	0.040***	-
	ν_{23}	0.191***	-
	ν_{13}	0.248***	-

* Principles of Wood Science and Technology: I. Solid Wood [46]
** Handbook of Finnish Plywood [37]
*** Derived by classical lamination theory [45]

4.4 Convergence study

Sharp corners are present in the model for some interlocking joint geometries. At these sharp corners, stresses tend to go to infinity independent of the mesh fineness which is caused by a stress singularity [47]. The degree of rounding of these corners varies for different connection designs by using different fillet radius or arc-like shapes. The stresses at these rounded corners do not tend to infinity anymore however very high peak stresses still occur [47]. There are two options to converge the mesh, namely through an h-refinement or a p-refinement study. The h-refinement discretizes the problem domain into smaller elements whereas the p-refinement uses higher-degree shape functions to achieve better accuracy [48]. An h-refinement study was done on a dovetail with fillet radius of 10 mm, considering mesh sizes of 2 mm to 0.05 mm. As illustrated in Figure 26, the maximum axial stress does not converge by using smaller mesh elements. However, the mesh selected for the numerical analyses is sufficiently fine to accurately describe the overall response of the structure in accordance with the following specifications.

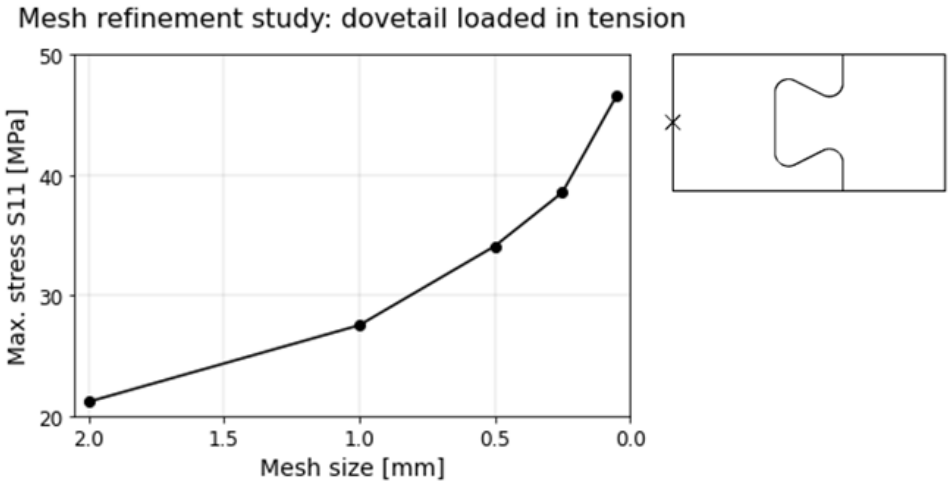

Figure 26: Mesh refinement study of a dovetail with fillet radius of 10 mm loaded in tension

For the variation study, first-order triangular mesh elements are used. The size of the mesh elements is chosen to be 5 times smaller than the smallest dimension occurring in the models, which is a fillet radius of 5 mm. Thus, the mesh size at the critical locations is assumed to be 1 mm. Lower mesh densities were used further away from the contacting edges and partitions to reduce computation time.

5 Parametric connection scripts

Python is one of the most popular and accessible programming languages nowadays and it is the standard programming language for Abaqus [44], [49]–[51]. Therefore, the codes for this research were written in Python. Two types of scripts were created: an input script and a post-processing script. The input script is run in Abaqus to perform the LEFEA and afterwards the results are analysed using the post-processing script. A flow chart is presented in Figure 27. The codes are added in Appendix C-G.

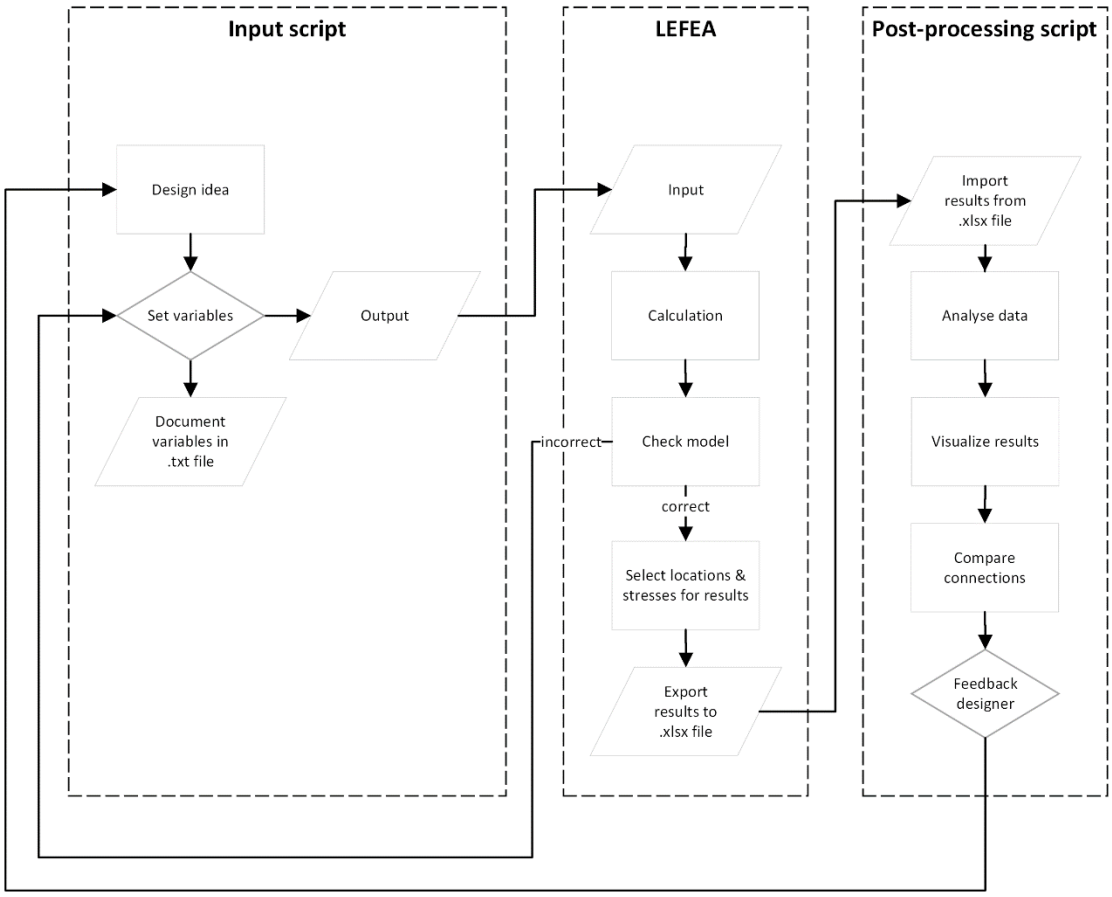

Figure 27: Parametric script flow chart

5.1 Input script

The input script is a parametric script which creates a Finite Element Model in Abaqus using object-oriented programming (OOP). OOP is an efficient way to build code in a modular way [52]. The code is structured and broken down into smaller manageable parts. Which makes it easier to understand, reuse, update or change the code. An input script is created for each connection shape and consists of four sections. Each connection shape has its own script, however the blueprint of each script is the same.

Import libraries

First, the math library and the Abaqus libraries are imported to use the functions from Abaqus.

Functions and methods

The second section consists of the functions and methods. Except for the class named 'definitions', the classes refer to the Abaqus modules: part, property, assembly, step, interaction, load, mesh and job. The methods are constructed the same way as one would build a model in the Abaqus interface. Most classes consist of a constructor and multiple functions. The values for the attributes corresponding to that class are defined after which they can be used in the functions of that class. For example, the class named 'Part' uses the values that are set for the dimensions of the connection. These are used in the functions to create the coordinates to create a part. After that, fillets and partitions can be created on that part.

Variables

The third section is where the parametric aspect comes into play. The variables are defined in this section which includes the dimensions, material properties, applied loads and mesh refinement of the interlocking timber connection. The definitions of the connection dimension are illustrated in Figures 21-23.

The equivalent linear elastic material properties for plywood are defined by specifying the engineering constants due to the orthotropic material characteristics. The corresponding parameters are:

- Density
- Young's modulus parallel to the grain, perpendicular to the grain and normal to the grain
- Poisson's ratio in the xy, xz and yz plane
- Shear modulus in the xy, xz and yz plane

In the load section, the maximum stresses present in the floor seam needs to be inserted. An assumption must be made on how many connections per meter will be applied. The applied loads on the connection are then defined using this information:

- Maximum tension stress
- Maximum compression stress
- Maximum shear stress

Mesh refinement is performed at certain locations in the design including:

- Local mesh size at partitions
- Local mesh size along the contacting surfaces
- Local mesh size at the side ends
- Global mesh size
- Global mesh shape

Function and method invocation

The order-dependent functions and methods are executed in the last section to create the Abaqus model. The variables from code section 3 are implemented in the functions and methods from code section 2. Instances are created for each class where their attribute values are specified using the constructor call. After that, functions are called to create the Abaqus model using these attributes.

5.2 LEFEA

When running the input script in Abaqus, the model is automatically generated and calculations are initiated. It is important to check if the model was created correctly. Maximum and minimum stresses and displacements can be obtained by running the field output script, which is added in Appendix F. Results at specific locations need to be obtain manually by following these steps:

- Create mesh node paths from the sets that are defined in the input script
- Create xy-data for these paths by selecting the y-coordinates to be plotted on the x-axis and the desired stresses on the y-axis
- Save xy-data to an Excel file

Ideally, the results at specific locations such as partitions were also obtained from the field output. However, the error kept occurring that the node set did not contain any nodes, node labels or coordinates. Therefore, the process had to be broken down into three steps namely the input script, manually running the model in the Abaqus interface and the post-processing script. When this error is fixed it would be possible to run all calculations in sequence from the command prompt, resulting in an even more time efficient process.

5.3 Post-processing script

A post-processing script is created for quick and neat data analytics and visualization. An example of the post-processing script is added in Appendix G.

Import libraries

Again, first the libraries are imported. The libraries needed to process the results are:

- Pandas is used to read data from .xlsx files
- Numpy is used for numerical computations like operations on arrays
- Matplotlib is used to visualize the results

Import & clean data

The results from the calculations in Abaqus are obtained by reading the Excel files. The data is stored in columns where each first column is the y-coordinate of the integration point from the mesh and each second column is the corresponding stress. The rows follow the order of the mesh sequence IDs, however the numbering of the mesh sequence does not logically follow the geometry. For example, on a section line the mesh sequence IDs from begin to end are: 11, 12, 13, 5, 14, 15, 9, 20. The code sorts the data according to the location of the result so that the stress distribution over the section line can be visualized in an xy-plot.

Analyse data

Stress patterns at section lines are created and average stresses are computed through iterations on the data. The maximum and average stresses are assessed to the failure criteria defined in section 4.5 ‘Failure criteria’.

6 Variation study

The most important conclusions of the variation study are discussed in this chapter. The complete results of the variation study are added in Appendix H, including peak stresses and deformations. Drawings of each connection design including the geometric parameters are added in Appendix I. The strength of the interlocking timber connections when loaded in tension and when loaded in shear is analysed by the numerical model which was presented in chapter '4. Numerical model' using the parametric script which was discussed in chapter '5. Parametric scripts'. Different designs are made for the three main connection shapes: dovetail, arrow and yin yang. For each variation study, one parameter is varied while all other parameters remain constant to determine the influence of each parameter.

The designs are criticized to the failure criteria stated in section '2.4 Failure criteria'. All designs are first assessed with failure criterium 1. The strength of the connection according to failure criteria 1 is presented as the maximum or minimum relative stress, which is obtained by dividing the peak stress by the design strength (Eq. 6-8). The best connections from each study are assessed with failure criterium 2. The strength of the connection according to failure criteria 2 is presented as the average relative stress, which is obtained by dividing the average stress by the design strength (Eq. 9-11). $S11^{+}$, $S22^{+}$ and $S12^{+}$ are the tension stress parallel, tension stress perpendicular and positive shear stress respectively. $S11^{-}$, $S22^{-}$ and $S12^{-}$ are the compression stress parallel, compression stress perpendicular and negative shear stress respectively. In addition, the stress distribution along the critical section is analysed. The material orientation and direction of the load application were illustrated in Figure 25 in section 4.2.

The variable and static parameters of each variation study are presented in Table 3. The drawings of the connections with geometric parameters can be found Figures 21-23 in section 4.1. Seven variation studies are performed on the dovetail shaped connection. The dovetail head width w_1 is dependent on the dovetail neck width w_2, since the dovetail shape is mirrored around its x-axis and y-axis when used in the floor seam. Four variation studies are performed on the arrow shaped connection. It is assumed that the arrow connections are mirrored along the x-axis when placed in the floor seam. Three variation studies are performed on the yin yang shaped connection. The yin yang is mirrored along its x-axis to create a symmetric shape. The width between the yin yangs (w_1) is dependent on the radius of the yin yangs (r_1), where a bigger radius results in a smaller width.

Table 3: Overview variation studies

Dovetail study	Variable parameter	Static parameters		
1	w_1: 95 - 55 mm w_2: 5 - 45 mm	h_1: 50 mm		fr_1: 5 mm
2	h_1: 20 - 190 mm	w_1: 60 mm w_2: 40 mm		fr_1: 5 mm
3	h_1: 20 - 190 mm	w_1: 80 mm w_2: 20 mm		fr_1: 5 mm
4	h_1: 40 - 190 mm	w_1: 80 mm w_2: 20 mm		fr_1: 10 mm
5	h_1: 50 - 190 mm	w_1: 80 mm w_2: 20 mm		fr_1: 15 mm
6	h_1: 40 - 190 mm	w_1: 60 mm w_2: 40 mm		fr_1: 10 mm
7	h_1: 40 - 180 mm	w_1: 60 mm w_2: 40 mm		fr_1: 15 mm
Arrow study	**Variable parameter**	**Static parameters**		
1	fr_3: 5 – 13 mm	h_1: 80 mm h_2: 30 mm	w_1: 90 mm w_2: 20 mm	fr_1: 5 mm fr_2: 5 mm fr_4: 5 mm
2	w_2: 20 - 50 mm	h_1: 80 mm h_2: 30 mm	w_1: 90 mm	fr_1: 5 mm fr_2: 5 mm fr_3: 5 mm fr_4: 5 mm
3	fr_1: 6 - 24 mm	h_1: 80 mm h_2: 30 mm	w_1: 90 mm w_2: 50 mm	fr_2: 5 mm fr_3: 5 mm fr_4: 5 mm
4	h_2: 15 - 50 mm	h_1: 90 mm	w_1: 90 mm w_2: 20 mm	fr_1: 5 mm fr_2: 5 mm fr_3: 5 mm fr_4: 5 mm
Yin Yang study	**Variable parameter**	**Static parameters**		
1	r_1: 10 – 18 mm w_1: 60 – 28 mm	fr_1: 5 mm		
2	fr_1: 5 – 10 mm	r_1: 18 mm w_1: 28 mm		
3	fr_1: 5 – 26 mm	r_1: 15 mm w_1: 40 mm		

6.1 Tension load application

Dovetail studies

The width w_2, height h_1 and fillet radius fr_1 were varied to create different dovetail configurations. The angle of the dovetail changes between 48-87° when either the width or the height is varied. Increasing the width w_2 results in a small reduction of peak stresses. As can be seen in Figure 28, the stress S11 spreads out over the width w_2 and a larger part of the dovetail is utilized. Moreover, stress S12 spreads out over the sloped dovetail sides which results in lower peak stresses due to the change of angle.

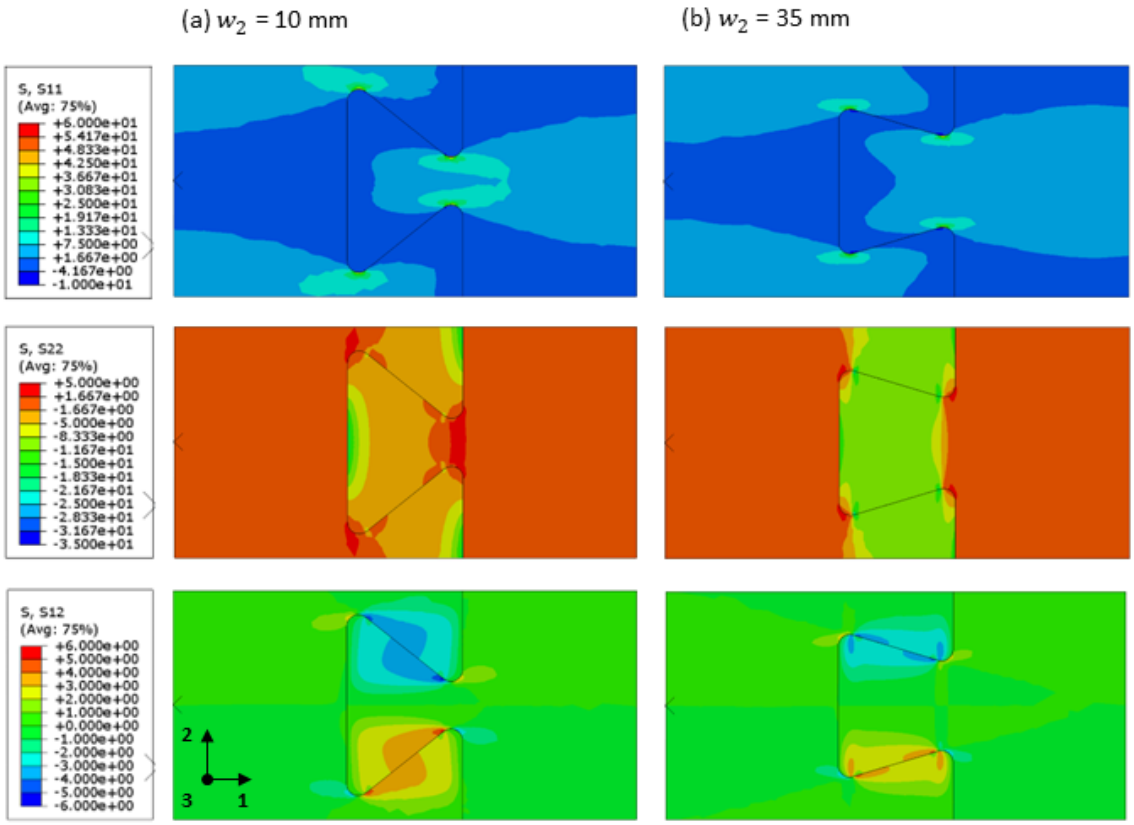

Figure 28: Stress distribution dovetail loaded in tension
(a) Dovetail study 1: h_1 = 50 mm, w_1 = 90 mm, w_2 = 10 mm, fr_1 = 5 mm
(b) Dovetail study 1: h_1 = 50 mm, w_1 = 65 mm, w_2 = 35 mm, fr_1 = 5 mm

Increasing the height h_1 significantly reduces the peak stresses and has the most influence compared to the other geometric parameters. This can also be seen in the stress distribution plots in Figure 29. The dovetail with a large height has much lower peak stresses than the dovetail with a small height. The peak stresses occur at the corners near the sloped sides. The stresses need to concentrate in a small area when a small height is applied. When h_1 is larger, the stresses can spread over the pressure contact area. The height parameter h_1 can be increased more per meter floor seam length than the width parameter w_2. For a 100 mm section of the floor seam length, the largest possible w_2 is 45 mm. However, h_1 can be increased further if the project of application allows a wider seam width. A maximum h_1 of 190 mm is now assumed, which is larger than the 100 mm section length. Thus, there is more space for strength improvement in the height direction than in the width direction.

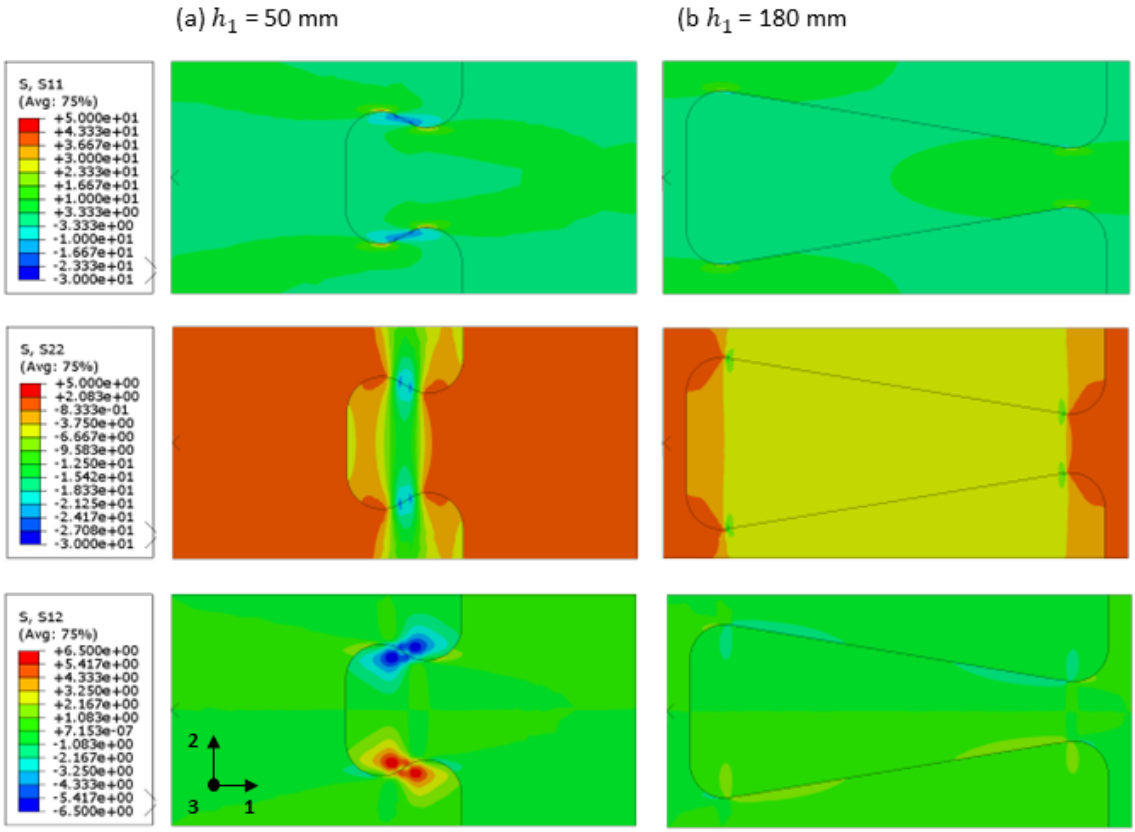

Figure 29: Stress distribution dovetail loaded in tension
(a) Dovetail study 5: h_1 = 50 mm, w_1 = 80 mm, w_2 = 20 mm, fr_1 = 15 mm
(b) Dovetail study 5: h_1 = 180 mm, w_1 = 80 mm, w_2 = 20 mm, fr_1 = 15 mm

Figure 30 illustrates the maximum relative stresses of the dovetails from study 3 where the height h_1 is varied between 20-190 mm. The static width w_2 is 20 mm and the fillet radius fr_1 is 5 mm. The maximum relative tension stress parallel is dominant for all dovetail in this study. A large reduction of this dominant peak stress is observed when increasing h_1. The difference between the governing stress and the other stresses is substantial. It can also be seen that the maximum and minimum relative shear stresses are equal for all dovetails. This is due to the fact that the geometry, load and boundary conditions are symmetric.

Most studies had a governing tension stress parallel. A few dovetail studies had a governing compression stress perpendicular. There is not a clear reason for this. All dovetails with a governing compression stress perpendicular had an angle > 75 degrees. However, a clear distinction could not be made as some dovetails with an angle > 75 degrees have a governing tension stress parallel.

Studies (4 & 5) that combine larger fillet radii fr_1 with w_2 of 20 mm perform better than studies (6 & 7) that combine larger fillet radii with a larger w_2 of 40 mm. A possible reason for this is that the dovetail can easily slide out if the angle is large and the corners are rounder. Studies 6 and 7 had larger displacements U1 (±0.5 mm) than studies 4 and 6 (±2 mm). Thus, rounding of the corners in the design leads to lower peak stresses, however sliding out of the interlocking shape should be prevented.

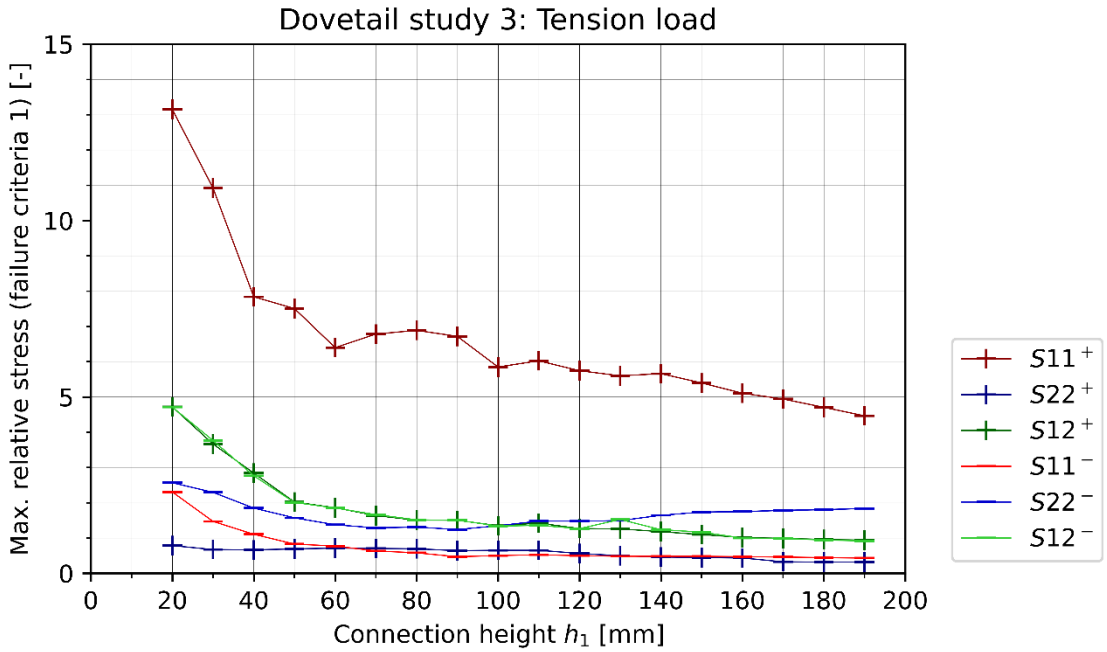

Figure 30: Dovetail study 3: maximum relative stresses (tension load)

The best performing dovetails are found in study 4 and 5. These studies both vary the height h_1 and have a static w_2 of 20 mm. Study 4 has a fillet radius of 10 mm whereas study 5 has a fillet radius of 15 mm. In both studies, tension stress parallel is dominant. The best dovetail from study 4 has a h_1 of 190 mm, angle of 81° and maximum relative tension stress parallel of 3.88. The best dovetail from study 5 has a h_1 of 180 mm, angle of 80.5° and maximum relative tension stress parallel of 3.87. The length of the smallest section at the dovetail's neck (illustrated in Figure 31 with dashed line) is 23.4 mm and 25.4 mm for the dovetail from study 4 and 5 respectively. The critical displacements U1 of these dovetails are 0.52 and 0.53 mm respectively. The displacement U1 varied between 0.45 and 3.21 mm for all dovetails.

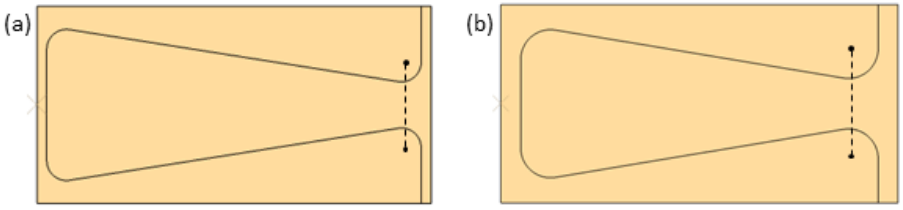

Figure 31: Most optimal dovetails loaded in tension
(a) Dovetail study 4: h_1 = 190 mm, w_1 = 80 mm, w_2 = 20 mm, fr_1 = 10 mm
(b) Dovetail study 5: h_1 = 180 mm, w_1 = 80 mm, w_2 = 20 mm, fr_1 = 15 mm

The tension load is transferred from one dovetail component to the other dovetail component by contact pressure. This means that the stresses must be transferred through the sloped sides of the dovetail connection. It was noticed that when the length of this sloped side was larger, which is the case when h_1 is larger, the peak stresses reduce since they can spread over the distance of the sloped sides. This can be seen in Figure 39a where the principal stresses are plotted for the most optimal dovetail from study 5. The minimal in-plane principal stresses spread out over the contact area (marked with a black circle). When h_1 increases, the angle of the sloped sides increases as well. In addition, the direction of the minimal in-plane principal stresses is more aligned with the perpendicular direction of the plywood. The compression strength of the applied plywood is the weakest in the perpendicular direction. It is also observed that the stress path of the dovetail is making less turns than the arrow and yin yang.

In all dovetail studies, peak stresses occurred locally at the corners in the designs. Figure 32 illustrates the relative tension stress parallel (S11) along the critical section of the two best dovetails (studies 4 and 5) on the left side. Here, it is visible that the peak stress is located in a small area around the corners which is roughly 20% of the partition length. All stresses along the critical section exceed failure criteria 1 as the relative stresses are all above 1.0. The difference between the peak stress and average stress is relatively small compared to some other dovetail designs. The peak stress is 2.49 and 2.78 times larger than the average stress respectively.

The dovetails from study 2 and 3 with a h_1 of 20 mm have much larger peak stresses which are situated in 10% of the dovetail partition length, see Figure 32. Moreover, the stresses of 80% of the critical section suffice failure criteria 1. However, this 80% of the dovetail section is not utilized a lot as the stresses are close to zero for a large part. While the peak stresses are located in a smaller area than studies 4 and 5, it is unlikely that a peak stress which is 12 times above the design strength can be redistributed along other fibres. It is expected that the dovetails from studies 4 and 5 in Figure 32 perform better even if a small redistribution of stresses takes place.

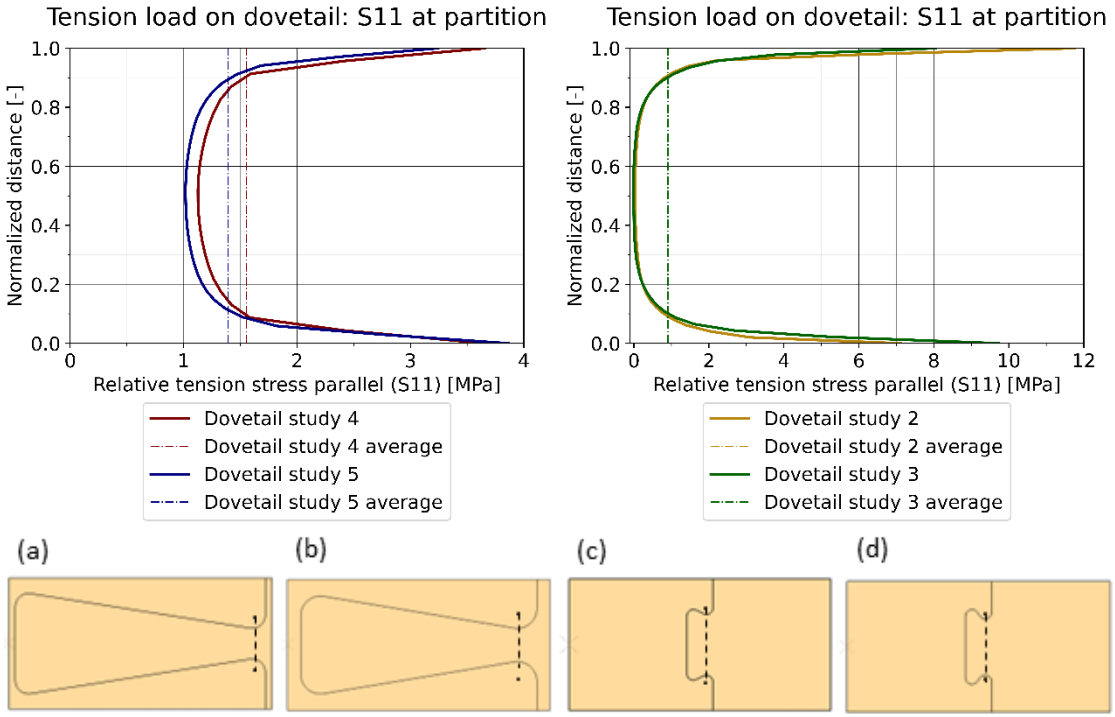

Figure 32: Stress distribution of dovetail along their critical section (tension load)
(a) Dovetail study 4: h_1 = 190 mm, w_1 = 80 mm, w_2 = 20 mm, fr_1 = 10 mm
(b) Dovetail study 5: h_1 = 180 mm, w_1 = 80 mm, w_2 = 20 mm, fr_1 = 15 mm
(c) Dovetail study 2: h_1 = 20 mm, w_1 = 60 mm, w_2 = 40 mm, fr_1 = 5 mm
(d) Dovetail study 3: h_1 = 20 mm, w_1 = 80 mm, w_2 = 20 mm, fr_1 = 5 mm

Arrow studies

The height h_2, width w_2 and fillet radii fr_1 and fr_3 were varied to create different arrow configurations. The dominant peak stress is mostly located at fr_3. Increasing fr_3 leads to a reduction of the peak stress and the location of the peak stress moves to fr_2 when fr_3 > 11 mm, see Figure 33. At this stage, there is not enough space left in the design to apply a larger fr_2 to further decrease the peak stress. Varying w_2 and fr_1 does not significantly influence the peak stresses. A larger h_2 results in a decrease of the peak stress as well.

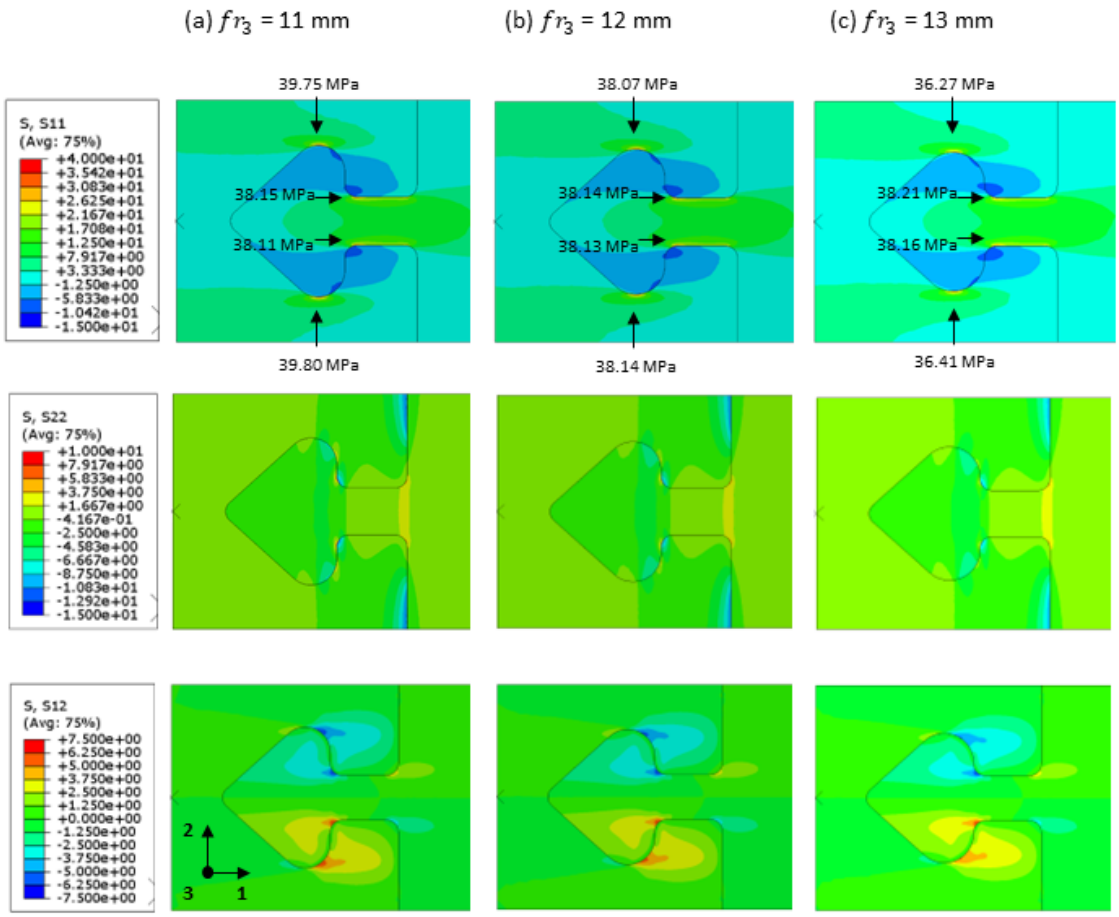

Figure 33: Stress distribution arrow loaded in tension

(a) Arrow study 1: h_1 = 80 mm, h_2 = 30 mm, w_1 = 90 mm, w_2 = 20 mm, $fr_{1,2,4}$ = 5 mm, fr_3 = 11 mm

(b) Arrow study 1: h_1 = 80 mm, h_2 = 30 mm, w_1 = 90 mm, w_2 = 20 mm, $fr_{1,2,4}$ = 5 mm, fr_3 = 12 mm

(c) Arrow study 1: h_1 = 80 mm, h_2 = 30 mm, w_1 = 90 mm, w_2 = 20 mm, $fr_{1,2,4}$ = 5 mm, fr_3 = 13 mm

In all cases, the maximum relative tension stress parallel was the dominant stress by far. It can be concluded that the arrow is not the most optimal shape for tension. When optimizing one geometric parameter, not enough space is left to optimize another parameter. There are a lot of corners in the design at which peak stresses initiate, however not all corners can be rounded enough to decrease these peaks.

The maximum relative stresses of arrow study 1, where fr_3 is varied, are presented in Figure 34. Both tension stress parallel and perpendicular decrease when increasing fr_3. Though the maximum tension stress parallel is the governing stress by far. The maximum relative shear stress is equal to the minimum relative shear stress for all arrow designs due to the symmetric geometry, load and boundary conditions.

Figure 34: Arrow study 1: maximum relative stresses (tension load)

The best performing arrow was found in study 3 and has a height h_1 of 80 mm and h_2 of 30 mm, width w_1 of 90 mm and w_2 of 20 mm and fillet radius fr_1, fr_2 and fr_4 of 5 mm and fillet radius fr_3 of 12 mm (Figure 35). The maximum relative tension stress parallel is 5.09 for this arrow, which is 32% higher than the best performing dovetail. A smaller height is used for this arrow compared to the best performing dovetails. However, when a connection with a small height is needed it is still better to apply a dovetail shape. A dovetail from study 5 with h_1 of 80 mm has a maximum relative tension stress of 4.64 and thus performs better on failure criteria 1 than the most optimal arrow with the same height. The critical displacement U1 of this arrow is 0.42 mm. The displacement U1 varied between 0.42 and 0.67 mm for all arrows.

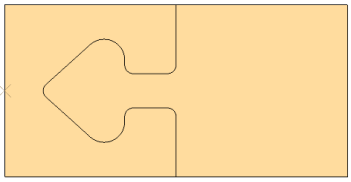

Figure 35: Most optimal arrow loaded in tension
Arrow study 3: h_1 = 80 mm, h_2 = 30 mm, w_1 = 90 mm, w_2 = 20 mm, $fr_{1,2,4}$ = 5 mm, fr_3 = 12 mm

The principal stress plot of the most optimal arrow can be found in Figure 39b. Contact pressure is exerted on the bottom flanges of the arrow (marked by the black circle). The stress path is making a double U-turn to go from one component to the other. Moreover, the pressure contact areas are a lot smaller than the dovetail. However, the pressure is directed parallel to the grain which is the strongest direction of the plywood. This could explain the relatively small difference in maximum relative stress between the best dovetail and the best arrow, despite the substantial difference in pressure contact area.

Yin yang studies

It should be noted that the yin yang is mirrored to create a symmetric design. Therefore, the total width w_t is double which means that the total applied load is double as well. The radius r_1 and fillet radius fr_1 were varied to create different yin yang configurations. Increasing r_1 significantly reduces the critical peak stress, which is straightforward since the interlocking area increases when increasing r_1, see Figure 36. Increasing the fillet radius fr_1 results in a slight decrease of critical peak stress. The peak stresses initiate at the fillet radii, rounder corners reduce these peaks by a more gradual inflow of forces. In all cases, tension stress parallel was the dominant stress by far. The yin yang shape is not ideal for tension loads. The shapes of the yin yangs are prone to bending and sliding out of the interlocking position.

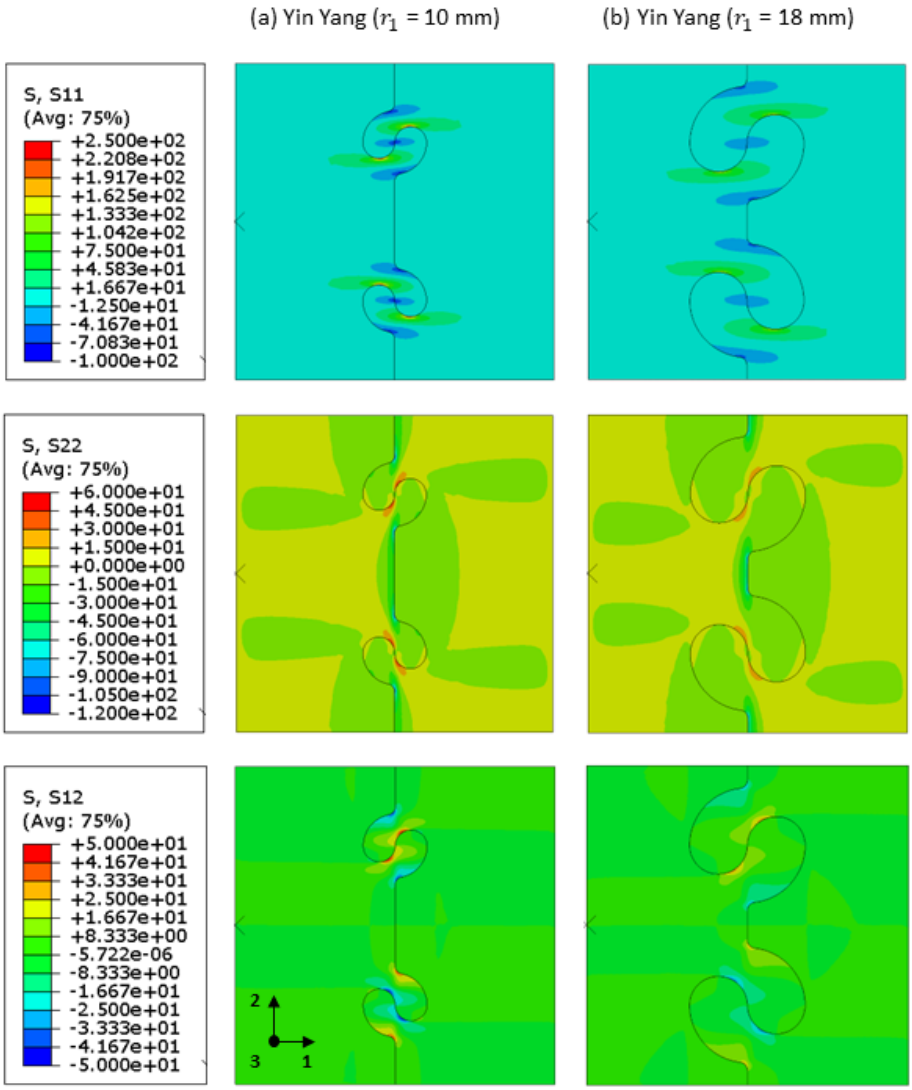

Figure 36: Stress distribution yin yang loaded in tension
(a) Yin yang study 1: r_1 = 10 mm, w_1 = 60 mm, fr_1 = 5 mm
(b) Yin yang study 1: r_1 = 18 mm, w_1 = 28 mm, fr_1 = 5 mm

The maximum relative stresses of yin yang study 3, where fr_1 is varied, are presented in Figure 37. A decrease of the stresses is observed for increasing fr_1. The maximum relative tension stress parallel is the governing stress by far. The maximum relative shear stress is equal to the minimum relative shear stress due to the symmetric geometry, load and boundary conditions.

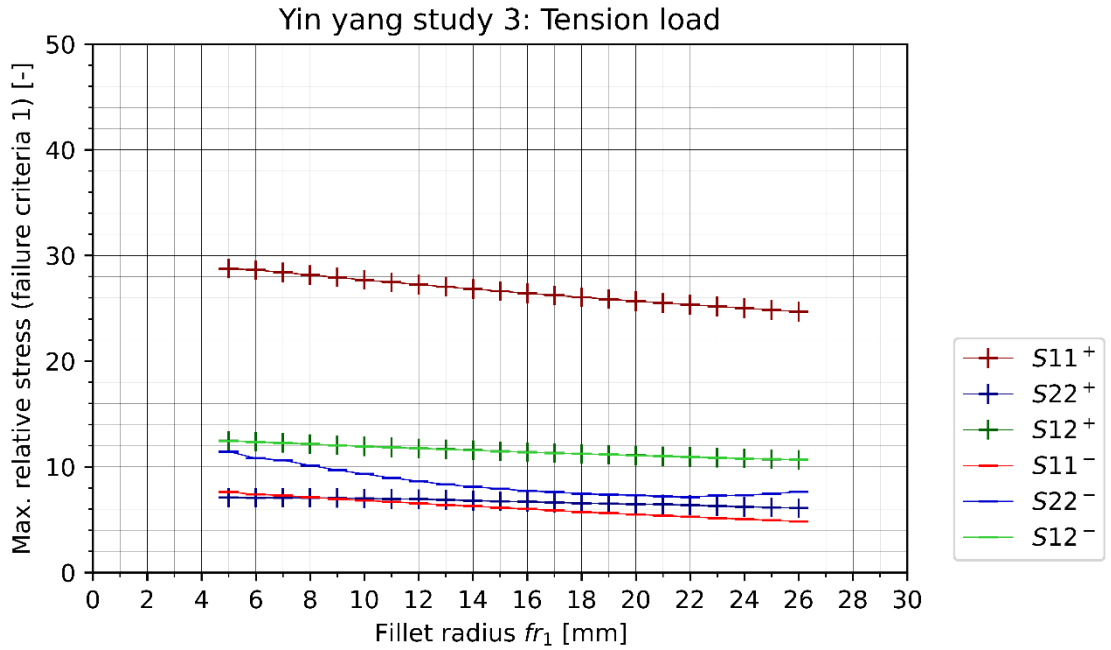

Figure 37: Yin yang study 3: maximum relative stresses (tension load)

The best performing yin yang loaded in tension is found in study 2 and has a fr_1 of 10 mm, r_1 of 15 mm and w_1 of 40 mm, see Figure 38. The maximum relative tension stress parallel is 21.75 for this yin yang, which is 462% higher than the best performing dovetail and 327% higher than the best performing arrow. The critical displacement U1 of this yin yang is 4.38 mm. The displacement U1 varied between 3.79 and 4.69 mm for all yin yangs. Hence, the yin yang shape performs drastically worse than the dovetail and arrow shape. The principal stress plot in Figure 39c shows that the pressure contact area is extremely small (marked by the black circle). The black dashed line illustrated the mirror axes to make the yin yang a symmetric connection design. Therefore, only the top or the bottom pressure contact area should be considered when comparing the pressure contact area of the yin yang to the other shapes. Moreover, the stress path needs to make a double U-turn to go from one component to the other component. These stresses need to squeeze together to fit in the small yin yang shapes and then squeeze even tighter to go through the pressure contact zone. The yin yang shape loaded in tension is prone to sliding and bending. The direction of the pressure is parallel to the grain which is the strongest direction of the plywood. However, the earlier mentioned aspects have a bigger influence on the tension strength of the yin yang.

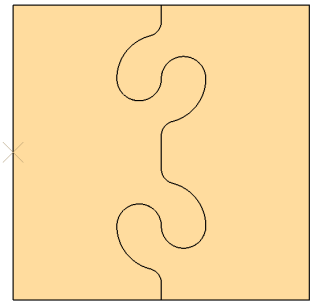

Figure 38: Most optimal yin yang loaded in tension
Yin yang study 2: r_1 = 15 mm, w_1 = 40 mm, fr_1 = 10 mm

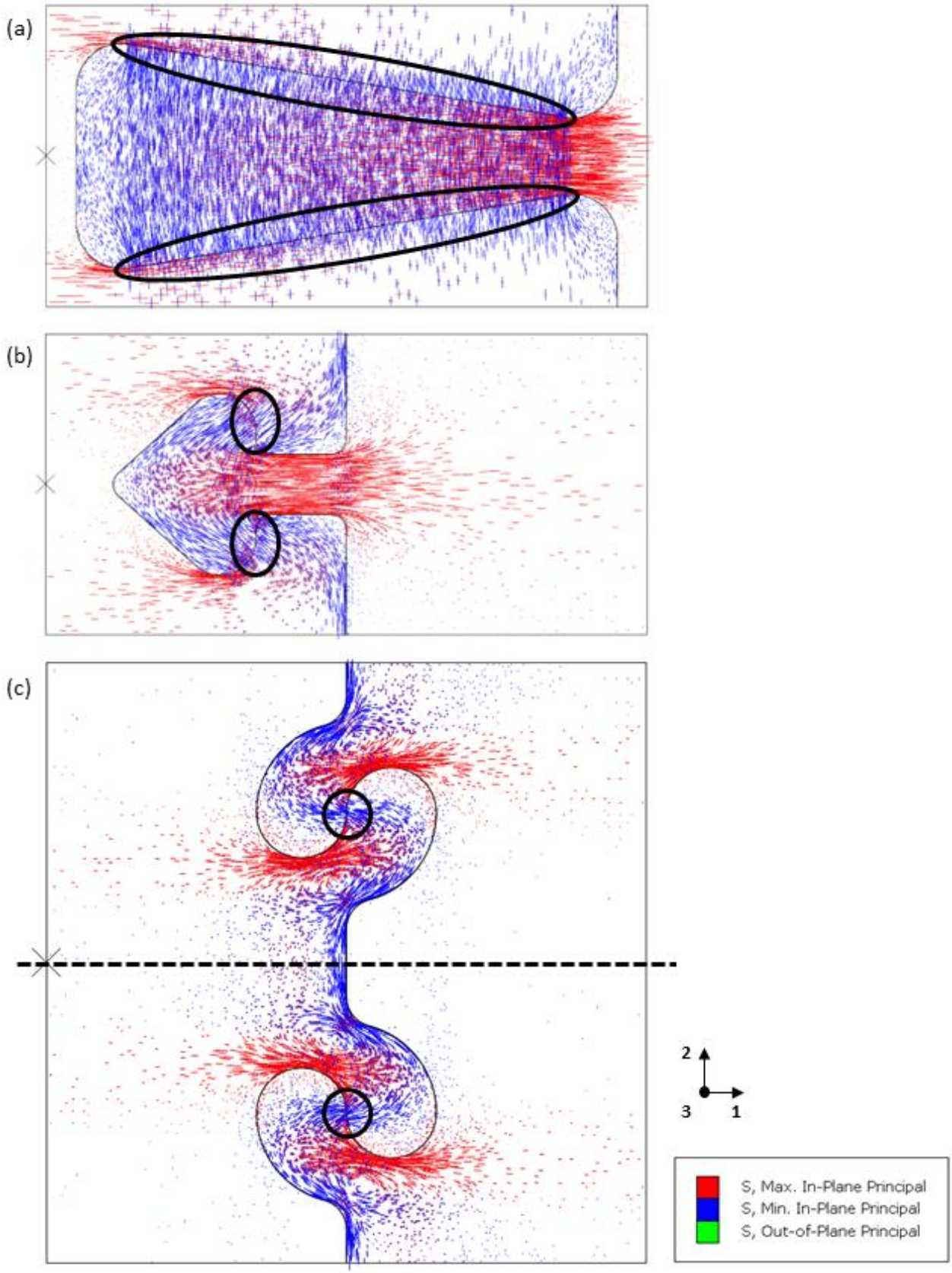

Figure 39: Principal stresses of the strongest (a) dovetail, (b) arrow and (c) yin yang loaded in tension

6.2 Shear load application

Dovetail

The width w_2, height h_1 and fillet radius fr_1 were varied to create different dovetail configurations. Increasing w_2 results in a decrease of the critical peak stress as can be seen in Figure 40. The stress distribution plot in Figure 41 shows that the shear stresses spread over the dovetail's neck width which results in lower peak stresses. Moreover, both S11 and S22 peak stresses are smaller for the dovetail with a larger w_2. A possible explanation for this reduction of peak stresses is that the angle of the sloped sides of the dovetail are more in favour. Consequently, a larger area is usable for pressure contact.

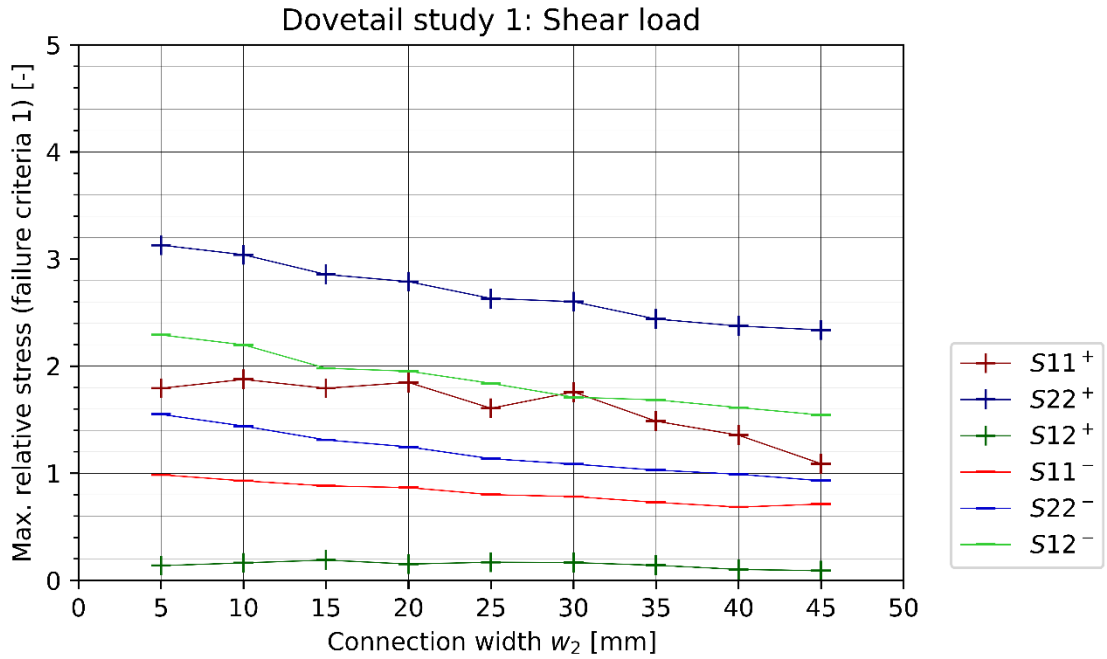

Figure 40: Dovetail study 1: maximum relative stresses (shear load)

Increasing fr_1 leads to the largest decrease of the critical peak stress. This was observed when comparing studies 2, 6, and 7 which have a constant w_2 of 40 mm and a constant fr_1 of 5, 10 and 15 mm respectively. The maximum relative tension stress perpendicular was smaller in the studies with larger fillet radii. This was also observed in studies 3, 4, and 5 which have a constant w_2 of 20 mm and a constant fr_1 of 5, 10 and 15 mm respectively. It should be noted that the length of the critical section increases a bit when the fillet radius increases. Therefore, the reduction of the maximum relative tension stress perpendicular could be caused by a combination of an increase in the width and an increase in the roundness of the corners.

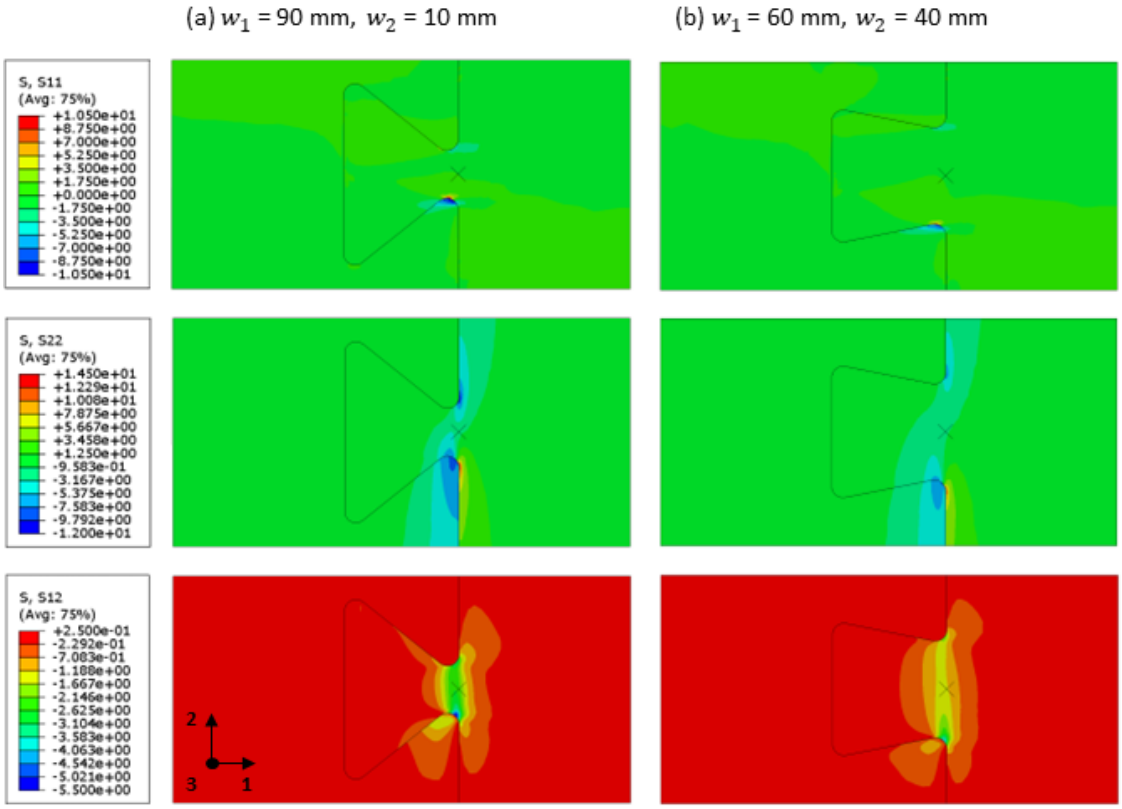

Figure 41: Stress distribution dovetail loaded in shear

(a) Dovetail study 1: h_1 = 50 mm, w_1 = 90 mm, w_2 = 10 mm, fr_1 = 5 mm

(b) Dovetail study 1: h_1 = 50 mm, w_1 = 60 mm, w_2 = 40 mm, fr_1 =15 mm

Varying the height h_1 does not have a large influence since the shear stresses are mainly present at the dovetail neck and do not spread to the dovetail head when applying a larger height, see Figure 42. Though the shear stresses and perpendicular axial stresses are able to spread more after the contact pressure area.

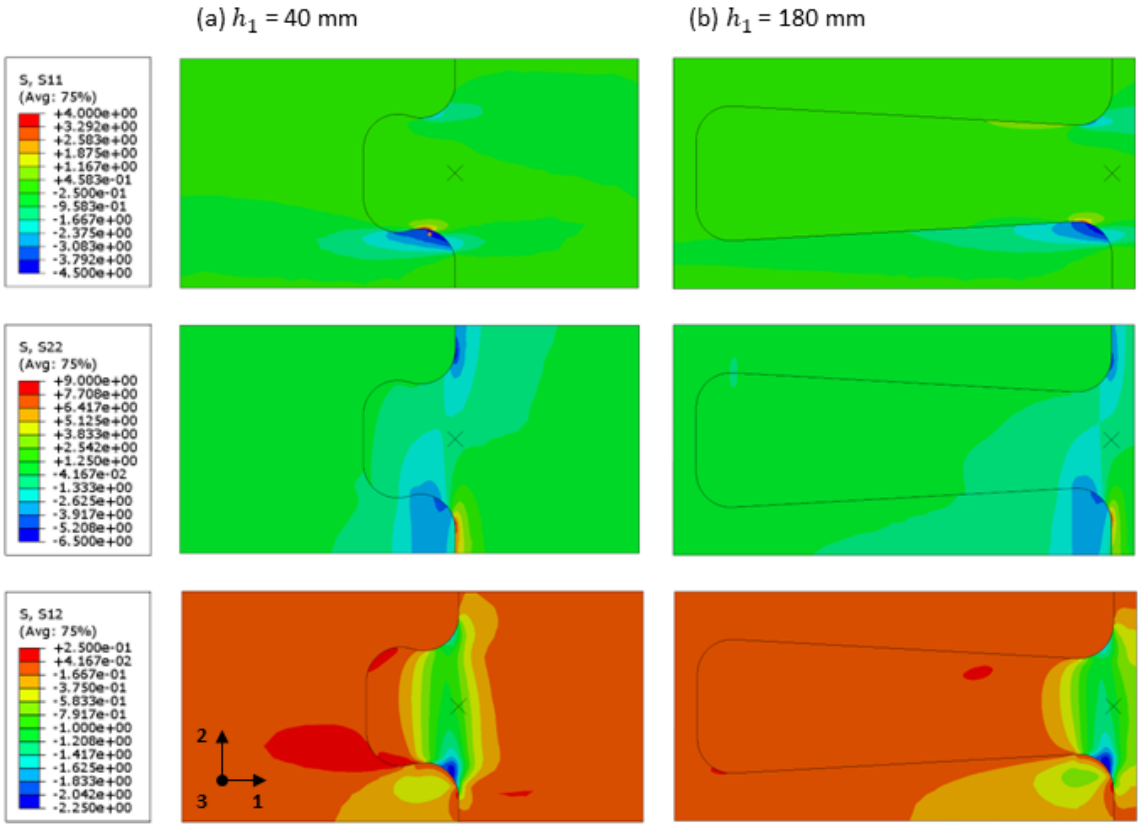

Figure 42: Stress distribution dovetail loaded in shear
(a) Dovetail study 5: h_1 = 50 mm, w_1 = 80 mm, w_2 = 20 mm, fr_1 = 15 mm
(b) Dovetail study 5: h_1 = 180 mm, w_1 = 80 mm, w_2 = 20 mm, fr_1 =15 mm

The dovetail which performs the best when loaded in shear has a h_1 of 190 mm, w_1 of 80 mm, w_2 of 20 mm and fr_1 of 15 mm (study 5). The maximum relative tension stress perpendicular has a value of 1.40. Two dovetails reached a close second place with a value of 1.48. These dovetails have dimensions h_1 of 190 mm, w_1 of 60 mm, w_2 of 40 mm and fr_1 of 10 mm (study 6) or h_1 of 180 mm, w_1 of 60 mm, w_2 of 40 mm and fr_1 of 15 mm (study 7). See Figure 43 for drawings of the most optimal dovetails loaded in shear. The critical displacements U2 of these dovetails are 0.12, 0.09 and 0.10 mm respectively. The displacement U2 varied between 0.08 and 0.13 mm for all dovetails. The most optimal dovetails have a large height although this was not a parameter with a large influence on the shear strength. They performed slightly better than other dovetails with smaller heights.

Figure 43: Most optimal dovetails loaded in shear
(a) Dovetail study 5: h_1 = 190 mm, w_1 = 80 mm, w_2 = 20 mm, fr_1 = 15 mm
(b) Dovetail study 6: h_1 = 190 mm, w_1 = 60 mm, w_2 = 40 mm, fr_1 =10 mm
(c) Dovetail study 7: h_1 = 180 mm, w_1 = 60 mm, w_2 = 40 mm, fr_1 =15 mm

Pressure contact is exerted on the bottom fillet of the dovetail neck (marked by the black circle), see the principal stress plot in Figure 53a. After which the stresses spread out over the other dovetail component. The direction of the contact pressure varies between the parallel and perpendicular fibre direction.

The best performing dovetails loaded in shear from each study are analysed using failure criteria 2. The relative shear stresses along the critical section are illustrated in Figure 44, where the average relative stresses are illustrated by the dashed lines. All dovetails exhibit roughly the same stress pattern over the normalized section length. The peak stress is located at the bottom end of the section line (near normalized distance of 0). The middle of the section line has the lowest shear stresses and at the top end of the section line (near normalized distance of 1) is a secondary peak stress. The average relative stress of all dovetails in Figure 44 suffice failure criteria 2.

Studies 1-3 have the smallest fillet radius of 5 mm. Their peak shear stresses are roughly equal, and these studies have the largest peak shear stress compared to the other studies. Their average stresses are 2.47, 2.10 and 2.34 times smaller than their peak stresses respectively. The difference between the peak stress and average stress becomes smaller when the fillet radius is larger. Study 4 and 6 have a fillet radius of 10 mm. Their peak stress is 1.86 and 1.67 times larger than the average stress respectively. Whereas study 5 and 7 with a fillet radius of 15 mm have a peak stress that is 1.33 and 1.52 times larger than their average stress. The average values approximately correlate to the length of the critical section.

The most optimal dovetail in shear according to failure criteria 2 is the dovetail from study 7 with h_1 = 180 mm, w_1 = 60 mm, w_2 = 40 mm and fr_1 = 15 mm. The average relative shear stress is 0.53. The most optimal dovetail in shear according to failure criteria 1 is the dovetail from study 5 which has the highest average relative shear stress of 0.78. However, the difference between its peak and average stress is the smallest. The resulting most optimal dovetail in shear analysed by criteria 1 or 2 is thus different. From the analysis using failure criteria 1 it was clear that the tension stress perpendicular was the governing stress. Failure criteria 2 is not applied on tension stresses, therefore the shear stress was analysed with this criterium instead. It is expected that the connections will fail from the perpendicular tension stresses and thus have a brittle failure mechanism. Therefore, the previously mentioned dovetail from study 5 is assumed to be to most optimal dovetail in shear.

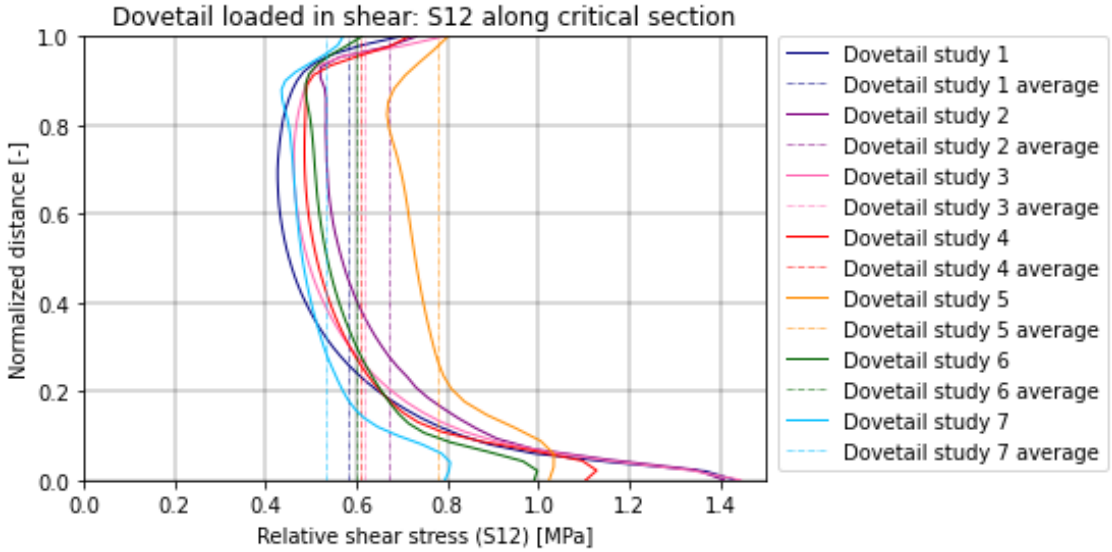

Figure 44: Shear stress (S12) distribution along the critical section of dovetails loaded in shear
(a) Dovetail study 1: h_1 = 50 mm, w_1 = 55 mm, w_2 = 45 mm, fr_1 = 5 mm
(b) Dovetail study 2: h_1 = 190 mm, w_1 = 60 mm, w_2 = 40 mm, fr_1 = 5 mm
(c) Dovetail study 3: h_1 = 20 mm, w_1 = 80 mm, w_2 = 20 mm, fr_1 = 5 mm
(d) Dovetail study 4: h_1 = 40 mm, w_1 = 80 mm, w_2 = 20 mm, fr_1 = 10 mm
(e) Dovetail study 5: h_1 = 190 mm, w_1 = 80 mm, w_2 = 20 mm, fr_1 = 15 mm
(f) Dovetail study 6: h_1 = 190 mm, w_1 = 60 mm, w_2 = 40 mm, fr_1 = 10 mm
(g) Dovetail study 7: h_1 = 180 mm, w_1 = 60 mm, w_2 = 40 mm, fr_1 = 15 mm

Arrow

Height h_2, width w_2 and fillet radii fr_1 and fr_3 were varied to create different arrow configurations. The critical peak stress is located at fr_1. Figure 45 shows that increasing fr_1 between 6-20 mm results in a reduction of the critical peak stress, while increasing fr_1 between 21-26 mm results in an increment of the critical peak stress. A possible reason for this could be that the peak stresses at fr_1 reduces for rounder corners, however when the corners are too round the connection becomes prone to sliding. The stress distribution plot in Figure 46 shows that all peak stresses are lower when a larger fillet radius is applied. Moreover, the area of the peak spreads over a larger area when a larger fillet radius is applied. The stress distribution plots of the arrows in Figure 46 look very similar to the stress distribution plots of the dovetails in Figures 41-42.

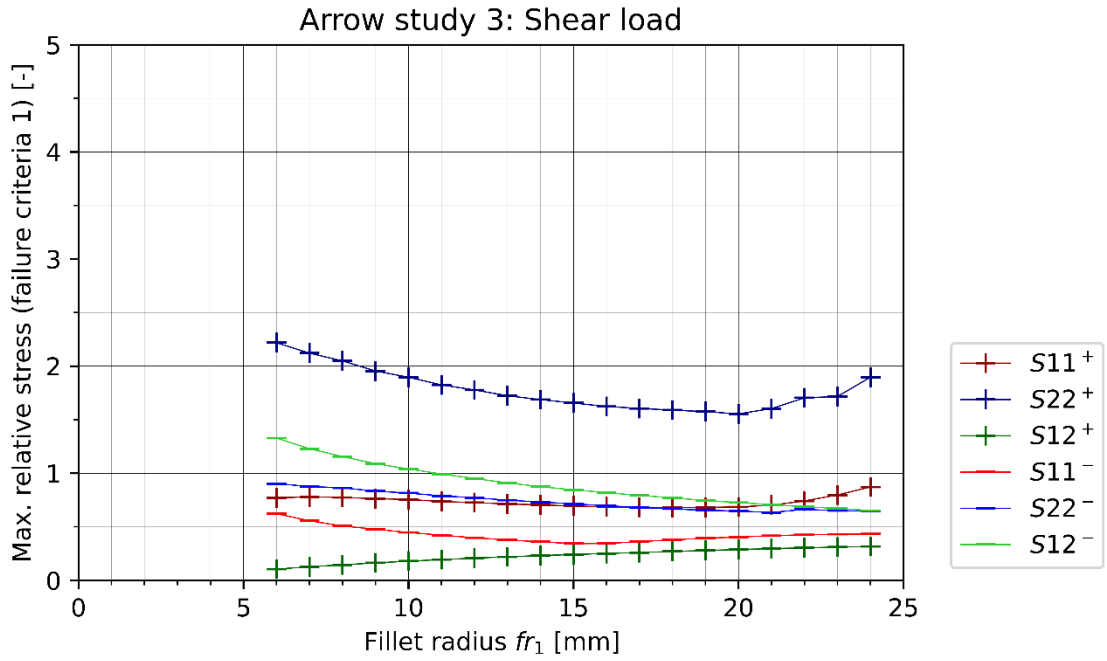

Figure 45: Arrow study 3: maximum relative stresses (shear load)

Increasing w_2 leads to a decrease of the critical peak stresses as well since the stresses are able to spread over the width. Increasing $w_2$and fr_1 both contribute to a larger critical section length. Therefore, the reduction of the maximum relative tension stress perpendicular could be caused by a combination of an increase in the width and an increase in the roundness of the corners as was observed in the dovetail studies as well.

Varying h_2 or fr_3 has no significant influence on the peak stress. Similar to the dovetail studies, the peak stress area does not spread over the height of the connection. Besides, the peak stress is not located at fr_3.

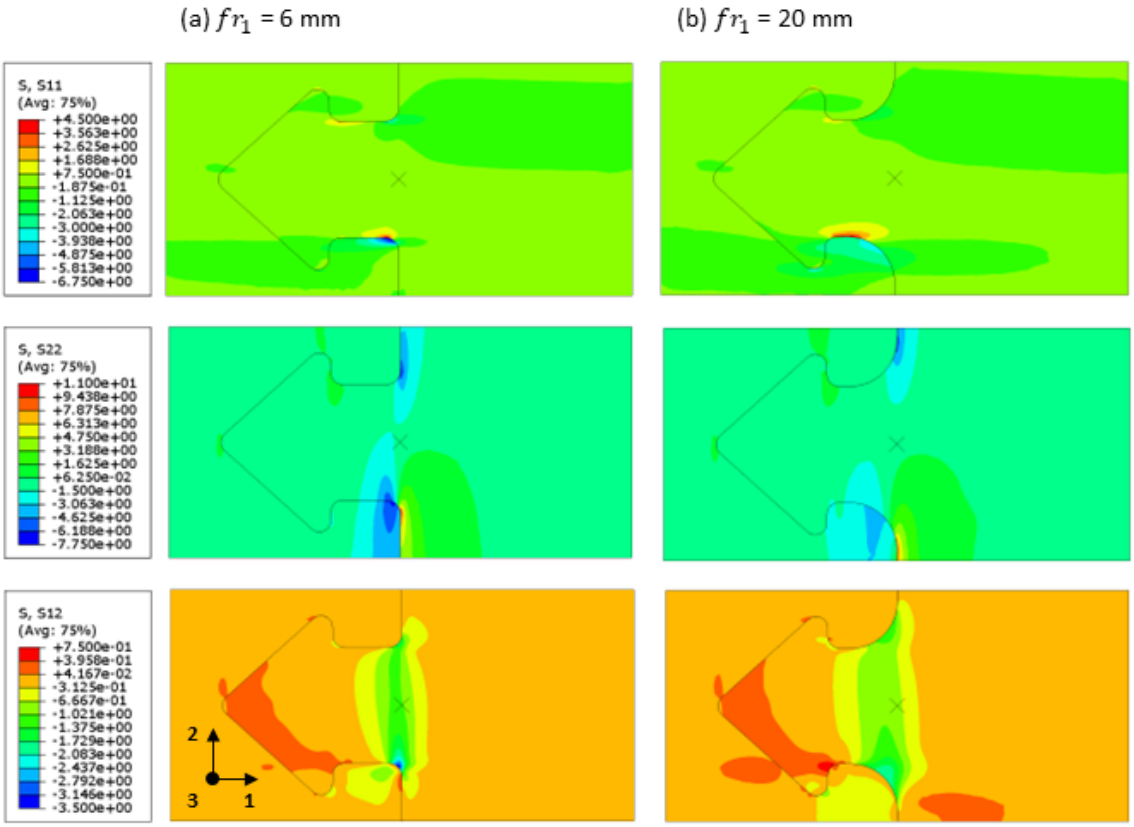

Figure 46: Stress distribution arrow loaded in shear
(a) Arrow study 3: h_1 = 80 mm, h_2 = 30 mm, w_1 = 90 mm, w_2 = 50 mm, fr_1 = 6 mm, $fr_{2,3,4}$ = 5 mm
(b) Arrow study 3: h_1 = 80 mm, h_2 = 30 mm, w_1 = 90 mm, w_2 = 50 mm, fr_1 = 20 mm, $fr_{2,3,4}$ = 5 mm

The best performing arrow is found in study 3 and has a height h_1 of 80 mm and h_2 of 30 mm, width w_1 of 90 mm and w_2 50 mm, fillet radius fr_1 of 20 mm and fillet radius fr_2, fr_3 and fr_4 of 5 mm (Figure 47). The maximum relative tension stress perpendicular has a value of 1.55, which is 11% higher than the best performing dovetail. The difference between an arrow and dovetail is minimal when comparing to the most optimal dovetail with a $h_1 \leq 80$ mm. The best performing dovetail that suffices this criterium has a h_1 of 50 mm (study 7) and maximum relative tension stress perpendicular of 1.57, i.e. 1% higher than the most optimal arrow. The critical displacement U2 of this arrow is 0.10 mm. The displacement U2 varied between 0.09 and 0.15 mm for all arrows.

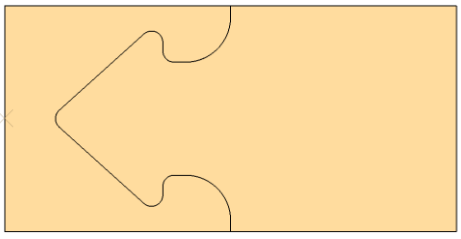

Figure 47: Most optimal arrow loaded in shear
Arrow study 3: h_1 = 80 mm, h_2 = 30 mm, w_1 = 90 mm, w_2 = 50 mm, fr_1 = 20 mm, $fr_{2,3,4}$ = 5 mm

Pressure contact is primarily exerted on the bottom part of the arrow near the bottom h_2 and fr_1 (marked by the large black circle), see the principal stress plot in Figure 53b. The direction of the primary contact pressure varies between the parallel and perpendicular fibre direction. Secondary pressure contact areas are observed near the bottom of the arrow flanges and above fr_4 (marked by the small black circles). The direction of the secondary contact pressure is in the vicinity of the parallel fibre direction. The area where the primary contact pressure spreads is smaller compared to the dovetail.

The best performing arrows loaded in shear from each study are analysed using failure criteria 2. The relative shear stresses along the critical section are illustrated in Figure 48, where the average relative stresses are illustrated by the dashed lines. The shear stress pattern is quite similar for the different arrows and comparable to the shear stress patterns of the dovetails in shear. The peak shear stress is located near the bottom end of the critical section (near normalized distance of 0), a secondary peak shear stress is located at the top end of the critical section (near normalized distance of 1) and the stresses decrease in between these ends.

The difference between the peak shear stress and the average shear stress is the largest for the arrow from study 2. Its peak stress is 2.45 times larger than its average stress. The other studies have a difference between 1.64 and 1.68 times the average stress. The average values approximately correlate to the length of the critical section, i.e. a larger section has a lower average shear stress. The peak shear stress reduces when increasing fr_1. Therefore, the large difference between the peak and average stress for the arrow in study 2 can be explained by the combination of a large width (w_2 of 50 mm) and small fillet radius (fr_1 of 5 mm).

The arrows from study 2 and 3 in Figure 48 suffice failure criteria 2 and the arrows from study 1 and 4 exceed failure criteria 2 with an average relative shear stress of 1.23. The most optimal arrow loaded in shear according to failure criteria 1 and 2 is identical; namely the arrow from study 3 which has a h_1 of 80 mm, h_2 of 30 mm, w_1 of 90 mm, w_2 of 50 mm, $fr_1$of 20 mm and $fr_{2,3,4}$ of 5 mm. The average relative shear stress of the most optimal dovetail is 23% higher than the most optimal arrow according to failure criteria 2. However, it is expected that the tension stress perpendicular will be the critical stress and therefore failure criteria 1 should be used for assessing the arrow's shear strength capacity.

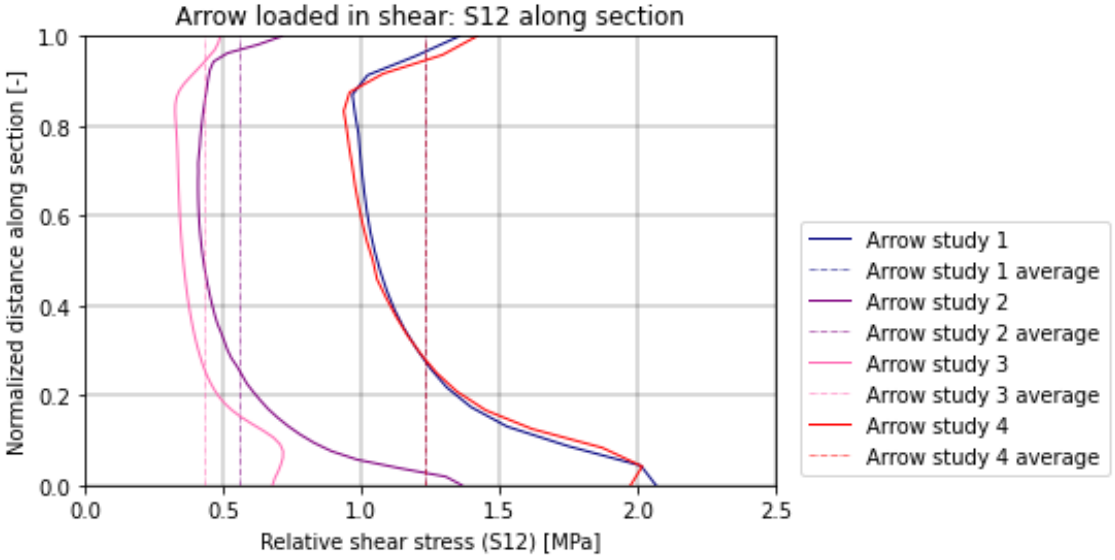

Figure 48: Shear stress (S12) distribution along the critical section of arrows loaded in shear
(a) Arrow study 3: h_1 = 80 mm, h_2 = 30 mm, w_1 = 90 mm, w_2 = 20 mm, $fr_{1,2,3,4}$ = 5 mm
(b) Arrow study 3: h_1 = 80 mm, h_2 = 30 mm, w_1 = 90 mm, w_2 = 50 mm, $fr_{1,2,3,4}$ = 5 mm
(c) Arrow study 3: h_1 = 80 mm, h_2 = 30 mm, w_1 = 90 mm, w_2 = 50 mm, fr_1 = 20 mm, $fr_{2,3,4}$ = 5 mm
(d) Arrow study 3: h_1 = 90 mm, h_2 = 50 mm, w_1 = 90 mm, w_2 = 20 mm, $fr_{1,2,3,4}$ = 5 mm

Yin yang

The radius r_1 and fillet radius fr_1 were varied to create different yin yang configurations. Increasing r_1 results in higher peak stresses. This seems illogical since a larger r_1 means a larger interlocking shape, however it was observed that the maximum relative tension stress perpendicular is located beneath the bottom yin yang, see Figure 49. The peak stress can spread over half of the width w_1, which dimension decreases when increasing r_1. Hence why the peak stress increases when increasing r_1.

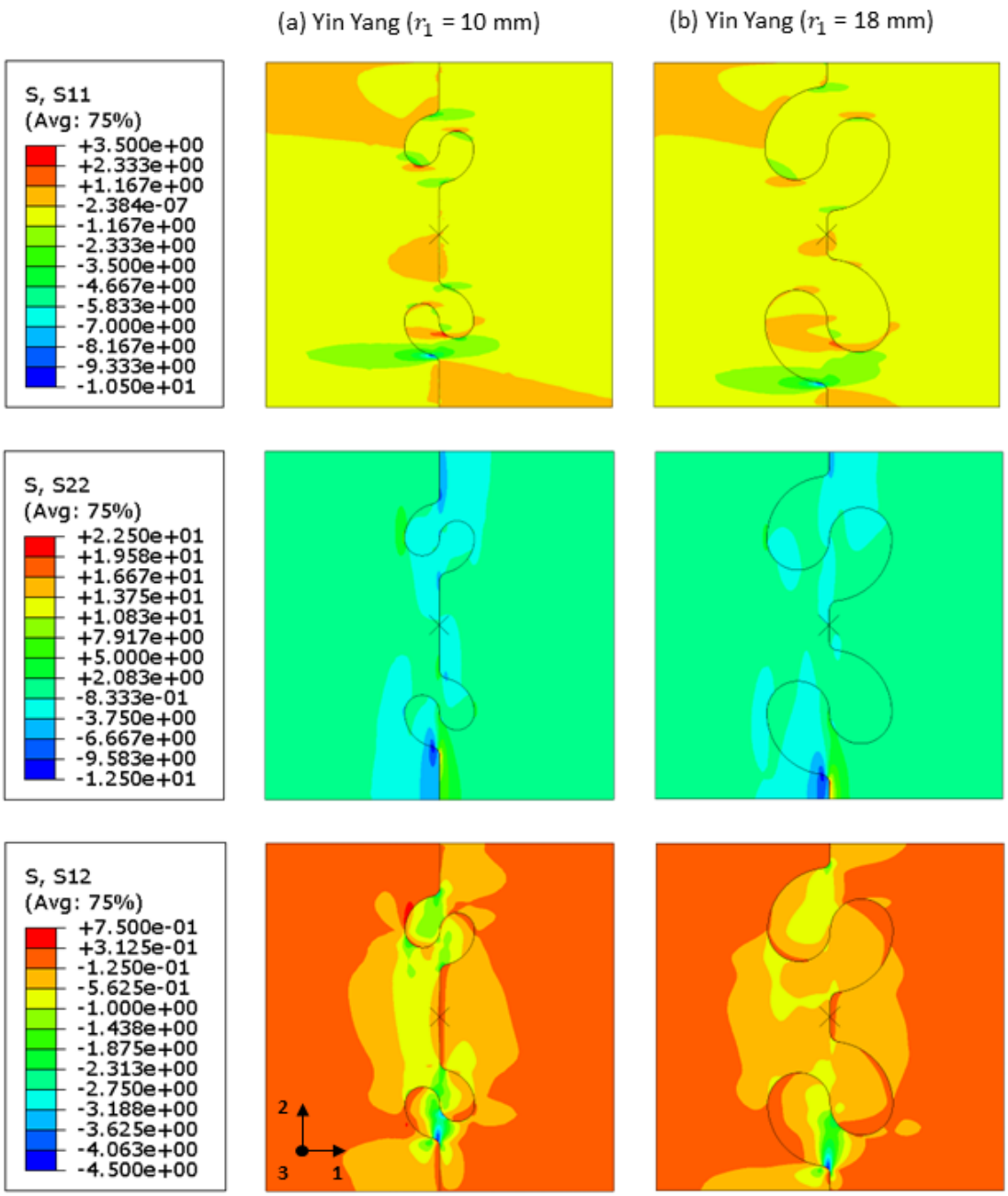

Figure 49: Stress distribution yin yang loaded in shear

(a) Yin yang study 1: r_1 = 10 mm, w_1 = 60 mm, fr_1 = 5 mm

(b) Yin yang study 1: r_1 = 18 mm, w_1 = 28 mm, fr_1 = 5 mm

The maximum tension stress perpendicular is the critical stress in all yin yang studies. The difference between the critical stress and the other stresses is substantial, therefore brittle tension failure is expected. A decrease of the critical stress is observed for fr_1 5 mm to 20 mm and an increase is observed for fr_1 20 mm to 26 mm, see Figure 50. The yin yang with a fr_1 of 20 mm performs the best and has a maximum relative tension stress perpendicular of 2.77. The maximum relative compression stress parallel makes jumps when varying fr_1. A possible reason is that the peak stress location shifts for different fr_1.

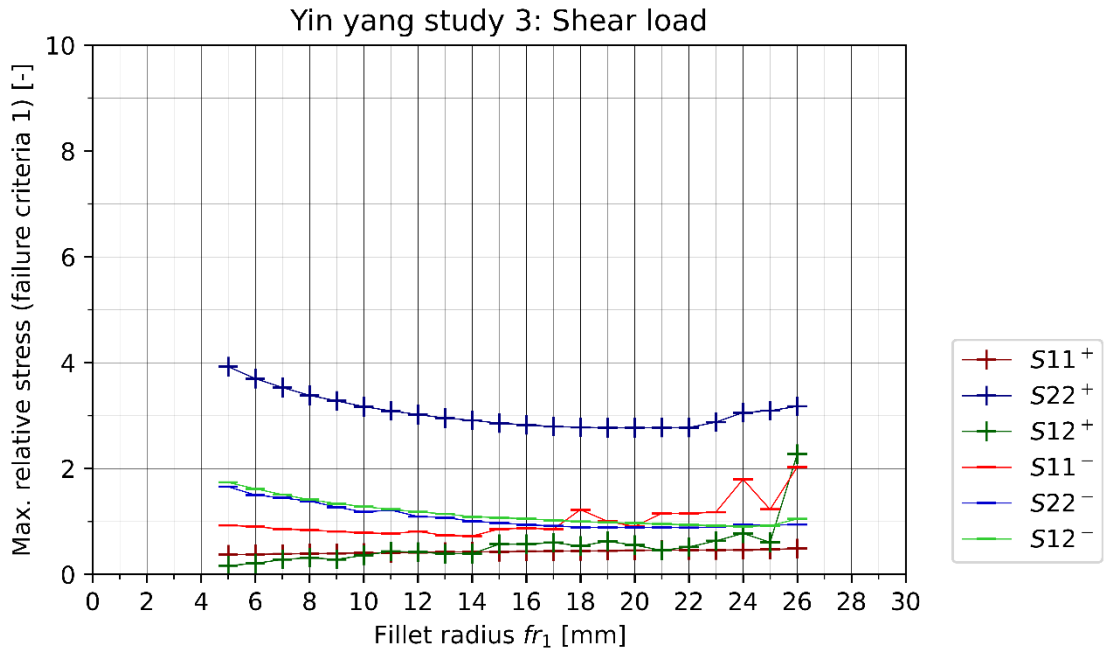

Figure 50: Yin yang study 3: maximum relative stresses (shear load)

The best performing yin yang can be found in study 3 and has a radius r_1 of 15 mm, w_1 of 40 mm and fillet radius fr_1 of 20 mm (Figure 51). The maximum relative tension stress perpendicular has a value of 2.77, which is 98% higher than the best performing dovetail and 79% higher than the best performing arrow. The critical displacement U2 of this yin yang is 0.15 mm. The displacement U2 varied between 0.13 and 0.16 mm for all yin yangs. Again, the yin yang shape performs a lot worse than the dovetail and arrow shape.

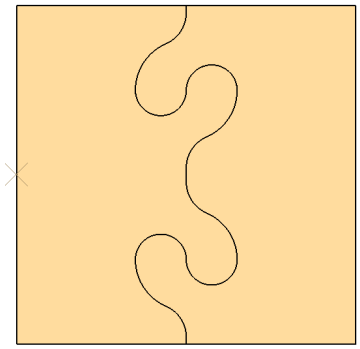

Figure 51: Most optimal yin yang loaded in shear
(a) Yin yang study 3: r_1 = 15 mm, w_1 = 40 mm, fr_1 = 20 mm

The pressure contact areas of the top yin yang differ from the bottom yin yang, see Figure 53c for the principal stress plot of the most optimal yin yang loaded in shear. The pressure contact area is located on the horizontal contact areas which have a rounded shape (marked by the black circles). The direction of the contact pressure is perpendicular to the grain, which is the weakest direction for the compression strength of the applied plywood. The highest concentration of in-plane principal stresses is found at the bottom pressure contact area. This area is situated near a fixed supported edge which might cause distortion of the results.

The best performing yin yangs loaded in shear from each study are analysed using failure criteria 2. The relative shear stresses along the critical section are illustrated in Figure 52, where the average relative stresses are illustrated by the dashed lines. The shear stress pattern of the yin yangs are different from the patterns of the dovetails and arrows. The peak shear stress is again located at the bottom end of the section line (near normalized distance of 0). However, the lowest stresses are now found near the top end of the section (near normalized distance of 1). All yin yangs in Figure 52 suffice failure criteria 2.

The yin yangs with the largest peak shear stresses also have the largest average shear stresses. The peak stress is 1.89, 1.92 and 1.57 times larger than the average stress for study 1, 2 and 3 respectively. The average values approximately correlate to the length of the critical section.

The most optimal yin yang in shear according to failure criteria is the yin yang from study 3 with a r_1 of 15 mm, w_1 of 40 mm and fr_1 of 20 mm. The average relative shear stress is 0.61, which is 15% higher than the most optimal dovetail and 42% higher than the most optimal arrow according to failure criteria 2. The difference between the peak shear stress and the average shear stress is the smallest for this yin yang. The same order of optimal designs result from the analysis using failure criteria 1 and 2. However, tension stress perpendicular is the governing stress and therefore brittle tension failure is expected.

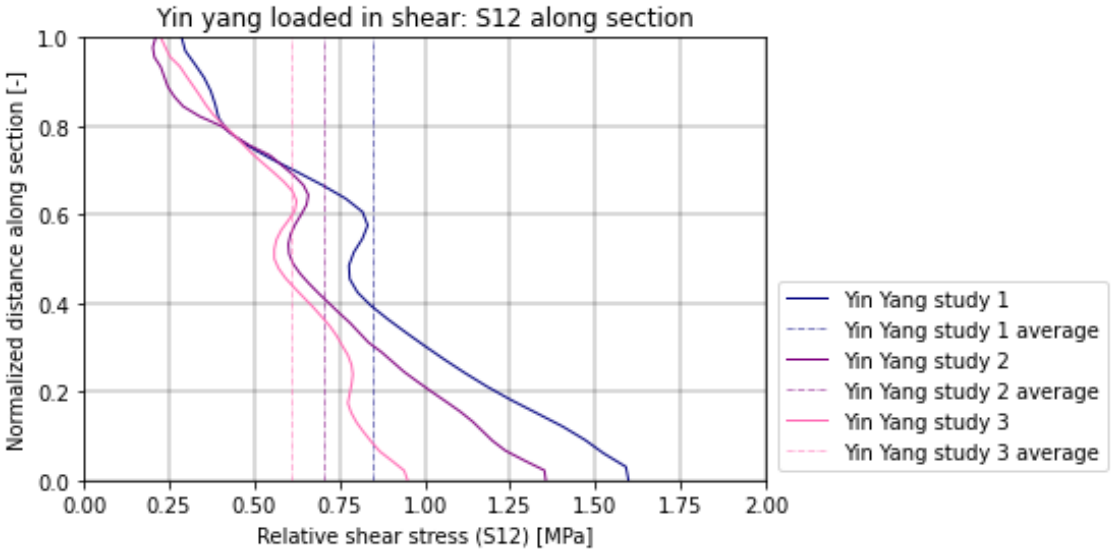

Figure 52: Shear stress (S12) distribution along the critical section of yin yangs loaded in shear
(a) Yin yang study 1: r_1 = 10 mm, w_1 = 60 mm, fr_1 = 5 mm
(b) Yin yang study 2: r_1 = 18 mm, w_1 = 28 mm, fr_1 = 9 mm
(c) Yin yang study 3: r_1 = 15 mm, w_1 = 40 mm, fr_1 = 20 mm

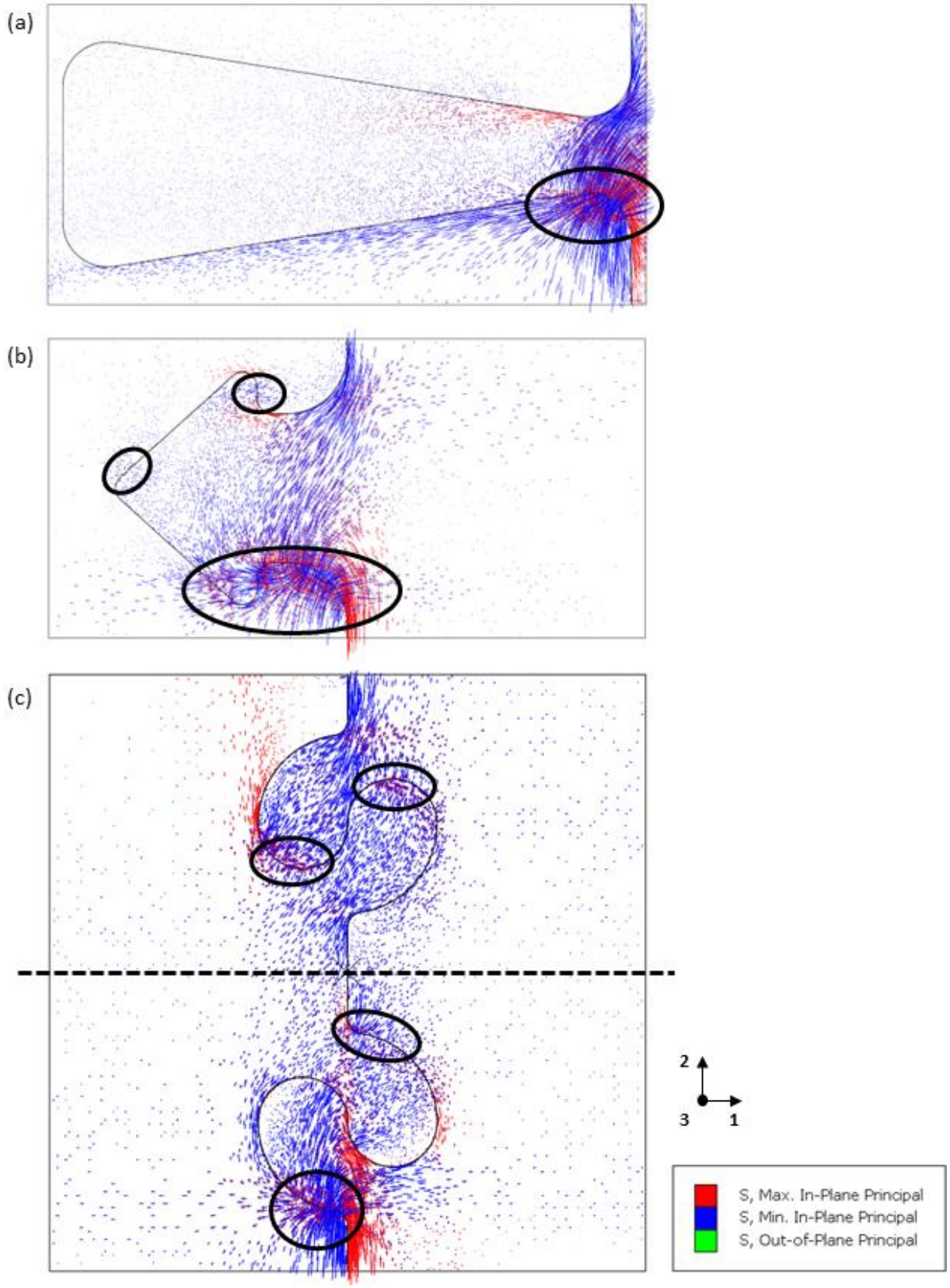

Figure 53: Principal stresses of (a) dovetail, (b) arrow and (c) yin yang loaded in shear

6.3 Conclusion

When assuming the values from the LEFEA analyses are correct, none of the connection designs loaded in either tension or shear would suffice failure criteria 1. A design or material with 3.87 times higher tension load capacity and 1.40 times higher shear load capacity is needed. It can be concluded that the tension load is more critical than the shear load as this was the case for every single design.

Almost all connection designs loaded in tension had a governing tension stress parallel to the grain. All connection designs loaded in shear had a governing tension stress perpendicular to the grain. It is expected that the connections will have a brittle failure mechanism caused by the tension stresses. Therefore, it is expected that failure criterium 1 gives a better indication on which connection has the largest strength capacity. Failure criterium 2 gives insight in the stress distribution. It can be concluded that the peak stresses are very locally situated at the corners in the designs. It is advised to conduct experimental research to determine the degree of plasticity.

For both tension and shear loads, the dovetail was the most efficient shape. The advantage of the dovetail is that it can accommodate large pressure contact areas on the sloped sides of the dovetail. This resulted in lower peak stresses and thus a larger tension and shear capacity. Its shape is symmetric and its geometric parameters can be optimized in such a way that both floor plates with interlocking timber joints have the optimized dimensions. A downside of the most optimal dovetail is that the contact pressure is directed perpendicular to the grain which is the weakest compression direction of the applied plywood. The direction of the contact pressure of the arrow was directed parallel to the grain which is the strongest compression direction of the applied plywood. However, the pressure contact area is a lot smaller compared to the dovetail. The yin yang performed drastically worse when loaded in tension and exceeds the failure criteria by far. The deformation of the most optimal yin yang loaded in tension is 8.25 times larger than the most optimal dovetail and 10.43 times larger than the most optimal arrow. Moreover, the deformation of the most optimal yin yang loaded in shear is roughly 1.5 times larger than the most optimal dovetail and arrow. Therefore, it is advised not to use yin yang shaped connections in plywood diaphragm floor seams. Even when the connection would be used for shear loads, it could be dangerous if there happens to be a small amount of tension since the connection might suddenly fail in tension.

Larger fillet radii at design corners generally result in lower peak stresses. However, attention is needed because too large fillet radii sometimes in combination with large angles can result in one joint component sliding out of the other joint component. Both tension and shear loads call for a wide dovetail neck. Yet only the tension load case profits from a tall dovetail height.

For the arrow design, a wider neck (w_2) results in a larger shear load capacity but in a smaller tension load capacity. For shear loads, the pressure is able to spread horizontally when a large neck width is applied. In other words, a larger area can be used for contact pressure. Whereas for tension loads, the pressure contact area deceases when the arrow neck width increases.

7 Example: Application to WikiHouse

This chapter elaborates on the application of the analysed interlocking timber connections from chapter '6. Variation study'. The first floor of the WikiHouse is used as example. The structural analysis of this first floor was presented in section 3.3. See Figures 18-19 for the stress and deformation plots.

This chapter elaborates on the application of the analysed interlocking timber connections from chapter '6. Variation study'. The first floor of the WikiHouse is used as example. The structural analysis of this first floor was presented in section 3.3. See Figures 18-19 for the stress and deformation plots.

According to failure criteria 1, there was no design which provides enough tension or shear strength capacity. When assuming that the peak stresses have correct values, the most ideal design for tension is still 3.87 times too weak and the most ideal design for shear is 1.40 times too weak. Several changes could be made to provide a solution which includes the use of a stronger timber species, thicker plate material or a different ply lay-up. For example, birch plywood of 18 mm thick and 13 plies has a tension strength which is about 4 times larger than spruce plywood of 18 mm. Using a different plate material results in a different relation between the plate's strength capacities. See Table 4 for a strength comparison between the two timber species. Therefore, it is important to calculate the LEFEA for the particular design with its new material properties. Another option is to use a different timber product such as LVL. LVL has its primary strength capacity in the parallel direction since most plies are oriented parallel to the grain. Since the interlocking timber connections from this variation study and the WikiHouse floor need strength in both directions this will not be a suitable solution.

Table 4: Comparison birch plywood to spruce plywood

	Tension		Compression		Shear	
	0°	90°	0°	90°	0°	90°
Spruce plywood, 18 mm [MPa]						
Design strength	7.5*	6*	12.53*	9.97*	2.63*	2.63*
Characteristic strength	10**	8**	16.7**	13.3**	3.5**	3.5**
Birch plywood, 18 mm [MPa]						
Design strength	29.4	26.8	20.4	18.6	7.1	7.1
Characteristic strength	39.2	35.8	27.2	24.8	9.5	9.5
Relation Birch to Spruce strength [%]						
	392	448	163	186	271	271

* Determined according to Dutch norm [36]
** Handbook of Finnish Plywood [37]

The primary fibre direction of the top and bottom plate of the box-structure at the first floor of the WikiHouse is directed from façade-to-façade wall. In the variation study it is assumed that the material orientation is parallel to the direction of the tension load. This means that the material orientation of the variation study (parallel to the grain) differs from the WikiHouse floor seams situation (perpendicular to the grain). There were no plywood or LVL plates with sufficient strength capacity while assessing the strengths with failure criteria 1 and using the perpendicular fibre direction. Thicker plate material has a slightly improved but insufficient strength capacity. Therefore, birch plywood of 18 mm thick with 13 orthogonally stacked plies will be applied while using the parallel fibre direction for the interlocking timber connections and the perpendicular fibre direction for the span between the two façades. This material provides enough strength capacity for the other structural elements, such as the bending moment of the floor. However, the box-structure was verified by experimental research and the structural calculations of the WikiHouse are based on those results. Thus, if the interlocking timber

connections were to be applied at the first floor of the WikiHouse and if the peak stresses exceed the strength capacity of the material that is applied in the WikiHouse now, additional testing on the box-structure is needed for verification.

The best performing connection for tension loads is the dovetail with h_1 of 180 mm, w_1 of 80 mm, w_2 of 20 mm and fr_1 of 15 mm (study 5). The governing stress is the maximum relative tension stress parallel which has a value of 3.87. The lack of tension stress capacity can be resolved by using birch plywood of 18 mm. However, this dovetail has a maximum relative compression stress of 2.38 which cannot be solved by using this material. The second-best performing connection for tension loads is another dovetail with h_1 of 190 mm, w_1 of 80 mm, w_2 of 20 mm and fr_1 of 10 mm (study 4). It has a maximum relative tension stress parallel of 3.88 and a maximum relative compression stress perpendicular of 1.93. This dovetail suffices the tensile failure criteria 1 and almost suffices the compression failure criteria 1 as illustrated in Figure 54. The tension stress parallel is utilized 99% and the compression stress perpendicular is utilized 103%. The compression stress perpendicular thus still exceeds failure criteria 1, however it is accepted since there is only 3% exceedance and plastic behaviour is expected for compression failure. Therefore, the latter mentioned dovetail is selected as the most optimal connection loaded in tension.

The best performing connection for shear loads is the dovetail with h_1 of 190 mm, w_1 80 of mm, w_2 of 20 mm and fr_1 of 15 mm. The governing stress is the maximum relative tension stress perpendicular which has a value of 1.40. Therefore, all stresses suffice failure criterium 1 when the connections are made from birch plywood. The shear capacity is only utilized for 51%. Figure 54 presents the dovetail utilization for best design for tension loads on the left and the best design for shear loads on the right according to failure criteria 1.

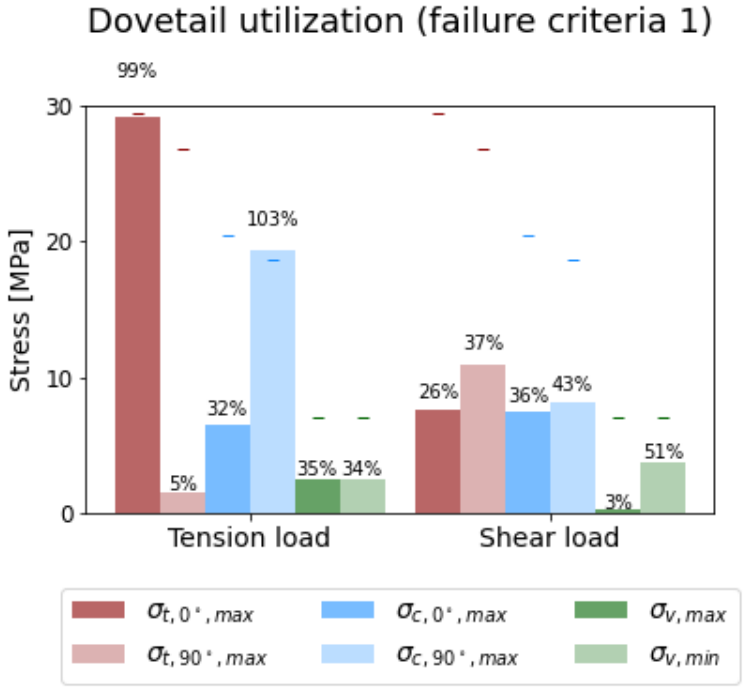

Figure 54: Dovetail utilization (failure criteria 1)

The way the box structure of the WikiHouse is built up now accommodates too little space for interlocking timber connections. The space between the vertical webs of two boxes is 114 mm, see Figure 12 for the connection seam. The webs need to be moved inwards so that more space is available for the connections in the floor seams. It is suggested to place the webs at 150 mm distance from the end of the horizontal plates as illustrated in Figure 55. Then the interlocking timber connections are placed inside the 2 times 100 mm from each plate. Accordingly, a minimum of 50 mm distance is kept between the horizontal connections (floor plate to floor plate) and vertical connections (box web to box plates).

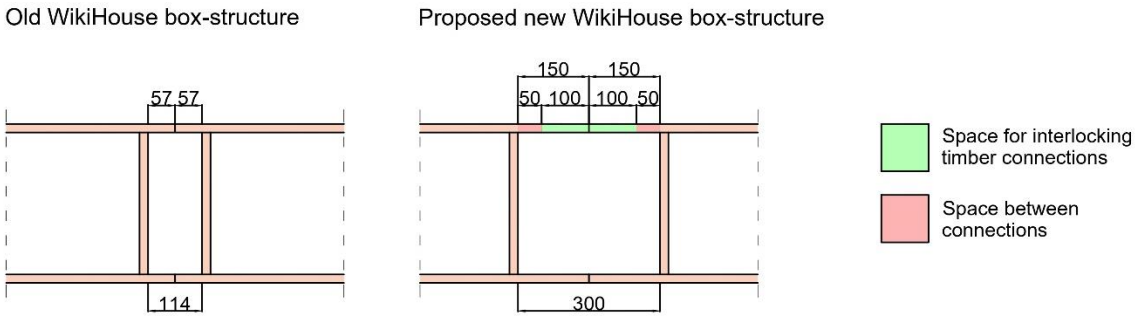

Figure 55: WikiHouse box-structure: old design and suggested new design

Two different loading zones can be distinguished on the first floor of the WikiHouse; a tension dominated zone and a shear dominated zone. The largest tension and compression stresses are present at the sides of the floor and the largest shear stresses are present in the middle of the floor. Moreover, the axial stress (S11) is at its minimum around the middle of the floor seams and the shear stress (S12) is at its minimum at the floor sides. The sides of the floor can be loaded either in tension or in compression depending on the wind direction. Compression is not a critical load case as determined earlier. Therefore, the floor sides are assumed as tension dominated zones and the middle of the floor is assumed as shear dominated zone. Figure 56 shows the proposed loading zones for the first floor of the WikiHouse, where the purple marking is the tension-dominated zone and the green marking is the shear-dominated zone.

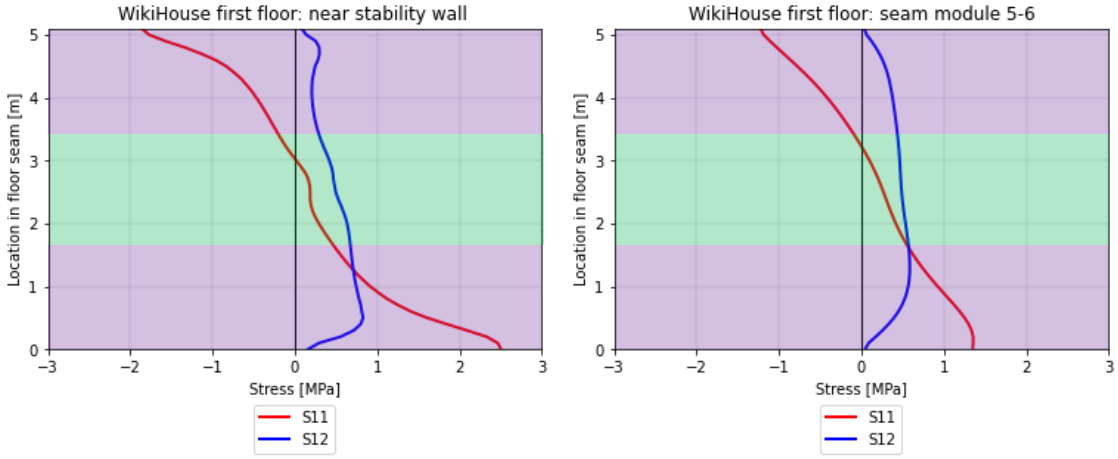

Figure 56: WikiHouse first floor: loading zones

Option 1: no variation along floor seam length

The optimal designs for the connection loaded in tension or shear do not have large geometric differences. The height of the tension loaded dovetail is 190 mm and the height of the shear loaded dovetail is 180 mm. The rest of the geometric parameters is equal for both designs. Moreover, it was concluded that varying the height for dovetails loaded in shear has minimal influence on the shear capacity. Therefore, the first option is to apply one design along the whole seam length. Since the tension capacity is more critical than the shear capacity, the design of the tension optimal dovetail will be used along all floor seams. When only applying one design for the critical load condition, time will be saved on creating loading zones and the probability on building errors is reduced. Figure 57 illustrates the application of the dovetail in the WikiHouse floor seam.

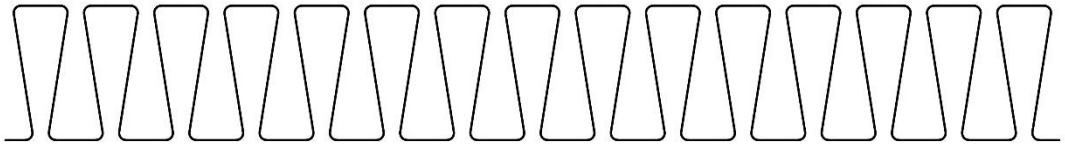

Figure 57: Application option 1: no variation along the floor seam length
(a) Dovetail study 4: h_1 = 190 mm, w_1 = 80 mm, w_2 = 20 mm, fr_1 = 10 mm

Option 2: variation in number of connections along floor seam length

The second option is to variate the number of connections along the floor seam length. The optimal dovetail design is not fully utilized when used as shear connection, only 51% of the shear capacity is used. Therefore, the suggestion is to apply the dovetail design every 100 mm in the tension-dominant zone and every 200 mm in the shear-dominant zone.

In addition, it was noticed that the stresses in the floor seams substantially reduce when the seam is located further away from the stability wall. Therefore, less dovetails need to be applied per meter floor length for those seams. The reduction between the seam at the stability wall (between module 4 and 5) and the seam between module 5 and 6 is 45% less tension stress, 33% less compression stress and 29% less shear stress. Larger reductions are found for the other seams as concluded from Figure 14. The proposed design for option 2 is illustrated in Figure 58. The CNC toolpath will be shorter when using less dovetails per meter resulting in a shorter production period. Moreover, less pieces need to interlock simultaneously during the construction process which might simplify the construction process.

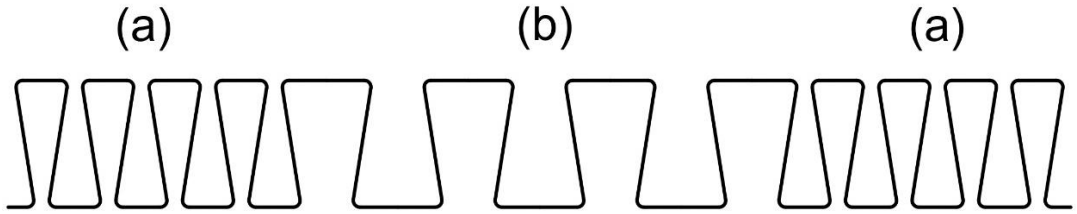

Figure 58: Application option 2: variation in number of connections along the floor seam length
*(a) **Tension-dominated zone.** 1x per 100 mm*
Dovetail study 4: h_1 = 190 mm, w_1 = 80 mm, w_2 = 20 mm, fr_1 = 10 mm
*(b) **Shear-dominated zone.** 1x per 200 mm*
Dovetail study 4: h_1 = 190 mm, w_1 = 80 mm, w_2 = 20 mm, fr_1 = 10 mm

Option 3: variation in connection height along floor seam length

Using the same principles of stress reduction from option 2, the last option is to use dovetails with varying heights along the seam length. A dovetail with a height of 190 mm is needed for the tension-dominated zone while a dovetail with a height of 20 mm suffices for the shear dominated zone. The utilization of the dovetail design for tension and the dovetail design for shear is presented in Figure 59. The dovetail for shear loads is utilized more in comparison to the dovetail in Figure 54. However, still roughly half of the dovetail's capacity is not used. The CNC toolpath will be shorter when using less dovetails per meter resulting in a shorter production period. The proposed design for option 3 is illustrated in Figure 60.

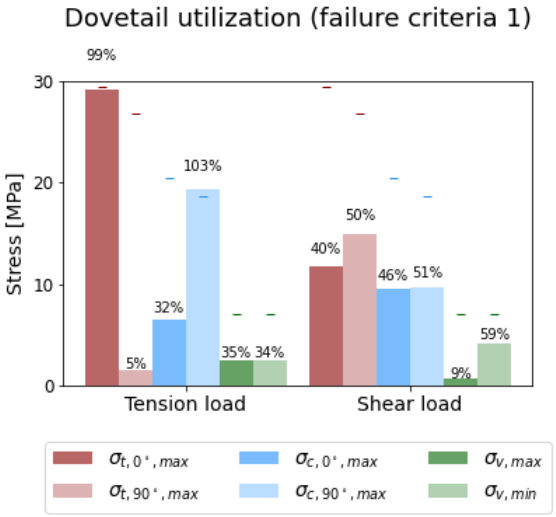

Figure 59: Dovetail utilization application option 3 (failure criteria 1)

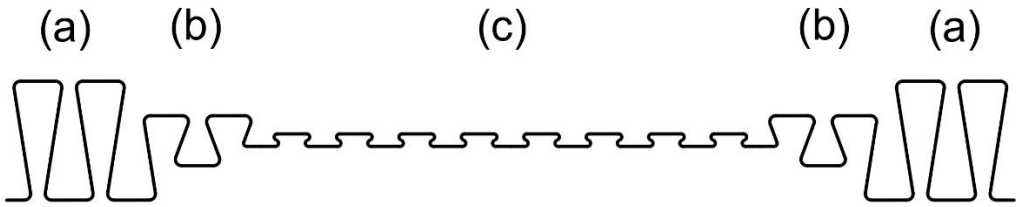

Figure 60: Application option 3: variation in connection height along the floor seam length

*(a) **Tension-dominated zone.** Dovetail study 4: h_1 = 190 mm, w_1 = 80 mm, w_2 = 20 mm, fr_1 = 10 mm*

*(b) **Shear-dominated zone.** Dovetail study 4: h_1 = 80 mm, w_1 = 80 mm, w_2 = 20 mm, fr_1 = 10 mm*

*(c) **Shear-dominated zone.** Dovetail study 3: h_1 = 20 mm, w_1 = 80 mm, w_2 = 20 mm, fr_1 = 5 mm*

8 Conclusion

In this thesis, Linear Elastic Finite Element Analyses were performed to analyse the influence of the shape of interlocking timber connections on their strength capacity. Dovetail, arrow and yin yang shaped connections with varying geometric parameters were investigated. Parametric scripts were created for automated creation of the Finite Element Models and for post-processing the results. The strength optimization study was performed using two failure criteria, where the peak or average stresses were compared to the design strength of the plywood.

It was difficult to determine the failure criteria for the optimization process due to the presence of high local peak stresses and lack of experimental data. The best performing designs could be determined by exclusively using failure criteria 1. In almost all cases, tension stresses were governing which leads to brittle failure mechanisms. On top of that, the analysis with failure criteria 2 led to the same results as the analysis of failure criteria 1. Though it is important to investigate the failure modes by experimental research.

The widths, heights, radii and fillet radii of dovetail, arrow and yin yang connections were varied. It can be concluded that the area of the pressure contact has a large influence on the strength of the connection for both tension and shear cases. The dovetail design was the most optimal design in both tension and shear. The pressure contact area increased when increasing the dovetail height. Contrary to the arrow and yin yang loaded in tension, the pressure of the dovetail was directed in the weakest direction of the plywood (compression perpendicular to the grain). The dovetail loaded in tension has the most optimal force path including the least turns. When larger fillet radii were applied at corners, the peak stresses decreased resulting in a stronger connection. A large width in combination with large filler radii contributed to higher shear strength capacity of the dovetail and arrow joint. The yin yang performed substantially worse in both tension and shear and therefore it is suggested to not use yin yang shaped connections.

Interlocking timber connections with larger deformations will slide out more resulting in a decreased pressure contact area. Therefore, it is expected that larger deformations lead to lower strength capacity. Designs with larger deformations often performed worse strength-wise. The most optimal designs had deformations due to tension loading of about 0.5 mm and deformations due to shear loading of about 0.1 mm. Note that these values need to be validated.

The order of most optimal connection to least optimal connection was investigated. It is uncertain if the designs have enough strength to be applied on the first floor of the WikiHouse since the peak stresses need to be validated. A suggestion was made for the application to the WikiHouse where it was assumed that the peak stresses from the LEFEA are correct values. In that case, the interlocking connections cannot be applied in the material that the WikiHouse box-structure is made of. The spruce plywood of 18 mm does not provide enough strength. However, birch plywood of 18 mm would provide enough strength and various options for application become available. The birch plywood should be applied parallel to the interlocking connections in the floor seam.

The first option is to use a single design along the floor seams since the designs of the most optimal connection loaded in tension or shear have minimal differences. The second and third option divide the floor seams in tension-dominated and shear-dominated loading zones. Moreover, a distinction is made for seams closer to the stability wall and seams further away from the stability wall. Higher stresses were found near the stability wall. The second option includes a larger density of dovetails per meter in tension-dominated zones and in seams closer to the stability wall. The third option includes dovetails with a larger height in tension-dominated zones and in seams closer to the stability wall. The second option is expected to be the most successful option.

The interlocking timber connection with the largest tension strength capacity made from 18 mm thick spruce plywood is a dovetail with h_1 of 180 mm, w_1 of 80 mm, w_2 of 20 mm and fr_1 of 15 mm. The interlocking timber connection with the largest tension strength capacity made from 18 mm thick birch plywood is a dovetail with h_1 of 190 mm, w_1 80 of mm, w_2 of 20 mm and fr_1 of 10 mm. When the results are validated, it can be determined which timber species needs to be applied. The interlocking timber connection with the largest shear strength capacity is a dovetail with h_1 of 190 mm, w_1 80 of mm, w_2 of 20 mm and fr_1 of 15 mm. There is no difference in the most optimal design for shear loads when using different timber species. All designs can be made with either 3-axis or 5-axis CNC machines.

9 Recommendation

Convergence
Peak stresses occurring at the corners in the designs complicated the definition of the failure criteria. It is expected that the interlocking timber connections fail under tension stresses and thus will have a brittle failure mechanism. However, it is unknown to what degree the stresses will redistribute. Since the LEFEA model could not converge, a constant mesh fineness was chosen for each simulation. It is strongly advised to conduct experimental research to converge the model and to obtain test data on this topic. The experimental data or a more advanced FEM model including plastic behaviour could validate the stresses and deformations from the LEFEA model. When testing, close attention to the test set-up is needed since the connections in a floor seam behave stiffer than a single connection without neighbour connections. It is proposed that the test specimen which are CNC manufactured are first acclimated in a climate room. Non-destructive moisture content measurements could be done by the oven dry method. Test results could be obtained by spraying a speckle pattern on the test specimen and measuring the strains with Digital Image Correlation cameras. This way the test results can be compared to the results from the LEFEA model. When the model is converged, not only the optimalisation order of the designs can be determined but also their maximum capacity. The degree of redistribution of stresses in tension and shear load cases can be determined and the failure criteria can be updated accordingly.

Optimization
The strength optimization was done by a variation study. Various shapes and dimensions were analysed but it could be possible that the most optimal shape and dimension is not among the connections analysed in this study. It would be very interesting if an optimization algorithm could be created to find the actual optimum. Jigsaw form and other random shapes.

Based on the results, it is not expected that separate puzzle pieces will improve the strength of the connections even if stronger timber material is used for the joint inlays. The assumption is that the connection will then fail first at the floor plate instead of at the joint inlay. However, joint inlays may simplify the construction process. The two floor plates can be easily aligned after which the joint inlays can be hammered into place. Hammering the connections to fit tightly together likely leads to larger connection stiffness. In addition, the shape in the thickness direction can be funnelled for easier hammering. Moreover, optimization along the floor seam length can be improved with the use of joint inlays. A larger number of joint inlays per meter can be applied in the tension-dominated zone than in the shear dominated zone. Furthermore, it was noticed that the stresses decreased substantially when further away from the stability wall of the WikiHouse. Thus, a smaller number of joint inlays per meter can be applied in seams that are located further away from the stability wall. The use of less joint inlays due to optimization along the floor seam length leads to a shorter construction time. Moreover, the joint inlays can possibly be made from scrap pieces of plywood that would otherwise have been thrown away.

Joint stiffness
The strength and deformation of the interlocking timber connections depend on the joint stiffness. Tolerances in the manufacturing process as well as shrinkage and swelling of the timber may cause gaps between the connection components which leads to a reduction of the joint stiffness. On the contrary, it is also possible that the joint is too tight before construction and causes pieces not to fit. Therefore, large interlocking elements may be a practical challenge as all elements need to fit perfectly at once. Furthermore, the friction between the timber components should be examined to determine the joint stiffness.

The deformation of the interlocking timber connection plays an important role in the whole timber structure. Deformation of the whole floor accumulates with deformation of each connection. Therefore, the length of the floor plays an important role in the deformation criteria to suffice to the Serviceability Limit State.

Loads normal to the plane of the connections

Loads normal to the plane of the interlocking timber connections applied in diaphragm floor seams are not included in this study. However, these loads, such as dead loads and live loads, are always present in the structure. It is important to investigate the influence of loading normal to the plane. For example, what if a heavy object is placed locally on the joint seam? What is the influence on the strength capacity of the joint?

Bibliography

[1] C. Robeller, 'Integral Mechanical Attachment for Timber Folded Plate Structures', 2015.

[2] J. Moradei *et al.*, 'Modern timber design approaches for traditional Japanese architecture: analytical, experimental, and numerical approaches for the Nuki joint', in *Proc. 60th IASS Annual Symposium - Form and Force,* Oct. 7-10, 2019. [Online]. Available: https://www.researchgate.net/publication/336474081

[3] The United Nations, 'Net Zero Coalition', *The United Nations*, 2021. https://www.un.org/climatechange

[4] Bouwend Nederland, 'Energieneutraal bouwen', *Nu bouwen aan morgen*, 2019. https://www.bouwendnederland.nl/nu-bouwen-aan-morgen/voorbeelden-uit-de-praktijk/energieneutraal-bouwen (accessed Sep. 06, 2022).

[5] M. Gray, 'How California Exported Its Worst Problem to Texas', *The Atlantic*, California, Aug. 10, 2022. Accessed: Sep. 06, 2022. [Online]. Available: https://www.theatlantic.com/ideas/archive/2022/08/housing-crisis-affordability-covid-everywhere-problem/671077/

[6] ANP, 'Woningtekort bedraagt bijna 400.000: vooral krapte in Amsterdam, Utrecht, Hilversum en Amersfoort', *Business Insider Nederland*, Jun. 22, 2022. Accessed: Sep. 06, 2022. [Online]. Available: https://www.businessinsider.nl/woningtekort-groter-ministerie-bzk-atlas-research/

[7] ANP, 'Woningtekort wordt komende jaren alleen erger', *De Telegraaf*, Utrecht, Feb. 10, 2022. Accessed: Sep. 06, 2022. [Online]. Available: https://www.telegraaf.nl/financieel/1321428662/woningtekort-wordt-komende-jaren-alleen-erger

[8] Cobouw, 'Bouw sluit 2022 goed af, maar de uitdagingen nemen toe', *Cobouw*, Feb. 24, 2023. https://www.cobouw.nl/311431/bouw-sluit-2022-goed-af-maar-de-uitdagingen-nemen-toe (accessed Mar. 06, 2023).

[9] W. S. Chang and M. F. Hsu, 'Rotational performance of traditional Nuki joints with gap II: The behavior of butted Nuki joint and its comparison with continuous Nuki joint', *Journal of Wood Science*, vol. 53, no. 5, pp. 401–407, Oct. 2007, doi: 10.1007/s10086-007-0880-1.

[10] J. Moradei *et al.*, 'Structural Characterization of Traditional Moment-Resisting Timber Joinery', in *Proc. 59th IASS Annual Symposium - Creativity in Structural Design*, Jul. 16-20, 2018. Accessed: Sep. 06, 2022. [Online]. Available: https://infoscience.epfl.ch/record/255197

[11] S. Mehra, C. O'Ceallaigh, A. Sotayo, Z. Guan, and A. M. Harte, 'Experimental characterisation of the moment-rotation behaviour of beam-beam connections using compressed wood connectors', *Eng Struct*, vol. 247, Nov. 2021, doi: 10.1016/j.engstruct.2021.113132.

[12] T. Tannert, D. Schmidt, and F. Lam, 'CNC Timber Processing in Research and Teaching', in *Proc. 51st International Convention of Society of Wood Science and Technology,* Nov. 10-12, 2008. Accessed: Sep. 06, 2022. [Online]. Available: https://www.swst.org/meetings/AM08/proceedings/WS-52.pdf

[13] E. V. Tagliaboschi, 'HexBox Canopy: A Rapid Assembly Segmented Timber Shell with Wedge Joints', University of Pisa, Pisa, 2020. doi: 10.13140/RG.2.2.28481.10084.

[14] C. Robeller, J. Gamerro, and Y. Weinand, 'Thétre Vidy Lausanne - A double-layered timber folded plate structure', *Journal of the International Association for Shell and Spatial Structures*, vol. 58, no. 4. Int. Association for Shell and Spatial Structures, pp. 295–314, Dec. 01, 2017. doi: 10.20898/j.iass.2017.194.864.

[15] M. Heesterman and K. Sweet, 'Robotic Connections: Customisable Joints for Timber Construction', 2018.

[16] A. Harte, 'Introduction to timber as an engineering material', *ICE Manual of Construction Materials*, 2009, doi: 10.1680/mocm.00000.0001.
[17] Rona, 'Spruce Scaffold Plank - 2" x 10" x 12"'. https://www.rona.ca/en/product/spruce-scaffold-plank-2-x-10-x-12-0971093
[18] Z. Cai and R. J. Ross, 'Wood Handbook, Chapter 12: Mechanical Properties of Wood-Based Composite Materials', 2010.
[19] P. Malanit and N. Laemsak, 'Effect of Strand Orientation on Physical and Mechanical Properties of Rubberwood Oriented Strandboard', 2007.
[20] S. Suzuki and K. Takeda, 'Production and properties of Japanese oriented strand board I: effect of strand length and orientation on strength properties of sugi oriented strand board', *The Japan Wood Research Society*, vol. 46, pp. 289–295, 2000.
[21] G. Havel, 'Construction Concerns: Timber Connections', *Fire Engineering*, Dec. 31, 2015. https://www.fireengineering.com/fire-prevention-protection/construction-concerns-timber-connections/#gref (accessed Mar. 10, 2023).
[22] K. N. Dew and D. K. Rosner, 'Lessons from the woodshop: Cultivating design with living materials', in *Conference on Human Factors in Computing Systems - Proceedings*, Association for Computing Machinery, Apr. 2018. doi: 10.1145/3173574.3174159.
[23] Lynch Brother Homes, 'Your local Joiners in Oxford', 2020. https://www.lynchbrotherhomes.co.uk/services/joiners-in-oxford/
[24] Australian Wood Review, 'Theo Cook's Impossible Dovetail', *Australian Wood Review*, Jun. 2017. [Online]. Available: https://www.woodreview.com.au/news/theo-cook-s-impossible-dovetail
[25] K. Seike, *The Art Of Japanese Joinery*. 1977.
[26] C. Lubchenko, 'Kanawa Tsugi by Dylan Iwakuni', Aug. 20, 2021. https://japanobjects.com/features/japanese-joinery
[27] W. Myers, 'Tusk Tenons…How Strong Are They?', 2016. https://woodandshop.com/will-myers-tusk-tenonshow-strong-are-they/
[28] M. Meier, 'Digital Fabrication for Designers', 2020. http://mkmra2.blogspot.com/2014/08/cnc-cut-wood-joinery.html
[29] K. Ron, 'Chigiri Tsugi by Dylan Iwakuni', Dec. 19, 2020. https://everydaymonkey.com/the-japanese-art-of-wood-joinery-is-incredibly-satisfying/
[30] A. Christiana, 'Butterfly Keys Made Easy', May 03, 2020. https://www.popularwoodworking.com/techniques/butterfly-keys-made-easy/
[31] M. A. Samboro and D. Kuswanto, 'Snap-fit joinery system using pinewood material elasticity properties', *Journal of Engineering and Technological Sciences*, vol. 52, no. 6, pp. 798–804, 2020, doi: 10.5614/j.eng.technol.sci.2020.52.6.2.
[32] Bayer MaterialScience, 'Snap-Fit Joints for Plastics - A Design Guide'. Accessed: Sep. 06, 2022. [Online]. Available: https://fab.cba.mit.edu/classes/S62.12/people/vernelle.noel/Plastic_Snap_fit_design.pdf
[33] C. Robeller and Y. Weinand, 'A 3D Cutting Method for Integral 1DOF Multiple-Tab-and-Slot Joints for Timber Plates, using 5-axis CNC Cutting Technology', 2016. [Online]. Available: https://www.researchgate.net/publication/316106442
[34] Open Systems Lab, 'Wikihouse', 2022. https://www.wikihouse.cc/ (accessed Aug. 10, 2022).
[35] T. Wang, Y. Wang, R. Crocetti, and M. Wålinder, 'In-plane mechanical properties of birch plywood', *Constr Build Mater*, vol. 340, Jul. 2022, doi: 10.1016/j.conbuildmat.2022.127852.
[36] Brussels: BSi, 'NEN-EN 1995, 2011. Eurocode 5: Ontwerp en berekening van houtconstructies - Part 1', 2011.
[37] UPM, *Handbook of Finnish Plywood*. 2007. [Online]. Available: www.wisa.com
[38] Stichting WikiHouseNL, 'De Stripmaker - realisatie', *WikiHouseNL*, Apr. 13, 2022. https://wikihousenl.cc/portfolio-item/destripmaker-2/ (accessed Sep. 06, 2022).

[39] Team Stadszaken.nl, 'WikiHouse: Almeers debuut zorgt voor wereldwijde interesse', *Stadszaken.nl*, Mar. 02, 2021. https://stadszaken.nl/artikel/3372/wikihouse-almeers-debuut-zorgt-voor-wereldwijde-interesse (accessed Sep. 06, 2022).
[40] Stichting WikiHouseNL, 'WikiHouseNL – Open Source Zelfbouw', 2022. https://wikihousenl.cc/ (accessed Aug. 10, 2022).
[41] A. Lier and G. J. Rozemeijer, 'Wikihouse Deel B: Berekening WikiHouse casco', Jun. 2021.
[42] A. Lier and G. J. Rozemeijer, 'Wikihouse fase 2 Detailberekeningen houtconstructie', Jun. 2021.
[43] Brussels: BSi, 'NEN-EN 1991, 2011. Eurocode 1: Belastingen op constructies - Deel 1', 2011.
[44] Dassault Systems, *Abaqus Scripting User's Guide*. 2016. [Online]. Available: http://130.149.89.49:2080/v2016/books/cmd/default.htm
[45] H. Yoshihara, 'Influence of the Specimen Depth to Length Ratio and Lamination Construction on Young's Modulus and In-Plane Shear Modulus of Plywood Measured by Flexural Vibration', 2012.
[46] F. F. P. Kollmann and W. A. Côté, *Principles of Wood Science and Technology: I Solid Wood*. Springer Berlin Heidelberg, 1968.
[47] H. Lee, 'Finite Element Simulations with ANSYS Workbench 14', pp. 1–602, 2012.
[48] K. Surana and J. Reddy, 'The Finite Element Method for Boundary Value Problems', *Mathematics and Computations*, Nov. 2016.
[49] StackOverflow, '2020 Developer Survey', *Stackoverflow*, 2020. https://insights.stackoverflow.com/survey/2020#technology-programming-scripting-and-markup-languages-professional-developers
[50] Github, 'PYPL PopularitY of Programming Language', *Github*, Mar. 2023. https://pypl.github.io/PYPL.html
[51] Dassault Systems, 'Introduction to Abaqus Scripting'. https://www.3ds.com/products-services/simulia/training/course-descriptions/introduction-to-abaqus-scripting/
[52] D. Phillips, 'Python 3 Object-Oriented Programming', *Build Robust and Maintainable Software with Object-oriented Design Patterns in Python 3.8*, no. 3, Oct. 2018.

After completing a course on Python coding, ChatGPT was used to learn more about Python coding. Moreover, ChatGPT was used for synonyms and paraphrasing ideas.

Appendix A: Structural drawings WikiHouse

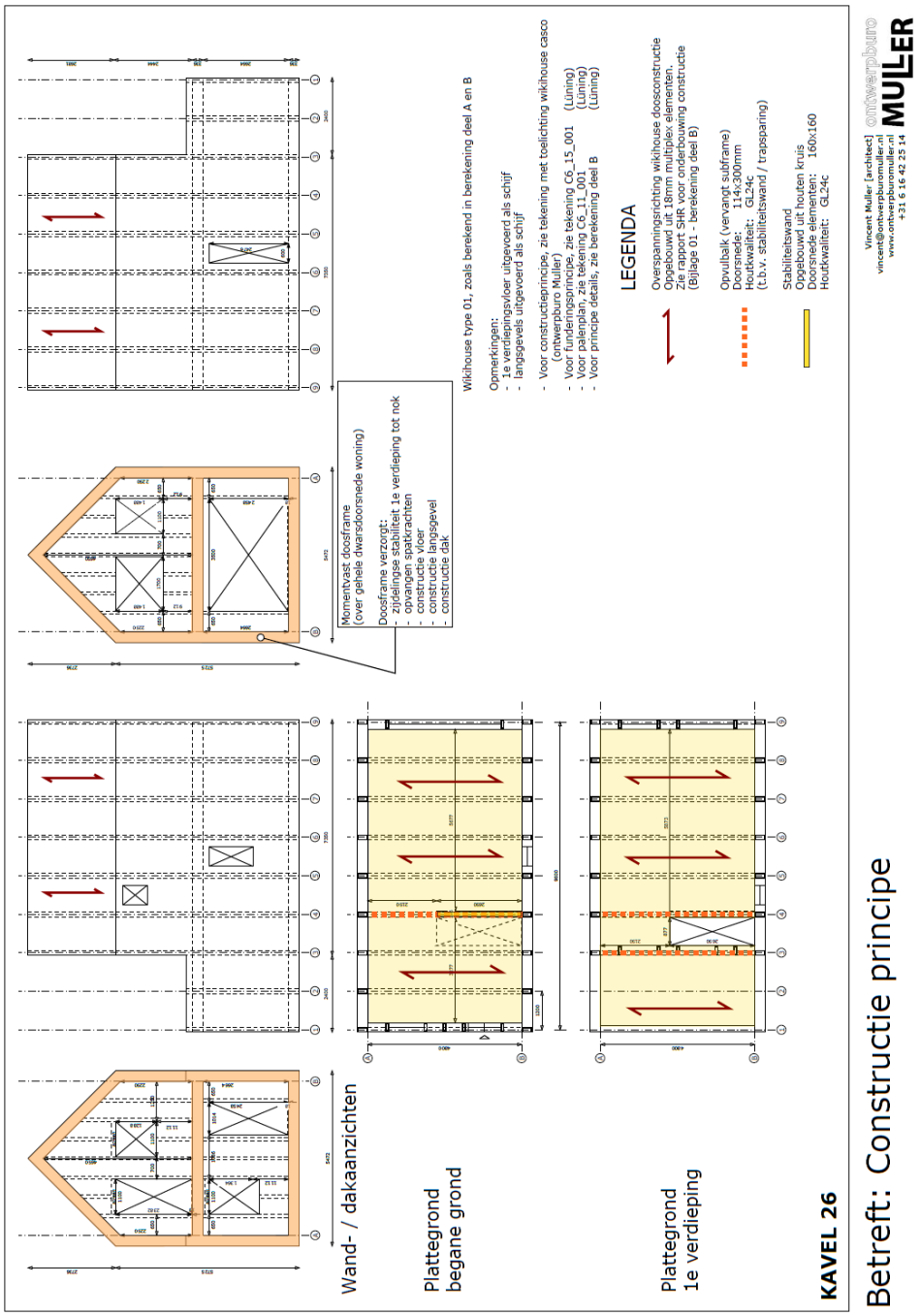

Figure A-I: Structure principle WikiHouse The Stripmaker lot 26 [41]

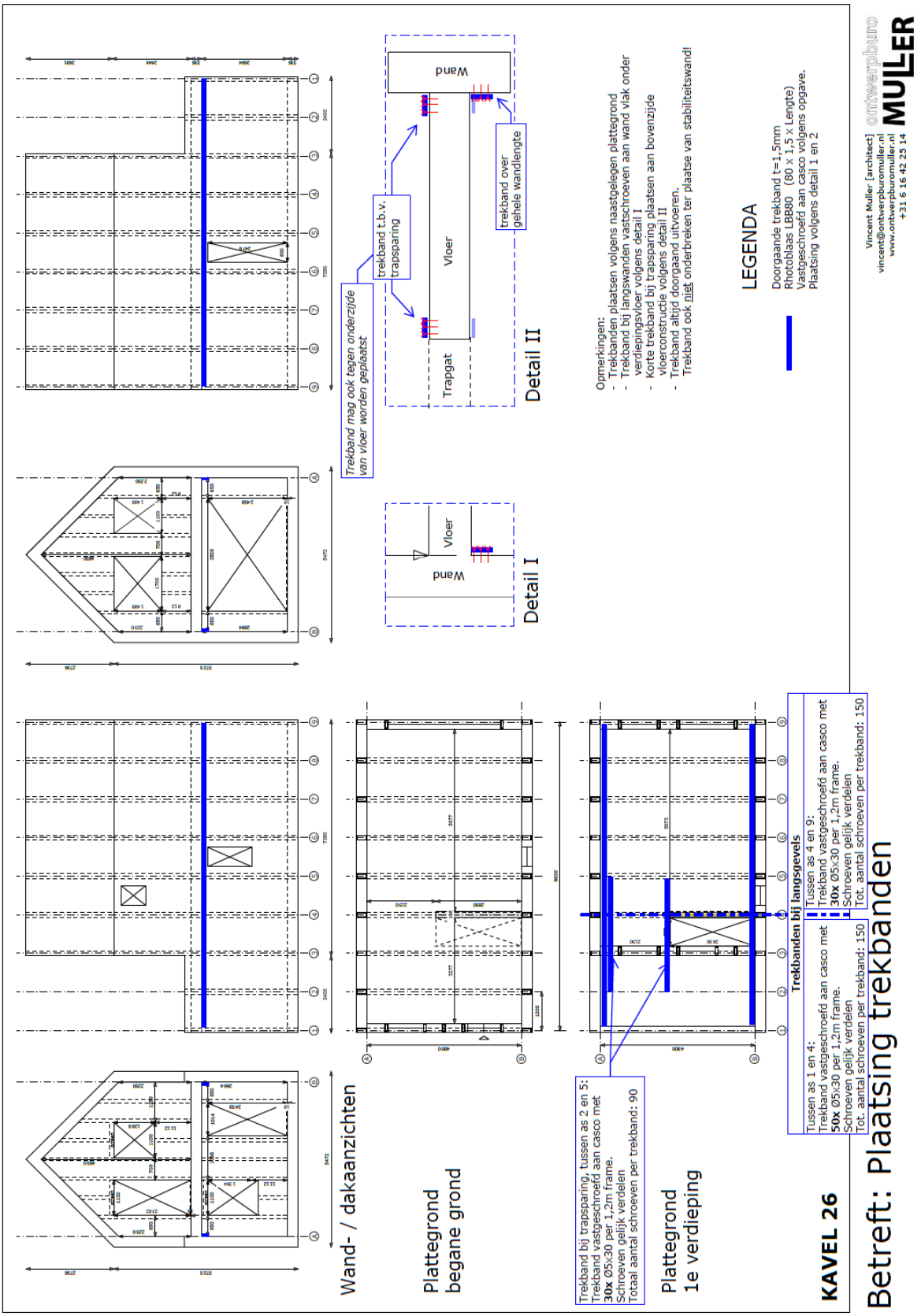

Figure A-II: Placement of ties WikiHouse The Stripmaker lot 26 [41]

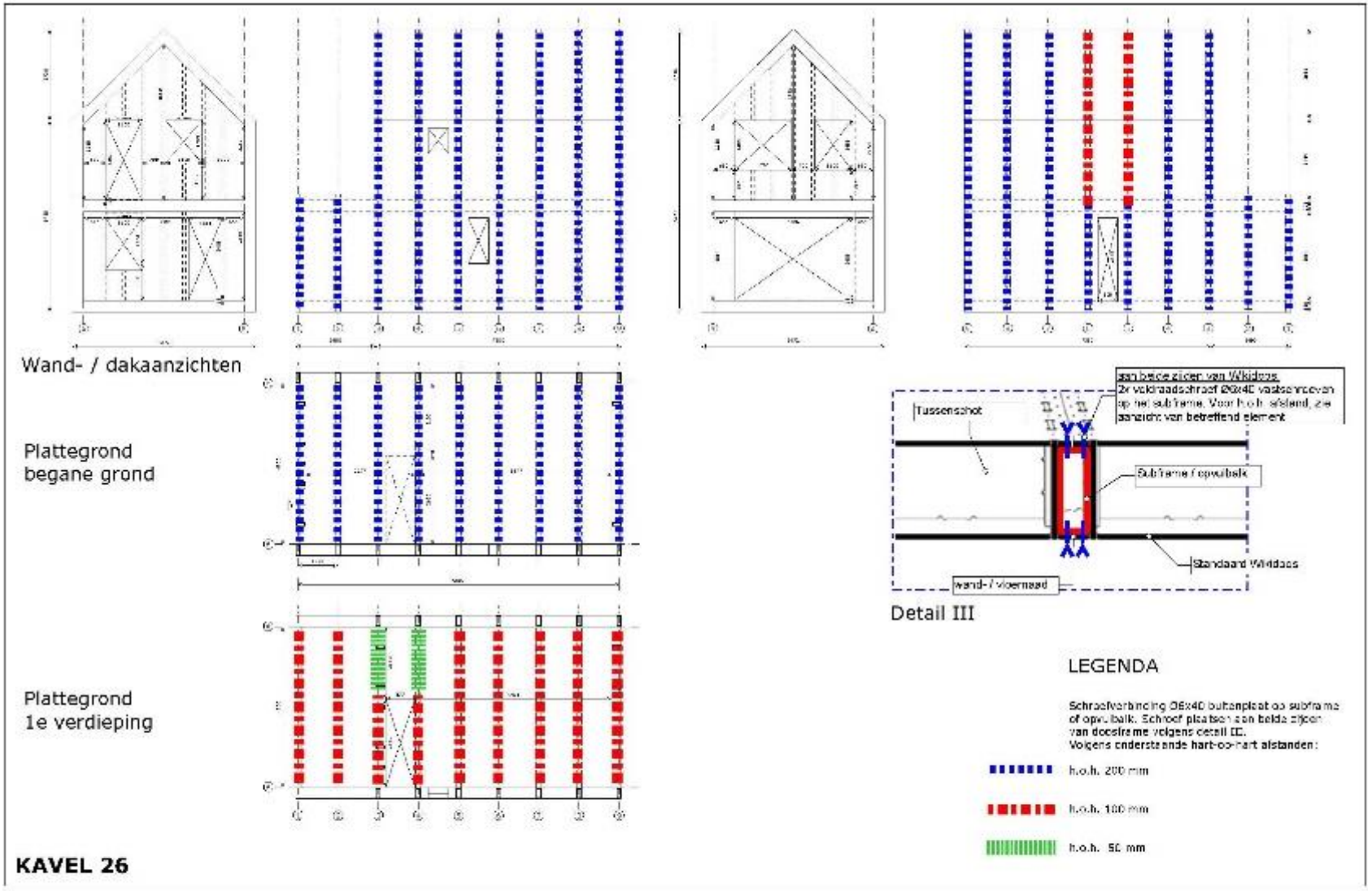

Figure A-III: Screw plan WikiHouse The Stripmaker lot 26 [41]

Appendix B: Structural report WikiHouse

The 2-storey WikiHouse consisting of 9 modules and a 45 degrees sloped roof has a residential function, thus calculated according to consequence class CC1. The timber structure is in climate class 1.

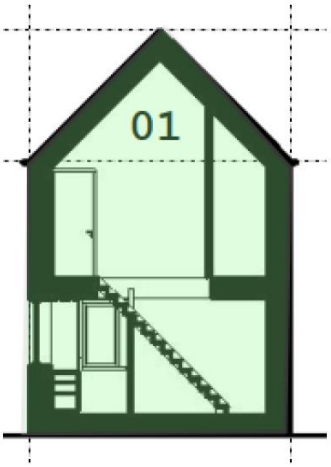

Figure B-I: Section of 2-storey WikiHouse consisting of 9 modules and a 45 degrees sloped roof [41]

The structure (excluding the foundation) consists of a spruce plywood box-structure, birch plywood corners and CLT stability cross. The build-up of the plywood box-structure is illustrated in Figure B-II. Material properties are given in Tables B-I – B-II.

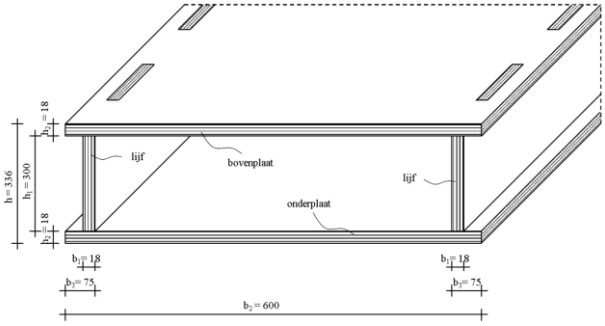

Figure B-II: Build-up of plywood box-structure [whalm]

Table B-I: Mechanical properties plywood [37]

								Characteristic strength						Mean modulus			
	Section properties							Bending		Compression		Tension		Bending		Tension and compression	
Lay-up	Type	Nominal thickness	Number of plies	T mean mm	A mm^2/mm	W mm^3/mm	I mm^4/mm	$f_{m,\parallel}$ N/mm^2	$f_{m,\perp}$ N/mm^2	$f_{c,\parallel}$ N/mm^2	$f_{c,\perp}$ N/mm^2	$f_{t,\parallel}$ N/mm^2	$f_{t,\perp}$ N/mm^2	$E_{m,\parallel}$ N/mm^2	$E_{m,\perp}$ N/mm^2	$E_{t/c,\parallel}$ N/mm^2	$E_{t/c,\perp}$ N/mm^2
Conifer (spruce) plywood, thick veneers																	
|-|-|-|	18/7-2.6	18	7	17.6	17.6	51.6	454	20.4	13.0	16.7	13.3	10.0	8.0	8170	3830	6682	5318
Birch plywood																	
|-|…|-|		18	13	17.6	17.6	51.6	454	40.2	34.1	27.2	24.8	39.2	35.8	10048	7452	9148	8352

Table B-II: Shear properties plywood [37]

Nominal thickness	Characteristic strength				Mean modulus of rigidity			
	Panel shear		Planar shear		Panel shear		Planar shear	
mm	$f_{v,\parallel}$ N/mm^2	$f_{v,\perp}$ N/mm^2	$f_{r,\parallel}$ N/mm^2	$f_{r,\perp}$ N/mm^2	$G_{v,\parallel}$ N/mm^2	$G_{v,\perp}$ N/mm^2	$G_{r,\parallel}$ N/mm^2	$G_{r,\perp}$ N/mm^2
Conifer (spruce) plywood, thick veneers								
13.0	16.7	13.3	10.0	8.0	8170	3830	6682	5318
Birch plywood								
34.1	27.2	24.8	39.2	35.8	10048	7452	9148	8352

Design strength plywood

The design strengths are calculated according to NEN-EN-1995 using equations A.1-A.5 [36].

$$f_{t,0,d} = \frac{f_{t,0,k}}{\gamma_M} \cdot k_{mod} \quad \text{(tensile strength parallel to grain)} \quad \text{(A.1)}$$

$$f_{t,90,d} = \frac{f_{t,90,k}}{\gamma_M} \cdot k_{mod} \quad \text{(tensile strength perpendicular to grain)} \quad \text{(A.2)}$$

$$f_{c,0,d} = \frac{f_{c,0,k}}{\gamma_M} \cdot k_{mod} \quad \text{(compression strength parallel to grain)} \quad \text{(A.3)}$$

$$f_{c,90,d} = \frac{f_{c,90,k}}{\gamma_M} \cdot k_{mod} \quad \text{(compression strength parallel to grain)} \quad \text{(A.4)}$$

$$f_{v,d} = \frac{f_{v,k}}{\gamma_M} \cdot k_{mod} \quad \text{(shear strength parallel and perpendicular to grain)} \quad \text{(A.5)}$$

The material factor γ_M for plywood is 1.2 [NEN-EN-1995 Table 2.3]. The duration factor k_{mod} for plywood in climate class 2 are presented in Table X-X. The duration factor with the shortest duration class should be used. In this case, the wind load has the shortest duration class in the load combinations. Therefore $k_{mod,short}$ is used to define the design strength.

Table B-III: Duration factor k_{mod} [NEN-EN-1995 Table 3.1]

Material		**Norm**	**Climate class**	**Duration class**				
				Permanent	**Long**	**Medium-long**	**Short**	**Very short**
Plywood		Type EN 636-2	2	0.6	0.7	0.8	0.9	1

Calculation design strengths:

$$f_{t,0,d} = \frac{f_{t,0,k}}{\gamma_M} \cdot k_{mod} = \frac{10}{1.2} \cdot 0.9 = 7.5\ MPa$$

$$f_{t,90,d} = \frac{f_{t,90,k}}{\gamma_M} \cdot k_{mod} = \frac{8}{1.2} \cdot 0.9 = 6\ MPa$$

$$f_{c,0,d} = \frac{f_{c,0,k}}{\gamma_M} \cdot k_{mod} = \frac{16.7}{1.2} \cdot 0.9 = 12.53\ MPa$$

$$f_{c,90,d} = \frac{f_{c,90,k}}{\gamma_M} \cdot k_{mod} = \frac{13.3}{1.2} \cdot 0.9 = 9.97\ MPa$$

$$f_{v,d} = \frac{f_{v,k}}{\gamma_M} \cdot k_{mod} = \frac{3.5}{1.2} \cdot 0.9 = 2.63\ MPa$$

Assumptions 2D frame analysis

A 2D frame analysis is performed to determine the forces in the plywood structure. From this calculation, the critical location to place the interlocking timber joints is determined. The 2D frame analysis is a line model of a single plywood module of which the properties are assumed to be similar to GL24c with a cross section of 100 x 236 mm^2 since these values are equal to the strengths from the experimental data.

The mechanical properties of the plywood boxes determined by laboratory tests are:

- Characteristic bending moment $M_k = 19.3\ \text{kNm}$
- Characteristic shear force $V_k = 24.0\ \text{kN}$
- Characteristic bending stiffness $EI_{mean} = 1.20996 \cdot 10^{12}\ N/mm^2 \cdot mm^4$

$$EI_{assumed} = E_{GL24c} \cdot I_{y,GL24c} = E_{GL24c} \cdot \frac{1}{12} \text{b}h^3 = 11000 \cdot 109535467 = 1.21 \cdot 10^{12}\ Nmm^2$$

Load cases

The load cases present on the WikiHouse are stated below in Table B-III. Corresponding values are calculated according to NEN-EN-1991. Each load case is elaborated in the sub sections. Hereafter, load combinations are made.

Table B-III: Load cases

Load case	Description
LC1	Permanent load
LC2	Snow load - centric
LC3	Snow load - eccentric
LC4	Wind load - left side
LC5	Wind load - front
LC6	Wind load - underpressure
LC7	Wind load - overpressure
LC8	Floor load - distributed
LC9	Floor load - concentrated

1. Permanent load (LC1)

The weight of the permanent loads of extracted from the structural report from Lüning.

Table B-IV: Permanent load [wiki]

	Per area		Per module of 1.2 m	
Description	Value	Unit	Value	Unit
Roof	0.65	kN/m^2	0.78	kN/m
Floors	0.75	kN/m^2	0.90	kN/m
Walls	0.50	kN/m^2	0.60	kN/m

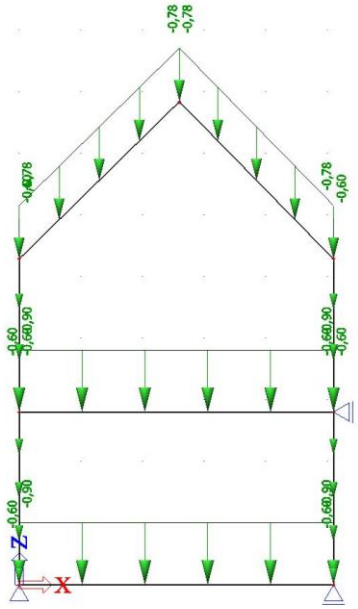

Figure B-III: Permanent load on 2D frame structure

2. Snow load – centric (LC2)

Adjacent roofs

The WikiHouse is situated next to other WikiHouses, thus snow accumulation resulting from adjacent roofs should be taken into account [NEN-EN-1991-1-3].

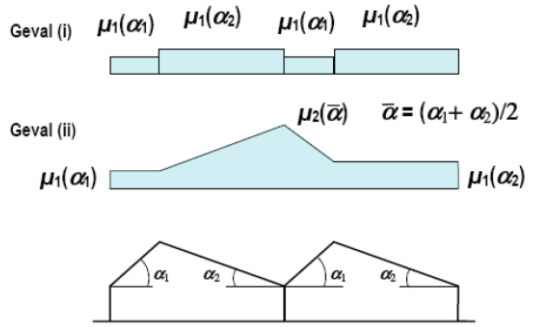

Figure B-IV: Snow accumulation [NEN-EN-1991-1-3 Figure 5.4]

$S_k = 0.70\ kN/m^2$ (characteristic snow force on the ground in the Netherlands)
$\mu_1 = 0.4 \quad for \quad \alpha = 45°$
$\mu_2 = 1.6 \quad for \quad \alpha = 45°$

$S_i = \mu_1 \cdot S_k = 0.4 \cdot 0.70 = 0.28\ kN/m^2$
$S_{ii} = \mu_2 \cdot S_k = 1.6 \cdot 0.70 = 1.12\ kN/m^2$

$S_{i,module} = S_i \cdot b = 0.28 \cdot 1.2 = 0.34\ kN/m^2$
$S_{ii,module} = S_{ii} \cdot b = 1.12 \cdot 1.2 = 1.34\ kN/m^2$

Adjacent taller structures

At the other side of the WikiHouse there is a taller structure.

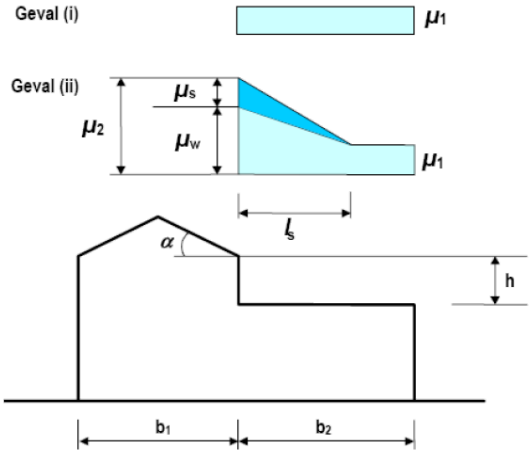

Figure B-V: Snow accumulation from taller structure [NEN-EN-1991-1-3 Figure 5.7]

$h = 2.6\ m$
$b_1 = 5.6\ m$
$b_2 = 5.6\ m$
$\alpha = 30° \quad for \quad 5.0 \leq l_s \leq 15$
$l_s = 2 \cdot h = 2 \cdot 2.6 = 5.2\ m$
$S_k = 0.70\ kN/m^2$
$\rho_{snow} = 2.0\ kN/m^3$

$\mu_1 = 0.8$

$\mu_w = \frac{b_1 + b_2}{2 \cdot h} \leq \frac{Y \cdot h}{S_k} = 2.15 \qquad 0.8 \leq \mu_w \leq 4.0$

$\mu_s = 0.5 \cdot \mu_1 = 0.5 \cdot 0.8 = 0.4$

$\mu_2 = 2.55$

$S_i = \mu_1 \cdot S_k = 0.8 \cdot 0.70 = 0.56\ kN/m^2$

$S_{ii} = \mu_2 \cdot S_k = 2.55 \cdot 0.70 = 1.79\ kN/m^2$

$S_{i,module} = S_i \cdot b = 0.56 \cdot 1.2 = 0.67\ kN/m^2$

$S_{ii,module} = S_{ii} \cdot b = 1.79 \cdot 1.2 = 2.15\, kN/m^2$

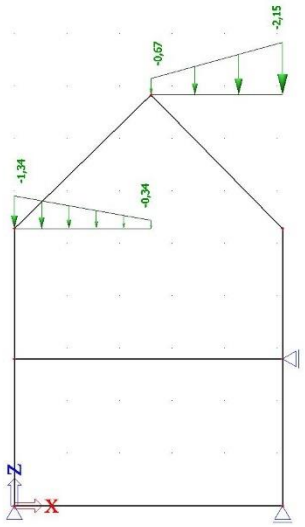

Figure B-VI: Centric snow load on 2D frame structure

3. Snow load – eccentric (LC3)

$S_{i,module} = 0.5 \cdot S_i \cdot b = 0.5 \cdot 0.28 \cdot 1.2 = 0.17\, kN/m^2$

$S_{ii,module} = 0.5 \cdot S_{ii} \cdot b = 0.5 \cdot 1.12 \cdot 1.2 = = 0.67\, kN/m^2$

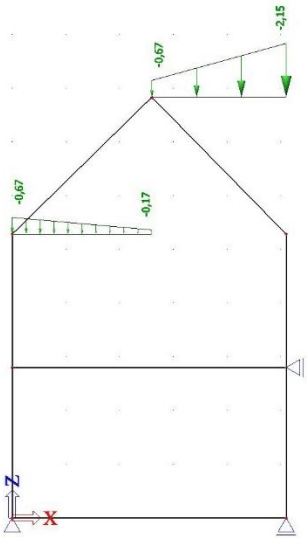

Figure B-VII: Eccentric snow load on 2D frame structure

4. Wind load – general properties (LC4-LC7)

Location: Almere-buiten

Wind zone 2, rural (NEN-EN-1991 4.2 Figure NB.1)

Ridge height = 8.2 m

$q_{p,k} = 0.79 + 0.2 \times (0.82 - 0.79) = 0.796\ kN/m^2 = 0.8\ kN/m^2$ (NEN-EN-1991 Table NB.5)

5. Wind load – left (LC4)

Table X: Wind parameters for wind left

Wind parameter	Value	Unit	Description
b	10.8	m	Dimension perpendicular to wind direction
d	5.1	m	Dimension parallel to wind direction
h	8.2	m	Height
e	10.8 (2.1d)	m	Min(b, 2h)
h/d	1.61	-	

Table X: External pressure coefficients for vertical facades (NEN-EN-1991 Figure 7.5 and Table NB.6)

	Value per zone					Unit
	A	B	C	D	E	
$C_{pe,10}$	-1.2	-0.8	-0.5	+0.8	-0.53	-
W_k	-0.96	-0.63	-0.40	+0.63	-0.42	kN/m^2
$W_{k,module}$	-1.15	-0.76	-0.48	+0.76	-0.50	kN/m
$W_{k,floor1}$*	-2.88	-1.89	-1.2	+1.89	-1.26	kN/m

*wind part to first floor assumed with façade height of 3.0 m

Figure B-VIII: Wind zones [NEN-EN-1991 Figure 7.5]

Table X: External pressure coefficients for gable roofs (NEN-EN-1991 Table NB.10)

	Value per zone					Unit
Zone	F	G	H	I	J	
$C_{pe,10}$ $(\alpha_{+45°})$	+0.7	+0.7	+0.6	-0.2	-0.3	-
W_k	+0.56	+0.56	+0.48	-0.16	-0.24	kN/m^2
$W_{k,module}$	+0.67	+0.67	+0.58	-0.19	-0.29	kN/m

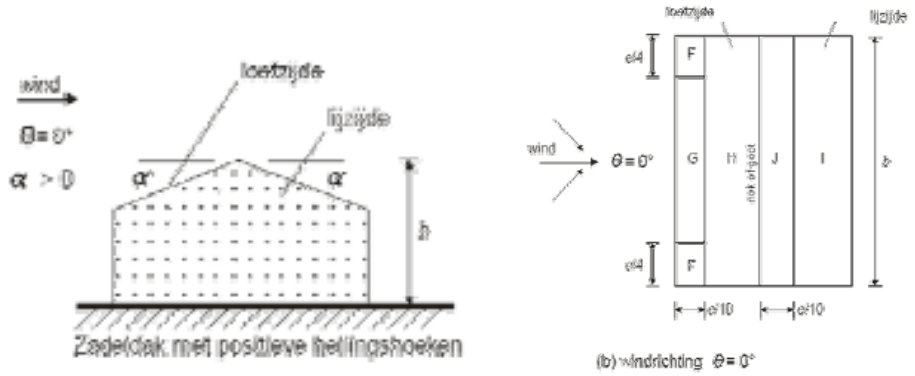

Figure B-IX: Wind zones [NEN-EN-1991]

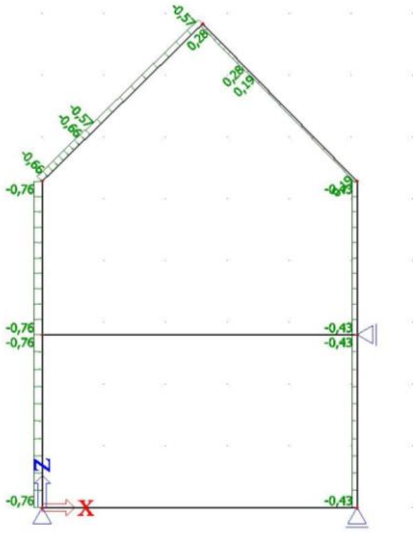

Figure B-X: Wind left on 2D frame

6. Wind load – front (LC5)

Table X: Wind parameters for wind front

Wind parameter	Value	Unit	Description
b	5.1	m	Dimension perpendicular to wind direction
d	10.8	m	Dimension parallel to wind direction
h	8.2	m	Height
e	5.1 (0.47d)	m	Min(b, 2h)
h/d	0.76	-	

Table X: External pressure coefficients for vertical facades (NEN-EN-1991 Figure 7.5 and Table NB.6)

	Value per zone					**Unit**
	A	**B**	**C**	**D**	**E**	
$C_{pe,10}$	-1.2	-0.8	-0.5	+0.8	-0.5	-
W_k	-0.96	-0.63	-0.40	+0.63	-0.40	kN/m^2
$W_{k,module}$	-1.15	-0.76	-0.48	+0.76	-0.48	kN/m
$W_{k,floor1}$*	-2.88	-1.89	-1.2	+1.89	-1.2	kN/m

*wind part to first floor assumed with façade height of 3.0 m

Figure B-XI: Wind zones [NEN-EN-1991 Figure 7.5]

Table B-XI: External pressure coefficients for gable roofs (NEN-EN-1991 Table NB.10)

	Value per zone					**Unit**
Zone	**F**	**G**	**H**	**I**	**J**	
$C_{pe,10}\ (\alpha_{+45°})$	+0.7	+0.7	+0.6	-0.2	-0.3	-
W_k	+0.56	+0.56	+0.48	-0.16	-0.24	kN/m^2
$W_{k,module}$	+0.67	+0.67	+0.58	-0.19	-0.29	kN/m

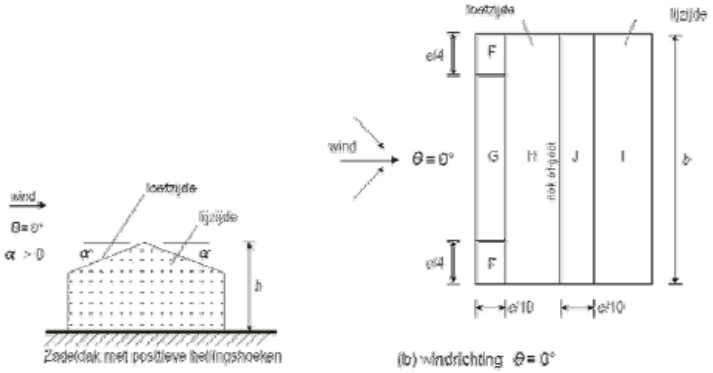

Figure B-XII: Wind zones [NEN-EN-1991]

Friction coefficient $c_{fr} = 0.02$ (for rough surface) [NEN-EN-1991 Table 7.10]

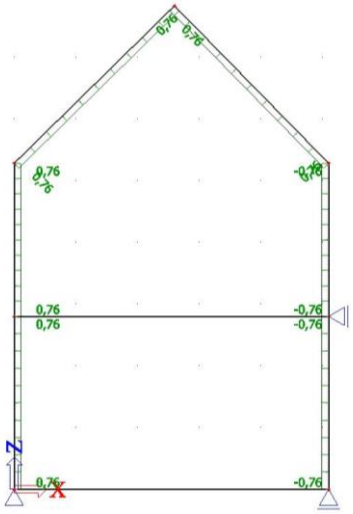

Figure B-XIII: Wind front on 2D frame

7. Wind load – underpressure (LC6)

Internal pressure coefficients:

$C_{pi} = -0.3$ [NEN-EN-1991 Figure 7.13]

$W_k = -0.24$

$W_{k,module} = -0.29$

$W_{k,floor} = -0.72$

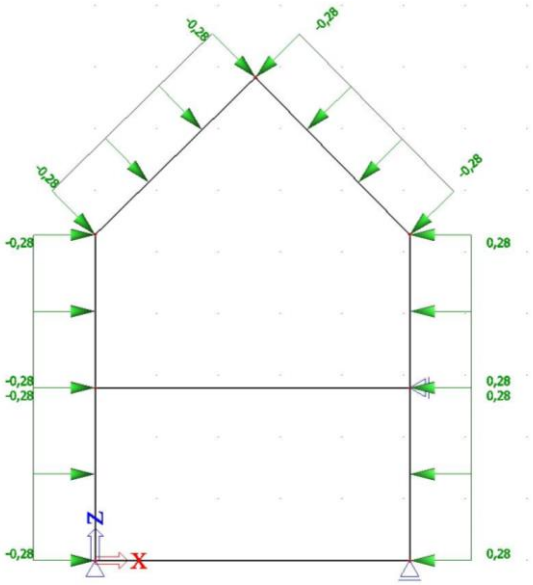

Figure B-XIV: Wind underpressure on 2D frame

8. Wind load – overpressure (LC7)

Internal pressure coefficients:

$C_{pi} = +0.2$ [NEN-EN-1991 Figure 7.13]

$W_k = +0.16$

$W_{k,module} = +0.19$

$W_{k,floor} = +0.48$

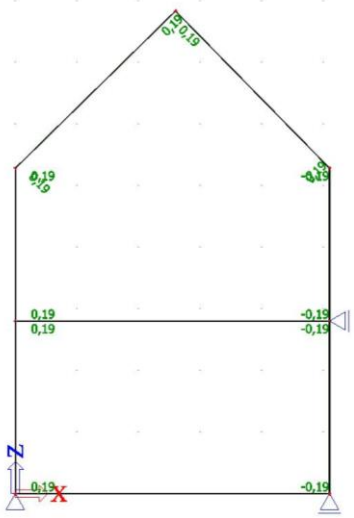

Figure B-XV: Wind overpressure on 2D frame

9. Floor load – distributed (LC8)

Table B-XI: External pressure coefficients for gable roofs [NEN-EN-1991 Table NB.10]

	Per area		Per module of 1.2 m	
Description	**Value**	**Unit**	**Value**	**Unit**
Live load residential	1.75	kN/m^2	2.1	kN/m
Separation walls	0.50	kN/m^2	0.6	kN/m
Total	2.25	kN/m^2	2.7	kN/m

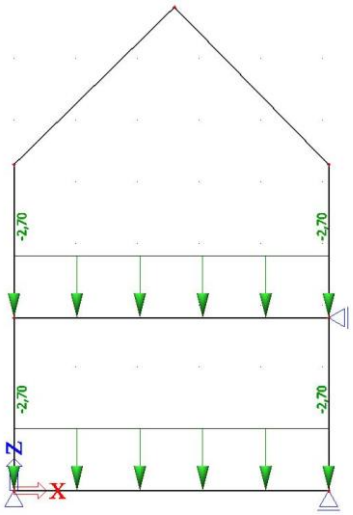

Figure B-XVI: Distributed floor load on 2D frame

10. Floor load – concentrated (LC9)

Live load residential: 3 kN

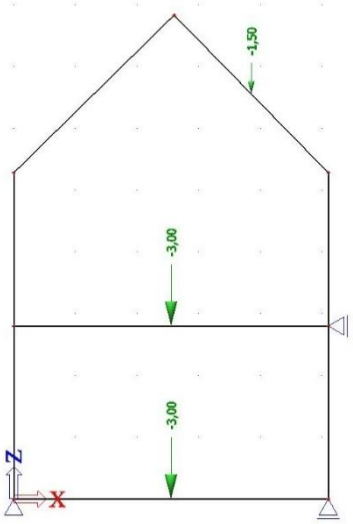

Figure B-XVII: Concentrated floor load on 2D frame

Load combinations

Table B-XII: Partial factors for CC1 for loads (STR/GEO) (group B) [NEN-EN 1990 Table NB.5]

CC	Permanent and temporary design situations	Permanent loads		Predominant variable load
		Unfavourable	Favourable	
1	6.10b	1.1 * G_k,j,sup	0.9 * G_k,j,inf	1.35 * Q_k,1

Table B-XII: Calculation values for loads using load combinations [NEN-EN-1990 Table A1.4]

Combination	Permanent loads G_d		Variable loads Q_d	
	Unfavourable	Favourable	Predominant	Other
Characteristic	G_k,j,sup	G_k,j,inf	Q_k,1	phi_0,i * Q_k,1
Frequent	G_k,j,sup	G_k,j,inf	phi_1,1 * Q_k,1	phi_2,i * Q_k,1
Quasi-permanent	G_k,j,sup	G_k,j,inf	phi_2,1 * Q_k,1	phi_2,i * Q_k,1

Table B-XIV: Phi-factors for buildings [NEN-EN-1990 Table NB2 - A1.1]

	Phi_0	Phi_1	Phi_2
Category A: residential	0.4	0.5	0.3
Snow load	0	0.2	0
Wind load	0	0.2	0

Table B-XV: Load combinations for the Ultimate Limit State

Load combi-nation	Description	Factor								
		LC1	LC2	LC3	LC4	LC5	LC6	LC7	LC8	LC9
C1	1.1*LC1 + 1.35*LC2	1.1	1.35							
C2	1.1*LC1 + 1.35*LC3	1.1		1.35						
C3	1.1*LC1 + 1.35*LC4 + 1.35*LC6	1.1			1.35		1.35			
C4	0.9*LC1 + 1.35*LC4 + 1.35*LC7	0.9			1.35			1.35		
C5	0.9*LC1 + 1.35*LC5 + 1.35*LC7	0.9				1.35		1.35		
C6	1.1*LC1 + 1.35*LC8	1.1							1.35	
C7	1.1*LC1 + 1.35*LC9	1.1								1.35
C8	1.1*LC1 + 1.35*LC2 + 0.54*LC8	1.1	1.35						0.54	
C9	1.1*LC1 + 1.35*LC3 + 0.54*LC8	1.1		1.35					0.54	
C10	1.1*LC1 + 1.35*LC4 + 1.35*LC6 + 0.54*LC8	1.1			1.35		1.35		0.54	
C11	0.9*LC1 + 1.35*LC4 + 1.35*LC7 + 0.54*LC8	0.9			1.35			1.35	0.54	
C12	0.9*LC1 + 1.35*LC5 + 1.35*LC7 + 0.54*LC8	0.9				1.35		1.35	0.54	

Table B-XVI: Load combinations for the Serviceability Limit State characteristic

Load combi-nation	Description	Factor								
		LC1	LC2	LC3	LC4	LC5	LC6	LC7	LC8	LC9
C101	LC1 + LC2	1	1							
C102	LC1 + LC3	1		1						
C103	LC1 + LC4 + LC6	1			1		1			
C104	LC1 + LC4 + LC7	1			1			1		
C105	LC1 + LC5 + LC7	1				1		1		
C106	LC1 + LC8	1							1	
C107	LC1 + LC9	1								1
C108	LC1 + LC2 + 0.4*LC8	1	1						0.4	
C109	LC1 + LC3 + 0.4*LC8	1		1					0.4	
C110	LC1 + LC4 + LC6 + 0.4*LC8	1			1		1		0.4	
C111	LC1 + LC4 + LC7 + 0.4*LC8	1			1			1	0.4	
C112	LC1 + LC5 + LC7 + 0.4*LC8	1				1		1	0.4	

Table B-XVII: Load combinations for the Serviceability Limit State quasi-permanent

Load combi-nation	Description	Factor								
		LC1	LC2	LC3	LC4	LC5	LC6	LC7	LC8	LC9
C201	LC1 + 0.3*LC8	1							0.3	
C202	LC1 + 0.3*LC9	1								0.3

WikiHouse 2D frame analysis

The results of the critical load cases are presented below. A study is done on the XZ-plane frame and a study is done on the first floor in plane YZ as a line with fixed support at the stability wall.

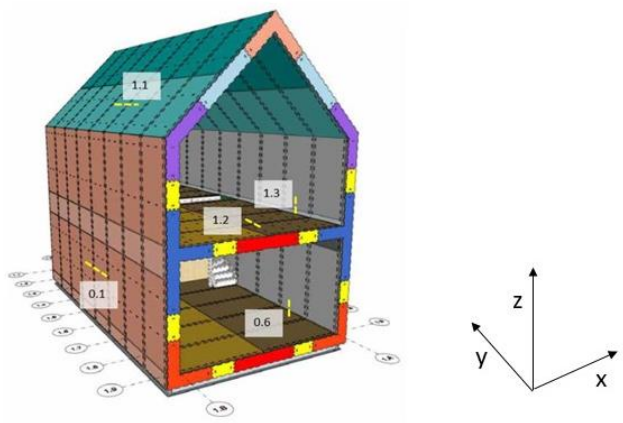

Figure B-XVIII: Coordinate system for WikiHouse 2D frame analysis [42]

SCIA calculation frame XZ

Maximum forces were found in the ULS load combinations. The critical load case for the ultimate limit state is CO8. The maximum tension force is 18.41 kN and occurs in the right bottom wall. The maximum compression force is 5.09 kN and occurs in the ground floor. The maximum shear force is 11.82 and -11.82 kN and occurs in both floors. The maximum bending moment is 9.09 kNm and occurs in the first floor.

ULS

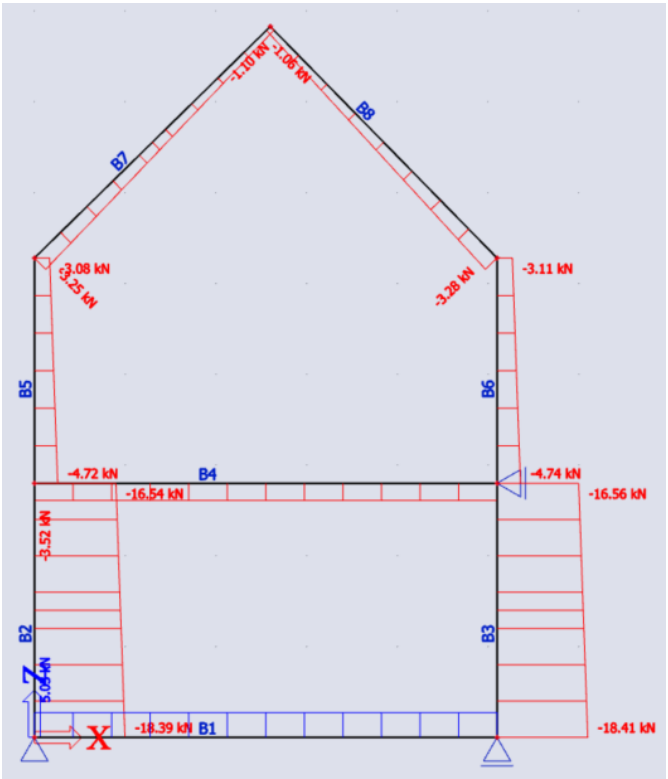

Figure B-XIX: Normal forces for load combination CO8, frame XZ

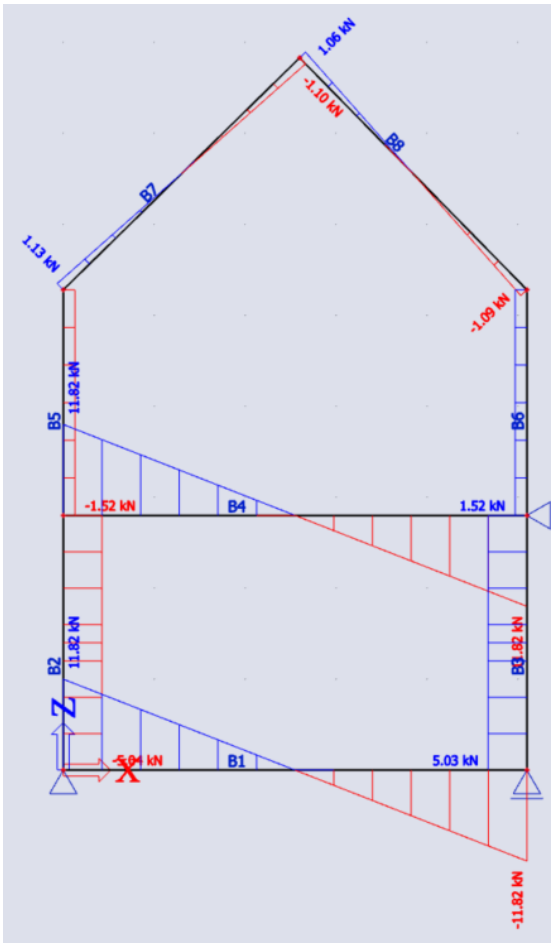

Figure B-XX: Shear forces for load combination CO8, frame XZ

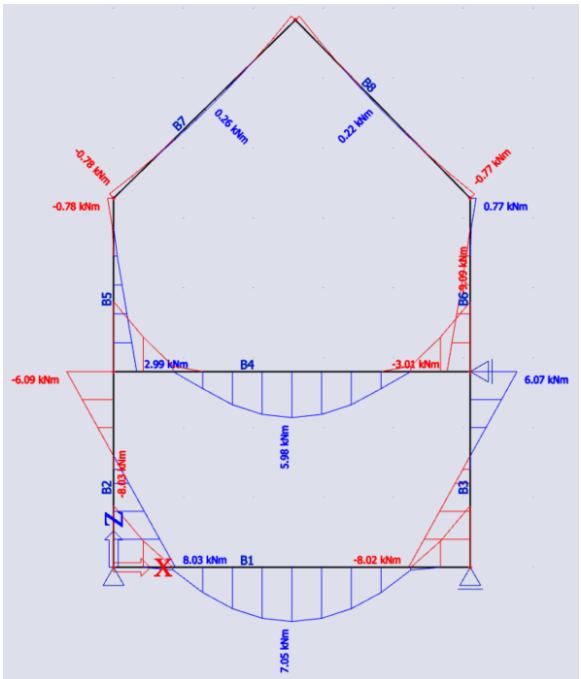

Figure B-XXI: Bending forces for load combination CO8, frame XZ

SCIA calculation frame YZ

The critical load combination is 1.35 times LC4 wind left plus 1.35 times LC7 wind overpressure. The first floor of the WikiHouse (seen from frame YZ) is represented as a line with a fixed support at the location of the stability wall at module 4, see Figure B-XXII. The maximum normal force is 19.21 kN, the maximum shear force is -47.22 kN and the maximum bending moment is 141.67 kNm.

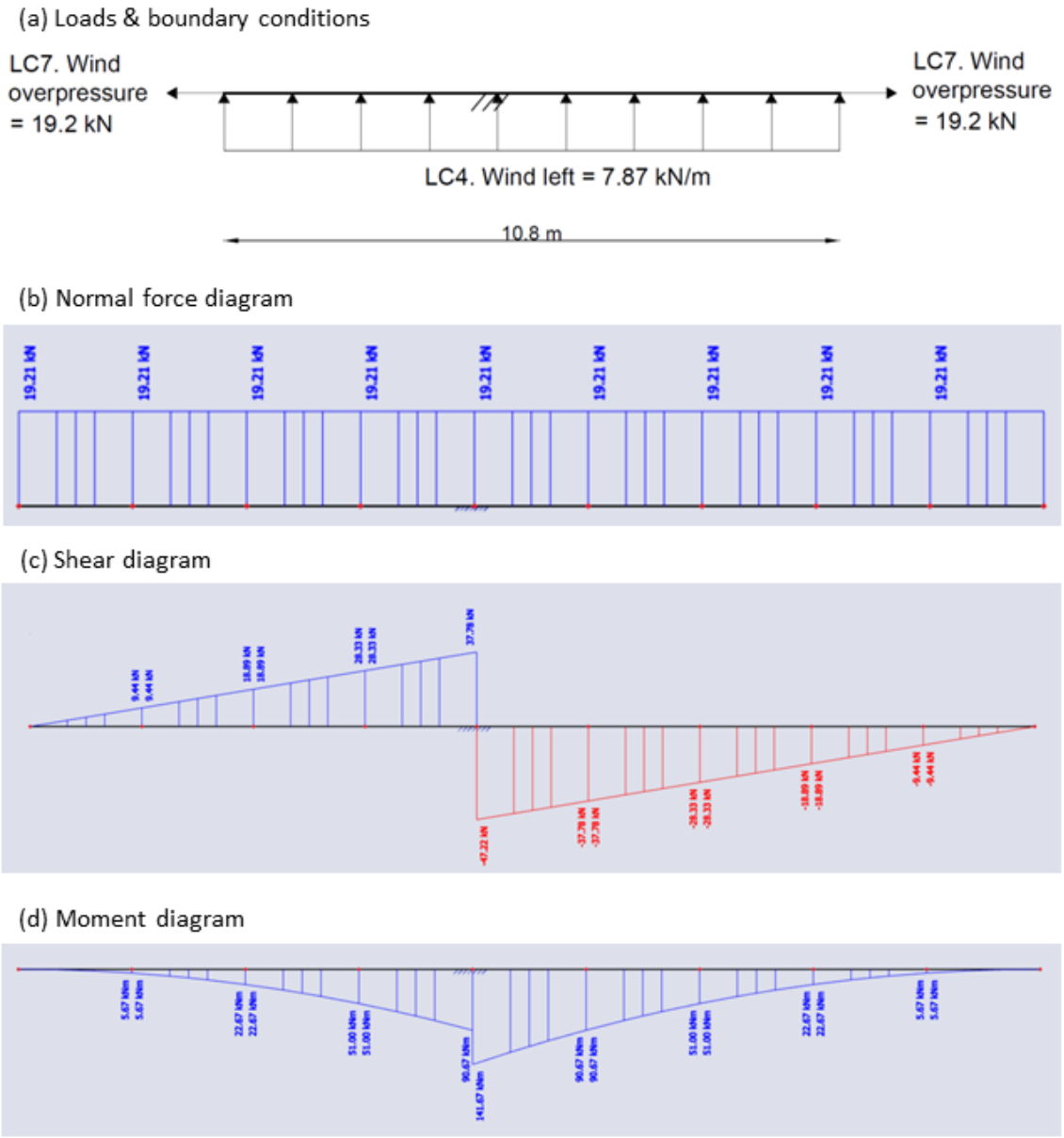

Figure B-XXII: Wind left on first floor WikiHouse (frame YZ)

Hand calculation frame YZ

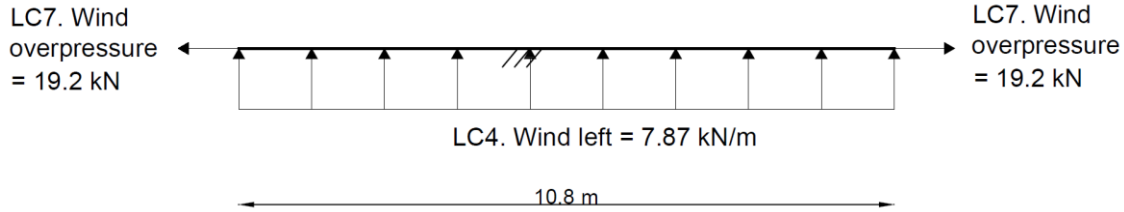

Figure B-XXIII: Loads and boundary conditions of first floor hand calculation

Load combination $\boldsymbol{C_{crit}} = \mathbf{1.35} \cdot (\boldsymbol{LC4} + \boldsymbol{LC7})$

$R_{x,SCIA} = 10.85\ kN$

$\frac{h}{d} = \frac{8.4}{5.5} = 1.53$

$correlation\ factor = 0.85 + \frac{(1.0 - 0.85)}{(5 - 1)} \cdot (1.53 - 1) = 0.87$

$F_{h,d} = \frac{0.87 \cdot 10.85}{1.2} = 7.87\ kN/m$

$Zone\ A = 1.35 \cdot 0.96 \cdot \frac{10.8}{5} \cdot 3 = 8.40\ kN$

$Zone\ B = 1.35 \cdot 0.63 \cdot (5.1 - \frac{10.8}{5}) \cdot 3 = 7.50\ kN$

$Overpressure = 1.35 \cdot 0.16 \cdot 5.1 \cdot 3 = 3.30\ kN$

$\sum F_v \uparrow^+ = 0: 7.87 \cdot 10.8 - R_V = 0$

$R_V = 85.00\ kN$

Part left:

$\sum \overset{+}{\underset{F_H}{\leftarrow}} = 0: 19.2 - R_{H,l} = 0$

$R_{H,l} = 19.20\ kN$

$\sum \overset{+}{\underset{M}{\curvearrowleft}} = 0: -7.87 \cdot 4.8 \cdot 2.4 + R_{M,l} = 0$

$R_{M,l} = 90.66\ kNm$

Part right:

$\sum \overset{+}{\underset{F_H}{\rightarrow}} = 0: 19.2 - R_{H,r} = 0$

$R_{H,r} = 19.2\ kN$

$\sum \overset{+}{\underset{M}{\curvearrowright}} = 0: -7.87 \cdot 6 \cdot 3 + R_{M,r} = 0$

$R_{M,r} = 141.66\ kN$

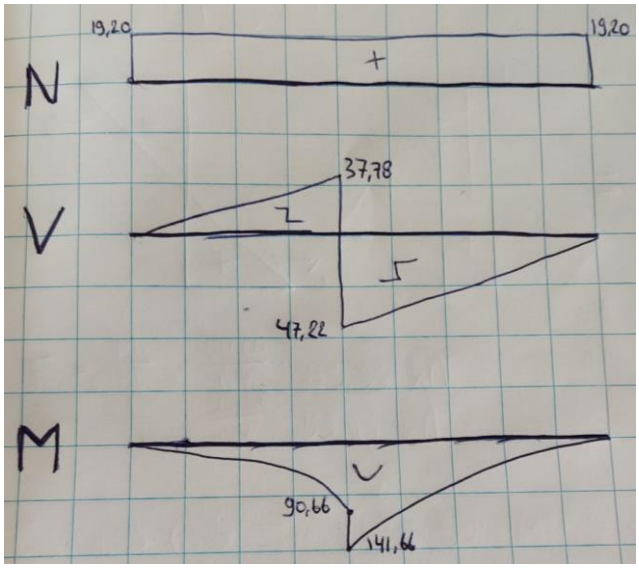

Figure B-XXIV: Force diagrams first floor hand calculation

$$\sigma_t = \frac{M_t}{W} + \frac{N_1}{A}$$
$$\sigma_c = -\frac{M_t}{W} + \frac{N_2}{A}$$

$$W = \frac{1}{6}bh^2 = \frac{1}{6} \cdot 18 \cdot 5100^2 = 78.03 \cdot 10^6\ mm^3$$
$M_R = 141.66\ kNm = 141.66 \cdot 10^6\ Nmm$ (right of stability wall)
$\sigma_{b,R} = \frac{M}{W} = \frac{141.66 \cdot 10^6}{78.03 \cdot 10^6} = 1.82\ N/mm^2$ (right of stability wall)
$M_L = 90.66\ kNm = 90.66 \cdot 10^6\ Nmm$ (left of stability wall)
$\sigma_{b,L} = \frac{M}{W} = \frac{90.66 \cdot 10^6}{78.03 \cdot 10^6} = 1.16\ N/mm^2$ (left of stability wall)

$$F_{V,1} = \frac{3}{2} \cdot 47.22 = 70.83\ kN$$
$$F_{V,2} = \frac{3}{2} \cdot 37.78 = 56.67\ kN$$

$$N_{A+O} = \frac{1.35 \cdot (0.96 + 0.16) \cdot 3000}{18 \cdot 1000} = 0.25\ N/mm^2$$
$$N_{B+O} = \frac{1.35 \cdot (0.63 + 0.16) \cdot 3000}{18 \cdot 1000} = 0.18\ N/mm^2$$

$\sigma_{t,R} = 1.82 + 0.25 = 2.07\ N/mm^2$ (right of stability wall)
$\sigma_{c,R} = -1.82 + 0.18 = -1.64\ N/mm^2$ (right of stability wall)
$\sigma_{v,R} = \frac{70.83}{18 \cdot 5.1} = 0.77\ N/mm^2$ (right of stability wall)

$\sigma_{t,L} = 1.16 + 0.25 = 1.41\ N/mm^2$ (left of stability wall)
$\sigma_{c,L} = -1.16 + 0.18 = -0.91\ N/mm^2$ (left of stability wall)
$\sigma_{v,L} = \frac{56.67}{18 \cdot 5.1} = 0.62\ N/mm^2$ (left of stability wall)

Appendix C: Input script dovetail

```
'''PARAMETRIC INPUT SCRIPT FOR ABAQUS CAE
INTERLOCKING TIMBER CONNECTION SHAPE: DOVETAIL'''



# 1. IMPORT LIBRARIES
# 1.1 Python libraries
import math
import csv
import numpy as np


# 1.2 Abaqus CAE libraries
# -*- coding: mbcs -*-
from part import *
from material import *
from section import *
from assembly import *
from step import *
from interaction import *
from load import *
from mesh import *
from optimization import *
from job import *
from sketch import *
from visualization import *
from xyPlot import*
from connectorBehavior import *
from odbAccess import*


#------------------------------------------------------------------


# 2. METHODS
class Definitions:
    def __init__(self,part_name_L, part_name_R, job_name_A, job_name_B, job_name_C,
    seq_L, seq_R):
        self.part_name_L = part_name_L
        self.part_name_R = part_name_R
        self.instance_name_L = part_name_L+'-1'
        self.instance_name_R = part_name_R+'-1'
        self.job_name_A = job_name_A
        self.job_name_B = job_name_B
        self.job_name_C = job_name_C
        self.seq_L = seq_L
        self.seq_R = seq_R


```

```
class Part:
    def __init__(self,h_t,w_t,h_1,w_1,w_2,fr):
        self.h_t = h_t
        self.w_t = w_t
        self.h_1 = h_1
        self.w_1 = w_1
        self.w_2 = w_2
        self.fr = fr
        self.angle = math.atan(h_1/((w_1-w_2)/2))    #[rad]


    def create_coords(self):
        xyCoords_L = [((-self.h_t),0), ((-self.h_t),self.w_t), ((self.h_1/2),self.w_t
        ), ((self.h_1/2),(self.w_t-(self.w_t-self.w_2)/2)),
            ((-self.h_1/2),(self.w_t-(self.w_t-self.w_1)/2)), ((-self.h_1/2),((self.
            w_t-self.w_1)/2)), ((self.h_1/2),((self.w_t-self.w_2)/2)),
            ((self.h_1/2),0), ((-self.h_t),0)]
        xyCoords_R = [(self.h_t,0), (self.h_t,self.w_t), ((self.h_1/2),self.w_t), ((
        self.h_1/2),(self.w_t-(self.w_t-self.w_2)/2)),
            ((-self.h_1/2),(self.w_t-(self.w_t-self.w_1)/2)), ((-self.h_1/2),((self.
            w_t-self.w_1)/2)), ((self.h_1/2),((self.w_t-self.w_2)/2)), ((self.h_1/2),0
            ), (self.h_t,0)]


        return xyCoords_L, xyCoords_R


    def create_part(self,xyCoords, part_name):

        mdb.models['Model-1'].ConstrainedSketch(name='__profile__', sheetSize=200.0)

        for i in range(len(xyCoords)-1):
            mdb.models['Model-1'].sketches['__profile__'].Line(point1=xyCoords[i],
            point2=xyCoords[i+1])

        mdb.models['Model-1'].Part(dimensionality=TWO_D_PLANAR, name=part_name,type=
        DEFORMABLE_BODY)
        mdb.models['Model-1'].parts[part_name].BaseShell(sketch=mdb.models['Model-1'].
        sketches['__profile__'])
        del mdb.models['Model-1'].sketches['__profile__']


    def create_fillets(self, part_name):
        mdb.models['Model-1'].ConstrainedSketch(name='__edit__', objectToCopy=
            mdb.models['Model-1'].parts[part_name].features['Shell planar-1'].sketch)
        mdb.models['Model-1'].parts[part_name].projectReferencesOntoSketch(filter=
            COPLANAR_EDGES, sketch=mdb.models['Model-1'].sketches['__edit__'],
            upToFeature=mdb.models['Model-1'].parts[part_name].features['Shell
            planar-1'])
        mdb.models['Model-1'].sketches['__edit__'].FilletByRadius(curve1=
            mdb.models['Model-1'].sketches['__edit__'].geometry[4], curve2=
            mdb.models['Model-1'].sketches['__edit__'].geometry[5], nearPoint1=(
            (self.h_1/2),(self.w_t-((self.w_t-self.w_2)/2)+(2*self.fr))), nearPoint2
            =(((self.h_1/2)-(2*self.fr*math.cos(math.pi/2-self.angle))),(self.w_t-((
            self.w_t-self.w_2)/2)+(2*self.fr*math.sin(math.pi/2-self.angle)))), radius
            =self.fr)
        mdb.models['Model-1'].sketches['__edit__'].FilletByRadius(curve1=
            mdb.models['Model-1'].sketches['__edit__'].geometry[5], curve2=
            mdb.models['Model-1'].sketches['__edit__'].geometry[6], nearPoint1=(
            ((-self.h_1/2)+(2*self.fr*math.cos(math.pi/2-self.angle))),(self.w_t-((
            self.w_t-self.w_1)/2)-(2*self.fr*math.sin(math.pi/2-self.angle)))),
            nearPoint2=((-self.h_1/2),(self.w_t-((self.w_t-self.w_1)/2)-(2*self.fr))),
             radius=self.fr)
```

```
98          mdb.models['Model-1'].sketches['__edit__'].FilletByRadius(curve1=
99              mdb.models['Model-1'].sketches['__edit__'].geometry[6], curve2=
100             mdb.models['Model-1'].sketches['__edit__'].geometry[7], nearPoint1=(
101             (-self.h_1/2),(((self.w_t-self.w_1)/2)+(2*self.fr))), nearPoint2=(((-self.
                h_1/2)+(2*self.fr*math.cos(math.pi/2-self.angle))),(((self.w_t-self.w_1)/2
                )+(2*self.fr*math.sin(math.pi/2-self.angle)))), radius=self.fr)
102         mdb.models['Model-1'].sketches['__edit__'].FilletByRadius(curve1=
103             mdb.models['Model-1'].sketches['__edit__'].geometry[7], curve2=
104             mdb.models['Model-1'].sketches['__edit__'].geometry[8], nearPoint1=(
105             ((self.h_1/2)-(2*self.fr*math.cos(math.pi/2-self.angle))),(((self.w_t-self
                .w_2)/2)-(2*self.fr*math.sin(math.pi/2-self.angle)))), nearPoint2=(((self.
                h_1/2),((self.w_t-self.w_2)/2)-(2*self.fr))), radius=self.fr)
106         mdb.models['Model-1'].parts[part_name].features['Shell planar-1'].setValues(
107             sketch=mdb.models['Model-1'].sketches['__edit__'])
108         del mdb.models['Model-1'].sketches['__edit__']
109         mdb.models['Model-1'].parts[part_name].regenerate()
110
111
112     def create_partition(self, part_name, int_edge1, int_edge2, loc):
113         mdb.models['Model-1'].parts[part_name].PartitionFaceByShortestPath(faces=mdb.
            models['Model-1'].parts[part_name].faces.getSequenceFromMask(('[#1 ]', ), ),
114             point1=mdb.models['Model-1'].parts[part_name].InterestingPoint(mdb.models[
                'Model-1'].parts[part_name].edges[int_edge1], loc),
115             point2=mdb.models['Model-1'].parts[part_name].InterestingPoint(mdb.models[
                'Model-1'].parts[part_name].edges[int_edge2], loc))
116
117
118 class Property:
119     def __init__(self,material_name, rho, E1, E2, E3, Nu12, Nu13, Nu23, G12, G13, G23,
         section_name, mat_rotation, rotation_axis, stack_dir):
120         self.material_name = material_name
121         self.rho = rho
122         self.E1 = E1
123         self.E2 = E2
124         self.E3 = E3
125         self.Nu12 = Nu12
126         self.Nu13 = Nu13
127         self.Nu23 = Nu23
128         self.G12 = G12
129         self.G13 = G13
130         self.G23 = G23
131         self.section_name = section_name
132         self.mat_rotation = mat_rotation
133         self.rotation_axis = rotation_axis
134         self.stack_dir = stack_dir
135
136
137     def create_material(self):
138         mdb.models['Model-1'].Material(name=self.material_name)
139         mdb.models['Model-1'].materials[self.material_name].Density(table=((self.rho,
            ), ))
140         mdb.models['Model-1'].materials[self.material_name].Elastic(table=((self.E1,
            self.E2, self.E3, self.Nu12, self.Nu13, self.Nu23,
141             self.G12, self.G13, self.G23), ), type=ENGINEERING_CONSTANTS)
142
143
144     def create_sol_hom_section(self):
145         mdb.models['Model-1'].HomogeneousSolidSection(self.section_name, self.
            material_name, thickness=None)
146
147
```

```
148         def assign_section_prop(self, part_name, seq):
149             mdb.models['Model-1'].parts[part_name].Set(faces=mdb.models['Model-1'].parts[
                part_name].faces.getSequenceFromMask((seq, ), ), name='Set-1')
150             mdb.models['Model-1'].parts[part_name].SectionAssignment(offset=0.0,
                offsetField='', offsetType=MIDDLE_SURFACE, region=
151                 mdb.models['Model-1'].parts[part_name].sets['Set-1'], sectionName=self.
                    section_name, thicknessAssignment=FROM_SECTION)
152
153
154         def create_mat_orient(self, part_name, seq):
155             mdb.models['Model-1'].parts[part_name].MaterialOrientation(
                additionalRotationType=self.mat_rotation, axis=self.rotation_axis,
156                 fieldName='', localCsys=None, orientationType=GLOBAL, region=Region(
157                 faces=mdb.models['Model-1'].parts[part_name].faces.getSequenceFromMask(
                    mask=(seq, ), )), stackDirection=self.stack_dir)
158
159
160
161     class Assembly:
162         def create_instances(self, part_name_L, part_name_R, instance_name_L,
            instance_name_R, dependency=OFF):
163             mdb.models['Model-1'].rootAssembly.DatumCsysByDefault(CARTESIAN)
164
165             instance_L = mdb.models['Model-1'].rootAssembly.Instance(dependent=dependency,
                 name=instance_name_L,
166                 part=mdb.models['Model-1'].parts[part_name_L])
167             instance_R = mdb.models['Model-1'].rootAssembly.Instance(dependent=dependency,
                 name=instance_name_R,
168                 part=mdb.models['Model-1'].parts[part_name_R])
169
170             return instance_L, instance_R
171
172
173         def create_ref_points(self, h_t, w_t, h_1):
174             RP_axial = mdb.models['Model-1'].rootAssembly.ReferencePoint(point=((-h_t),(
                w_t/2),0))
175             RP_shear = mdb.models['Model-1'].rootAssembly.ReferencePoint(point=(h_1/2,(w_t
                /2),0))
176
177             return RP_axial, RP_shear
178
179
180         def create_set_from_RP(self, set_name, RP_point):
181             mdb.models['Model-1'].rootAssembly.Set(name=set_name, referencePoints=(mdb.
                models['Model-1'].rootAssembly.referencePoints[RP_point], ))
182
183
184         def create_set_from_instance(self, instance_name, set_name, seq):
185             mdb.models['Model-1'].rootAssembly.Set(edges=mdb.models['Model-1'].
                rootAssembly.instances[instance_name].edges.getSequenceFromMask(
186                 (seq, ), ), name=set_name)
187
188
189         def create_set_from_2instances(self, instance_name_L, instance_name_R, set_name,
            seq_L, seq_R):
190             mdb.models['Model-1'].rootAssembly.Set(edges=mdb.models['Model-1'].
                rootAssembly.instances[instance_name_L].edges.getSequenceFromMask(
191                 mask=(seq_L, ), )+\
192                     mdb.models['Model-1'].rootAssembly.instances[instance_name_R].edges.
                        getSequenceFromMask(mask=(seq_R, ), ), name=set_name)
193
194
195
```

```
205 class Interaction:
206     def __init__(self, int_prop_name, general_int_name):
207         self.int_prop_name = int_prop_name
208         self.general_int_name = general_int_name
209 
210 
211     def create_contact_int_prop(self):
212         mdb.models['Model-1'].ContactProperty(self.int_prop_name)
213         mdb.models['Model-1'].interactionProperties[self.int_prop_name].
            TangentialBehavior(formulation=FRICTIONLESS)
214 
215 
216     def create_general_interaction(self,step_name, previous_step='Initial'):
217         mdb.models['Model-1'].StaticStep(name=step_name, previous=previous_step)
218         mdb.models['Model-1'].ContactProperty(self.int_prop_name)
219         mdb.models['Model-1'].interactionProperties[self.int_prop_name].
            TangentialBehavior(formulation=FRICTIONLESS)
220         mdb.models['Model-1'].ContactStd(createStepName='Initial', name=self.
            general_int_name)
221         mdb.models['Model-1'].interactions[self.general_int_name].includedPairs.
            setValuesInStep(stepName='Initial', useAllstar=ON)
222         mdb.models['Model-1'].interactions[self.general_int_name].
            contactPropertyAssignments.appendInStep(
223             assignments=((GLOBAL, SELF, self.int_prop_name), ), stepName='Initial')
224 
225 
226 class Load:
227     def __init__(self, stress_t, stress_c, stress_s,):
228         self.stress_t = stress_t
229         self.stress_c = stress_c
230         self.stress_s = stress_s
231 
232 
233     def create_tie_rigid_body_constraint(self,RBC_name,set_name_region, set_name_RP):
234         mdb.models['Model-1'].RigidBody(name=RBC_name, tieRegion=mdb.models['Model-1'
            ].rootAssembly.sets[set_name_region], refPointRegion=
235             mdb.models['Model-1'].rootAssembly.sets[set_name_RP])
236 
237 
238     def define_loads(self,h_t, w_t, fh, fw):
239         load_t = self.stress_t/fh*h_t       #Tensile point load [N]
240         load_c = self.stress_c/fh*h_t       #Compressive point load [N]
241         load_s = self.stress_s/fw*w_t       #Shear point load [N]
242 
243         return load_t, load_c, load_s
244 
245 
246     def create_load(self,load_name, F1, F2, RP_set, step_name='Load'):
247         mdb.models['Model-1'].ConcentratedForce(cf1=F1, cf2=F2, createStepName=
            step_name, distributionType=UNIFORM, field='',
248             localCsys=None, name=load_name, region=mdb.models['Model-1'].rootAssembly.
                sets[RP_set])
249 
250 
251     def create_displacement_BC_fixed(self, BC_name, set_name, step_name='Initial'):
252         mdb.models['Model-1'].DisplacementBC(amplitude=UNSET, createStepName=step_name
            ,
253             distributionType=UNIFORM, fieldName='', localCsys=None, name=BC_name,
254             region=mdb.models['Model-1'].rootAssembly.sets[set_name], u1=SET, u2=SET,
                ur3=SET)
255 
256 
```

```
257         def create_displacement_BC_roller(self, BC_name, set_name, fixed_dir, step_name=
            'Initial'):
258             if fixed_dir=='u1':
259                 mdb.models['Model-1'].DisplacementBC(amplitude=UNSET, createStepName=
                    step_name,
260                     distributionType=UNIFORM, fieldName='', localCsys=None, name=BC_name,
261                     region=mdb.models['Model-1'].rootAssembly.sets[set_name], u1=SET, u2=
                        UNSET, ur3=UNSET)
262             elif fixed_dir=='u2':
263                 mdb.models['Model-1'].DisplacementBC(amplitude=UNSET, createStepName=
                    step_name,
264                     distributionType=UNIFORM, fieldName='', localCsys=None, name=BC_name,
265                     region=mdb.models['Model-1'].rootAssembly.sets[set_name], u1=UNSET, u2
                        =SET, ur3=UNSET)
266             else:
267                 pass
268
269
270         def create_Ysym_BC(self, sym_name, set_name, step_name='Initial'):
271             mdb.models['Model-1'].YsymmBC(createStepName='Initial', localCsys=None, name=
272                 sym_name, region=mdb.models['Model-1'].rootAssembly.sets[set_name])
273
274
275
276     class Mesh:
277         def seed_edge_by_number(self, instance_name, seq, mesh_number):
278             mdb.models['Model-1'].rootAssembly.seedEdgeByNumber(constraint=FINER, edges=
279                 mdb.models['Model-1'].rootAssembly.instances[instance_name].edges.
                    getSequenceFromMask(
280                     (seq, ), ), number=mesh_number)
281
282         def seed_edge_by_size(self, instance_name, seq, mesh_size):
283             mdb.models['Model-1'].rootAssembly.seedEdgeBySize(constraint=FINER,
                deviationFactor=0.1, edges=
284                 mdb.models['Model-1'].rootAssembly.instances[instance_name].edges.
                    getSequenceFromMask((seq, ), ), size=mesh_size)
285
286         def seed_2edges_by_size(self, instance_name_L, instance_name_R, seq_L, seq_R,
            mesh_size):
287             mdb.models['Model-1'].rootAssembly.seedEdgeBySize(constraint=FINER,
                deviationFactor=0.1, edges=
288                 mdb.models['Model-1'].rootAssembly.instances[instance_name_L].edges.
                    getSequenceFromMask(mask=(seq_L, ), )+\
289                 mdb.models['Model-1'].rootAssembly.instances[instance_name_R].edges.
                    getSequenceFromMask(mask=(seq_R, ), ), size=mesh_size)
290
291         def seed_global(self, instance_name_L, instance_name_R, mesh_size):
292             mdb.models['Model-1'].rootAssembly.seedPartInstance(deviationFactor=0.1,
                minSizeFactor=0.1, regions=(
293                 mdb.models['Model-1'].rootAssembly.instances[instance_name_L],
294                 mdb.models['Model-1'].rootAssembly.instances[instance_name_R]), size=
                    mesh_size)
295
296         def define_mesh_shape(self,instance_name_L, instance_name_R,mesh_shape):
297             mdb.models['Model-1'].rootAssembly.setMeshControls(elemShape=mesh_shape,
                regions=
298                 mdb.models['Model-1'].rootAssembly.instances[instance_name_L].faces.
                    getSequenceFromMask(
299                     mask=('[#1 ]', ), )+\
300                 mdb.models['Model-1'].rootAssembly.instances[instance_name_R].faces.
                    getSequenceFromMask(
301                     mask=('[#7 ]', ), ))
302             #Choose mesh_shape: QUAD_DOMINATED, QUAD or TRI. By default, QUAD_DOMINATED
                is chosen.
303
```

```
304         def generate_mesh(self, instance_name_L, instance_name_R):
305             mdb.models['Model-1'].rootAssembly.generateMesh(regions=(mdb.models['Model-1'
            ].rootAssembly.instances[instance_name_L],
306                 mdb.models['Model-1'].rootAssembly.instances[instance_name_R]))
307
308
309
310     class Job:
311         def create_job(self,job_name):
312            mdb.Job(atTime=None, contactPrint=OFF, description='', echoPrint=OFF,
               explicitPrecision=SINGLE, getMemoryFromAnalysis=True,
313                 historyPrint=OFF, memory=90, memoryUnits=PERCENTAGE, model='Model-1',
                    modelPrint=OFF, multiprocessingMode=DEFAULT,
314                 name=job_name, nodalOutputPrecision=SINGLE, numCpus=1, numGPUs=0, queue=
                    None, resultsFormat=ODB, scratch='', type=ANALYSIS,
315                 userSubroutine='', waitHours=0, waitMinutes=0)
316
317
318         def submit_job(self, job_name):
319             mdb.jobs[job_name].submit(consistencyChecking=OFF)
320
321
322         def supress_constraint(self, constraint):
323             mdb.models['Model-1'].constraints[constraint].suppress()
324
325         def resume_constraint(self, constraint):
326             mdb.models['Model-1'].constraints[constraint].resume()
327
328         def supress_load(self, load):
329             mdb.models['Model-1'].loads[load].suppress()
330
331         def resume_load(self, load):
332             mdb.models['Model-1'].loads[load].resume()
333
334         def supress_BC(self, boundary_condition):
335             mdb.models['Model-1'].boundaryConditions[boundary_condition].suppress()
336
337         def resume_BC(self, boundary_condition):
338             mdb.models['Model-1'].boundaryConditions[boundary_condition].resume()
339
340
341     #-------------------------------------------------------------------
342
343
344     # 3. VARIABLES
345     '''Define your variables in this section.'''
346
347     # 3.1 Load-length factor
348     '''Assumption: 10 connections per meter floor. However, this assumption can be
        changed by changing the load-length factor.
349     Example 1: When the load-length factor is 2, you assume that there are 5 connections
        per meter.
350     Example 2: When the load-length factor is 0.5, you assume that there are 20
        connections per meter.'''
351     myFh = 1                        #load height factor
352     myFw = 1                        #load width factor
353
354     # 3.2 Total dimensions of one element
355     myH_t = myFh*100                  #Total height of one plywood element [mm]
356     myW_t = myFw*100                  #Total width of one plywood element [mm]
357
358     # 3.3 Dimensions dovetail connection
359     '''Look at Figure X for the corresponding dimensions on the connection
        illustration.'''
```

```
myH_1 = 50                    #height 1 [mm]
myW_1 = 85                    #width 1 [mm]
myW_2 = 15                    #width 2 [mm]
myFr = 5                     #fillet radius [mm]

# 3.4 Define material properties
'''The equivalent properties need to be defined below. The equivalent Poisson's ratio can be calculated according
to the classical lamination theory using the Poisson's ratio of the timber species used for the plywood.
In this case, spruce timber is used.'''
myMaterial_name = 'Conifer plywood thick veneers 18 mm'
myRho = 8300.0                #Density [tonne/mm3]
myE1 = 6682.0                 #Young's Modulus longitudinal direction [MPa]
myE2 = 5318.0                 #Young's Modulus transverse direction [MPa]
myE3 = 5318.0                 #Young's Modulus radial direction [MPa] (This property is irrelevant for a 2D planar simulation, though a non-zero value should be included)
myNu12 = 0.040                #Poisson's ratio longitudinal transeverse plane [-]
myNu13 = 0.191                #Poisson's ratio longitudinal radial plane [-] (This property is irrelevant for a 2D planar simulation)
myNu23 = 0.248                #Poisson's ratio transeverse radial plane [-] (This property is irrelevant for a 2D planar simulation)
myG12 = 350.0                 #Shear Modulus longitudinal transverse plane [MPa]
myG13 = 52.0                  #Shear Modulus longitudinal radial plane [MPa]
myG23 = 38.0                  #Shear Modulus transeverse radial plane [MPa]


# 3.5 Define loads
myName_load_t = 'A - Tension parallel'        #Tensile load applied parallel to the grain
myName_load_c = 'B - Compression parallel'    #Compression load applied parallel to the grain
myName_load_s = 'C - Shear (panel)'           #Shear load in-plane
myStress_t = -2.51                            #Tensile stress (parallel) [MPa]
myStress_c = 1.86                             #Compressive stress (parallel) [MPa]
myStress_s = -0.83                            #Shear stress (panel) [MPa]

# 3.6 Define mesh refinement
    # 3.6.1 Mesh edge seeding by size
'''A smooth transition of mesh fineness between adjacent elements results in a better mesh quality.
Always check the quality of your mesh in Abaqus CAE.'''
myMesh_s_p = 1                                #Size of local mesh elements at partition [mm]
myMesh_s_c = 1                                #Size of local mesh elements along connection part [mm]
myMesh_s_e = 16                               #Size of local mesh elements at the ends of the parts [mm]
myMesh_s_g = 8                                #Size of global mesh elements [mm]

    # 3.6.2 Mesh element shape
myMesh_shape = QUAD   #Choose: QUAD, QUAD_DOMINATED OR TRI. Write everything in upper case.

# 3.7 Define job names
'''It is important to give each simulation a different job name,
otherwise jobs will be overwritten and data will be lost'''
A = str(myH_1).replace(".","")
B = str(myW_1).replace(".","")
C = str(myW_2).replace(".","")
D = str(myMesh_shape)
E = str(myMesh_s_p).replace(".","")
F = str(myMesh_s_c).replace(".","")
G = str(myMesh_s_e).replace(".","")
H = str(myMesh_s_g).replace(".","")
I = str(myFr).replace(".","")
```

```
414
415 myJob_name_A = 'A_D_h1-{}_w1-{}_w2-{}_{}_{}-{}-{}-{}_fr-{}_sym'.format(A, B, C, D, E,
    F, G, H, I)  #Tension job with symmetry axes
416 myJob_name_B = 'B_D_h1-{}_w1-{}_w2-{}_{}_{}-{}-{}-{}_fr-{}_sym'.format(A, B, C, D, E,
    F, G, H, I)  #Compression job with symmetry axes
417 myJob_name_C = 'C_D_h1-{}_w1-{}_w2-{}_{}_{}-{}-{}-{}_fr-{}'.format(A, B, C, D, E, F, G
    , H, I)      #Shear job
418
419
420 #-------------------------------------------------------------------
421
422
423 # 4. CREATE ABAQUS MODEL
424 '''The script below uses the parameters you defined in the previous sections.
425 Nothing needs to be adjusted in section 3.'''
426 # 4.1 Define parameters
427 definitions = Definitions(part_name_L='part_L', part_name_R='part_R', job_name_A=
    myJob_name_A, job_name_B=myJob_name_B,
428     job_name_C=myJob_name_C, seq_L='[#1 ]', seq_R='[#7 ]')
429
430
431 # 4.2 Part module
432 part = Part(myH_t, myW_t, myH_1, myW_1, myW_2, myFr)
433
434 xyCoords_L, xyCoords_R = part.create_coords()
435
436 part_L = part.create_part(xyCoords=xyCoords_L, part_name=definitions.part_name_L)
437 part_R = part.create_part(xyCoords=xyCoords_R, part_name=definitions.part_name_R)
438
439 fillets_L = part.create_fillets(part_name=definitions.part_name_L)
440 fillets_R = part.create_fillets(part_name=definitions.part_name_R)
441
442 partition_axial = part.create_partition(part_name=definitions.part_name_R, int_edge1=4
    , int_edge2=10, loc=CENTER)
443 partition_shear = part.create_partition(part_name=definitions.part_name_R, int_edge1=7
    , int_edge2=1, loc=MIDDLE)
444
445 # 4.3 Property module
446 material = Property(material_name=myMaterial_name, rho=myRho, E1=myE1, E2=myE2, E3=
    myE3, Nu12=myNu12, Nu13=myNu13, Nu23=myNu23, G12=myG12, G13=myG13,
447     G23=myG23, section_name='sol_hom_2D', mat_rotation=ROTATION_NONE, rotation_axis=
        AXIS_3, stack_dir=STACK_3)
448
449 create_material = material.create_material()
450
451 sol_hom_section = material.create_sol_hom_section()
452
453 section_L = material.assign_section_prop(definitions.part_name_L, definitions.seq_L)
454 section_R = material.assign_section_prop(definitions.part_name_R, definitions.seq_R)
455
456 mat_orient_L = material.create_mat_orient(definitions.part_name_L, definitions.seq_L)
457 mat_orient_R = material.create_mat_orient(definitions.part_name_R, definitions.seq_R)
458
459
460 # 4.4 Assembly module
461 assembly = Assembly()
462
463 instances = assembly.create_instances(definitions.part_name_L, definitions.part_name_R
    , definitions.instance_name_L,
464     definitions.instance_name_R, dependency=OFF)
465
466 ref_points = assembly.create_ref_points(part.h_t, part.w_t, part.h_1)
467
468 set_RP_axial = assembly.create_set_from_RP(set_name='RP_AXIAL', RP_point=6)
469 set_RP_shear = assembly.create_set_from_RP(set_name='RP_SHEAR', RP_point=7)
```

```
470
471
472 set_BC_axial = assembly.create_set_from_instance(definitions.instance_name_R, set_name
    ='FIXED_AXIAL', seq='[#10 ]')
473 set_BC_shear = assembly.create_set_from_instance(definitions.instance_name_L, set_name
    ='FIXED_SHEAR', seq='[#c01 ]')
474 set_RBC_axial = assembly.create_set_from_instance(definitions.instance_name_L,
    set_name='RBC_AXIAL', seq='[#800 ]')
475 set_RBC_shear = assembly.create_set_from_instance(definitions.instance_name_R,
    set_name='RBC_SHEAR', seq='[#38 ]')
476 set_partition_axial = assembly.create_set_from_instance(definitions.instance_name_R,
    set_name='PARTITION_AXIAL', seq='[#200 ]')
477 set_partition_shear = assembly.create_set_from_instance(definitions.instance_name_R,
    set_name='PARTITION_SHEAR', seq='[#1 ]')
478 set_con_L = assembly.create_set_from_instance(definitions.instance_name_L, set_name=
    'CON_L', seq='[#3fe ]')
479 set_con_R = assembly.create_set_from_instance(definitions.instance_name_R, set_name=
    'CON_R', seq='[#3fdc6 ]')
480 set_con_side_bot_L = assembly.create_set_from_instance(definitions.instance_name_L,
    set_name='CON_SIDE_BOT_L', seq='[#8 ]')
481 set_con_side_bot_R = assembly.create_set_from_instance(definitions.instance_name_R,
    set_name='CON_SIDE_BOT_R', seq='[#10000 ]')
482 set_con_side_top_L = assembly.create_set_from_instance(definitions.instance_name_L,
    set_name='CON_SIDE_TOP_L', seq='[#80 ]')
483 set_con_side_top_R = assembly.create_set_from_instance(definitions.instance_name_R,
    set_name='CON_SIDE_TOP_R', seq='[#1000 ]')
484 set_con_top_L = assembly.create_set_from_instance(definitions.instance_name_L,
    set_name='CON_TOP_L', seq='[#20 ]')
485 set_con_top_R = assembly.create_set_from_instance(definitions.instance_name_R,
    set_name='CON_TOP_R', seq='[#4000 ]')
486 set_con_top_L = assembly.create_set_from_instance(definitions.instance_name_L,
    set_name='BOT_L', seq='[#2 ]')
487 set_con_top_R = assembly.create_set_from_instance(definitions.instance_name_R,
    set_name='BOT_R', seq='[#4 ]')
488 set_fillets_L = assembly.create_set_from_instance(definitions.instance_name_L,
    set_name='FILLETS_L', seq='[#154 ]')
489 set_fillets_R = assembly.create_set_from_instance(definitions.instance_name_R,
    set_name='FILLETS_R', seq='[#2ad82 ]')
490
491 set_Y_SYM = assembly.create_set_from_2instances(definitions.instance_name_L,
    definitions.instance_name_R, set_name='Y_SYM', seq_L='[#401 ]', seq_R='[#28 ]')
492 set_ends = assembly.create_set_from_2instances(definitions.instance_name_L,
    definitions.instance_name_R, set_name='ENDS', seq_L='[#800 ]', seq_R='[#10 ]')
493
494
495 #4.5 Step module
496 step = Step(step_name='Load')
497
498 load_step = step.create_static_general_step()
499
500
501 # 4.6 Interaction module
502 interaction = Interaction(int_prop_name='Frictionless', general_int_name='General
    contact')
503
504 frictionless = interaction.create_contact_int_prop()
505 global_int = interaction.create_general_interaction(step.step_name)
506
507
508 # 4.7 Load module
509 load = Load(myStress_t, myStress_c, myStress_s)
510
```

```
RBC_axial = load.create_tie_rigid_body_constraint(RBC_name='RBC_AXIAL',set_name_region
='RBC_AXIAL', set_name_RP='RP_AXIAL')
RBC_shear = load.create_tie_rigid_body_constraint(RBC_name='RBC_SHEAR',set_name_region
='RBC_SHEAR', set_name_RP='RP_SHEAR')

load_t, load_c, load_s = load.define_loads(h_t=100, w_t=100, fh=1, fw=1,)

tension_load = load.create_load(load_name=myName_load_t, F1=load_t, F2=0, RP_set=
'RP_AXIAL')
compression_load = load.create_load(load_name=myName_load_c, F1=load_c, F2=0, RP_set=
'RP_AXIAL')
shear_load = load.create_load(load_name=myName_load_s, F1=0, F2=load_s, RP_set=
'RP_SHEAR')

BC_fixed_axial = load.create_displacement_BC_fixed(BC_name='FIXED_AXIAL', set_name=
'FIXED_AXIAL')
BC_fixed_shear = load.create_displacement_BC_fixed(BC_name='FIXED_SHEAR', set_name=
'FIXED_SHEAR')

BC_roller_shear = load.create_displacement_BC_roller(BC_name='ROLLER_SHEAR', set_name=
'RP_SHEAR', fixed_dir='u1')

Y_sym = load.create_Ysym_BC(sym_name='Y_SYM', set_name='Y_SYM')


# 4.8 Mesh module
mesh = Mesh()

seed_partition_axial = mesh.seed_edge_by_size(definitions.instance_name_R, seq='[#200
]', mesh_size=myMesh_s_p)
seed_partition_shear = mesh.seed_edge_by_size(definitions.instance_name_R, seq='[#1 ]'
, mesh_size=myMesh_s_p)

seed_con_L = mesh.seed_edge_by_size(definitions.instance_name_L, seq='[#3fe ]',
mesh_size=myMesh_s_c)
seed_con_R = mesh.seed_edge_by_size(definitions.instance_name_R, seq='[#3fdc6 ]',
mesh_size=myMesh_s_c)

seed_ends = mesh.seed_2edges_by_size(definitions.instance_name_L, definitions.
instance_name_R, seq_L='[#800 ]', seq_R='[#10 ]', mesh_size=myMesh_s_e)

seed_global = mesh.seed_global(definitions.instance_name_L, definitions.
instance_name_R, mesh_size=myMesh_s_g)

mesh_shape_def = mesh.define_mesh_shape(definitions.instance_name_L, definitions.
instance_name_R, mesh_shape=myMesh_shape)

mesh_generation = mesh.generate_mesh(definitions.instance_name_L, definitions.
instance_name_R)


# 4.9 Job module
job = Job()

create_job_A = job.create_job(definitions.job_name_A)
#create_job_B = job.create_job(definitions.job_name_B)      #Activate this job to
include compression test
create_job_C = job.create_job(definitions.job_name_C)

#Tension
job.supress_constraint('RBC_SHEAR')
job.supress_load(myName_load_c)
job.supress_load(myName_load_s)
job.supress_BC('FIXED_SHEAR')
job.supress_BC('ROLLER_SHEAR')
```

```
559
560 submit_job_A = job.submit_job(definitions.job_name_A)
561
562 #Compression
563 job.supress_load(myName_load_t)
564 job.resume_load(myName_load_c)
565
566 #submit_job_B = job.submit_job(definitions.job_name_B)      #Activate this job to
    include compression test
567
568 #Shear
569 job.supress_constraint('RBC_AXIAL')
570 job.resume_constraint('RBC_SHEAR')
571 job.supress_load(myName_load_c)
572 job.resume_load(myName_load_s)
573 job.supress_BC('FIXED_AXIAL')
574 job.supress_BC('Y_SYM')
575 job.resume_BC('FIXED_SHEAR')
576 job.resume_BC('ROLLER_SHEAR')
577
578 submit_job_C = job.submit_job(definitions.job_name_C)
579
580 #-------------------------------------------------------------------------
```

Appendix D: Input script arrow

The biggest difference between the input script for the arrow compared to the input script for the dovetail is the coordinates. Therefore, only the function to create coordinates is presented below.

```
50  class Part:
51      def __init__(self,h_t,w_t,h_1,h_2,w_1,w_2,fr_1,fr_2,fr_3,fr_4):
52          self.h_t = h_t
53          self.w_t = w_t
54          self.h_1 = h_1
55          self.h_2 = h_2
56          self.w_1 = w_1
57          self.w_2 = w_2
58          self.fr_1 = fr_1
59          self.fr_2 = fr_2
60          self.fr_3 = fr_3
61          self.fr_4 = fr_4
62
63
64      def create_coords(self):
65          xyCoords_L = [(0,(self.w_t/2)), (0,(self.w_2/2)), (-self.h_2,(self.w_2/2)), (-
            self.h_2,(self.w_1/2)), (-self.h_1, 0), (-self.h_2,(-self.w_1/2)),
66                        (-self.h_2,(-self.w_2/2)), (0,(-self.w_2/2)), (0,(-self.w_t/2)),
                           (-self.h_t, (-self.w_t/2)), (-self.h_t, (self.w_t/2)),(0,(self.
                          w_t/2))]
67
68          xyCoords_R = [(0,(self.w_t/2)), (0,(self.w_2/2)), (-self.h_2,(self.w_2/2)), (-
            self.h_2,(self.w_1/2)), (-self.h_1, 0), (-self.h_2,(-self.w_1/2)),
69                        (-self.h_2,(-self.w_2/2)), (0,(-self.w_2/2)), (0,(-self.w_t/2)),
                           (self.h_t, (-self.w_t/2)), (self.h_t, (self.w_t/2)),(0,(self.
                          w_t/2))]
70
71          return xyCoords_L, xyCoords_R
72
73
74      def create_part(self,xyCoords, part_name):
75
76          mdb.models['Model-1'].ConstrainedSketch(name='__profile__', sheetSize=200.0)
77
78          for i in range(len(xyCoords)-1):
79              mdb.models['Model-1'].sketches['__profile__'].Line(point1=xyCoords[i],
                point2=xyCoords[i+1])
80
81          mdb.models['Model-1'].Part(dimensionality=TWO_D_PLANAR, name=part_name,type=
            DEFORMABLE_BODY)
82          mdb.models['Model-1'].parts[part_name].BaseShell(sketch=mdb.models['Model-1'].
            sketches['__profile__'])
83          del mdb.models['Model-1'].sketches['__profile__']
84
85
```

```
    def create_fillets(self, part_name):
        mdb.models['Model-1'].ConstrainedSketch(name='__edit__', objectToCopy=
            mdb.models['Model-1'].parts[part_name].features['Shell planar-1'].sketch)
        mdb.models['Model-1'].parts[part_name].projectReferencesOntoSketch(filter=
            COPLANAR_EDGES, sketch=mdb.models['Model-1'].sketches['__edit__'],
            upToFeature=mdb.models['Model-1'].parts[part_name].features['Shell
            planar-1'])
        mdb.models['Model-1'].sketches['__edit__'].FilletByRadius(curve1=
            mdb.models['Model-1'].sketches['__edit__'].geometry[2], curve2=
            mdb.models['Model-1'].sketches['__edit__'].geometry[3], nearPoint1=(
            0,(self.w_t/4)), nearPoint2=(-self.h_2/2,(self.w_2/2)), radius=self.fr_1)
        mdb.models['Model-1'].sketches['__edit__'].FilletByRadius(curve1=
            mdb.models['Model-1'].sketches['__edit__'].geometry[3], curve2=
            mdb.models['Model-1'].sketches['__edit__'].geometry[4], nearPoint1=(
            -self.h_2/2,(self.w_2/2)), nearPoint2=(-self.h_2,((self.w_2/2)+((self.w_1/
            2-self.w_2/2)/2))), radius=self.fr_2)
        mdb.models['Model-1'].sketches['__edit__'].FilletByRadius(curve1=
            mdb.models['Model-1'].sketches['__edit__'].geometry[4], curve2=
            mdb.models['Model-1'].sketches['__edit__'].geometry[5], nearPoint1=(
            -self.h_2,((self.w_2/2)+((self.w_1/2-self.w_2/2)/2))), nearPoint2=((-self.
            h_1)+((self.h_1-self.h_2)/2),(self.w_2/2)), radius=self.fr_3)
        mdb.models['Model-1'].sketches['__edit__'].FilletByRadius(curve1=
            mdb.models['Model-1'].sketches['__edit__'].geometry[5], curve2=
            mdb.models['Model-1'].sketches['__edit__'].geometry[6], nearPoint1=(
            ((-self.h_1)+((self.h_1-self.h_2)/2)),(self.w_2/2)), nearPoint2=(((-self.
            h_1)+((self.h_1-self.h_2)/2)),(-self.w_2/2)), radius=self.fr_4)
        mdb.models['Model-1'].sketches['__edit__'].FilletByRadius(curve1=
            mdb.models['Model-1'].sketches['__edit__'].geometry[6], curve2=
            mdb.models['Model-1'].sketches['__edit__'].geometry[7], nearPoint1=(
            ((-self.h_1)+((self.h_1-self.h_2)/2)),(-self.w_2/2)), nearPoint2=(-self.
            h_2,-((self.w_2/2)+((self.w_1/2-self.w_2/2)/2))), radius=self.fr_3)
        mdb.models['Model-1'].sketches['__edit__'].FilletByRadius(curve1=
            mdb.models['Model-1'].sketches['__edit__'].geometry[7], curve2=
            mdb.models['Model-1'].sketches['__edit__'].geometry[8], nearPoint1=(
            -self.h_2,-((self.w_2/2)+((self.w_1/2-self.w_2/2)/2))), nearPoint2=(-self.
            h_2/2,-(self.w_2/2)), radius=self.fr_2)
        mdb.models['Model-1'].sketches['__edit__'].FilletByRadius(curve1=
            mdb.models['Model-1'].sketches['__edit__'].geometry[8], curve2=
            mdb.models['Model-1'].sketches['__edit__'].geometry[9], nearPoint1=(
            -self.h_2/2,-(self.w_2/2)), nearPoint2=(0,-(self.w_t/4)), radius=self.fr_1
            )
        mdb.models['Model-1'].parts[part_name].features['Shell planar-1'].setValues(
            sketch=mdb.models['Model-1'].sketches['__edit__'])
        del mdb.models['Model-1'].sketches['__edit__']
        mdb.models['Model-1'].parts[part_name].regenerate()
```

Appendix E: Input script yin yang

The biggest difference between the input script for the yin yang compared to the input script for the dovetail is the coordinates. Therefore, only the function to create coordinates is presented below.

```
48  class Part:
49      def __init__(self,h_t,w_t,r_1,fr,w_1):
50          self.h_t = h_t
51          self.w_t = w_t
52          self.r_1 = r_1
53          self.fr = fr
54          self.w_1 = w_1
55
56
57
58      def create_coords(self):
59          xyCoords_arc = [(-self.r_1,(-2*self.r_1-self.w_1/2)), (-2*self.r_1,(-2*self.
            r_1-self.w_1/2)), (0,(-2*self.r_1-self.w_1/2)),
60                                  (self.r_1,(-2*self.r_1-self.w_1/2)), (2*self.r_1,(-2*
                                    self.r_1-self.w_1/2)), (0,(-2*self.r_1-self.w_1/2)),
61                                  (0,(-2*self.r_1-self.w_1/2)), (0,(-4*self.r_1-self.w_1/
                                    2)), (-2*self.r_1,(-2*self.r_1-self.w_1/2)),
62                                  (0,(-2*self.r_1-self.w_1/2)), (0,-self.w_1/2), (2*self.
                                    r_1,(-2*self.r_1-self.w_1/2)),
63                                  (-self.r_1,(2*self.r_1+self.w_1/2)), (0,(2*self.r_1+
                                    self.w_1/2)), (-2*self.r_1,(2*self.r_1+self.w_1/2)),
64                                  (self.r_1,(2*self.r_1+self.w_1/2)), (0,(2*self.r_1+self
                                    .w_1/2)), (2*self.r_1,(2*self.r_1+self.w_1/2)),
65                                  (0,(2*self.r 1+self.w 1/2)), (-2*self.r 1,(2*self.r 1+
                                    self.w_1/2)), (0,(4*self.r_1+self.w_1/2)),
66                                  (0,(2*self.r_1+self.w_1/2)), (2*self.r_1,(2*self.r_1+
                                    self.w_1/2)), (0,self.w_1/2)]
67
68          xyCoords_mid = [(0,-(self.w_1/2)), (0,(self.w_1/2))]
69
70          xyCoords_L = [(0,-(self.w_t-(self.w_1/2))), (0,-self.w_t), (-self.h_t,-self.
            w_t), (-self.h_t,self.w_t), (0,self.w_t), (0,(self.w_t-(self.w_1/2)))]
71
72          xyCoords_R = [(0,-(self.w_t-(self.w_1/2))), (0,-self.w_t), (self.h_t,-self.w_t
            ), (self.h_t,self.w_t), (0,self.w_t), (0,(self.w_t-(self.w_1/2)))]
```

Appendix F: Post-processing script peak stresses and deformations

```
'''POST-PROCESSING SCRIPT FOR ABAQUS CAE
GLOBAL DEFORMATIONS AND STRESSES'''


# 1. DEFINITIONS
name = 'YY_r1-15_fr1-5_w1-40_TRI_1-1-8-4'
output_A = 'A_'+name+'_sym'
output_C = 'C_'+name


# 2. TENSION JOB
odb_A = session.openOdb(output_A+'.odb')      #Tension output

# 2.1 Field outputs
A_U = odb_A.steps['Load'].frames[-1].fieldOutputs['U']
A_S = odb_A.steps['Load'].frames[-1].fieldOutputs['S']

# 2.1.1 Displacement data
'''Data container order (U1, U2)'''
A_U1 = []
A_U2 = []

for displacement in A_U.values:
    A_U1.append(displacement.data[0])
    A_U2.append(displacement.data[1])

max_A_U1 = max(A_U1)
min_A_U1 = min(A_U1)
max_A_U2 = max(A_U2)
min_A_U2 = min(A_U2)

# 2.1.2 Stress data
'''Data container order (S11, S22, S33, S12, S13, S23)'''
A_S11 = []
A_S22 = []
A_S12 = []

for stress in A_S.values:
    A_S11.append(stress.data[0])
    A_S22.append(stress.data[1])
    A_S12.append(stress.data[3])

max_A_S11 = max(A_S11)
min_A_S11 = min(A_S11)
max_A_S22 = max(A_S22)
min_A_S22 = min(A_S22)
max_A_S12 = max(A_S12)
min_A_S12 = min(A_S12)

```

```python
# 2.3 Close output database
odb_A.close()

# 3. SHEAR JOB
odb_C = session.openOdb(output_C+'.odb')      #Shear output

# 3.1 Field outputs
C_U = odb_C.steps['Load'].frames[-1].fieldOutputs['U']
C_S = odb_C.steps['Load'].frames[-1].fieldOutputs['S']

# 3.1.1 Displacement data
'''Data container order (U1, U2)'''
C_U1 = []
C_U2 = []

for displacement in C_U.values:
    C_U1.append(displacement.data[0])
    C_U2.append(displacement.data[1])

max_C_U1 = max(C_U1)
min_C_U1 = min(C_U1)
max_C_U2 = max(C_U2)
min_C_U2 = min(C_U2)

# 3.1.2 Stress data
'''Data container order (S11, S22, S33, S12, S13, S23)'''
C_S11 = []
C_S22 = []
C_S12 = []

for stress in C_S.values:
    C_S11.append(stress.data[0])
    C_S22.append(stress.data[1])
    C_S12.append(stress.data[3])

max_C_S11 = max(C_S11)
min_C_S11 = min(C_S11)
max_C_S22 = max(C_S22)
min_C_S22 = min(C_S22)
max_C_S12 = max(C_S12)
min_C_S12 = min(C_S12)

# 3.3 Close output database
odb_C.close()


#Store all envelope data in a single list
envelope = [max_A_U1, min_A_U1, max_A_U2, min_A_U2,
            max_A_S11, min_A_S11, max_A_S22, min_A_S22, max_A_S12, min_A_S12,
            max_C_U1, min_C_U1, max_C_U2, min_C_U2,
            max_C_S11, min_C_S11, max_C_S22, min_C_S22, max_C_S12, min_C_S12]

print(envelope)
print(name)
```

Appendix G: Post-processing script average stresses

```
5   # 1. IMPORT LIBRARIES
6   import pandas as pd
7   import numpy as np
8   import matplotlib.pyplot as plt
9
10  # 2. IMPORT DATA INTO DATAFRAMES
11  df0 = pd.read_excel(
    r'C:\Users\Lüning\Documents\Afstuderen\Simulation_files\D_h1-50_w1-85_w2-15_TRI_1-1-1-
    16-8_fr-5.xlsx', header=None)
12  df1 = pd.read_excel(
    r'C:\Users\Lüning\Documents\Afstuderen\Simulation_files\D_h1-50_w1-85_w2-15_TRI_1-1-1-
    16-8_fr-10.xlsx', header=None)
13  df2 = pd.read_excel(
    r'C:\Users\Lüning\Documents\Afstuderen\Simulation_files\D_h1-50_w1-85_w2-15_TRI_1-1-1-
    16-8_fr-15.xlsx', header=None)
14  df3 = pd.read_excel(
    r'C:\Users\Lüning\Documents\Afstuderen\Simulation_files\D_h1-50_w1-80_w2-20_TRI_1-1-1-
    16-8_fr-5.xlsx', header=None)
15  df4 = pd.read_excel(
    r'C:\Users\Lüning\Documents\Afstuderen\Simulation_files\D_h1-50_w1-80_w2-20_TRI_1-1-1-
    16-8_fr-10.xlsx', header=None)
16  df5 = pd.read_excel(
    r'C:\Users\Lüning\Documents\Afstuderen\Simulation_files\D_h1-50_w1-80_w2-20_TRI_1-1-1-
    16-8_fr-15.xlsx', header=None)
17  df6 = pd.read_excel(
    r'C:\Users\Lüning\Documents\Afstuderen\Simulation_files\D_h1-50_w1-75_w2-25_TRI_1-1-1-
    16-8_fr-5.xlsx', header=None)
18  df7 = pd.read_excel(
    r'C:\Users\Lüning\Documents\Afstuderen\Simulation_files\D_h1-50_w1-75_w2-25_TRI_1-1-1-
    16-8_fr-10.xlsx', header=None)
19  df8 = pd.read_excel(
    r'C:\Users\Lüning\Documents\Afstuderen\Simulation_files\D_h1-50_w1-75_w2-25_TRI_1-1-1-
    16-8_fr-15.xlsx', header=None)
20  df9 = pd.read_excel(
    r'C:\Users\Lüning\Documents\Afstuderen\Simulation_files\D_h1-50_w1-70_w2-30_TRI_1-1-1-
    16-8_fr-5.xlsx', header=None)
21  df10 = pd.read_excel(
    r'C:\Users\Lüning\Documents\Afstuderen\Simulation_files\D_h1-50_w1-70_w2-30_TRI_1-1-1-
    16-8_fr-10.xlsx', header=None)
22  df11 = pd.read_excel(
    r'C:\Users\Lüning\Documents\Afstuderen\Simulation_files\D_h1-50_w1-70_w2-30_TRI_1-1-1-
    16-8_fr-15.xlsx', header=None)
23  df12 = pd.read_excel(
    r'C:\Users\Lüning\Documents\Afstuderen\Simulation_files\D_h1-50_w1-65_w2-35_TRI_1-1-1-
    16-8_fr-5.xlsx', header=None)
24  df13 = pd.read_excel(
    r'C:\Users\Lüning\Documents\Afstuderen\Simulation_files\D_h1-50_w1-65_w2-35_TRI_1-1-1-
    16-8_fr-10.xlsx', header=None)
```

```
df14 = pd.read_excel(
r'C:\Users\Lüning\Documents\Afstuderen\Simulation_files\D_h1-50_w1-65_w2-35_TRI_1-1-1-16-8_fr-15.xlsx', header=None)
df15 = pd.read_excel(
r'C:\Users\Lüning\Documents\Afstuderen\Simulation_files\D_h1-50_w1-60_w2-40_TRI_1-1-1-16-8_fr-5.xlsx', header=None)
df16 = pd.read_excel(
r'C:\Users\Lüning\Documents\Afstuderen\Simulation_files\D_h1-50_w1-60_w2-40_TRI_1-1-1-16-8_fr-10.xlsx', header=None)
df17 = pd.read_excel(
r'C:\Users\Lüning\Documents\Afstuderen\Simulation_files\D_h1-50_w1-60_w2-40_TRI_1-1-1-16-8_fr-15.xlsx', header=None)

dataframes = [df0, df1, df2, df3, df4, df5, df6, df7, df8, df9, df10, df11, df12, df13, df14, df15, df16, df17]


# 3. MANIPULATE DATA
#Max. stresses
max_A_S11_PARTITION = [df.iloc[:, 1].max() for df in dataframes]
max_A_S12_CON_SIDE_BOT_L = [df.iloc[:, 3].max() for df in dataframes]
max_A_S12_CON_SIDE_BOT_R = [df.iloc[:, 5].max() for df in dataframes]
max_A_S12_CON_SIDE_TOP_L = [df.iloc[:, 7].max() for df in dataframes]
max_A_S12_CON_SIDE_TOP_R = [df.iloc[:, 9].max() for df in dataframes]
max_A_S22_CON_TOP_R = [df.iloc[:, 11].max() for df in dataframes]
max_A_S22_PARTITION = [df.iloc[:, 13].max() for df in dataframes]
max_A_C_S12_PARTITION = [df.iloc[:, 15].max() for df in dataframes]

#Min. stresses
min_A_S11_PARTITION = [df.iloc[:, 1].min() for df in dataframes]
min_A_S12_CON_SIDE_BOT_L = [df.iloc[:, 3].min() for df in dataframes]
min_A_S12_CON_SIDE_BOT_R = [df.iloc[:, 5].min() for df in dataframes]
min_A_S12_CON_SIDE_TOP_L = [df.iloc[:, 7].min() for df in dataframes]
min_A_S12_CON_SIDE_TOP_R = [df.iloc[:, 9].min() for df in dataframes]
min_A_S22_CON_TOP_R = [df.iloc[:, 11].min() for df in dataframes]
min_A_S22_PARTITION = [df.iloc[:, 13].min() for df in dataframes]
min_A_C_S12_PARTITION = [df.iloc[:, 15].min() for df in dataframes]

#w_2
w_2 = [15, 15, 15,
       20, 20, 20,
       25, 25, 25,
       30, 30, 30,
       35, 35, 35,
       40, 40, 40]

#Failure criteria - scenerio 1
f_t0d = 7.5
f_t90d = 6
f_c0d = -12.53
f_c90d = -9.97
f_v0d = 2.63
f_v90d = 2.63


#Sorted data
for i, df in enumerate(dataframes):
    headers = [f"DF{i}_A_S11_PARTITION", "-",
               f"DF{i}_A_S12_CON_SIDE_BOT_L", "-",
               f"DF{i}_A_S12_CON_SIDE_BOT_R", "-",
               f"DF{i}_A_S12_CON_SIDE_TOP_L", "-",
               f"DF{i}_A_S12_CON_SIDE_TOP_R", "-",
               f"DF{i}_A_S22_CON_TOP_R", "-",
               f"DF{i}_A_S22_PARTITION", "-",
               f"DF{i}_C_S12_PARTITION", "-"]

```

```
    data = {}

    for j in range(0, len(headers), 2):
        data[headers[j]] = {"x": df.iloc[:, j].dropna(), "y": df.iloc[:, j+1].dropna()}

    sorted_data = {}

    for name, values in data.items():
        x = values["x"]
        y = values["y"]
        sorted_data_values = sorted(zip(x, y), key=lambda x: x[0])
        x_sorted = [x for x, y in sorted_data_values]
        normalized_x = (x_sorted - np.min(x_sorted)) / (np.max(x_sorted) - np.min(x_sorted))
        sorted_data[name + "_SORTED"] = {"x": normalized_x, "y": [y for x, y in sorted_data_values]}



# 4. PLOT STYLE DEFINITIONS
df_labels = ["D1a", "D1b", "D1c",
             "D2a", "D2b", "D2c",
             "D3a", "D3b", "D3c",
             "D4a", "D4b", "D4c",
             "D5a", "D5b", "D5c",
             "D6a", "D6b", "D6c"]

bw_colors = ['silver', 'silver', 'silver',
             'darkgray', 'darkgray', 'darkgray',
             'gray', 'gray', 'gray',
             'dimgray', 'dimgray', 'dimgray',
             'darkslategray', 'darkslategray', 'darkslategray',
             'black', 'black', 'black']

dark_colors = ['saddlebrown', 'saddlebrown', 'saddlebrown',
               'maroon', 'maroon', 'maroon',
               'indigo', 'indigo', 'indigo',
               'navy', 'navy', 'navy',
               'darkgreen', 'darkgreen', 'darkgreen',
               'darkslategray', 'darkslategray', 'darkslategray']

bright_colors = ['black', 'black', 'black',
               'darkred', 'darkred', 'darkred',
               'darkgreen', 'darkgreen', 'darkgreen',
               'darkblue', 'darkblue', 'darkblue',
               'rebeccapurple', 'rebeccapurple', 'rebeccapurple',
               'deeppink', 'deeppink', 'deeppink']

light_colors = ['grey', 'grey', 'grey',
               'red', 'red', 'red',
               'green', 'green', 'green',
               'blue', 'blue', 'blue',
               'mediumorchid', 'mediumorchid', 'mediumorchid',
               'pink', 'pink', 'pink']

line_styles = ['-', '--', '-.',
               '-', '--', '-.',
               '-', '--', '-.',
               '-', '--', '-.',
               '-', '--', '-.',
               '-', '--', '-.']        #solid, dashed, dashdotted

```

```
markers = ["x", ".", "+",
           "x", ".", "+",
           "x", ".", "+",
           "x", ".", "+",
           "x", ".", "+",
           "x", ".", "+"]              #square, point, triangle_up


# 5. CREATE STRESS PLOTS (MAX VALUES)
#Tension load case
for i in range(len(w_2)):
    plt.scatter(w_2[i], max_A_S11_PARTITION[i], c=dark_colors[i], marker=markers[i],
    label=df_labels[i])

plt.grid(which='both', color='black', linewidth=0.1)
plt.legend(bbox_to_anchor=(0.5, -0.15), loc="upper center", ncol=6)
plt.xlabel("Smallest connection width w_2 [mm]")
plt.ylabel("Max. axial stress (S11) at partition [MPa]")
plt.title("Variation study dovetails 1-6: Tension load case")
plt.savefig(
r"C:\Users\Lüning\Documents\Afstuderen\Simulation_files\Variation_study_dovetails1-6_A
_S_11_partition_1.png", dpi=1000, bbox_inches="tight")
plt.show()


for i in range(len(w_2)):
    plt.scatter(w_2[i], max_A_S12_CON_SIDE_BOT_L[i], c=dark_colors[i], marker=markers[
    i], label=df_labels[i])

plt.grid(which='both', color='black', linewidth=0.1)
plt.legend(bbox_to_anchor=(0.5, -0.15), loc="upper center", ncol=6)
plt.xlabel("Smallest connection width w_2 [mm]")
plt.ylabel("Max. shear stress (S12) at connection side [MPa]")
plt.title("Variation study dovetails 1-6: Tension load case")
plt.savefig(
r"C:\Users\Lüning\Documents\Afstuderen\Simulation_files\Variation_study_dovetails1-6_A
_S12_side_1.png", dpi=1000, bbox_inches="tight")
plt.show()


for i in range(len(w_2)):
    plt.scatter(w_2[i], max_A_S22_CON_TOP_R[i], c=dark_colors[i], marker=markers[i],
    label=df_labels[i])

plt.grid(which='both', color='black', linewidth=0.1)
plt.legend(bbox_to_anchor=(0.5, -0.15), loc="upper center", ncol=6)
plt.xlabel("Smallest connection width w_2 [mm]")
plt.ylabel("Max. axial stress (S22) at connection top [MPa]")
plt.title("Variation study dovetails 1-6: Tension load case")
plt.savefig(
r"C:\Users\Lüning\Documents\Afstuderen\Simulation_files\Variation_study_dovetails1-6_A
_S22_top_1.png", dpi=1000, bbox_inches="tight")
plt.show()

for i in range(len(w_2)):
    plt.scatter(w_2[i], max_A_S22_PARTITION[i], c=dark_colors[i], marker=markers[i],
    label=df_labels[i])

plt.grid(which='both', color='black', linewidth=0.1)
plt.legend(bbox_to_anchor=(0.5, -0.15), loc="upper center", ncol=6)
plt.xlabel("Smallest connection width w_2 [mm]")
plt.ylabel("Max. axial stress (S22) at partition [MPa]")
plt.title("Variation study dovetails 1-6: Tension load case")
plt.savefig(
r"C:\Users\Lüning\Documents\Afstuderen\Simulation_files\Variation_study_dovetails1-6_A
_S22_partition_1.png", dpi=1000, bbox_inches="tight")
```

```
196 plt.show()
197
198
199
200 #Shear load case
201 for i in range(len(w_2)):
202     plt.scatter(w_2[i], min_A_C_S12_PARTITION[i], c=dark_colors[i], marker=markers[i],
      label=df_labels[i])
203
204 plt.grid(which='both', color='black', linewidth=0.1)
205 plt.legend(bbox_to_anchor=(0.5, -0.15), loc="upper center", ncol=6)
206 plt.xlabel("Smallest connection width w_2 [mm]")
207 plt.ylabel("Max. shear stress (S12) at partition [MPa]")
208 plt.title("Variation study dovetails 1-6: Shear load case")
209 plt.savefig(
    r"C:\Users\Lüning\Documents\Afstuderen\Simulation_files\Variation_study_dovetails1-6_C
    _partition_1.png", dpi=1000, bbox_inches="tight")
210 plt.show()
211
212
213
214 # 6. CREATE OPTIMIZATION PLOTS (MAX VALUES)
215 #Tension load case
216 for i in range(len(w_2)):
217     plt.scatter(x=w_2[i], y=(max_A_S11_PARTITION[i]/f_t0d), c=dark_colors[i], marker=
    markers[i], label=df_labels[i])
218
219 plt.grid(which='both', color='black', linewidth=0.1)
220 plt.legend(bbox_to_anchor=(0.5, -0.15), loc="upper center", ncol=6)
221 plt.xlabel("Smallest connection width w_2 [mm]")
222 plt.ylabel("Optimization grade: S11 at partition [-]")
223 plt.title("Variation study dovetails 1-6: Tension load case")
224 plt.savefig(
    r"C:\Users\Lüning\Documents\Afstuderen\Simulation_files\Variation_study_dovetails1-6_A
    _S_11_partition_opt1.png", dpi=1000, bbox_inches="tight")
225 plt.show()
226
227
228 for i in range(len(w_2)):
229     plt.scatter(x=w_2[i], y=(max_A_S12_CON_SIDE_BOT_L[i]/f_v0d), c=dark_colors[i],
    marker=markers[i], label=df labels[i])
230
231 plt.grid(which='both', color='black', linewidth=0.1)
232 plt.legend(bbox_to_anchor=(0.5, -0.15), loc="upper center", ncol=6)
233 plt.xlabel("Smallest connection width w_2 [mm]")
234 plt.ylabel("Optimization grade: S12 at connection side [-]")
235 plt.title("Variation study dovetails 1-6: Tension load case")
236 plt.savefig(
    r"C:\Users\Lüning\Documents\Afstuderen\Simulation_files\Variation_study_dovetails1-6_A
    _S12_side_opt1.png", dpi=1000, bbox_inches="tight")
237 plt.show()
238
239
240 for i in range(len(w_2)):
241     plt.scatter(x=w_2[i], y=(max_A_S22_CON_TOP_R[i]/f_c90d), c=dark_colors[i], marker=
    markers[i], label=df_labels[i])
242
243 plt.grid(which='both', color='black', linewidth=0.1)
244 plt.legend(bbox_to_anchor=(0.5, -0.15), loc="upper center", ncol=6)
245 plt.xlabel("Smallest connection width w_2 [mm]")
246 plt.ylabel("Optimization grade: S22 at connection top [-]")
247 plt.title("Variation study dovetails 1-6: Tension load case")
248 plt.savefig(
    r"C:\Users\Lüning\Documents\Afstuderen\Simulation_files\Variation_study_dovetails1-6_A
    _S22_top_opt1.png", dpi=1000, bbox_inches="tight")
249 plt.show()
```

```
250
251 for i in range(len(w_2)):
252     plt.scatter(x=w_2[i], y=(max_A_S22_PARTITION[i]/f_t90d), c=dark_colors[i], marker=
    markers[i], label=df_labels[i])
253
254 plt.grid(which='both', color='black', linewidth=0.1)
255 plt.legend(bbox_to_anchor=(0.5, -0.15), loc="upper center", ncol=6)
256 plt.xlabel("Smallest connection width w_2 [mm]")
257 plt.ylabel("Optimization grade: S22 at partition [-]")
258 plt.title("Variation study dovetails 1-6: Tension load case")
259 plt.savefig(
    r"C:\Users\Lüning\Documents\Afstuderen\Simulation_files\Variation_study_dovetails1-6_A
    _S22_partition_opt1.png", dpi=1000, bbox_inches="tight")
260 plt.show()
261
262
263
264 #Shear load case
265 for i in range(len(w_2)):
266     plt.scatter(x=w_2[i], y=(min_A_C_S12_PARTITION[i]/-f_v0d), c=dark_colors[i],
    marker=markers[i], label=df_labels[i])
267
268 plt.grid(which='both', color='black', linewidth=0.1)
269 plt.legend(bbox_to_anchor=(0.5, -0.15), loc="upper center", ncol=6)
270 plt.xlabel("Smallest connection width w_2 [mm]")
271 plt.ylabel("Optimization grade: S12 at partition [-]")
272 plt.title("Variation study dovetails 1-6: Shear load case")
273 plt.savefig(
    r"C:\Users\Lüning\Documents\Afstuderen\Simulation_files\Variation_study_dovetails1-6_C
    _partition_opt1.png", dpi=1000, bbox_inches="tight")
274 plt.show()
275
276
277
278
279 # Plot the data
280 for i,d in enumerate(zero_dicts):
281     #Stresses
282     plt.plot(d["x"], d["y"], label=df_labels[i], color=dark_colors[i], linewidth=0.3)
283     #Average stresses
284     average_y = np.mean(d["y"])
285     plt.axhline(y=average_y, label=df_labels[i]+" average", color=light_colors[i],
    linewidth=0.3, linestyle='-.')
286
287     #plt.xlim(0, 1)
288     #plt.ylim(0, 100)
289     #plt.xticks(np.arange(0, 1.1, 0.1))
290     #plt.yticks(np.arange(0, 110, 10))
291     plt.grid(which='both', color='black', linewidth=0.1)
292     plt.xlabel("Smallest connection width w_2 [mm]")
293     plt.ylabel("Max. axial stress (S11) at partition [MPa]")
294     plt.title("Variation study dovetail 1-6: Tension load case")
295
296     #plt.grid(color='black', linewidth=0.2)
297 plt.legend(bbox_to_anchor=(0.5, -0.15), loc="upper center")
298 #plt.legend(loc='lower center')
299 #plt.savefig(r"C:\Users\Lüning\Documents\Afstuderen\Simulation_files\A_S11_PARTITION_m
    eshrefinement.png", dpi=1000, bbox_inches="tight")
300 plt.show()
301
302
303
```

```
#DATAFRAME0
#Divide data into pairs of columns and drop empty rows
headers0 = ["DF0_A_S11_PARTITION", "-",
            "DF0_A_S12_CON_SIDE_BOT_L", "-",
            "DF0_A_S12_CON_SIDE_BOT_R", "-",
            "DF0_A_S12_CON_SIDE_TOP_L", "-",
            "DF0_A_S12_CON_SIDE_TOP_R", "-",
            "DF0_A_S22_CON_TOP_R", "-",
            "DF0_A_S22_PARTITION", "-",
            "DF0_C_S12_PARTITION", "-"]

data0 = {}

for i in range(0, len(headers0),2):
    data0[headers0[i]] = {"x": df0.iloc[:, i].dropna(), "y": df0.iloc[:, i+1].dropna
    ()}


#Order and normalize
sorted_data0 = {}

for name, values in data0.items():
    x = values["x"]
    y = values["y"]
    sorted_data = sorted(zip(x, y), key=lambda x: x[0])
    x = [x for x, y in sorted_data]
    normalized_x = (x - np.min(x)) / (np.max(x) - np.min(x))
    sorted_data0[name+"_SORTED"] = {"x": normalized_x, "y": [y for x, y in sorted_data
    ]}


sorted_data_name = f"sorted_data{i}"
locals()[sorted_data_name] = sorted_data


#plots
df_labels = ["Dovetail 50-60-40-5",
             "Dovetail 50-60-40-10",
             "Dovetail 50-60-40-15",
             "Dovetail 50-60-40-5",
             "Dovetail 50-60-40-5"]

dark_colors = ['black',
               'darkred',
               'darkgreen',
               'darkblue',
               'rebeccapurple']

light_colors = ['grey',
                'red',
                'green',
                'blue',
                'mediumorchid']

# 0. PLOT THE FIRST DICTIONARY OF SORTED_DATA0, SORTED_DATA1, SORTED_DATA2,
SORTED_DATA3, AND SORTED_DATA4

```

```
# Get the first dictionary from each sorted_data variable
zero_dicts = [list(sorted_data0.values())[0],
              list(sorted_data1.values())[0],
              list(sorted_data2.values())[0],
              list(sorted_data3.values())[0],
              list(sorted_data4.values())[0]]

# Plot the data
for i,d in enumerate(zero_dicts):
    #Stresses
    plt.plot(d["x"], d["y"], label=df_labels[i], color=dark_colors[i], linewidth=0.3)
    #Average stresses
    average_y = np.mean(d["y"])
    plt.axhline(y=average_y, label=df_labels[i]+" average", color=light_colors[i],
    linewidth=0.3, linestyle='-.')

    plt.xlim(0, 1)
    #plt.ylim(0, 100)
    plt.xticks(np.arange(0, 1.1, 0.1))
    #plt.yticks(np.arange(0, 110, 10))
    plt.grid(which='both', color='black', linewidth=0.1)
    plt.xlabel("Normalized distance along partition [-]")
    plt.ylabel("Axial stress (S11) [MPa]")
    plt.title("Tension load on dovetail: S11 at partition")

    #plt.grid(color='black', linewidth=0.2)
plt.legend(bbox_to_anchor=(0.5, -0.15), loc="upper center")
#plt.legend(loc='lower center')
plt.savefig(
r"C:\Users\Lüning\Documents\Afstuderen\Simulation_files\A_S11_PARTITION_meshrefinement
.png", dpi=1000, bbox_inches="tight")
plt.show()
```

Appendix H: Variation study results

Tension load applications

Dovetail

Dovetail study 1

In dovetail study 1, the width w_2 is varied from 5 to 45 mm. These dovetails have a static height h_1 of 50 mm and fillet radius fr_1 of 5 mm. The maximum relative tension stress parallel is governing for all dovetails except the dovetail with w_2 of 45 mm. Increasing w_2 up to 40 mm results in a slightly lower peak stress. However, compression stress perpendicular increases rapidly for a w_2 of 30 mm to 45 mm. At a w_2 of 45 mm the compression stress perpendicular becomes dominant. A dovetail with a w_2 of 40 mm performs the best in this study where the maximum relative tension stress parallel has a value of 6.46.

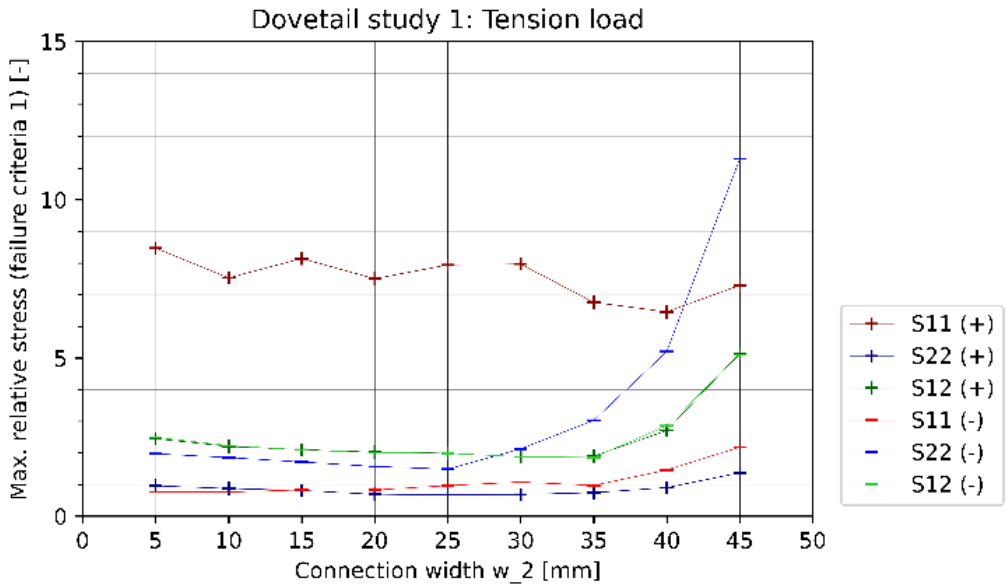

Figure H-TD-I: Dovetail study 1 (tension): max. relative stresses (failure criteria 1)

Dovetail study 2

The height h_1 of the dovetail is varied from 20 to 190 mm. The width w_2 is 40 mm and the fillet radius fr_1 is 5 mm. A reduction of the peak stresses is observed, especially for tension stress parallel which reduces from 12.07 to 3.88. Tension stress parallel is the critical stress for h_1 between 20 and 100 mm, whereas compression stress perpendicular is critical for h_1 between 110 and 180 mm. The most optimal dovetail has a h_1 of 180 mm and maximum relative compression stress perpendicular of 4.35.

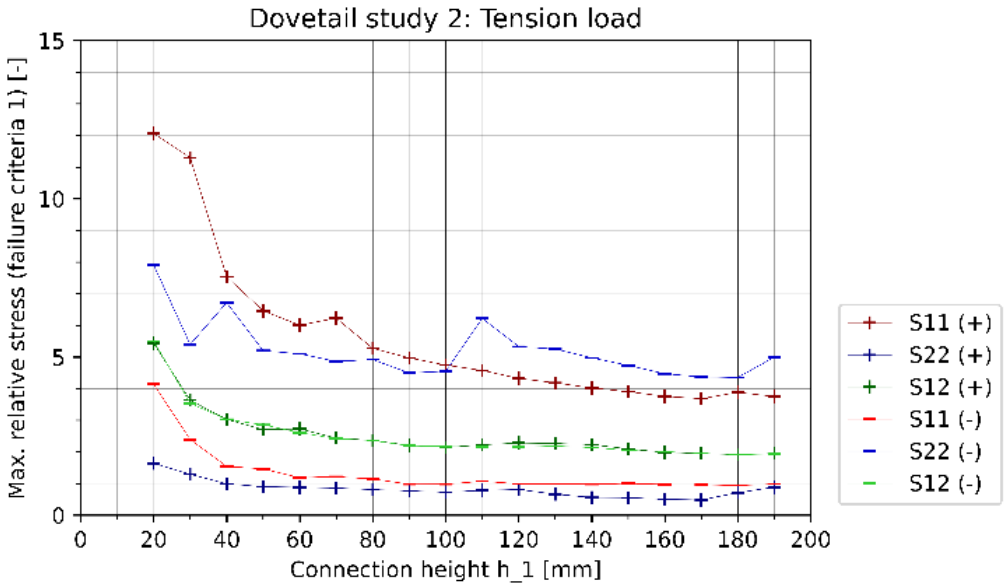

Figure H-TD-II: Dovetail study 2 (tension): max. relative stresses (failure criteria 1)

Dovetail study 3

Another height variation study is performed with a static width w_2 of 20 mm and fillet radius fr_1 of 5 mm. The height h_1 is varied from 20 mm to 190 mm. A reduction of stresses is observed for larger dovetail heights. Tension stress parallel is dominant for all dovetails by far. The optimal dovetail configuration is found at h_1 of 190 mm which has a maximum relative tension stress parallel of 4.46.

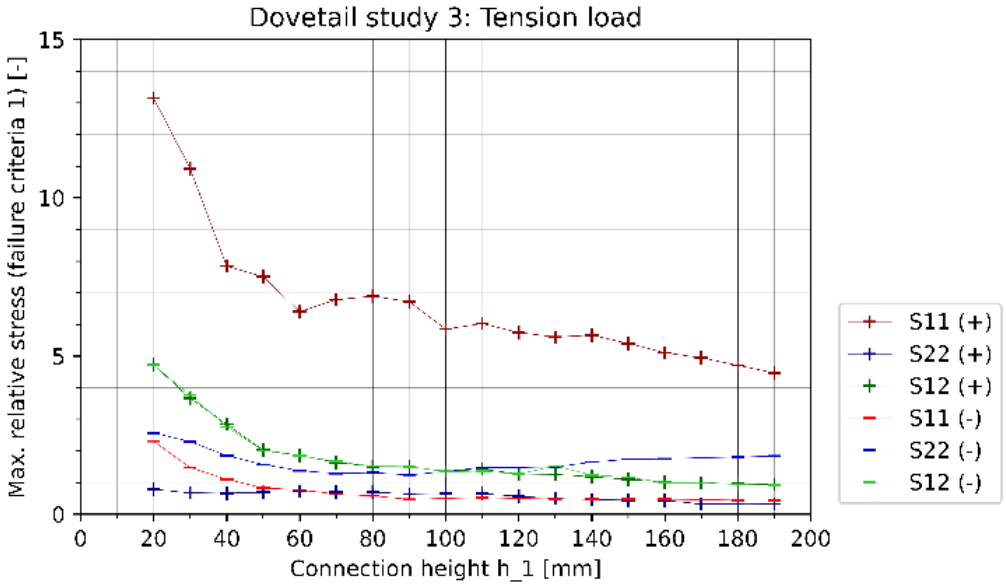

Figure H-TD-III: Dovetail study 3 (tension): max. relative stresses (failure criteria 1)

Dovetail study 4

In dovetail study 4, the height h_1 is varied from 40 to 190 mm while the static width is w_2 20 mm and the static fillet radius fr_1 is 10 mm. A reduction of stresses is observed for dovetails with larger h_1. Tension stress parallel is dominant for all dovetails and the best performing dovetail has a height h_1 of 190 mm with a maximum relative tension stress parallel of 3.88.

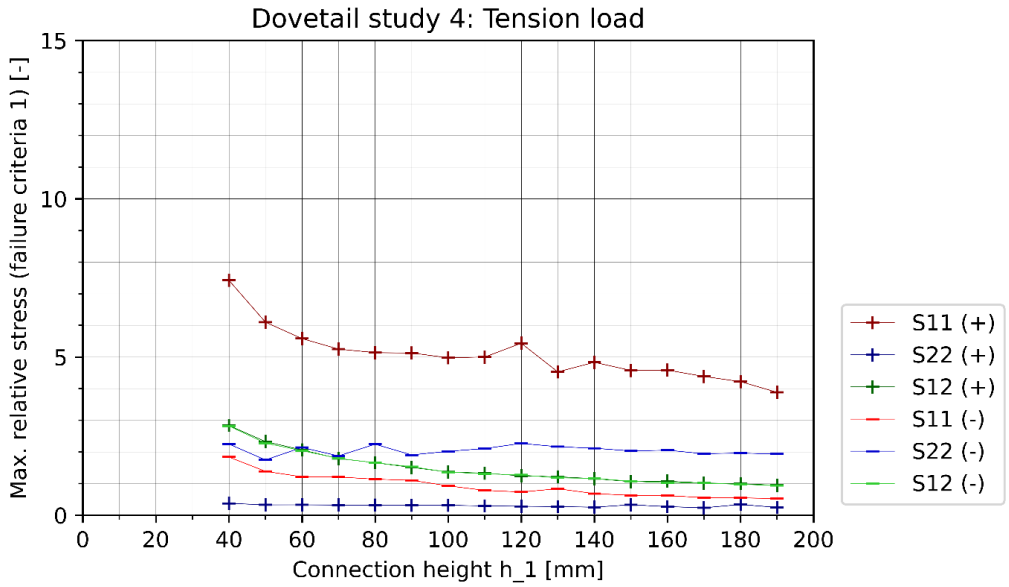

Figure H-TD-IV: Dovetail study 4 (tension): max. relative stresses (failure criteria 1)

Dovetail study 5

In dovetail study 5, the height h_1 is varied from 50 to 190 mm while the static width is w_2 20 mm and the static fillet radius fr_1 is 15 mm. A small reduction of stresses is observed for dovetails with larger h_1. Tension stress parallel is dominant for all dovetails and the best performing dovetail has a height h_1 of 180 mm with a maximum relative tension stress parallel of 3.87.

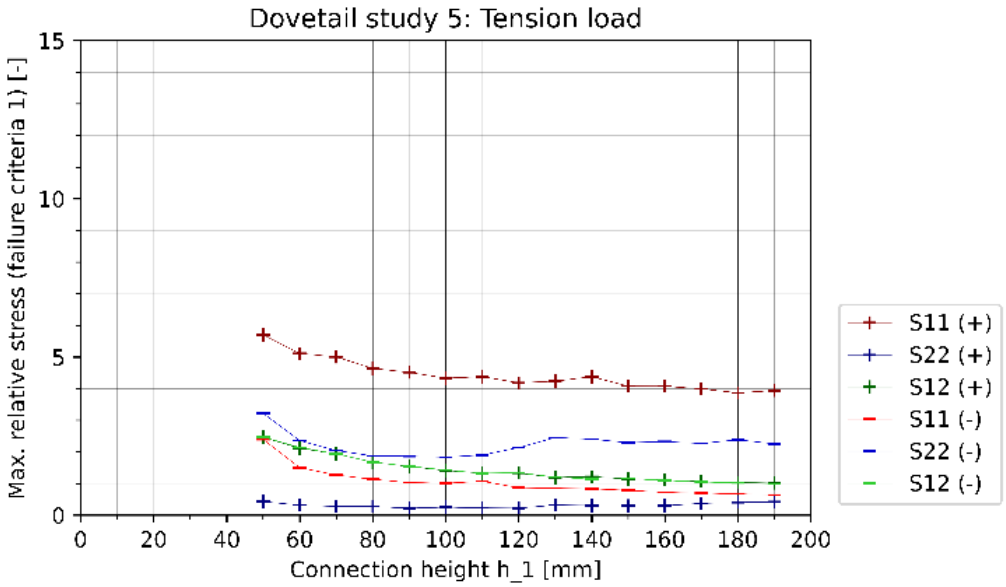

Figure H-TD-V: Dovetail study 5 (tension): max. relative stresses (failure criteria 1)

Dovetail study 6

The heights h_1 of the dovetails in study 7 vary from 40 mm to 190 mm. The static width w_2 is 40 mm and the fillet radius fr_1 is 10 mm. In contrast to the other dovetails studies, the compressions stress perpendicular is dominant for all dovetails. A reduction of stresses is observed for dovetails with larger h_1. The best performing dovetail has a height h_1 of 160 mm with a maximum relative compression stress perpendicular of 3.59.

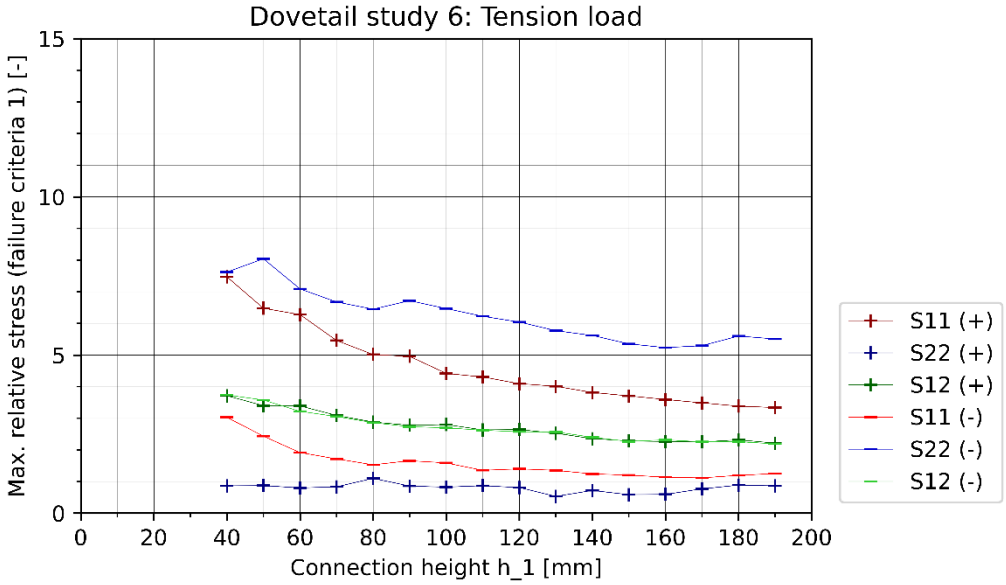

Figure H-TD-VI: Dovetail study 6 (tension): max. relative stresses (failure criteria 1)

Dovetail study 7

The heights h_1 of the dovetails in study 7 vary from 40 mm to 180 mm. The static width w_2 is 40 mm and the fillet radius fr_1 is 15 mm. In contrast to the other dovetails studies, the compressions stress perpendicular is dominant for all dovetails. A reduction of stresses is observed for dovetails with larger h_1. The best performing dovetail has a height h_1 of 160 mm with a maximum relative compression stress perpendicular of 5.77.

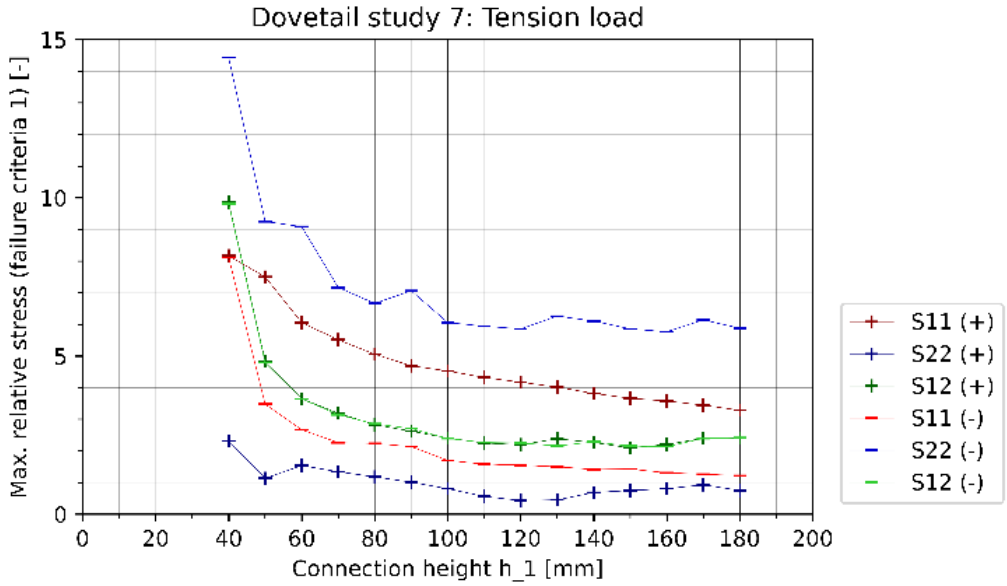

Figure H-TD-VII: Dovetail study 7 (tension): max. relative stresses (failure criteria 1)

Arrow

Arrow study 1

All arrows in this study have a height h_1 of 80 mm and h_2 of 30 mm, width w_1 of 90 mm and w_2 20 mm and fillet radius fr_1, fr_2 and fr_4 of 5 mm. The fillet radius fr_3 is varied from 5 to 13 mm. Larger fillet radii fr_3 were not possible in the geometry. The maximum relative tension stress parallel is governing for all dovetails and reduces for increasing fr_3. The best performing arrow has a fr_3 of 12 mm and a maximum relative tension stress parallel of 5.09. It was observed that for fr_3 of 12 mm and larger, the peak stress location shifts from fr_3 to fr_2. This can be seen in the stress distribution plot in Figure X. The peak stress at fr3 decreases for larger fr3. However, the peak stress at fr2 exceeds the peak stress at fr3 for fr3 is > 11 mm.

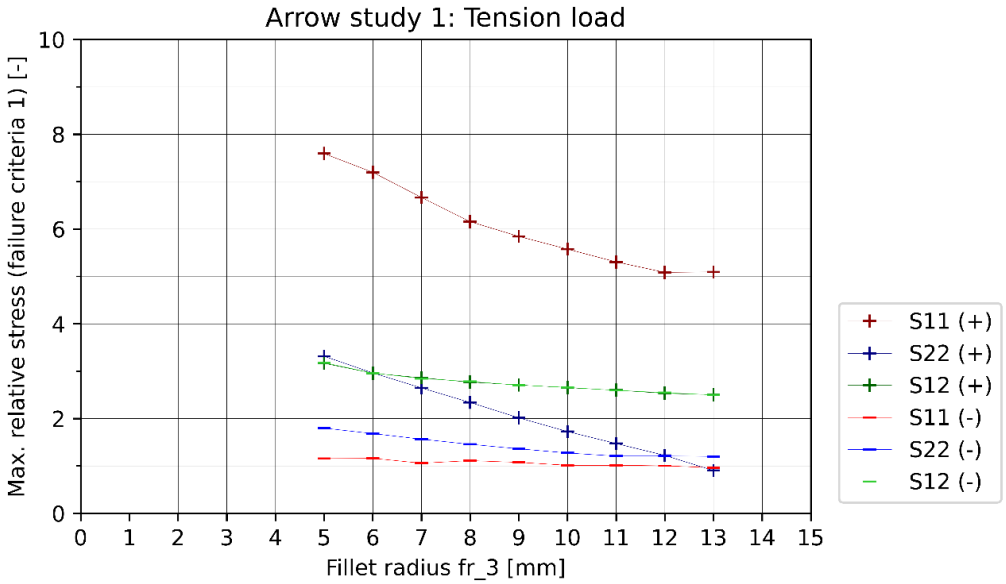

Figure H-TA-I: Arrow study 1 (tension): max. relative stresses (failure criteria 1)

Arrow study 2

Width w_2 is varied from 20 to 50 mm. All arrows in this study have a height h_1 of 80 mm and h_2 of 30 mm, width w_1 of 90 mm and fillet radius fr_1, fr_2, fr_3 and fr_4 of 5 mm. The maximum relative tension stress parallel is dominant for all arrows. There is no significant influence on the peak stresses for arrows with various w_2. The arrow with a w_2 of 50 mm has the lowest maximum relative stress of 7.46 whereas the arrow with w_2 of 25 mm has the highest maximum relative stress of 7.62.

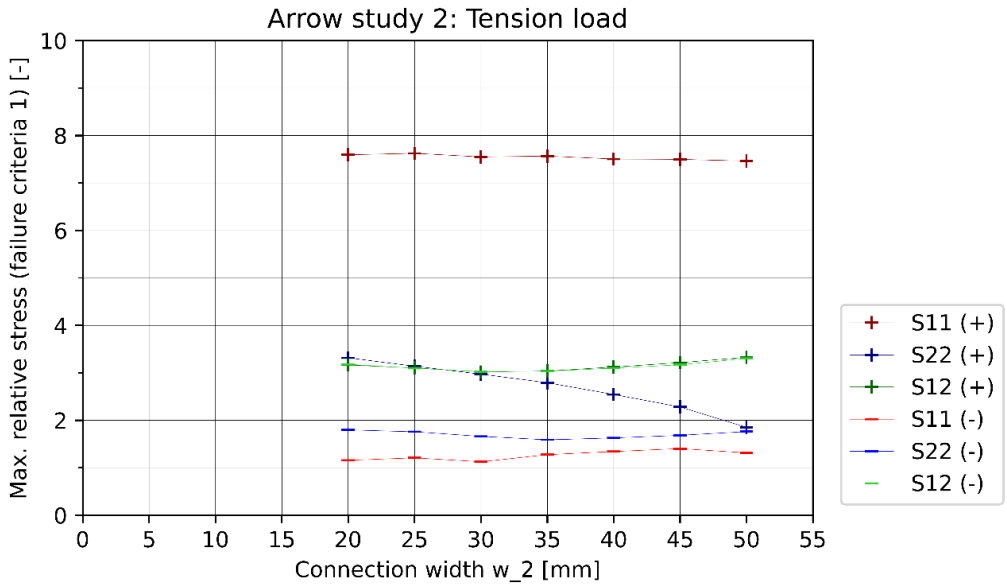

Figure H-TA-II: Arrow study 2 (tension): max. relative stresses (failure criteria 1)

Arrow study 3

Fillet radius fr_1 is varied from 6 to 24 mm. All arrows in this study have a height h_1 of 80 mm and h_2 of 30 mm, width w_1 of 90 mm and w_2 50 mm and fillet radius fr_2, fr_3 and fr_4 of 5 mm. All stresses remain roughly constant for the different fillet radius fr_1, see Fig. Larger fillet radii fr_1 than 24 mm were not possible in the geometry. The arrow with fr_1 is 15 mm has the lowest maximum relative tension stress parallel of 7.44.

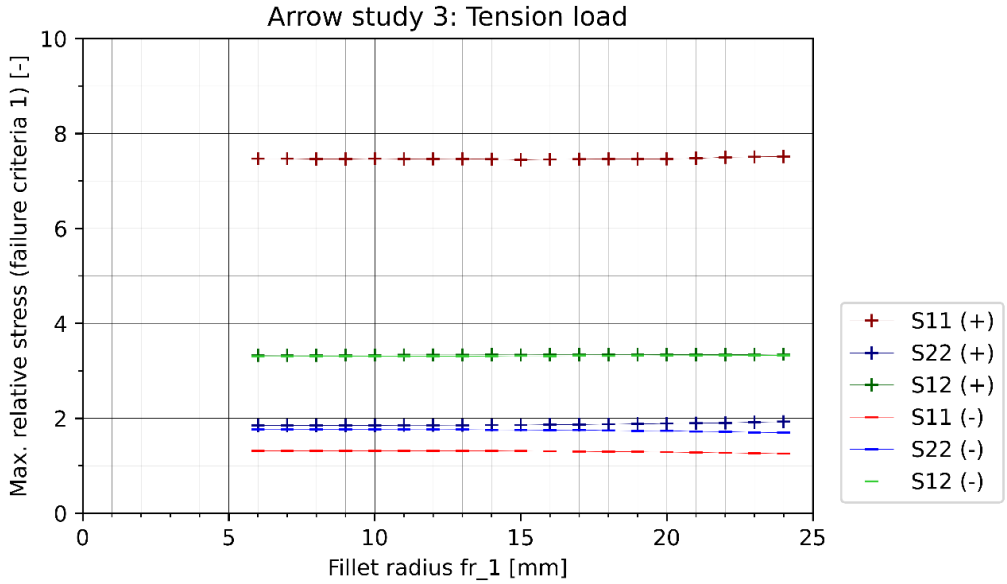

Figure H-TA-III: Arrow study 3 (tension): max. relative stresses (failure criteria 1)

Arrow study 4

Height h_2 is varied from 15 to 50 mm. All arrows in this study have a height h_1 of 90 mm, width w_1 of 90 mm and w_2 of 20 mm and fillet radius fr_1, fr_2, fr_3 and fr_4 of 5 mm. The maximum relative tension stress parallel is dominant for all arrows. A reduction of the peak stress is observed for arrows with a larger h_2. The best performing arrow has a height h_2 of 50 mm and maximum relative tension stress parallel of 6.59.

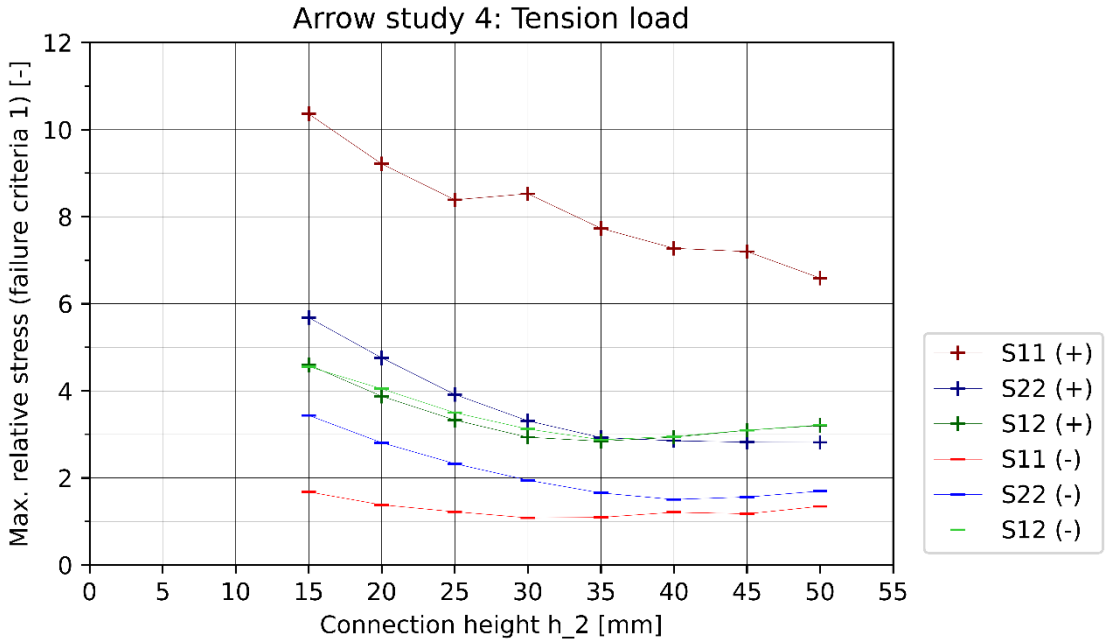

Figure H-TA-IV: Arrow study 4 (tension): max. relative stresses (failure criteria 1)

Yin Yang

Yin yang study 1

Radius r_1 is varied from 10 to 18 mm. Width w_1 is dependent on r_1 and varies from 60 to 28 mm. A static fillet radius fr_1 of 5 mm is applied. For all the yin yang connections, the maximum relative tension stress parallel is dominant by far. A yin yang with a larger radius obviously performs better than a yin yang with a smaller radius since more length of the floor seam has an interlocking shape. The best performing yin yang has a r_1 of 18 mm with a maximum relative tension stress parallel of 22.60.

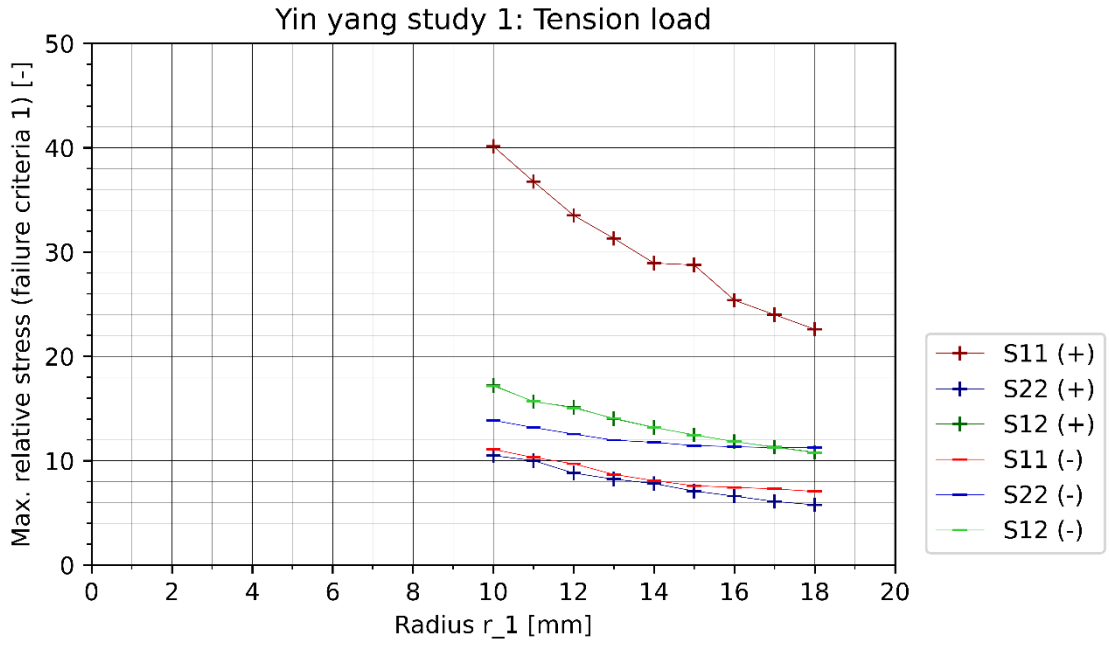

Figure H-TYY-I: Yin yang study 1 (tension): max. relative stresses (failure criteria 1)

Yin yang study 2

Fillet radius fr_1 is varied from 5 to 10 mm. Larger fillet radii were not possible in the geometry. The static radius r_1 is 18 mm and the width w_1 is 28 mm. Applying a larger fr_1 does not significantly reduce the peak stresses. Tension stress parallel is the critical stress for all yin yangs, which varies from 22.60 when fr_1 is 5 mm to 21.75 when fr_1 is 10 mm.

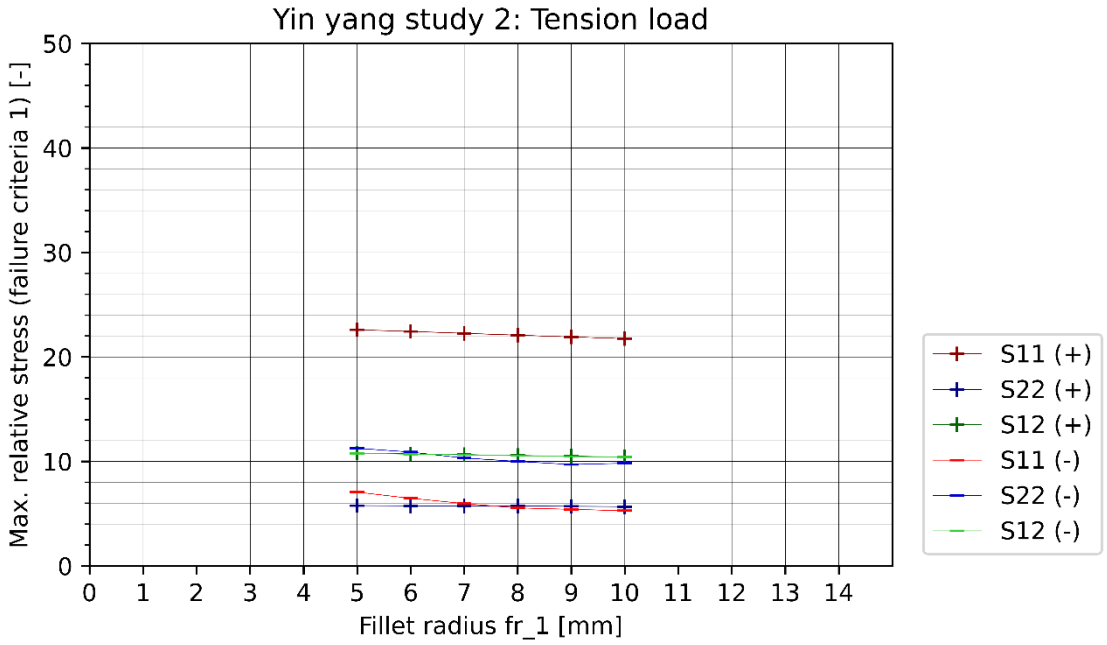

Figure H-TYY-II: Yin yang study 2 (tension): max. relative stresses (failure criteria 1)

Yin yang study 3

The yin yangs in this study have a static radius r_1 of 15 mm and a width w_1 of 40 mm. The fillet radius fr_1 is varied from 5 to 26 mm. Larger fillet radii were not possible in the geometry. A peak stress reduction is observed for increasing the fillet radius. Tension stress parallel is the critical stress for all yin yangs, which varies from 28.76 for fr_1 of 5 mm to 24.68 for fr_1 of 26 mm.

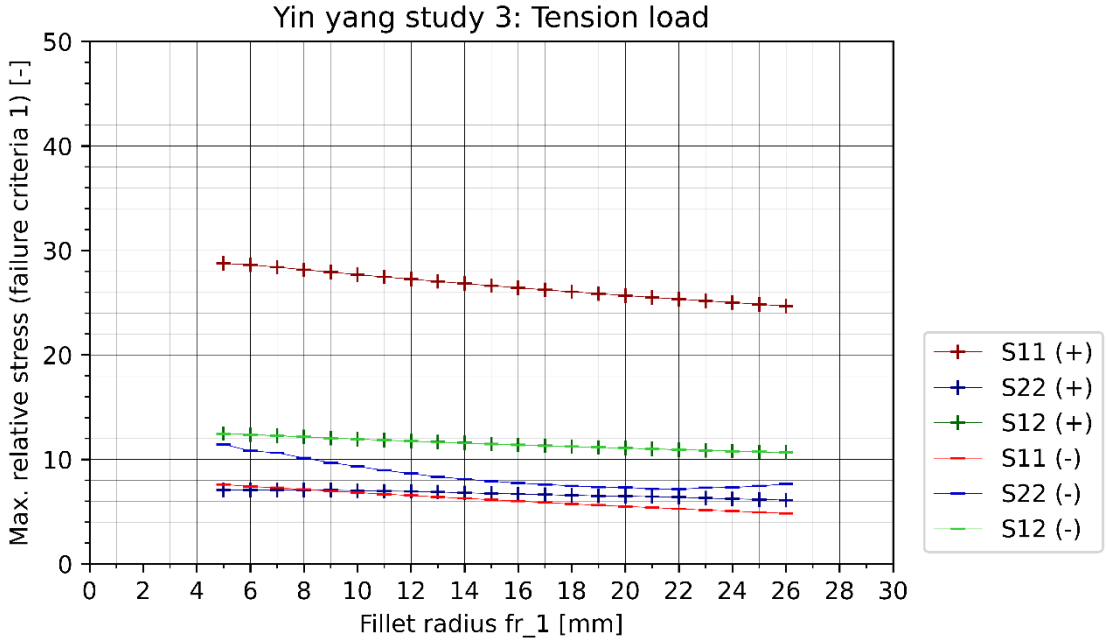

Figure H-TYY-III: Yin yang study 3 (tension): max. relative stresses (failure criteria 1)

Shear load application

Dovetail

Dovetail study 1

In dovetail study 1, the width w_2 is varied from 5 to 45 mm. These dovetails have a static height h_1 of 50 mm and fillet radius fr_1 of 5 mm. A reduction of the peak stresses can be observed when increasing w_2. Tension stress perpendicular is critical for all dovetails in this study. The dovetail with a width w_2 of 45 mm has the lowest maximum relative tension stress perpendicular of 2.34.

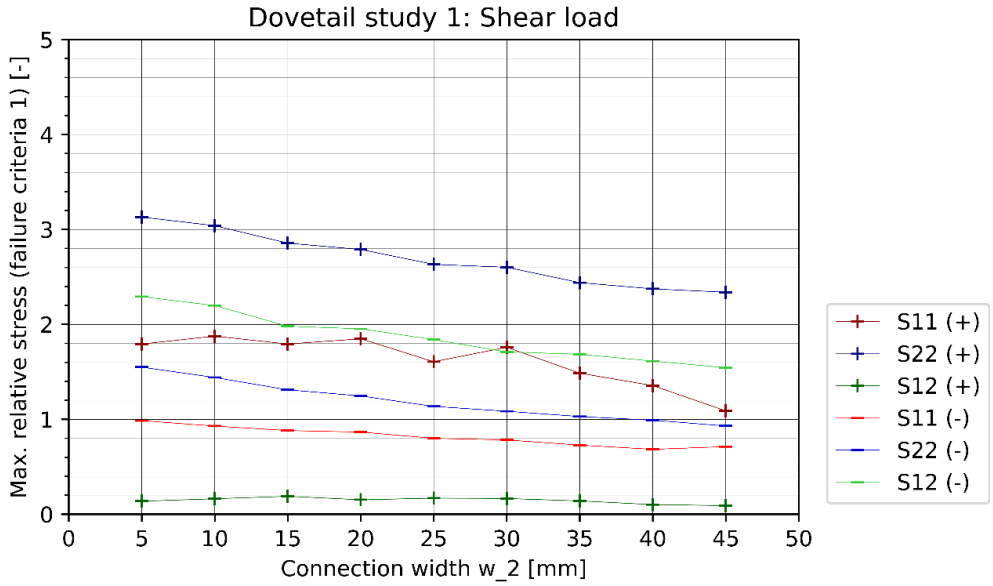

Figure H-SD-I: Dovetail study 1 (shear): max. relative stresses (failure criteria 1)

Dovetail study 2

The height h_1 of the dovetail is varied from 20 to 190 mm. The width w_2 is 40 mm and the fillet radius fr_1 is 5 mm. The maximum relative tension stress perpendicular is dominant for all dovetails. Overall, a small reduction of the governing stress can be observed, except for h_1 between 120-160 mm. The strongest dovetail from this study has a h_1 of 190 mm and maximum relative tension stress perpendicular of 1.85.

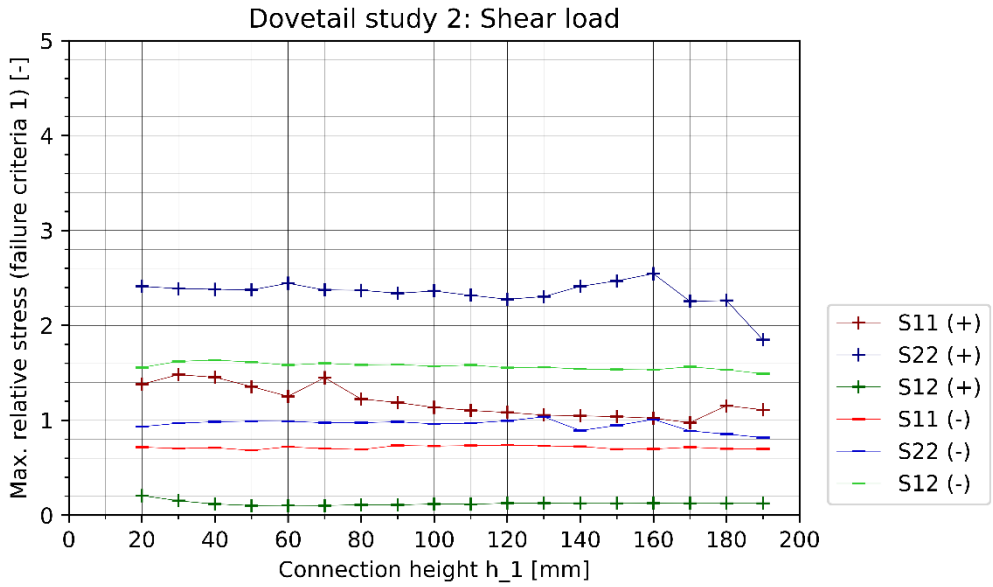

Figure H-SD-II: Dovetail study 2 (shear): max. relative stresses (failure criteria 1)

Dovetail study 3

Another height variation study is performed with a static width w_2 of 20 mm and fillet radius fr_1 of 5 mm. The height h_1 is varied from 20 mm to 190 mm. The maximum relative tension stress perpendicular is dominant for all dovetails and increases when increasing h_1. The best performing dovetail has a h_1 of 20 mm and a maximum relative tension stress perpendicular of 2.48.

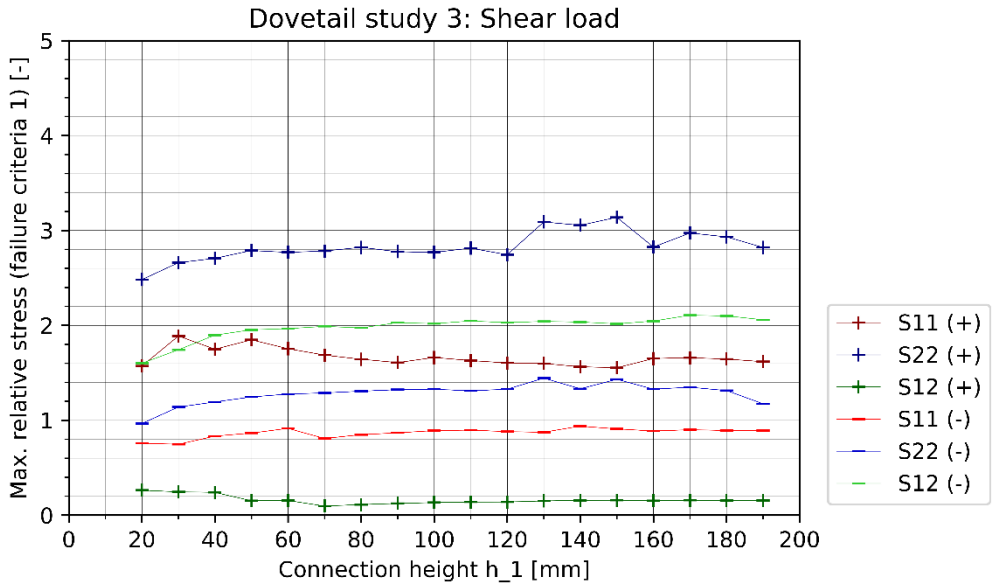

Figure H-SD-III: Dovetail study 3 (shear): max. relative stresses (failure criteria 1)

Dovetail study 4

In dovetail study 4, the height h_1 is varied from 40 to 190 mm while the static width is w_2 20 mm and the static fillet radius fr_1 is 10 mm. The stresses remain almost constant for varying h_1. The maximum relative tension stress perpendicular is dominant for all dovetails. The most optimal dovetail from this study has a h_1 of 40 mm and has a maximum relative tension stress perpendicular of 1.90.

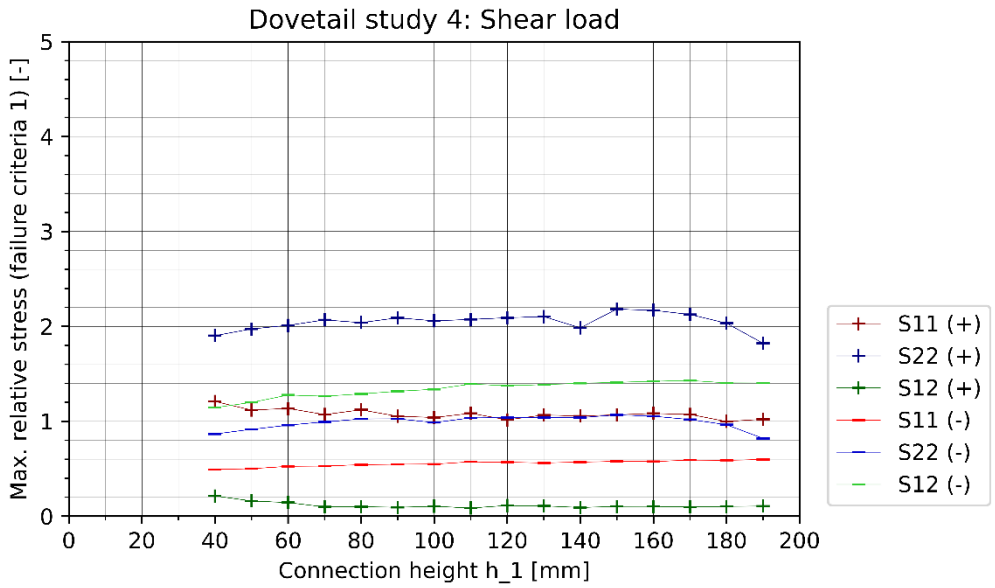

Figure H-SD-IV: Dovetail study 4 (shear): max. relative stresses (failure criteria 1)

Dovetail study 5

In dovetail study 5, the height h_1 is varied from 50 to 190 mm while the static width is w_2 20 mm and the static fillet radius fr_1 is 15 mm. The height h_1 of the dovetail does not have a big influence on the peak stresses. As can be seen in Figure X, all stresses remain roughly constant while varying the width. The dovetail with a height h_1 has a maximum relative tension stress perpendicular of 1.40.

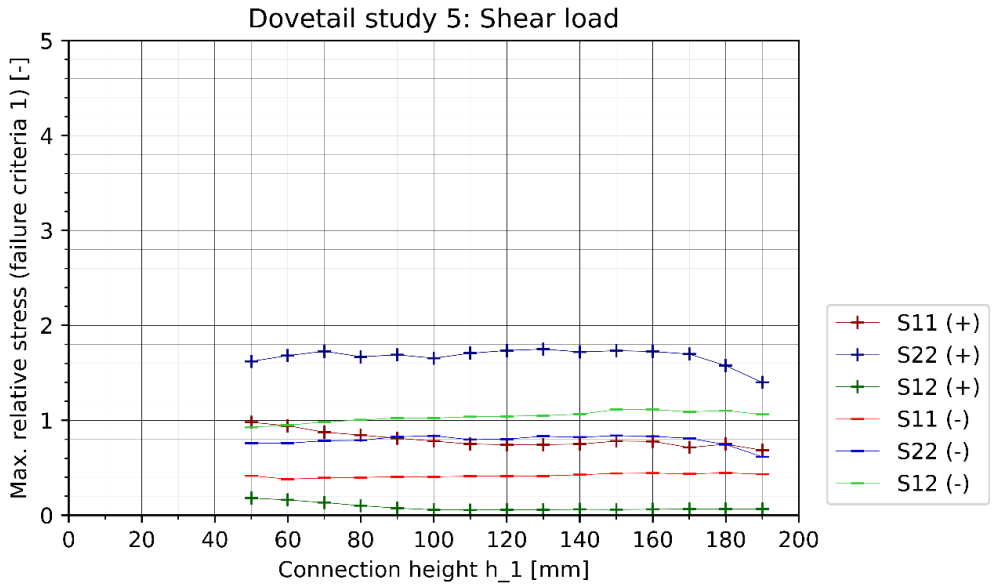

Figure H-SD-V: Dovetail study 5 (shear): max. relative stresses (failure criteria 1)

Dovetail study 6

The heights h_1 of the dovetails in study 7 vary from 40 mm to 190 mm. The static width w_2 is 40 mm and the fillet radius fr_1 is 10 mm. The stresses vary a bit when varying the h_1, the governing stress varies from 1.48 to 2.04. The maximum relative tension stress perpendicular is dominant for all dovetails. The best performing dovetail has a h_1 of 190 mm and a maximum relative tension stress perpendicular of 1.48.

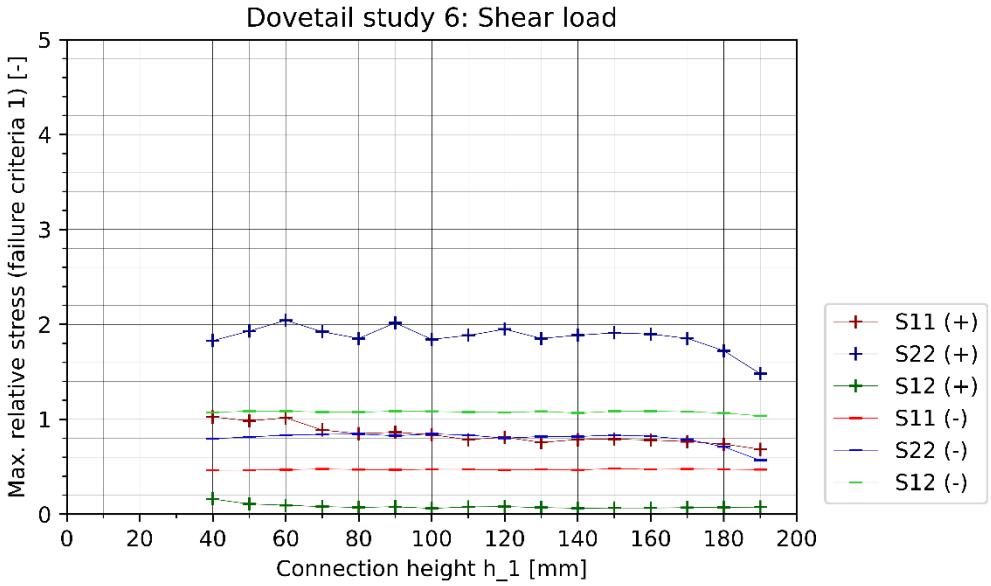

Figure H-SD-VI: Dovetail study 6 (shear): max. relative stresses (failure criteria 1)

Dovetail study 7

The heights h_1 of the dovetails in study 7 vary from 40 mm to 180 mm. The static width w_2 is 40 mm and the fillet radius fr_1 is 15 mm. The stresses remain more or less constant for different connection heights h_1. A dovetail with h_1 of 180 mm performs the best, though differences to other dovetails in this study are minimal. The tension stress perpendicular is dominant and has a value of 1.48. The peak stresses are lower by using rounder edges as can be seen in the stress distribution plots in Figure X.

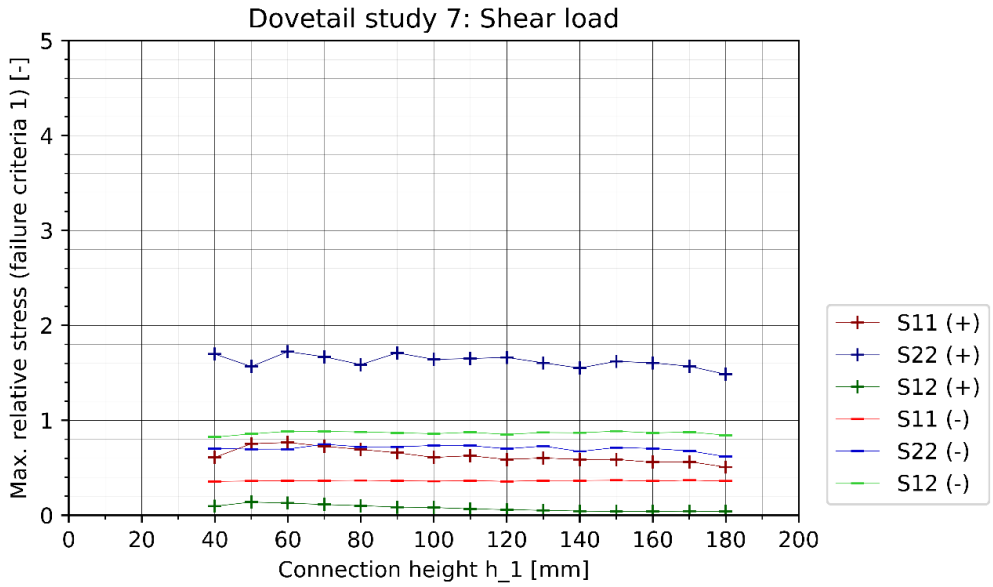

Figure H-SD-VII: Dovetail study 7 (shear): max. relative stresses (failure criteria 1)

Arrow

Arrow study 1

Fillet radius fr_3 is varied from 5 to 13 mm. All arrows in this study have a height h_1 of 80 mm and h_2 of 30 mm, width w_1 of 90 mm and w_2 20 mm and fillet radius fr_1, fr_2 and fr_4 of 5 mm. The maximum relative tension stress perpendicular is governing and constant at a value of 3.21 for all arrows.

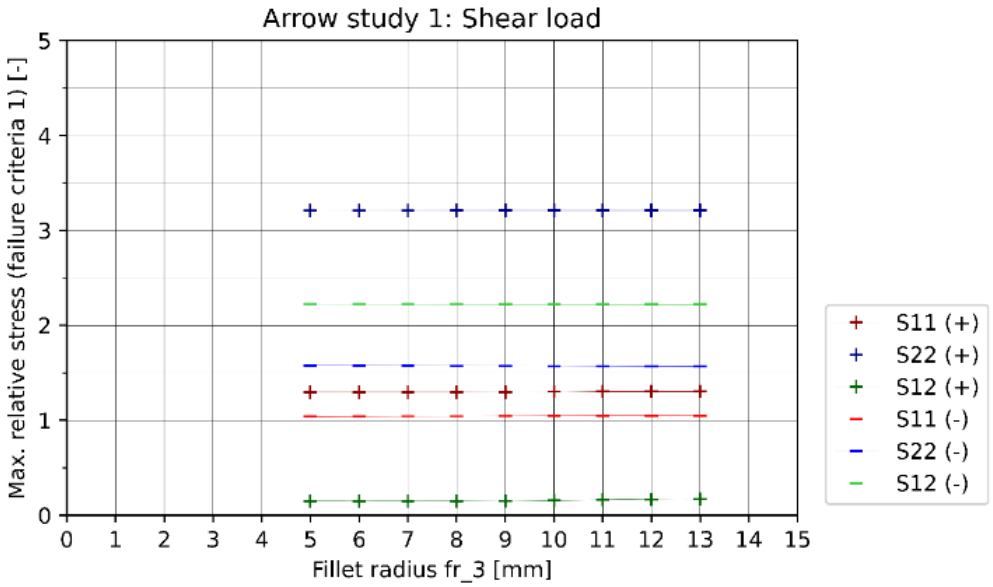

Figure H-SA-I: Arrow study 1 (shear): max. relative stresses (failure criteria 1)

Arrow study 2

Width w_2 is varied from 20 to 50 mm. All arrows in this study have a height h_1 of 80 mm and h_2 of 30 mm, width w_1 of 90 mm and fillet radii fr_1, fr_2, fr_3 and fr_4 of 5 mm. The maximum relative tension stress perpendicular is dominant for all different widths and reduces when increasing w_2. The order of stresses from dominant to not dominant is $S22^+$, $S12^-$, $S22^-$, $S11^+$, $S11^-$, $S12^+$ which is identical to study 1. The strongest arrow has a w_2 of 50 mm and a maximum relative tension stress perpendicular of 2.39.

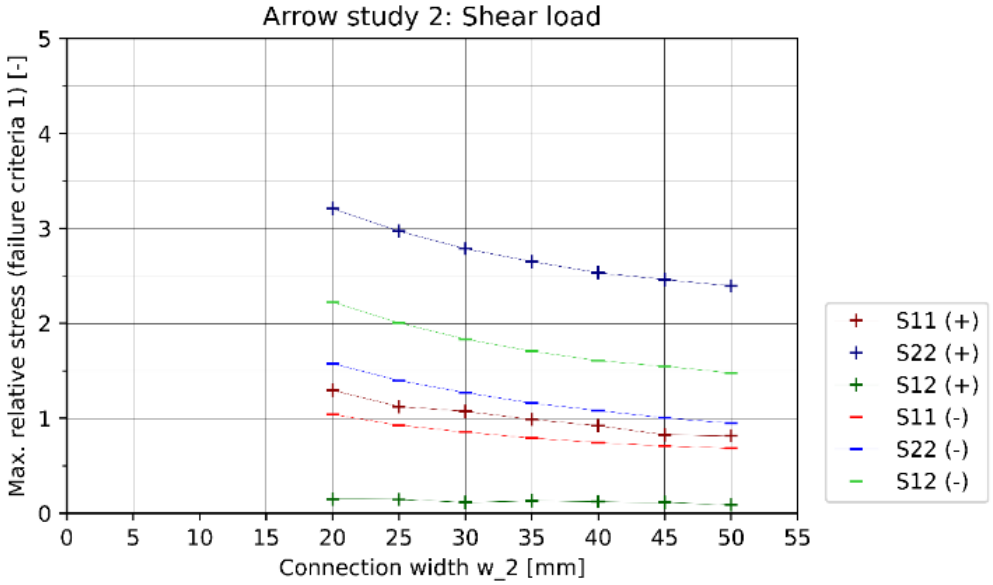

Figure H-SA-I: Arrow study 1 (shear): max. relative stresses (failure criteria 1)

Arrow study 3

Fillet radius fr_1 is varied from 6 to 24 mm. All arrows in this study have a height h_1 of 80 mm and h_2 of 30 mm, width w_1 of 90 mm and w_2 50 mm and fillet radii fr_2, fr_3 and fr_4 of 5 mm. Tension stress perpendicular is critical for all arrows. This stress reduces when increasing fr_1 from 6 to 20 mm. Though, this stress increases when increasing fr_1 from 21 to 26 mm. The best performing arrow has a fr_1 of 20 mm where the maximum relative tension stress perpendicular is 1.55.

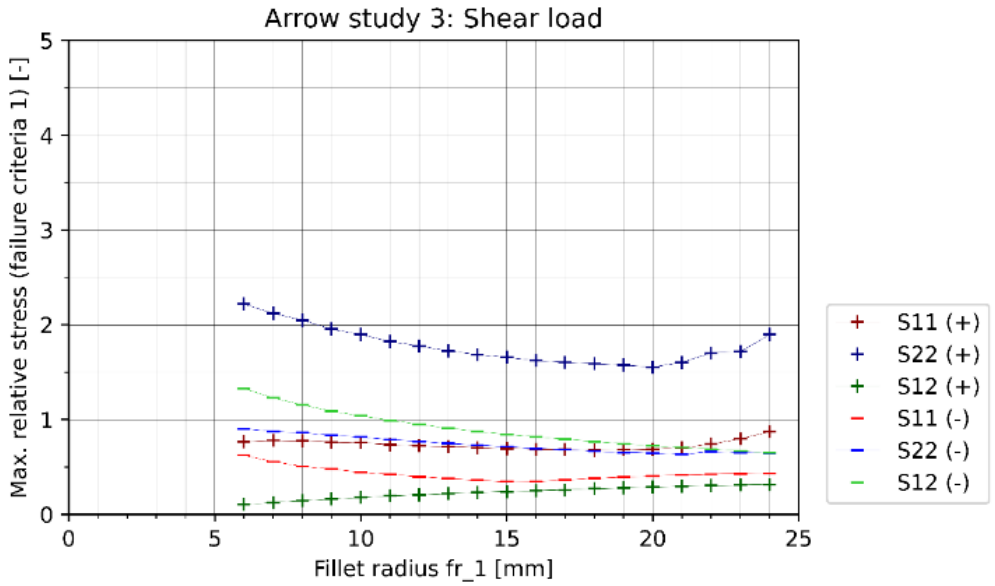

Figure H-SA-III: Arrow study 3 (shear): max. relative stresses (failure criteria 1)

Arrow study 4

Height h_2 is varied from 15 to 50 mm. All arrows in this study have a height h_1 of 90 mm, width w_1 of 90 mm and w_2 of 20 mm and fillet radii fr_1, fr_2, fr_3 and fr_4 of 5 mm. All stresses remain roughly constant while varying h_2. Tension stress perpendicular is critical for all arrows, where the lowest value of 2.96 is found for h_2 is 50 mm and the highest value of 2.98 is found for h_2 is 20 mm. The order of stress dominancy is identical to study 1 and 2.

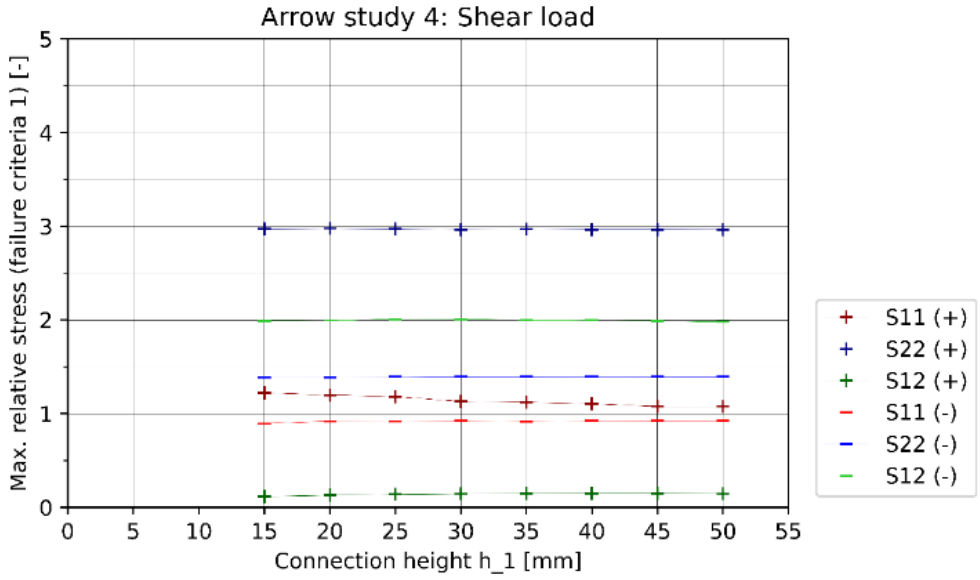

Figure H-SA-IV: Arrow study 4 (shear): max. relative stresses (failure criteria 1)

Yin Yang

Yin yang study 1

Radius r_1 is varied from 10 to 18 mm. Width w_1 is dependent on r_1 and varies from 60 to 28 mm. A static fillet radius fr_1 of 5 mm is applied. The maximum relative tension stress perpendicular is critical in all cases and increases for larger r_1. The lowest value of 3.80 is found for a yin yang with r_1 of 13 mm.

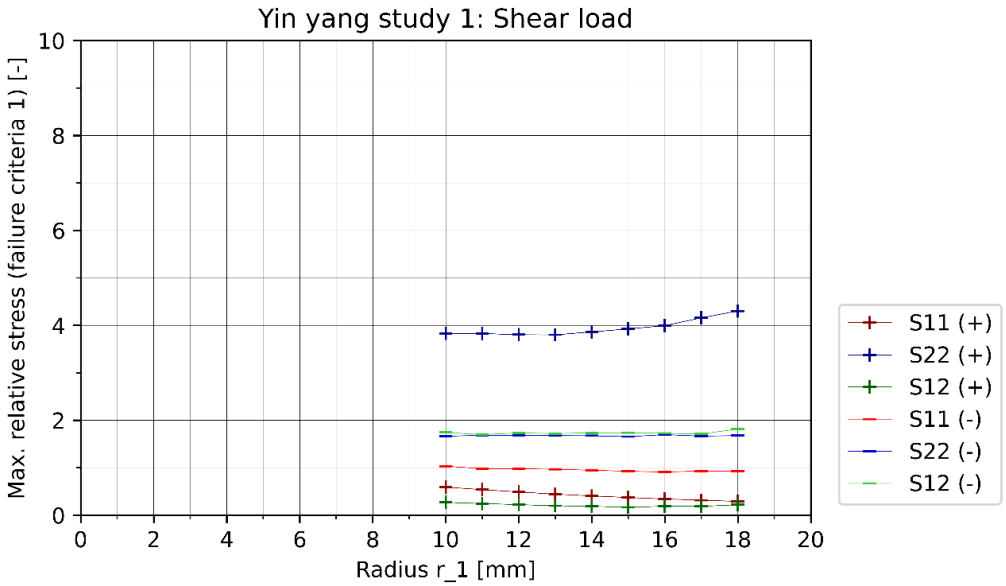

Figure H-SYY-I: Yin yang study 1 (shear): max. relative stresses (failure criteria 1)

Yin yang study 2

Fillet radius fr_1 is varied from 5 to 10 mm. The static radius r_1 is 18 mm and the width w_1 is 28 mm. The maximum relative tension stress perpendicular is critical in all cases and decreases when increasing fr_1 between 5 mm and 9 mm. The yin yang with a fr_1 of 9 mm has the lowest maximum relative tension stress perpendicular with a value of 3.69.

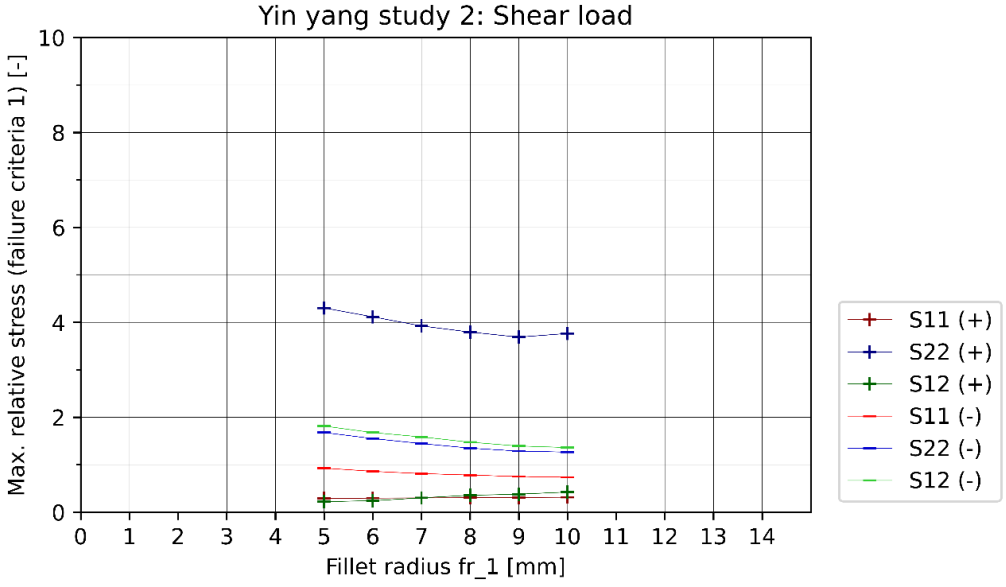

Figure H-SYY-II: Yin yang study 2 (shear): max. relative stresses (failure criteria 1)

Yin yang study 3

The yin yangs in this study have a static radius r_1 of 15 mm and a width w_1 of 40 mm. The fillet radius fr_1 is varied from 5 to 26 mm. The maximum tension stress perpendicular is critical in all cases. A decrease is observed for fr_1 5 mm to 20 mm and an increase is observed for fr_1 20 mm to 26 mm. The yin yang with a fr_1 of 20 mm performs the best and has a maximum relative tension stress perpendicular of 2.77. The maximum relative compression stress parallel makes jumps when varying fr_1. A possible reason is that the peak stress location shifts for different fr_1.

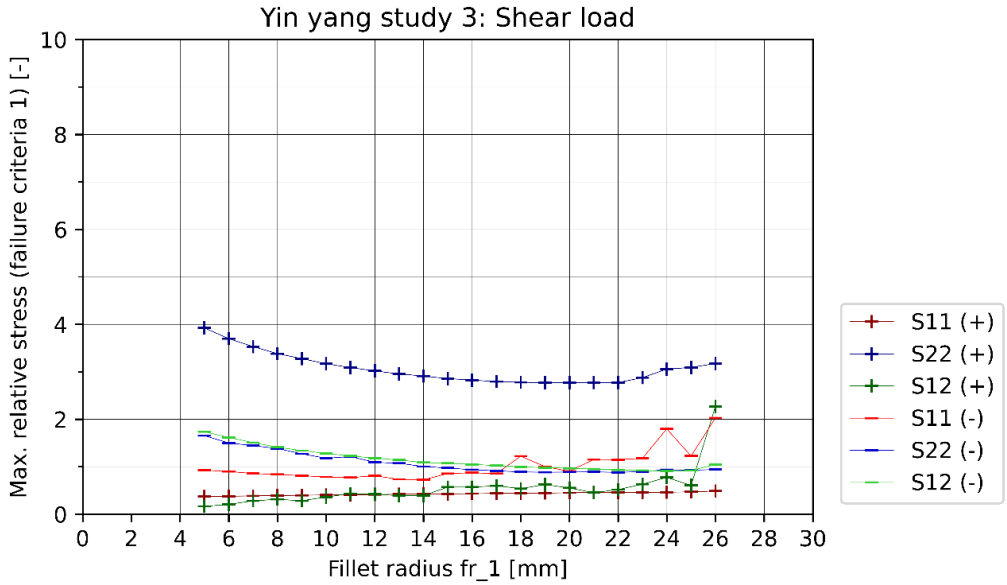

Figure H-SYY-III: Yin yang study 3 (shear): max. relative stresses (failure criteria 1)

Appendix I: Connection designs

Dovetails study 1
Varying w_2: 5 - 45 mm

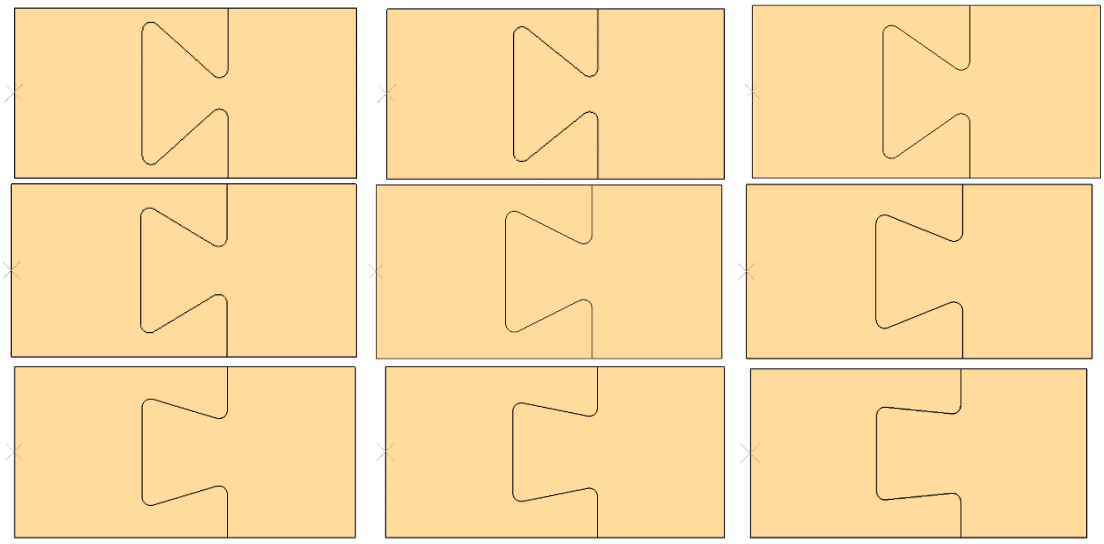

Dovetails study 2
Varying h_1: 20 - 190 mm

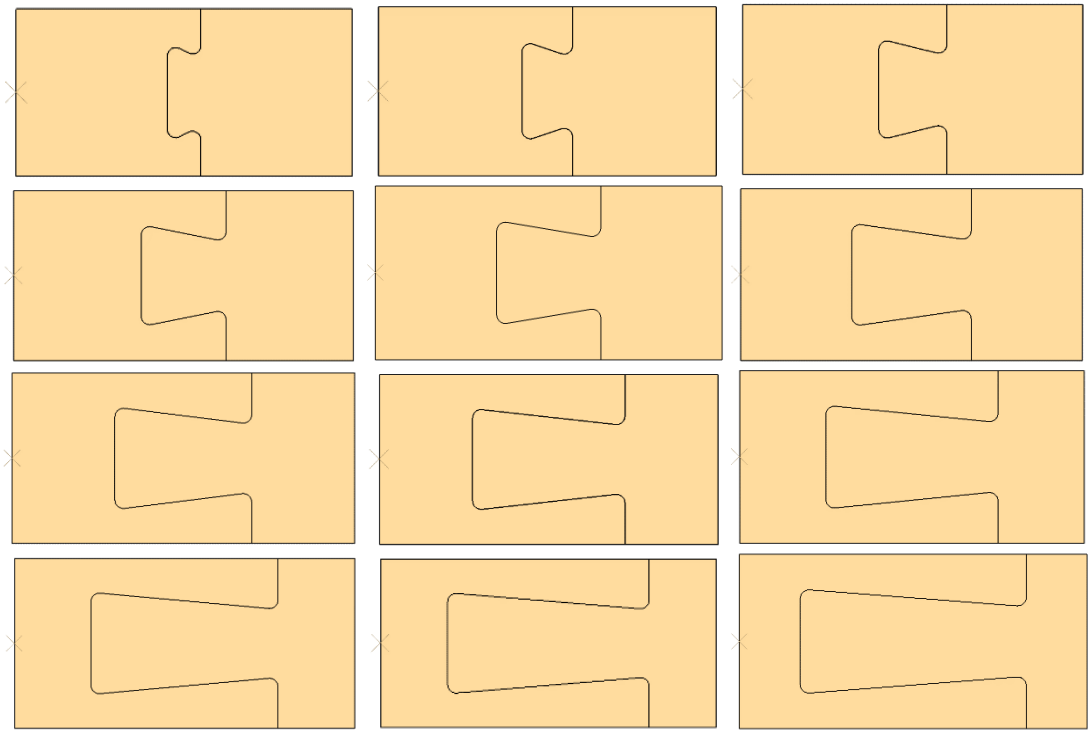

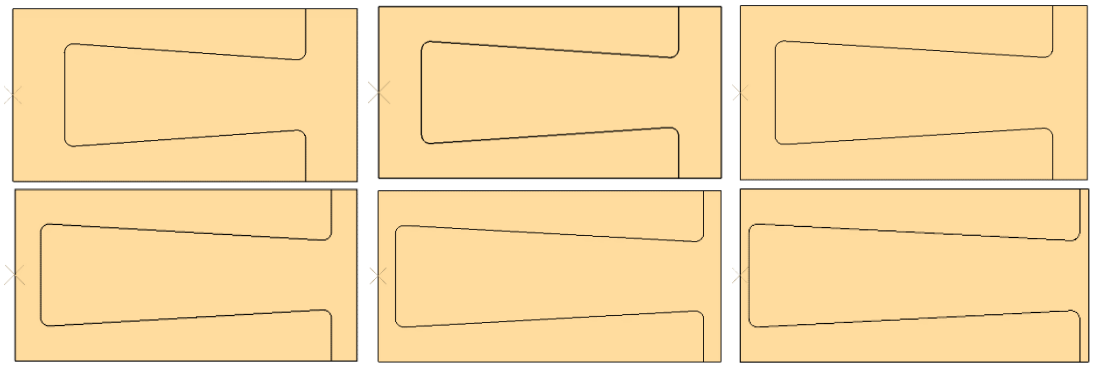

Dovetails study 3

Varying h_1: 20 - 190 mm

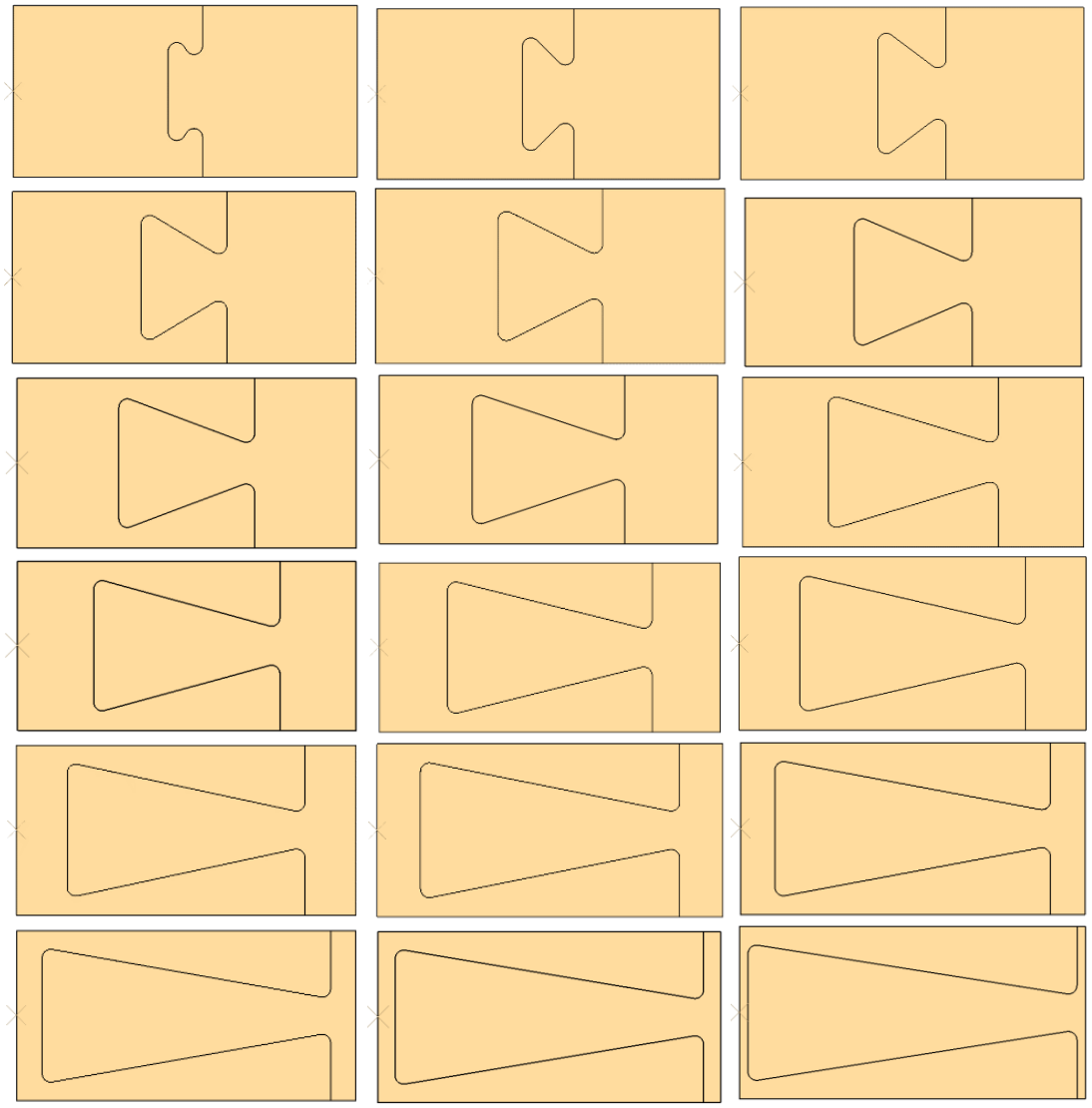

Dovetails study 4

Varying h_1: 40 - 190 mm

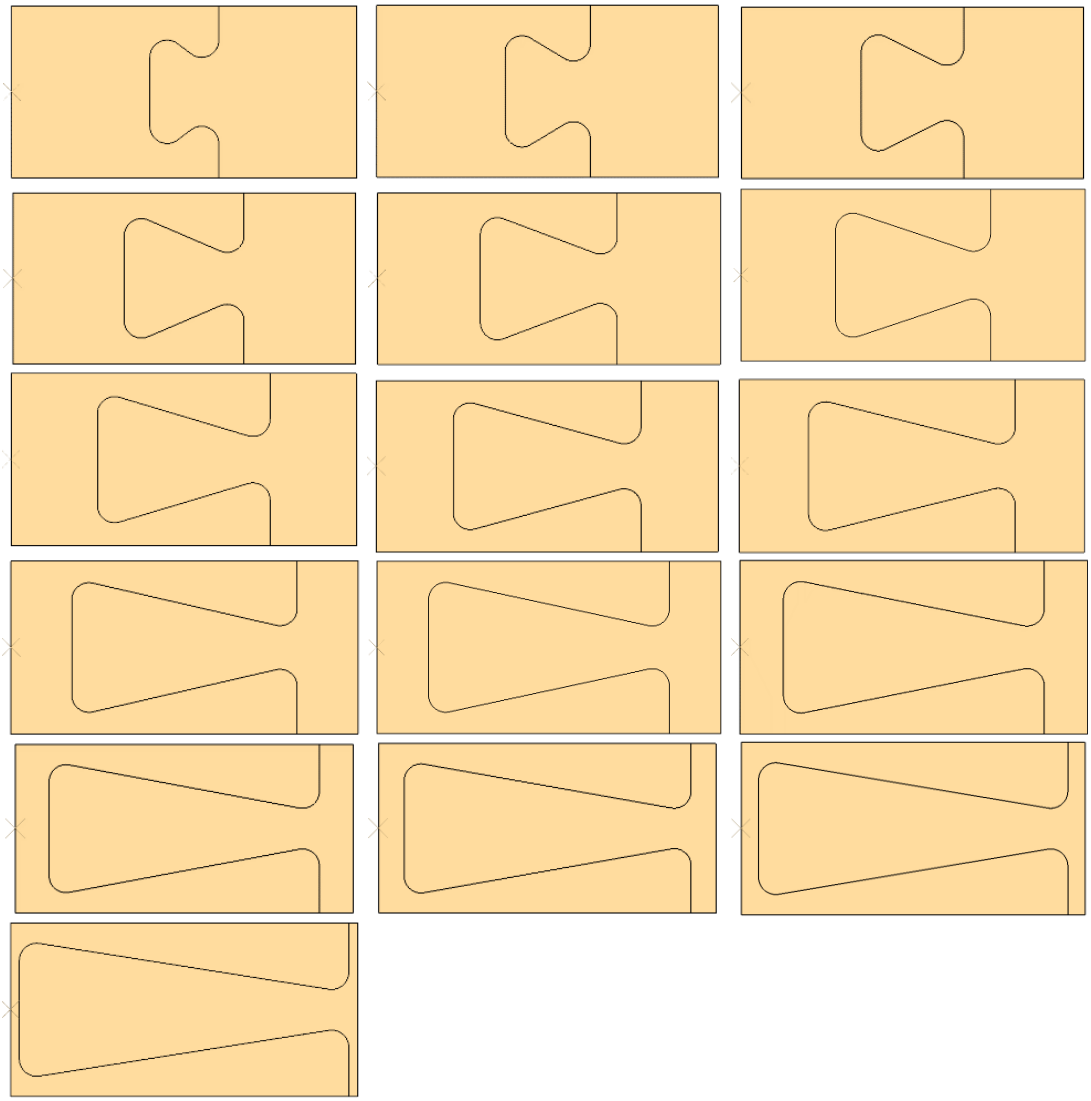

Dovetails study 5

Varying h_1: 50 - 190 mm

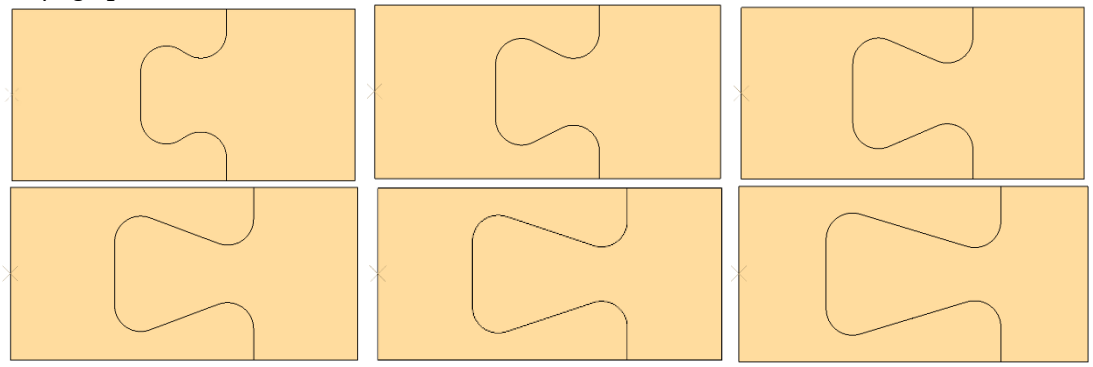

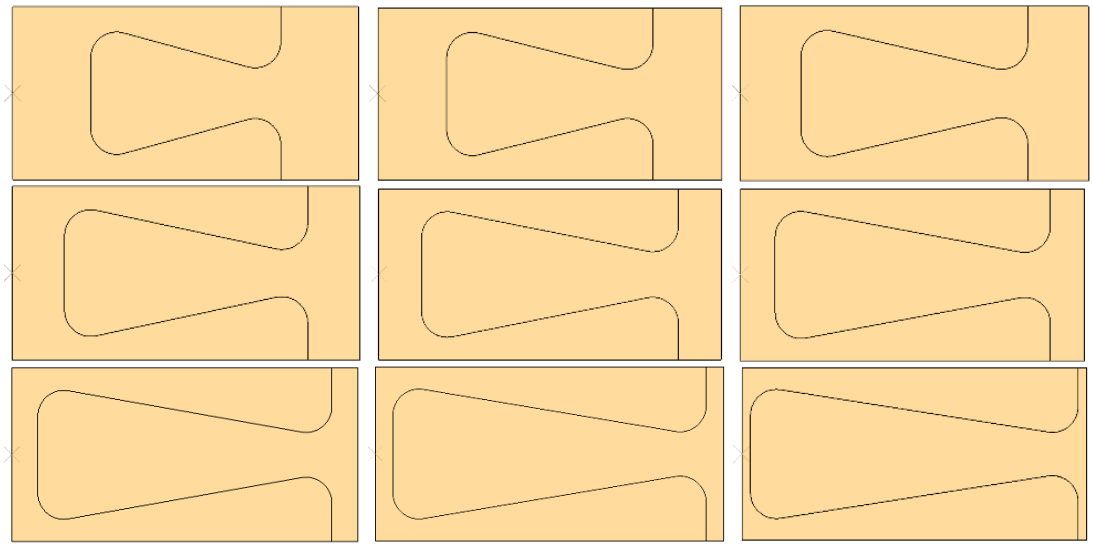

Dovetails study 6

Varying h_1: 40 - 190 mm

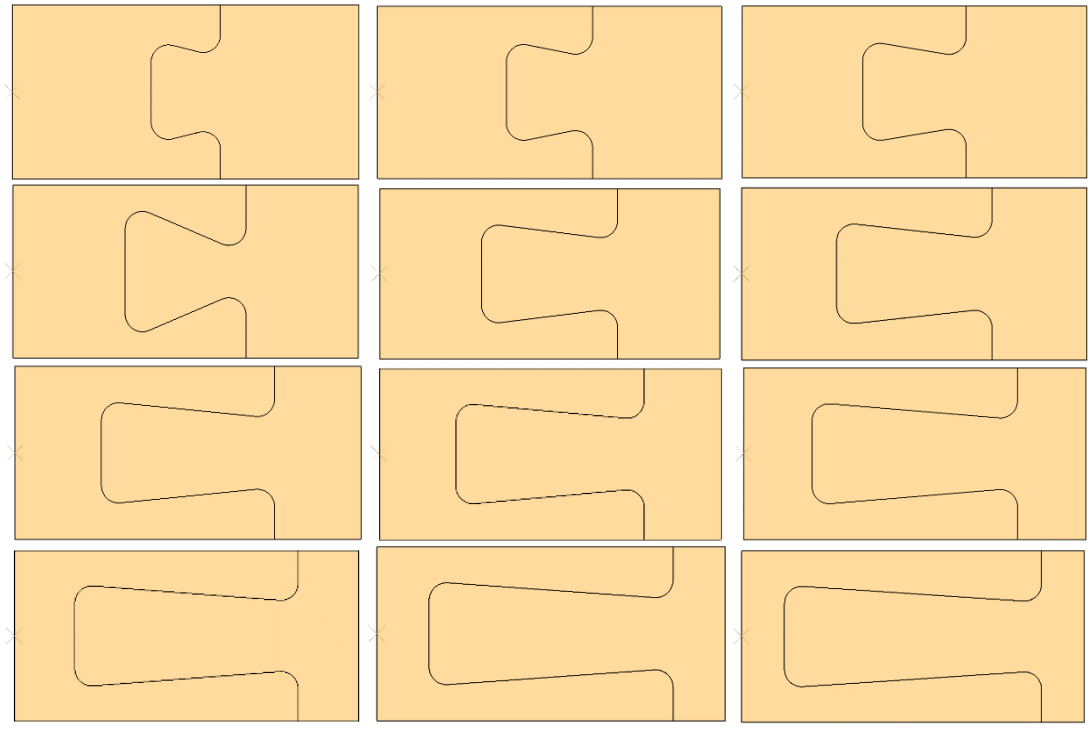

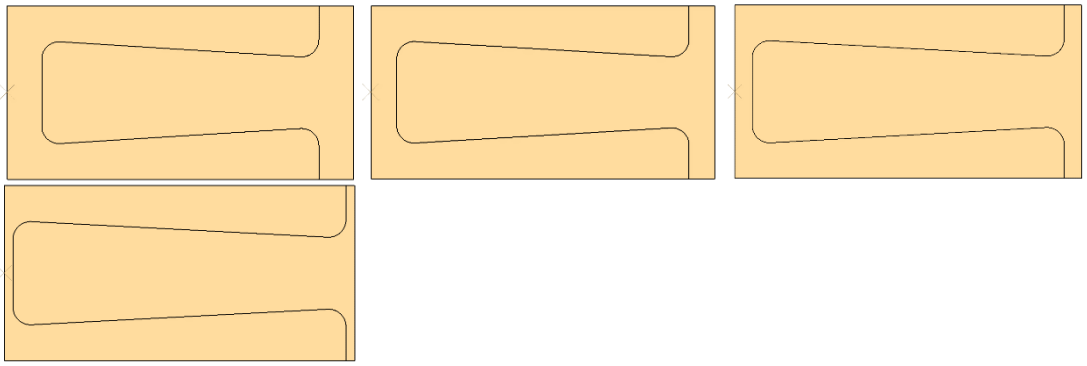

Dovetails study 7

Varying h_1: 40 - 180 mm

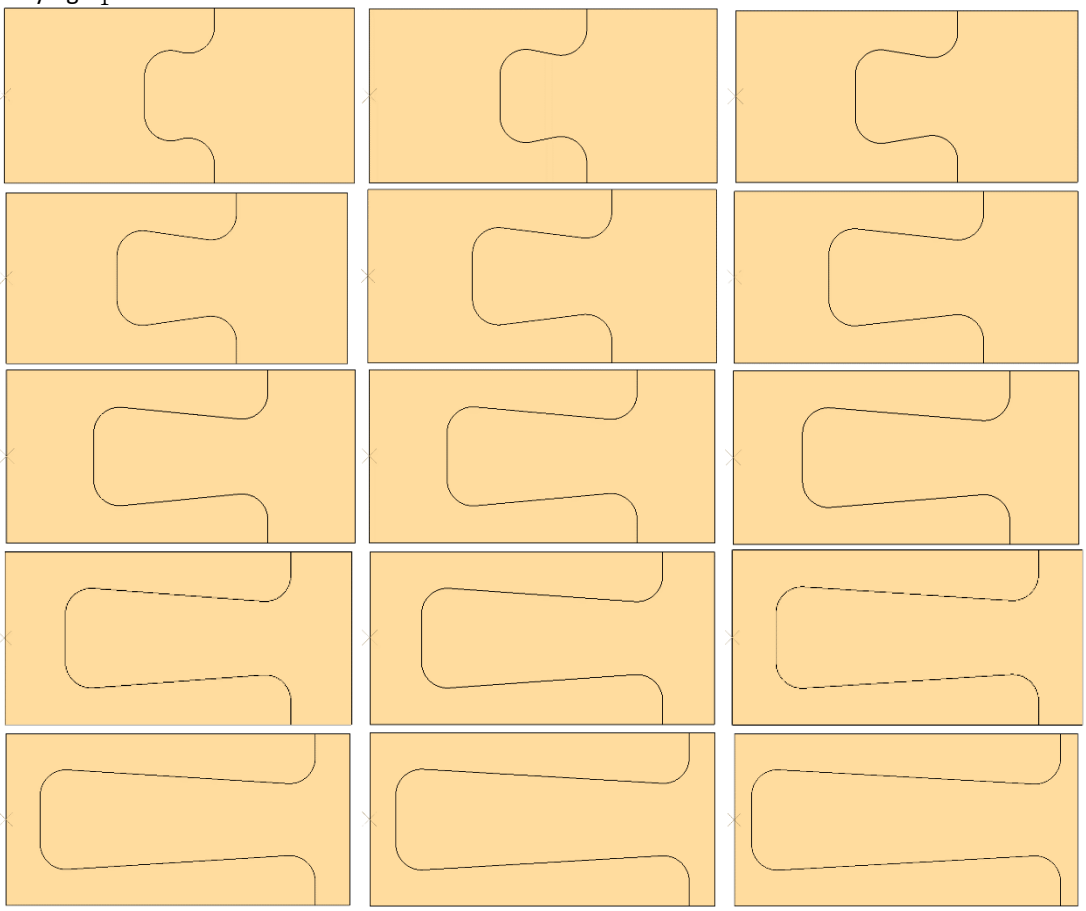

Arrows study 1

Varying fr_3: 5 – 13 mm

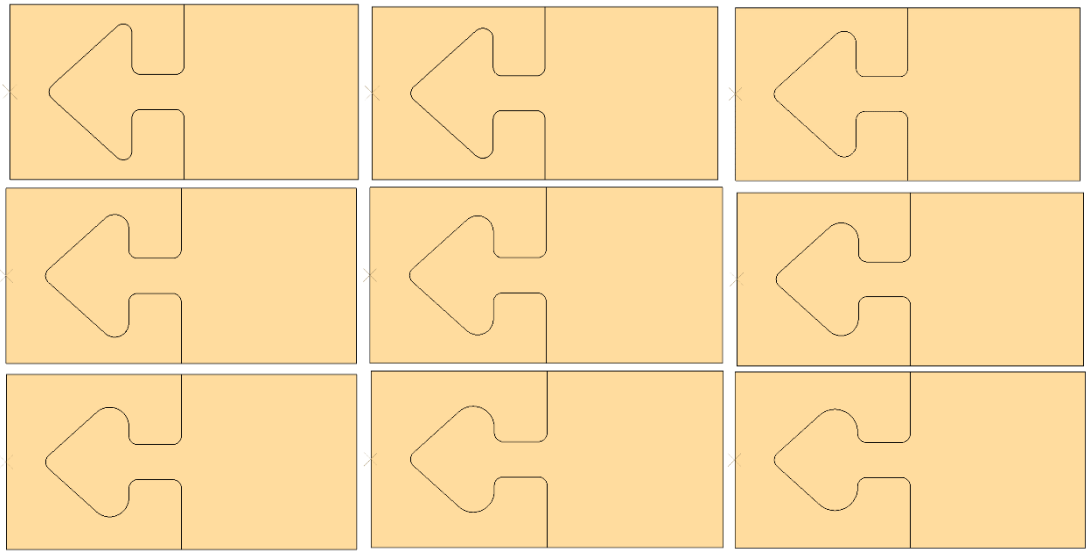

Arrows study 2

Varying w_2: 20 - 50 mm

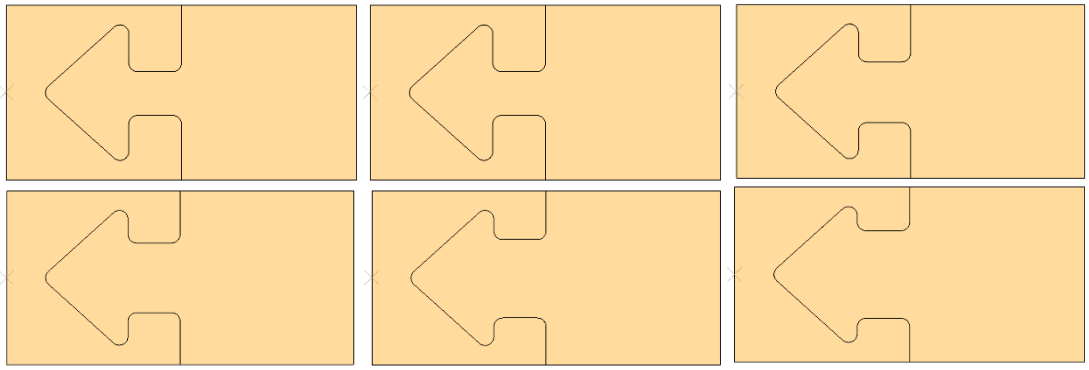

Arrows study 3

Varying fr_1: 6 - 24 mm

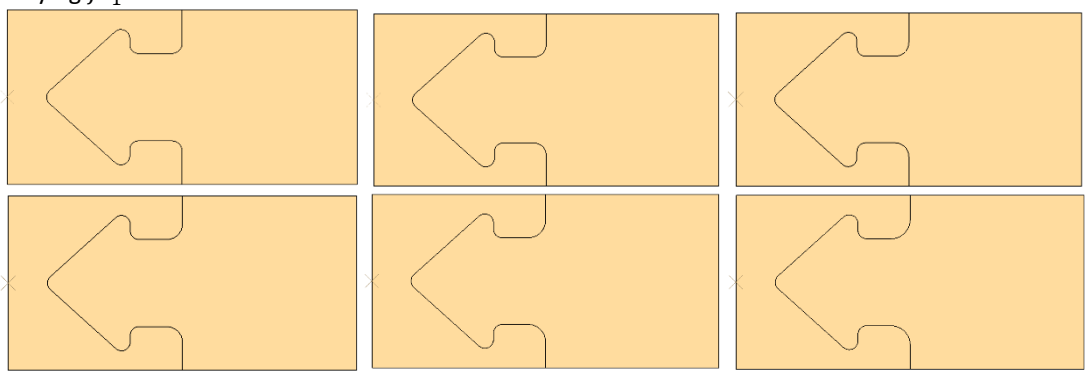

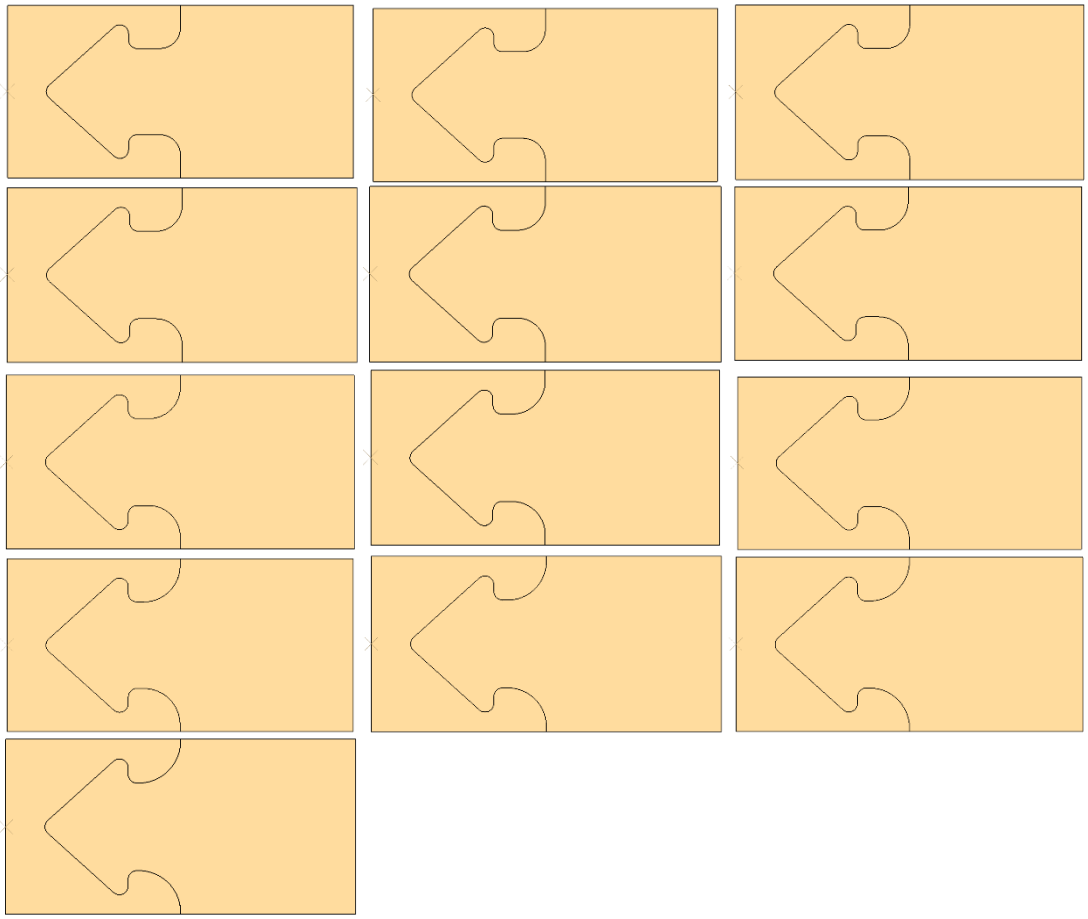

Arrows study 4

Varying h_2: 15 - 50 mm

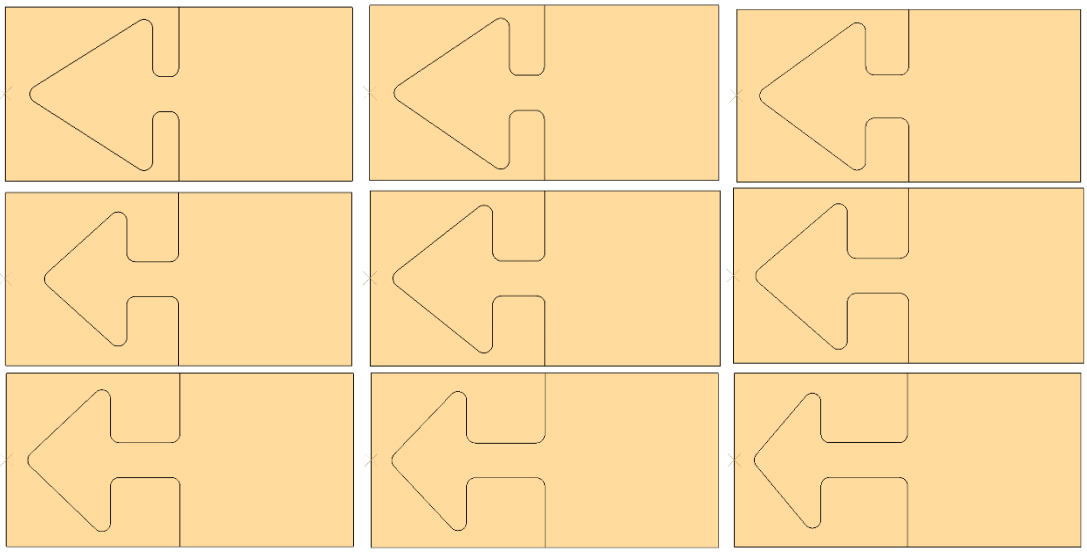

Yin yang study 1

Varying r_1: 10 – 18 mm

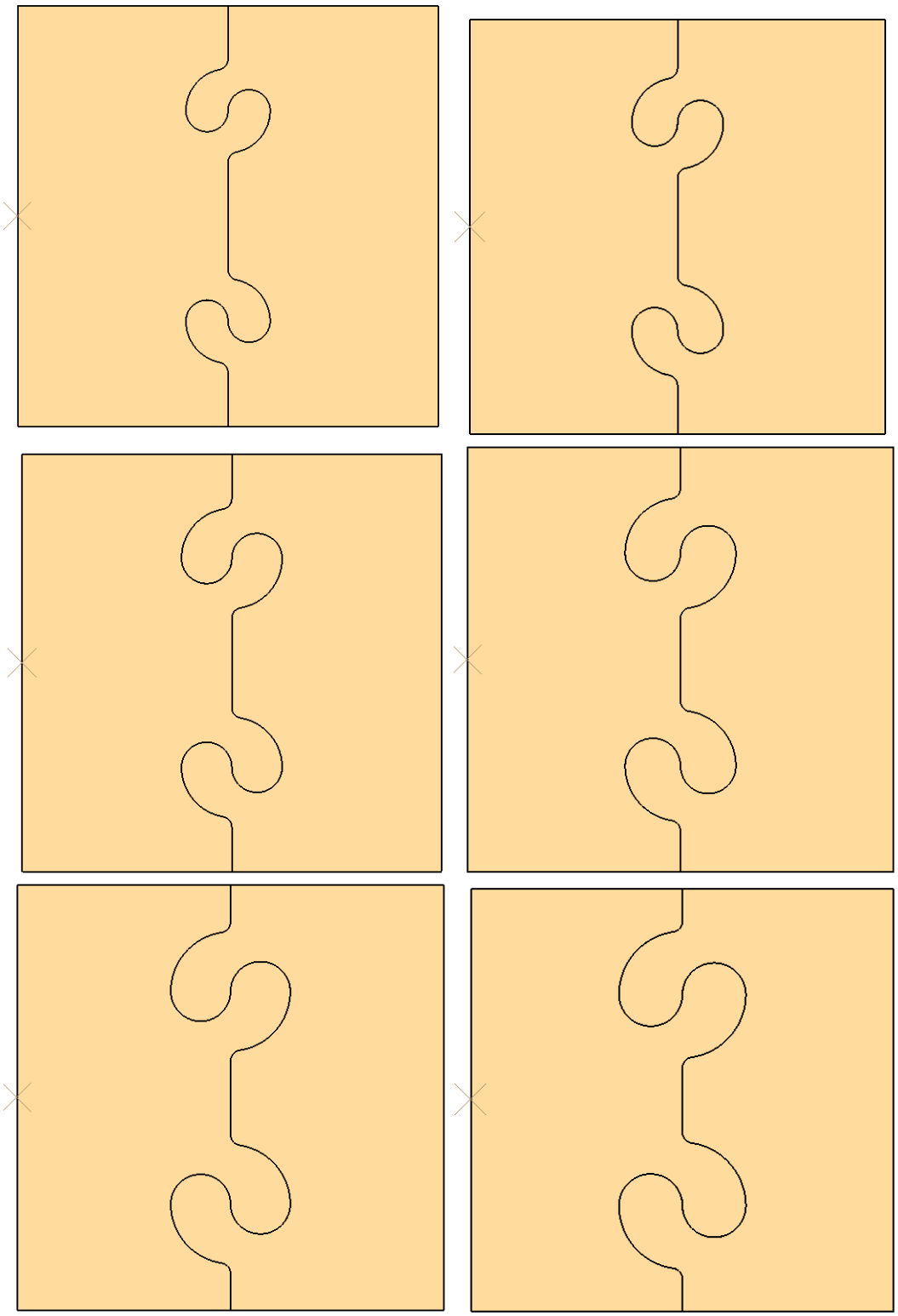

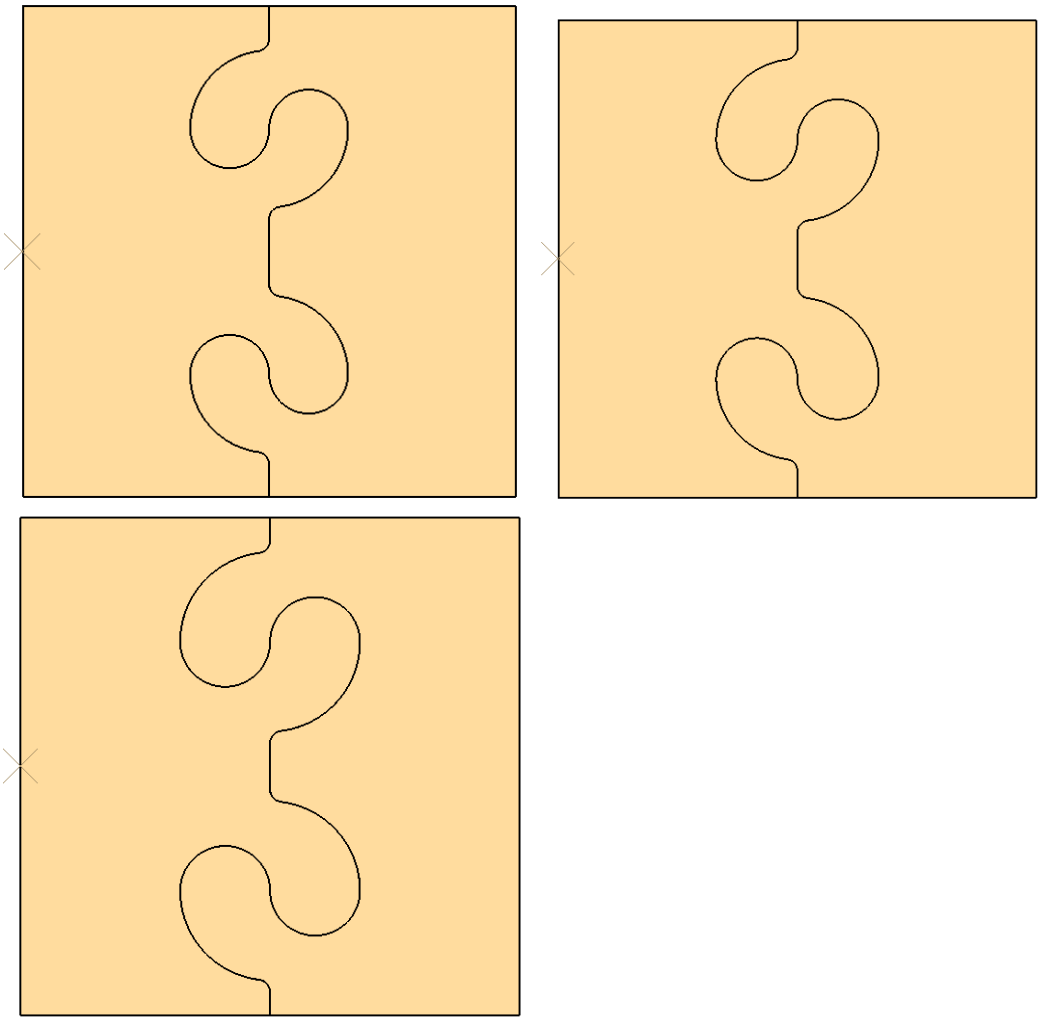

Yin yang study 2
Varying fr_1: 5 – 10 mm

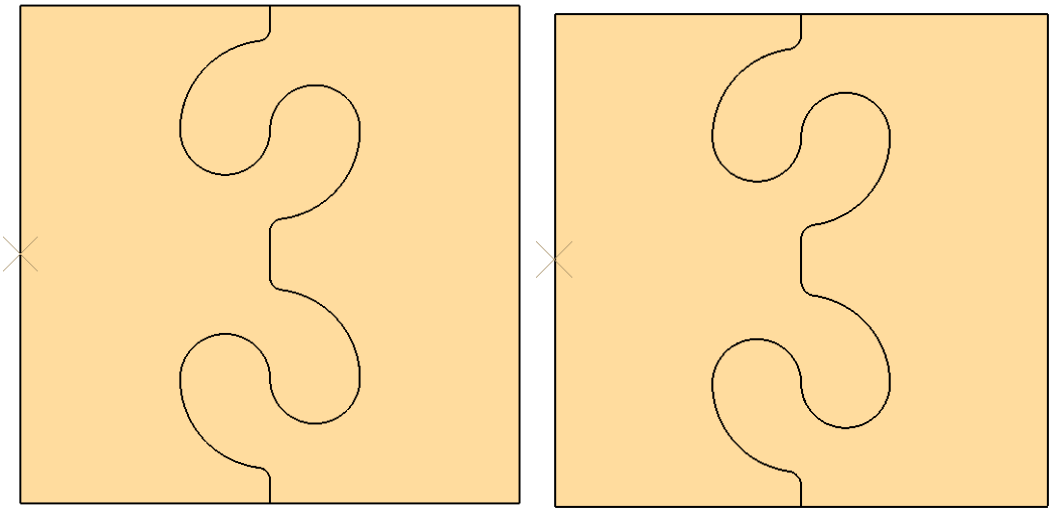

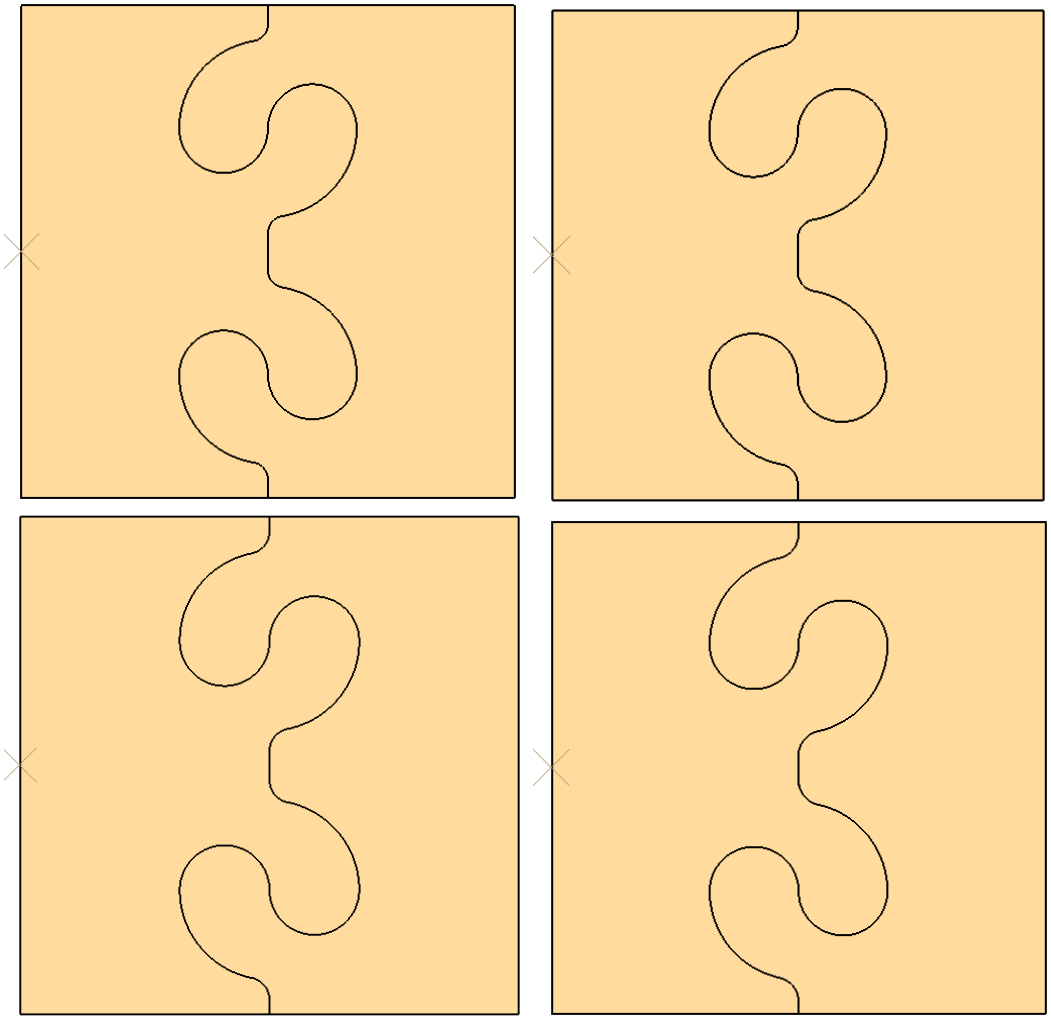

Yin Yang study 3
Varying fr_1: 5 – 26 mm